THESIS APPROVAL

GRADUATE SCHOOL, KASETSART UNIVERSITY

Master of Engineering (Chemical Engineering)

DEGREE

Chemical Engineering	Chemical Engineering
FIELD	**DEPARTMENT**

TITLE: Gas Holdup via Electrical Resistance Tomography and Residence Time Distribution via Stimulus-Response Tracer Technique in an External-loop Gas Lift Reactor

NAME: Miss Olrarat Wongsirikajorn

THIS THESIS HAS BEEN ACCEPTED BY

THESIS ADVISOR

(Associate Professor Sunun Limtrakul, D.Sc.)

DEPARTMENT HEAD

(Associate Professor Phungphai Phanawadee, D.Sc.)

APPROVED BY THE GRADUATE SCHOOL ON

DEAN

(Associate Professor Gunjana Theeragool, D.Agr.)

THESIS

GAS HOLDUP VIA ELECTRICAL RESISTANCE TOMOGRAPHY AND RESIDENCE TIME DISTRIBUTION VIA STIMULUS-RESPONSE TRACER TECHNIQUE IN AN EXTERNAL-LOOP GAS LIFT REACTOR

OLRARAT WONGSIRIKAJORN

A Thesis Submitted in Partial Fulfillment of
the Requirements for the Degree of
Master of Engineering (Chemical Engineering)
Graduate School, Kasetsart University
2009

Olrarat Wongsirikajorn 2009: Gas Holdup via Electrical Resistance Tomography and Residence Time Distribution via Stimulus-Response Tracer Technique in an External-loop Gas Lift Reactor. Master of Engineering (Chemical Engineering), Major Field: Chemical Engineering, Department of Chemical Engineering. Thesis Advisor: Associate Professor Sunun Limtrakul, D.Sc. 193 pages.

Hydrodynamics in an external-loop gas lift reactor was studied. The gas holdup by ERT system and the residence time distribution (RTD) by a stimulus-response tracer technique were investigated with the effects of superficial gas velocities in the riser and downcomer in the range of 0.51-10.23 cm/s and 0-3.07 cm/s, respectively. Water and air were used as system fluids. A dual-plane ERT system was used for measuring cross-sectional gas holdup distributions of both columns. The ranges of gas holdup values in the riser and downcomer are 0.079-0.238 and 0.037-0.157, respectively. The gas holdup was approximately axis-symmetric and was decreased from the center to the wall both of columns. The gas holdup in both columns was increased with an increasing of superficial gas velocity. Gas holdup in the riser is always higher than that in the downcomer. The mean value and the fluctuation of mixing index were increased with an increasing of the superficial gas velocities of both columns. A stimulus-responses technique with a pulse input signal was used to obtain RTD. The dispersion model was used to obtain the vessel dispersion number (*D/uL*) in both columns. (*D/uL*) values of the riser and downcomer are in the range of 0.23-1.51 and 0.08-0.9, respectively and increase with an increasing of superficial gas velocity. It can be concluded that the fluid flow behavior is large deviation from plug flow and is more close to a mixed flow. The results from both methods lead to the conclusions that the fluid flow in the riser approaches a mixed flow and the mixing is higher than that in the downcomer. Increasing superficial gas velocities increases the mixing in both columns.

_____ _____ ___ / ___ / ___

Student's signature Thesis Advisor's signature

ACKNOWLEDGEMENTS

This major undertaking has received the whole-hearted support of many individuals. I would like to express my gratitude to all those who gave me the possibility to complete this thesis. I would like to thank the Department of Chemical Engineering Faculty of Engineering Kasetsart University for giving me permission to study this thesis. I am deeply indebted to my supervisor Assoc. Prof. Dr. Sunun Limtrakul and co-supervisor Assoc. Prof. Dr. Terdthai Vatanatham whose help, effort, tolerance, stimulating suggestions me in all the time of this thesis.

I deeply thank to my chairperson Asst. Prof. Dr. Manop Charoenchaitrakool, my external examiner Assoc. Prof. Dr. Thawatchai charinpanichkul and Asst. Prof. Dr. Chaiwat Chaikul. Furthermore, I would like to thank the Kasetsart University Research and Development Institute (KURDI), Department of Chemical Engineering, Kasetsart University, National Research Council of Thailand (NRCT) and Center of Excellence for Petroleum, Petrochemicals, Advanced Materials, S&T Postgraduate Education and Research Development Office (PERDO) for financial support.

My heartfelt appreciation also goes to my colleagues, Miss Sirirat Janjaturaphan, and Mr. Chinnawat Thawornkuno from Kasetsart University. I would love to thank them for all their help, support, interest, valuable hints and experience sharing. Especially, I am obliged to Mr. Somchai Pattarameth, Mr. Marco Castillo, Mr. Gary Bolton, Mr. Octave Levenspiel, and Mr. Scott Fogler for all their assistance on the theory, technique, expertise and professional advice. My close friend Mr. Phuwaphat Klongpramong was of great help in difficult times. My senior, Mr. Parinya Kongprom looked close at the final version of the thesis for English style and grammar, both correcting and offering suggestions for improvement. Especially, I would like to give my special thanks to my family whose patient love enabled me to complete this thesis.

Olrarat Wongsirikajorn

April 2009

TABLE OF CONTENTS

Page

LIST OF TABLES

LIST OF TABLES (Continued)

LIST OF TABLES (Continued)

LIST OF FIGURES

LIST OF FIGURES (Continued)

LIST OF FIGURES (Co ntinued)

LIST OF FIGURES (Continued)

LIST OF FIGURES (Continued)

LIST OF FIGURES (Continued)

LIST OF FIGURES (Continued)

LIST OF FIGURES (Continued)

LIST OF FIGURES (Continued)

LIST OF FIGURES (Continued)

LIST OF FIGURES (Continued)

Appendix Figure **Page**

LIST OF FIGURES (Continued)

Appendix Figure **Page**

LIST OF FIGURES (Continued)

Appendix Figure **Page**

LIST OF FIGURES (Continued)

Appendix Figure **Page**

LIST OF FIGURES (Continued)

Appendix Figure **Page**

LIST OF ABBREVIATIONS

a_D	=	surface area per volume of liquid in all bubble (cm^2/cm^3)
a_l	=	surface area per volume of liquid not include bubble
A_d	=	cross-sectional area of a downcomer (cm^2)
A_r	=	cross-sectional area of a riser (cm^2)
C	=	concentration (g/ml)
d_B	=	bubble size (mm)
d_d	=	diameter of the downcomer column (cm)
d_r	=	diameter of the riser column (cm)
D	=	axial dispersion coefficient for flowing fluid (m^2/s)
E	=	RTD for the dispersion model (exit age distribution, (1/t))
E_L	=	the effective dispersion coefficient in the liquid
E_{Lo}	=	overall axial dispersion coefficient for the reactor as a whole
E_θ	=	dimensionless exit age distribution of RTD for the dispersion model
F_g	=	gas flow rate (m^3/s)
g	=	gas
h_D	=	dispersion height corresponds to the distance from the surface (cm)
h_t	=	the vertical distance between the manometer taps (cm)
Δh_m	=	the manometer reading
H_d	=	height of the downcomer column (cm)
H_L	=	height of liquid (cm)
H_r	=	height of the riser column (cm)
I	=	current (A)
K_B	=	empirical coefficients (in downcomer)
K_T	=	empirical coefficients (in riser)
l	=	liquid
N	=	number of equal-size mixed flow reactors in series

LIST OF ABBREVIATIONS (Continued)

N	=	number of mixing cell
N	=	number of pixel
P	=	pressure (kg/m·s^2)
Pe	=	Peclect Number
ΔP	=	pressure drop (kg/m·s^2)
t	=	time (s)
t_c	=	average of time in circulation one loop (s)
t_c	=	circulation time
t_m	=	mixing time (s)
$\bar{t}$	=	V / v, reactor holding time or mean residence time of fluid in a flow reactor (s)
T	=	temperature (^{o}C)
u_b	=	bubble velocity (cm/s)
u_L	=	local axial liquid velocity (cm/s)
U_l	=	superficial liquid velocity (m/s)
U_{Lc}	=	liquid circulation velocity (cm/s)
U_{Ld}	=	liquid circulation velocity in the downcomer (cm/s)
U_{Ld}	=	superficial liquid velocity in the riser (m/s)
U_{Lr}	=	liquid circulation velocity in the riser (cm/s)
U_{Lr}	=	superficial liquid velocity in the downcomer (m/s)
U_{Sg}	=	superficial gas velocity (cm/s)
U_{sgr}	=	superficial gas velocity gas in the riser (cm/s)
U_{sgd}	=	superficial gas velocity gas in the downcomer (cm/s)
v_d	=	volumetric flow rate of the downcomer column (l/min)
v_r	=	volumetric flow rate of the riser column (l/min)
V	=	electrical potential difference (Volt)

LIST OF ABBREVIATIONS (Continued)

V_{gl}	=	slip velocity (m/s)
V_G	=	volume of gas (cm^3)
V_{Gr}	=	volume of gas in the riser column
V_L	=	volume of liquid (cm^3)
V_{Lr}	=	volume of liquid in the riser column
V_{Lr}	=	actual liquid velocity in the riser (m/s)
$\dot{V}_{Lr}$	=	velocity of liquid circulation in the riser
V_{Ld}	=	actual liquid velocity in the downcomer (m/s)
x_c	=	distance in circulation or circulation path length (cm)
Δz	=	distance between two levels of the column
ε	=	local gas holdup
ε_{gr}	=	gas holdup in riser column
ε_{gd}	=	gas holdup in downcomer column
ε_g	=	gas holdup in the gas-liquid system
ω	=	function of the reactor geometry and of the properties of the liquid
ν	=	function of the flow regime as well as by reactor geometry
α	=	volume fraction of the dispersed material
σ	=	conductivity (mS/cm)
σ_1	=	conductivity of the continuous phase (mS/cm)
σ_2	=	conductivity of the dispersed phase (mS/cm)
σ_{mc}	=	reconstructed measured conductivity (mS/cm)
σ^2	=	variance of a tracer curve or distribution function (s^2)
ρ_L	=	density of liquid (kg/m^3)
θ	=	dimensionless time units
τ	=	space-time (s)
$k_L a_L$	=	overall volumetric mass transfer coefficient

LIST OF ABBREVIATIONS (Continued)

$k_L a_D$	=	overall volumetric mass transfer coefficient
MFR	=	mixed flow reactor
PFR	=	plug flow reactor
RTD	=	residence time distribution
$\frac{D}{uL}$	=	vessel dispersion number

GAS HOLDUP VIA ELECTRICAL RESISTANCE TOMOGRAPHY AND RESIDENCE TIME DISTRIBUTION VIA STIMULUS-RESPONSE TRACER TECHNIQUE IN AN EXTERNAL-LOOP GAS LIFT REACTOR

INTRODUCTION

Gas lift reactors consist of a liquid pool which is divided into two distinct zones. The difference of the gas holdup results in different bulk densities of the fluid in these two zones. This leads to circulation of the fluid in the reactor. This class of reactor is very attractive for use in the chemical process industry and biotechnology due to their design flexibility, low power requirement, and less pressure drop with further advantages of good mass and heat transfer. The rate of liquid circulation depends on gas flow rate. Two basic classes of the gas lift are distinguished: (i) the internal-loop gas lift reactor (IL-GLR) and (ii) the external-loop gas lift reactor (EL-GLR). The EL-GLR has greater flexibility (Weiland and Onken, 1981) and its performance could be manipulated better by controlling parameters for the individual sections. EL-GLR is selected in this study. Gas holdup is an important hydrodynamic parameter in the reactor. It affects to mass and heat transfer in the system. Gas holdup measurements usually provide overall average information, i.e., level measurement, pressure measurement. However, local gas holdup information is important for accuracy design and performance prediction. Local gas holdup measurements require a non-invasive technique to avoid disturbing the flow pattern in the system.

An electrical resistance tomography (ERT) system is one of non-invasive technique that produce a cross-sectional image showing the distribution of electrical conductivity of the contents of the fluids in the vessel from measurements taking at the boundary of the vessel. Multiple electrodes are arranged around the boundary of the vessel at fixed locations in such a way that they make electrical contact with the fluid inside the vessel but do not affect the flow. The technique has been used in

many fields such as petroleum, chemical, metallurgy and pharmacy etc, especially in the measurement of two-phase/multi-phase flows (Vereechen *et al.,* 1996; Wang *et al.,* 1999; Bolton *et al.,* 2004; Fransolet *et al.,* 2005; Razzak *et al.,* 2007; Giguere *et al.,* 2008).

The residence time distribution (RTD) is one of the most informative characterizations that describe mixing behavior in a reactor. It is a probability distribution function that describes the amount of time a fluid element spends inside the reactor. The knowledge of the liquid RTD is important for a number of reasons (Danckwerts, 1953) allowing an accurate kinetic modeling of the system, help rector design to achieve or preserve a desired flow pattern, and to compare the behavior of real reactors to their ideal models. Furthermore, this is useful in estimating the yield of a given reaction and designing future reactors (MacMullin and Weber, 1935). The RTD in loop reactors is mainly due to recirculation, usually provided by axial dispersion model (Naseau *et al.,* 1996; Cho *et al.,* 2000; Teixeira *et al.,* 2001; Hoppe *et al.,* 2002; Forret *et al.,* 2003; Camargo *et al.,* 2005; Dahhan *et al.,* 2006; LEE *et al.,* 2007). In streamline flow of fluids through pipes, axial mixing is mainly due to fluid velocity gradients, whereas radial mixing is due to molecular diffusion alone. Axial dispersion depends on the flow rates, the axial dispersion coefficient, and length of tubes. A standard way to estimate the degree of dispersion in loop reactors is by the experimental measurement of the RTD.

A stimulus-response tracer technique is a well-established method in investigation of a flow process dynamics and evaluation of residence time distribution (RTD). The principle of a tracer experiment consists of a common impulse-response method: injection of a tracer at the inlet of a system followed by the measurement of some relevant property of the outlet solution (e.g. the solution electrical conductivity) is the most commonly used RTD experiment in loop reactors (Ruffer *et al.,* 1994; Melo *et al.,* 2001; Minsker *et al.,* 2004; Zhang *et al.,* 2005; NIE *et al.,* 2006).

Therefore, this work focused on investigation of hydrodynamics and mixing index behavior (i.e., gas holdup, residence time distribution) in an external-loop gas

lift reactor by electrical resistance tomography (ERT) system and a stimulus-response tracer technique were used in the measurements. In addition, the effects of superficial gas velocities in the riser and downcomer on the gas holdup and RTD were also investigated.

OBJECTIVES

To investigate the hydrodynamic and mixing behavior within an external-loop gas lift reactor. The scopes of the work are listed below:

1. To study the radial distribution of gas and liquid phase across the sectional areas of riser and downcomer in an external-loop gas lift reactor by using method of Electrical Resistance Tomography (ERT).

2. To study the Residence Time Distribution (RTD) by stimulus-response tracer technique.

3. Air and tap water were used as gas and liquid phases, respectively in an external-loop gas lift reactor.

4. To study the effect of superficial gas velocities on the gas holdup and residence time distribution.

5. To find the parameter from Dispersion model, dimensionless group of dispersion model that can demonstrate the flow pattern.

LITERATURE REVIEW

1. General gas lift reactors

General gas lift reactors consist of a liquid pool which is divided into two distinct zones, only one of which is usually sparged by gas. The different gas holdup in the gassed and ungassed zones results in different bulk densities of the fluid in these regions. This leads to circulation of the fluid in the reactor. The part of the reactor containing the gas-liquid up flow is the riser and the region containing the down flowing fluid is known as the downcomer.

Gas lift reactors have been employed for any gas-liquid or gas-slurry contacting processes. The practical application depends on the ability to achieve the required rates of momentum, heat and mass transfer at acceptable capital and operating costs. The technical and economic feasibility of using gas lift devices has been conclusively established for a number of processes. These reactors have been used in aerobic fermentations, for treatment of wastewater and other similar operations.

Despite numerous successes, the industrial application of gas lift reactors remains limited principally because the basic knowledge needed for their design is not widely available in the open literature (Chisti and Moo-Young, 1987). The limited information which is accessible frequently shows wide variations and conflicting claims. Consequently, a reliable design basis is still far from established for airlift reactors (Chisti and Moo-Young, 1987). Until recently, the important parameters such as the induced liquid circulation rate, could not be satisfactorily predicted except in particular situations and then only in low viscosity Newtonian fluids.

1.1 Classification of gas lift reactors

Two basic classes of the gas lift may be distinguished: (i) the internal-loop gas lift where what would otherwise be a simple bubble column has been split into a riser and a downcomer by an internal baffle; and (ii) the external- or outer-loop gas lift reactors where the riser and the downcomer are two quite separate tubes connected by horizontal sections near the top and the bottom. Internal- and external-loop reactors may be further subdivided depending on the peculiarities. Internal-loop gas lift, for example, may be of the split-cylinder type or they may have a concentric draught-tube configuration. In the latter, either the draught-tube or the annulus may be gas sparged. The draught-tube and the vertical baffle (in the split-cylinder mode) may themselves be subdivided (Blenke, 1979; Chisti and Moo-Young, 1987) into sections to increase communication between the riser and the downcomer. Multiple concentric draught-tubes have also been studied (Margaritis and Sheppard, 1981).

The external-loop reactors have a less variety, but several designs of the horizontal connections between the riser and the downcomer, particularly the top connection, may be appropriate. Further modifications could be introduced into the head-space region of the reactor where gas-liquid separation takes place, and depending on the separator efficiency the reactor performance may be significantly influenced (Siegel, 1986).

Internal- and external-loop gas lift reactors usually have circular cross-sections, but rectangular and square cross-sections which have practical applications in industry are also a definite option and have indeed been studied (Chisti, 1986; Chisti and Moo-Young, 1988a; Gasner, 1974; Piggott, 1985; Siegel, 1986). Gas sparger types, both in the static and the dynamic sparger classes, and their location in the riser and/or the downcomer may be altered to give different performances for different purposes. Multiple gas injection points in the reactor may also be beneficial. In addition, the downcomer and/or the riser may contain such internal such sieve plates (Wesrlake, 1986), static mixers (Stejskal and Potucek, 1985) and baffles projecting from the walls (Lin, 1976). Some other aspects may be found elsewhere

(Chisti and Moo-Young, 1987; Merchuk, 1986; Merchuk and Siegel, 1988; Onken and Weiland, 1983).

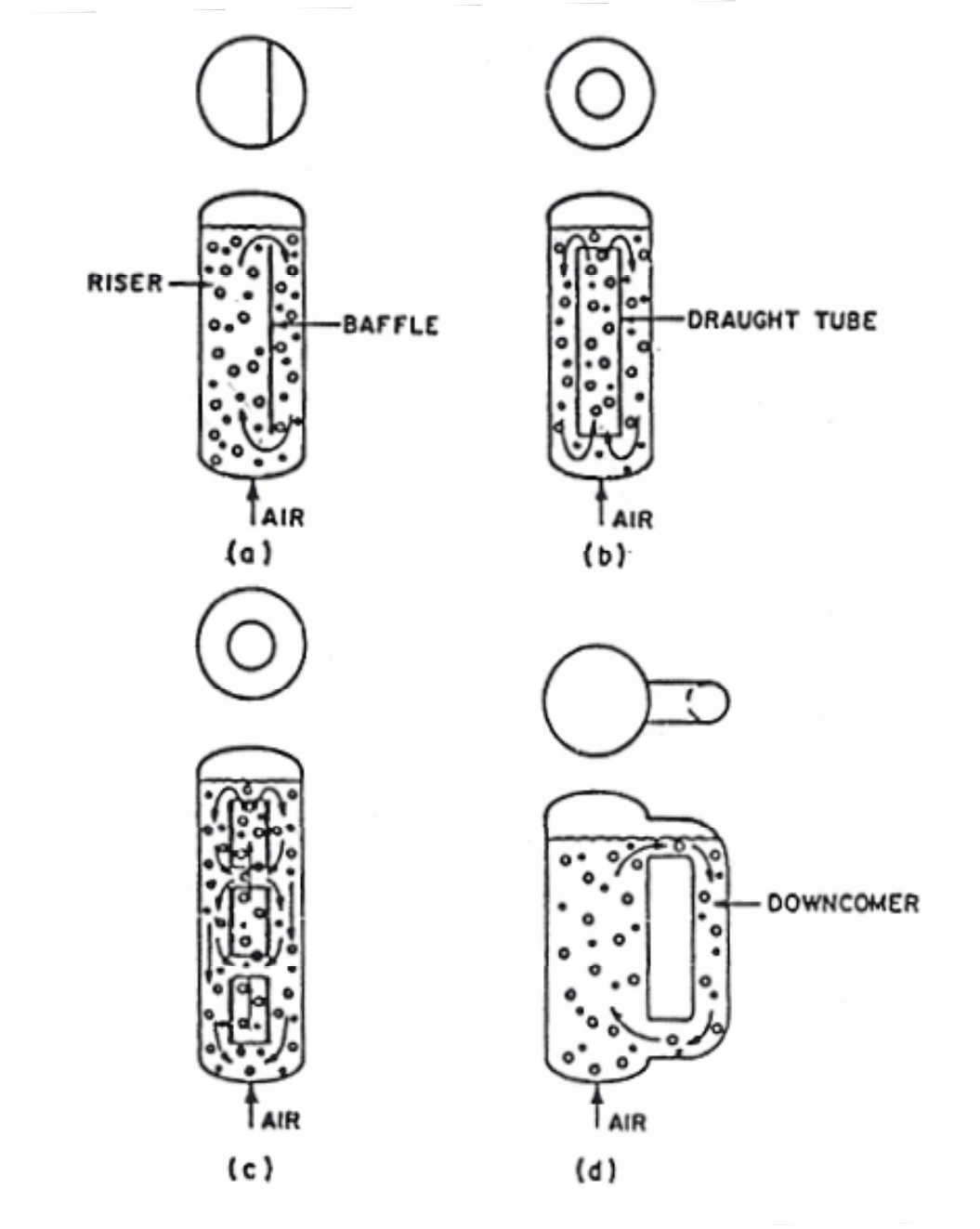

Figure 1 Types of gas lift reactors. (a) Split-cylinder internal-loop; (b) Concentric draught-tube internal-loop; (c) Draught-tube internal-loop with vertically split draught-tube; (d) External-loop.

Source: Airlift Bioreactor, Chisti (1989)

1.2 Bubble column vs. the gas lift reactor

The hydrodynamic behaviors of bubble column and gas lift reactors are very different. The main distinction between co-current or counter-current bubble columns and gas lift reactors is that in the latter the rate of liquid circulation depends on, and is determined by, the gas flow rate, whereas in the former types the liquid flow is independent of gas flow. Because of the long residence times that are typically necessary in a bioreactor, large liquid throughputs are not possible in bubble columns without significant recycle rates. In gas lift reactors, on the other hand, quite high linear liquid velocities may be generated without the need for any external recirculating mechanism. The consequent turbulence postpones the incipient slugging in the gas lift to higher gas velocities than usual in bubble columns (Merchuk, 1986; Weiland and Onken, 1981). Also, the gas velocities for liquid blowout condition (*i.e.,* spray formation) are lower (Chisti and Moo-Young, 1987) in the bubble columns than in gas lift reactors. As a result of theses effects the operating range of the gas lift reactors in terms of the possible gas and liquid superficial velocities in them is broader (Merchuk, 1986; Weiland and Onken, 1981) than for the bubble column reactor.

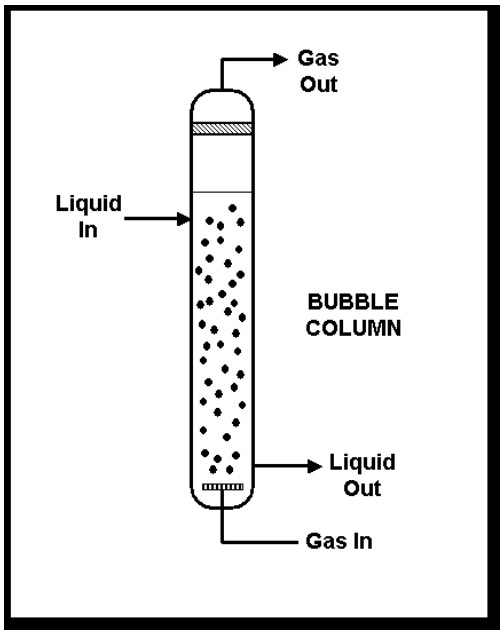

Figure 2 A bubble column (schematic). Gas is sparged in the bottom of the column; the liquid flows down to the column.

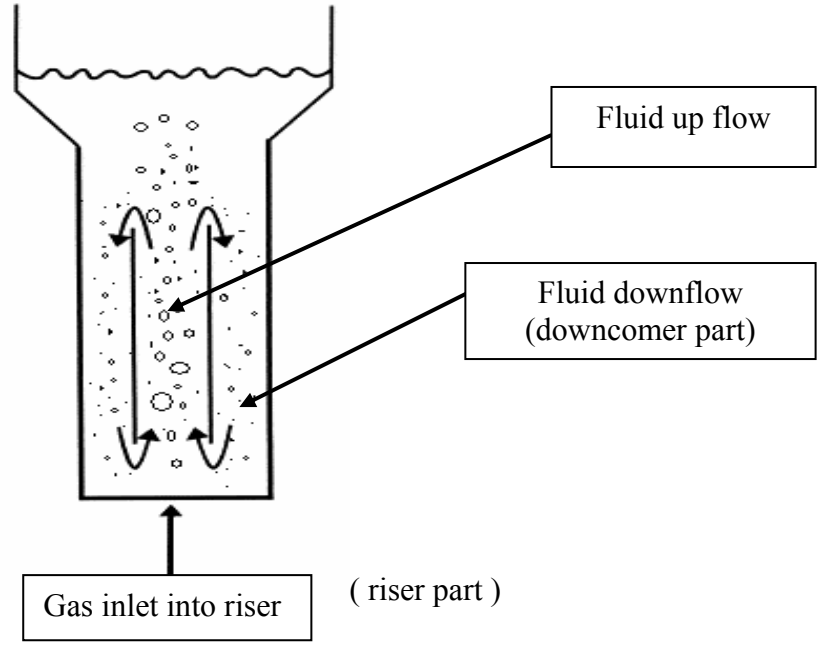

Figure 3 A gas lift reactor (schematic). Gas is sparged in the annular riser (inside column); the liquid flows down to the downcomer (outside column).

1.3 Advantages of gas lift reactors

This class of reactor is very attractive for use in the chemical process industry and biotechnology due to their design flexibility, low power requirement, and less pressure drop with further advantages of good mass and heat transfer. The rate of liquid circulation depends on gas flow rate. Two basic classes of the gas lift are distinguished: (i) the internal-loop gas lift reactor (IL-GLR) and (ii) the external-loop gas lift reactor (EL-GLR). The EL-GLR has greater flexibility (Weiland & Onken, 1981) and its performance could be manipulated better by controlling parameters for the individual sections.

2. Hydrodynamics of an external-loop gas lift reactor

Several methods are used for measuring the hydrodynamics in an external-loop gas lift reactor. The fractional gas holdup in the different sections is the critical parameter which determines the reactor hydrodynamics. Most studies about gas lift reactors have been focused on estimating the evolution of gas holdup in each section of the reactor with superficial gas velocity (Hills, 1976; Merchuk and Stein, 1981; Siegel, Merchuk and Schugerl, 1986; Joshi Ranade *et al.,* 1990; Dhaouadi, 1997a).

For many investigators, the superficial circulation velocity of the liquid phase is often identified as the key parameter for design. Consequently, many models and correlations have been proposed in order to predict the liquid velocity in gas lift reactors (Bello *et al.,* 1984; Chisti *et al.,* 1988; Siegel *et al.,* 1986; Popoic and Robindon, 1988; Gavrilescu and Tudose, 1995; Dhaouadi, 1997a).

It appears clearly that global parameters have been widely studied, but that little attention has been paid to the local characteristics of the flow. Firstly, the axial evolution of the cross-sectional gas holdup has been rarely studied, except by Merchuk and Stein (1981) and by Young *et al.* (1991). Secondly, only the works of Okada *et al.* (1993) and of Young *et al.* (1991) proposed an experimental description of the radial evolution of the local gas holdup and of the local axial velocity of both

phases. Thirdly, the bubble rise velocity could be calculated by cross correlating the two probe fiber signals (Tiefng Wang *et al.,* 2003).

Hydrodynamics at the global scale has been investigated on reactors using conventional techniques. The manometric technique has been used for average gas holdup ε_{gr} measurements using piezo-resistive pressure sensors (PR25, 0-150 mbar & 0-500 mbar, Keller GmbH, Germany) mounted flush to the wall at several heights in the riser. This technique has been shown to be useful for identification of the prevailing hydrodynamic regime. The example methods for calculating gas holdup, superficial velocity and liquid circulation velocity have shown as follow:

The gas holdup values in the riser and the downcomer zones have been obtained by measuring the differential pressure between two sampling ports using two inverted U-tube manometers. The gas holdup in each section has been calculated using the equation:

$$\varepsilon_g = \frac{\Delta h_m}{h_t} \tag{1}$$

where h_t is the vertical distance between the manometer taps and Δh_m is the manometer reading.

Bello *et al.* (1985a) using data of their own and additional data from other sources proposed the following linear equations to relate the downcomer and the riser gas holdups

$$\varepsilon_d = 0.79\varepsilon_r - 0.057 \tag{2}$$

for the external-loop devices applied to air-water only. Similar work was extended to more complex fluids by others (Chisti *et al.,* 1986; Chisti and Moo-Young, 1987). However, the direct relationships between ε_d and ε_r as found by Bello *et al.* (1985a)

and Chisti *et al.* (1986) make sense also because the riser and the downcomer liquid velocities are similarly related to each other.

The lower downcomer gas holdups in the external-loop gas lifts relative to the concentric-tube reactors (see Equation 2) were due to the geometric peculiarity of the external-loop devices in which the horizontal connection between the riser and the downcomer allowed most of the gas to separate from the liquid and little gas was carried to the downcomer.

Local hydrodynamics in the riser have been investigated and analyzed in detail by Vial *et al.* (2002). Local gas holdup exhibits flat profiles in the homogeneous regime while it seems nearly parabolic in the transition and the heterogeneous regime. This is proved by fitting the following relation on experimental profiles as a function of the dimensionless diameter $\phi = 2r / D_R$, adjusting ε_{gr} and the exponent n:

$$\varepsilon_{gr} = \left\langle \varepsilon_{gr} \right\rangle \frac{n+2}{n}\left(1-\phi^n\right) \tag{3}$$

where n is higher than 8 in the homogeneous regime and that it tends to 4 for high U_{gr} values. Conversely to the classical intuition, local axial liquid velocity u_L profiles are never flat in air lift reactors, even in the homogeneous regime. Liquid u_L and bubble u_b velocity profiles tend even to become flatter in the transition and the heterogeneous regime than in the homogeneous regime.

Local measuring techniques were applied on reactors involved in the analysis of radial gas holdup profiles with an optical fibred probe (RBI, France) which detects the phase around the probe tip on the basis of its refractive index. A system with two parallel fibres placed on the same optical probe was used to estimate bubble size.

Local time-averaged liquid velocity and RMS velocity are measured in the axial and the tangential directions with a one-component Laser Doppler Anemometer

Aerometrics equipped with a RSA-1000L processor which operates in the backward scattering mode (Ch. Vial *et al.,* 2002).

The gas holdup could be measured by the usual manometric method. The method measures the pressure difference ΔP between the two levels of the column (Kaustubha *et al.,* 2006). The gas holdup is related to the pressure drop by

$$\Delta P = \left(1 - \varepsilon_g\right)\rho_L g \Delta z \tag{4}$$

Other method for calculating of the fractional gas holdup in the riser section of the column at different gas flow rates as follow by: (Hossein *et al.,* 2005);

$$\varepsilon_{gr} = \frac{V_{Gr}}{V_{Gr} + V_{Lr}} \tag{5}$$

where V_{Gr} is volume of gas in the riser column; V_{Lr} is volume of liquid in the riser column.

The overall liquid circulation velocity in the riser U_{Lr} could be predicted from an energy balance using the following equation:

$$U_{Lr} = \left[\frac{2gh_D(\varepsilon_r - \varepsilon_d)}{K_T/(1-\varepsilon_r)^2 + K_B(A_r/A_d)^2\left[1/(1-\varepsilon_d)^2\right]}\right]^{0.5} \tag{6}$$

where two empirical coefficients K_T (that takes the effects of pressure drop in the riser and the separator section into account), K_B (that accounts for pressure drop in the downcomer and the junction) and dispersion height h_D corresponds to the distance from the surface in which a gas phase could be observed in the riser.

Accordingly, liquid circulation depends on the superficial gas velocity and this dependence is claimed (Bello *et al.,* 1984; EI Gabbani, 1977; Merchuk, 1986; Merchuk, 1986a; Onken and Weiland, 1983; Siegel *et al.,* 1986) to be of the form:

$$U_{Lr} = \omega U_{Gr}^{V} \tag{7}$$

In which ω is a function of the reactor geometry and of the properties of the liquid, whereas ν determined by the flow regime as well as by reactor geometry (Onken and Weiland, 1983). Equation 7 is purely empirical and the exact nature of the dependence of ω on gas lift geometry in any generalized form is unknown.

In two very different external-loop gas lift reactors using water or water-like fluids independent investigators (Merchuk, 1986a; Onken and Weiland, 1980) found the exponent v in Equation 7 to be approximately 0.4. Some other work complied by Merchuk (1986) also substantiated this point.

Furthermore, the gas holdup strongly affects the liquid circulation velocity. Since a correlation for the gas holdup in terms of the basic parameters of the multi-stage an external-loop gas lift reactor has already been developed, and as liquid circulation velocity and gas holdup are interdependent, the following equation has been obtained relating liquid circulation velocity with the system fractional gas holdup (Kaustubha *et al.,* 2006):

$$U_{Lc} = 0.248\varepsilon_g^{1.91} \tag{8}$$

where ε_g is fractional gas holdup, dimensionless; U_{Lc} is superficial liquid velocity, m/s.

A new way of determining the limits of the flow regimes is presented here; it is based on the classical slip velocity approach of (Wallis, 1969):

$$V_{gl} = \frac{U_g}{\varepsilon_g} - \frac{U_l}{1-\varepsilon_g} \tag{9}$$

where V_{gl} is slip velocity, m/s; ε_g is fractional gas holdup, dimensionless; U_g is superficial gas velocity, m/s; U_l is superficial liquid velocity, m/s.

However superficial velocity has value not equal to velocity of liquid at real flow in pipe because has bubble contaminate in liquid (J. B. SNPE *et al.,* 1995). Relation of these as follows:

$$V_{Lr} = \frac{U_{Lr}}{1-\varepsilon_r} \tag{10}$$

$$V_{Ld} = \frac{U_{Ld}}{1-\varepsilon_d} \tag{11}$$

where U_{Lr} is superficial liquid velocity in the riser, m/s; U_{Ld} is superficial liquid velocity in the downcomer, m/s; V_{Lr} is actual liquid velocity in the riser, m/s; V_{Ld} is actual liquid velocity in the downcomer, m/s; ε_r is fractional gas holdup in the riser, dimensionless; ε_d is fractional gas holdup in the downcomer, dimensionless.

The available empirical correlations for liquid velocity in gas lift reactors are useful in understanding the various factors which influence liquid circulation; however, such correlations do not have a sufficient predictive potential for satisfactory reactor design as illustrated by the following example:

Figure 4, some data could be compared for an external-loop gas lift reactor some data on liquid circulation velocity with the prediction of Bello *et al.* (1984). The data in Figure 4 was obtained (Herskowitz and Merchuk, 1986) on air-water and following the equation:

$$\dot{V}_{Lr} = 2.62 U_{Gr}^{0.63} \tag{12}$$

which was calculated by the present writer. The data (Herskowitz and Merchuk, 1986) was from a reactor with A_d / A_r of 0.219 and a liquid height of about 2 m. These dimensions corresponded closely to the ranges that were used by Bello *et al.* (1984). The equation recommended by Bello *et al.* (1984) is also shown on Figure 4. This equation and the data do not compare even within ± 30% of the data set. Morever, notice the discrepancy in the slopes of the two lines (*i.e.,* in the exponents on the U_{Gr} term).

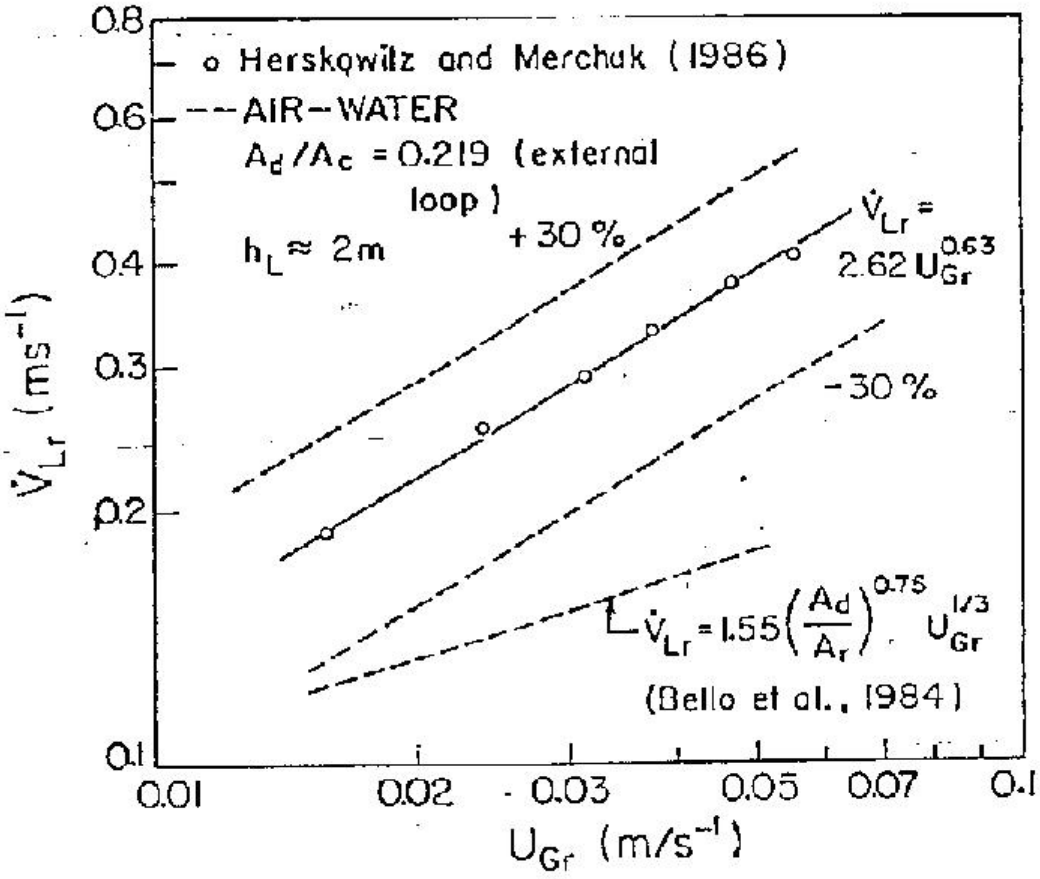

Figure 4 Liquid velocity vs. gas flow rate (external-loop). Comparison of liquid circulation data of Herskowitz and Merchuk (1986) with the correlation of Bello *et al.* (1984).

Source: Chisti (1989) Airlift bioreactor**.**

Most of the available correlations on mixing and liquid circulation in gas lift reactors are summarized in Table 1. Other work on liquid circulation exists, but it has not led to explicit equations.

Table 1 Liquid circulation and mixing correlations in gas lift reactors.

Reactor Type and Reference	Equation	Parameter Range
1. External-loop, Bello *et al,* 1981	$V_{Lr} = \omega\left[\frac{A_d}{A_r}\right]^{\nu} U_{Gr}^{1/3}$ $\omega = 1.55, \nu = 0.74 \pm 0.04$ $t_c = \omega\left[\frac{A_d}{A_r}\right]^{\nu} U_{Gr}^{1/3}$ $\omega = 2.3, \nu = -0.46$ $\left(\frac{t_m}{t_c}\right) = \omega\left[\frac{A_d}{A_r}\right]^{\nu}$ (99% of complete mixing) $\omega = 5.2, \nu = 0.46$	Water 0.15 *M* NaCl $h_D = 1.8m$ $d_r = 0.152m$ $\frac{A_d}{A_r} = 0.11, 0.25, 0.44$ $B = 0.25m$ $L_c = 0.10m$
2. External-loop. Kawagoe and Robinson (1980)	$U_{Lr} \alpha \ U_{Gr}^{\nu}$ $\nu \approx 0.48$ for $U_{Gr} < 0.03 ms^{-1}$	Air-water $d_r = 0.152m$ $\frac{A_d}{A_r} = 0.44$

Table 1 (Continued)

Reactor Type and Reference	Equation	Parameter Range
3. External-loop. Onken and Weiland (1980)	$U_{Lr} \alpha \ U_{Gr}^{\nu}$ $\nu \approx 0.4$	Water and Newtonian media, $\mu_L \approx 1-16mPas,$ $d_r = 0.10m,$ $d_d = 0.05m,$ $h_D \approx 8.5m$ $0.006 \le U_{Gr}(ms^{-1}) \le 0.16$
4. External-loop. Lin *et al.* (1976)	$\frac{t_m}{t_c} = \frac{\overline{U}_{Lc} x_c}{19.89 E_L \tau^{0.188}}$ $\tau = \frac{C_t - C_{t\infty}}{C_{t\infty}}$	Air-water $h_L < 2m$ $d_r = 0.152m$ $\frac{A_d}{A_r} = 0.11$
5. External-loop. Popovic and Robinson (1984)	$U_{Lr} = \omega U_{Gr}^{0.322} \left[\frac{A_d}{A_r}\right]^{0.784} \mu_{ap}^{-0.385}$ $\omega = 0.052$ (bubble flow) $\omega = 0.0204$ (slug flow) $\mu_{ap} = K(5000U_{Gr})^{n-1}$ Note: U_{Gr} unit cms^{-1}	CMC in water, $\mu_{ap} = 0.015 - 0.5Pas$ U_{Gr} not specified. $h_D = 1.8m$ $d_r = 0.152m$ $\frac{A_d}{A_r} = 0.11,0.25,0.44$ $B = 0.25m$ $L_c = 0.10m$

Table 1 (Continued)

Reactor Type and Reference	Equation	Parameter Range
6. External-loop. Merchuk and Stein (1981)	$\frac{U_{Gr}}{\varepsilon_r} = 1.03(U_{Lr} + U_{Gr}) + 0.33$	Apparently water. $0 \le (U_{Lr} + U_{Gr}) \le 1.40 ms^{-1}$ $0.2 < \frac{U_{Gr}}{\varepsilon_r} < 1.80 ms^{-1}$ $d_r = 0.14m; \frac{A_d}{A_r} = 1.0,$ $L_r = L_d = 4.05m$ $L_{ap} \approx 0.35m, \varepsilon_d = 0$ always

In case of the overall volumetric mass transfer coefficient ($k_L a_L$ or $k_L a_D$) and the gas holdup have been frequently studied in gas lift reactors. All the main correlations for these parameters are compiled in Table 2. Notice that apart from the gas holdup correlation of Miyahara *et al.* (1986) all other equations in Table 2 may be reduced, for a given fluid and reactor geometry, to simple power law type functions of gas velocity. Even though all the equations in Table 2 are purely empirical, the hydrodynamic theory (Chisti and Moo-Young, 1988c) does indeed support the observed form of the relationship between gas holdup (or $k_L a_L$) and the gas velocity.

Table 2 Gas holdup and mass transfer correlations for gas lift reactors.

Reactor Type and Reference	Equation	Parameter Range
1. External-loop, Bello *et al.,* 1985.	$k_L a_D = 0.76\left[1+\frac{A_d}{A_r}\right]^{-2} U_{Gr}^{0.8}$ or in terms of the power input: $k_L a_D = 5.5\times10^{-4}\left[1+\frac{A_d}{A_r}\right]^{-1.2} \times (P_a/V_b)^{0.8}$ $\varepsilon_r = 3.4\times10^{-3}\left[1+\frac{A_d}{A_r}\right]^{-1} (P_G/V_D)^{2/3}$	Air-water or aqueous salt solution (0.15 $kmolm^{-3}$ NaCl); $d_e or d_t = 0.152m$; $h_D = 1.8m$; $U_{Gr} = 0.0137 to 0.086 ms^{-1}$ (bubble flow only) $\frac{A_d}{A_r} = 0.11 to 0.69$
2. External-loop, as in 1. Bello *et al.,* 1985a.	Liquid velocity effects: $\frac{k_L a_D h_D}{U_L} = 2.28\left[\frac{U_{Gr}}{U_L}\right]^{0.8}\left[1+\frac{A_d}{A_r}\right]^{-1}$ For water and salt solution; and $\varepsilon_r = 0.16\left[\frac{U_{Gr}}{U_L}\right]^{\alpha}\left[1+\frac{A_d}{A_r}\right]$ $\alpha = 0.56$ (water) $\alpha = 0.58$ (salt solution)	Air-water or aqueous salt solution (0.15 $kmolm^{-3}$ NaCl); $d_e or d_t = 0.152m$; $h_D = 1.8m$; $U_{Gr} = 0.0137 to 0.086 ms^{-1}$ (bubble flow only) $\frac{A_d}{A_r} = 0.11 to 0.69$

Table 2 (Continued)

Reactor Type and Reference	Equation	Parameter Range
3. External-loop, Chisti *et al.* 1986	$\varepsilon_r = 0.65\left[1+\frac{A_d}{A_r}\right]^{-0.258} U_{Gr}^{0.803\pm0.078C_S}$ $k_L a_L = \left[1+\frac{A_d}{A_r}\right]^{-1}(0.349-0.102C_S)$ $\times U_{Gr}^{0.837\pm0.002}$	Water; aqueous salt solution (0.15 $kmolm^{-3}$ NaCl); salt solution + 1, 2 or 3 dry wt./vol. % Solka-Floc (KS-1016) cellulose fibre; geometric details in Figure 1. $d_r = 0.152m; L_L = 1.75m;$ $\frac{A_d}{A_r} = 0.25;0.44;$ 52 holes $d_C = 0.001m.$
4. External-loop, as in Popovic and Robinson, 1984	$k_L a_L = 1.911\times10^{-4} U_{Gr}^{0.525}$ $\times\left[1+\frac{A_d}{A_r}\right]^{-0.853} \mu_{ap}^{-0.88}$ and $\varepsilon_r = 0.22 U_{Gr}^{0.8504}\left[1+\frac{A_d}{A_r}\right]^{-1.0518} \mu_{ap}^{-0.1039}$ μ_{ap} based on shear rates calculated using: $\gamma = 5000 U_{Gr}$ which is due to Nishikawa, 1977	Non-Newtonian CMC solutions; $\frac{A_d}{A_r} = 0,0.11,0.25,0.44;$ $\mu_{ap} = 0.015 to 0.5 Pas;$ U_{Gr} not specified. The gas velocity of Popovic and Robinson has unit cms^{-1}.

3. Electrical Resistance Tomography

3.1 General information

Electrical Resistance Tomography System (ERT) is a measurement technique for obtaining information about the contents of process vessels and pipelines. Multiple electrodes are arranged around the boundary of the vessel at fixed locations in such a way that they make electrical contact with the fluid inside the vessel but do not affect the flow or movement of materials.

A typical application is real time monitoring of multi-component flows within process engineering units. Specific applications where Electrical Resistance Tomography System (ERT) has been successfully exploited include solid/liquid and liquid/gas mixing, hydro-cyclones, packed columns, flotation columns, precipitation processes, liquid-liquid extraction and hydraulic conveying. In principle, Electrical Resistance Tomography System (ERT) could be used to investigate and monitor any process where the main continuous phase is at least slightly conducting and the other phases and components have differing values of conductivity.

3.2 Operating principles

An Electrical Resistance Tomography System (ERT) produces a cross-sectional image showing the distribution of electrical conductivity of the contents of a process vessel or pipeline from measurements taken at the boundary of the vessel. The P2000 system injects a current between a pair of electrodes and measures the resultant voltage difference between remaining electrode pairs according to a predefined measurement protocol. This interrogates an entire ‘slice’ through the measurement zone- analogous to a ‘body-scan’ in medical imaging. A single measurement set consists of over 100 voltage measurements- the exact number depends on the pre-defined measurement protocol.

3.3 Electrode geometry and construction

The most common electrode geometry shows electrodes arranged at equal intervals around the boundary of a circular vessel. Alternative arrangements include electrodes arranged around a square cross-section and a vertical series of electrodes. The electrodes are connected to the data acquisition system by co-axial cable which assists in reducing the effect of extraneous environmental noise and interference. The outer sheath of the co-axial cable is coupled to the feedback path of a voltage buffer to provide further noise immunity and the inner core is capacitive coupled to the input of the voltage buffer.

The material for electrode construction depends largely on the process application. The material should be more conductive than fluids being imaged to prevent problems due to contact impedance. Typically the electrode material is stainless steel, brass or silver palladium alloy. The dimensions of the electrodes are a function of the vessel diameter, range of conductivity to be measured, velocity of materials and the required imaging speed. ITS have the capability to provide optimum sensor designs.

A spare electrode referred to as the ground electrode, positioned away from the measurement electrodes but in electrical contact with the internal fluid is required to ensure all voltage measurements are fixed against a common ground source.

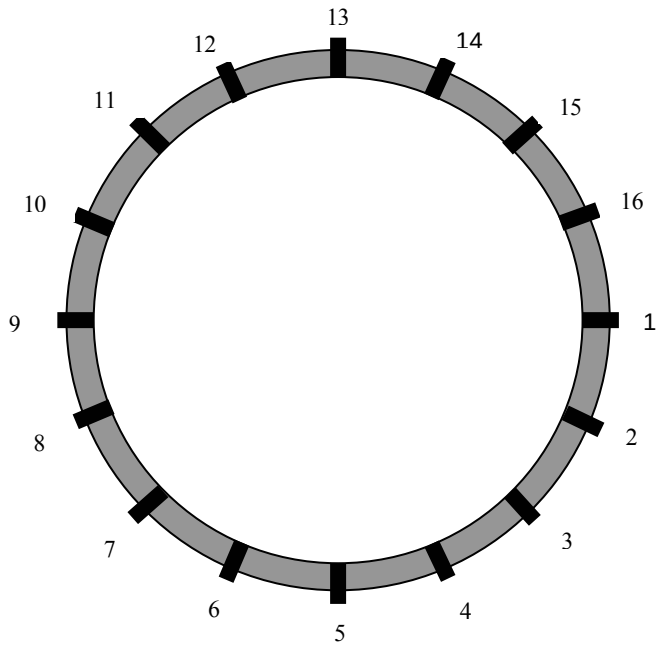

Figure 5 Schematic diagram of electrode arrangement and placement.

3.4 P2000 Data acquisition system for ERT

The Data Acquisition System (DAS) is responsible for obtaining the quantitative data describing the state of the conductivity distribution inside the pipeline. The data must be collected quickly and accurately in order to track small changes of conductivity in real-time thus allowing the image reconstruction algorithm to provide an accurate measurement of the true conductivity distribution.

A sine-wave voltage output is fed into a voltage-to-current converter (referred to as a voltage controlled current source – VCCS). Current is used in preference to voltage as the electrical 'probe' due to the variation of contact impedance between electrodes and the fluid inside the sensor. The VCCS circuit maintains constant amplitude over a wide range of resistance loads by employing two operational amplifiers and an analogue switch arrangement in the feedback path of one of the op-amps.

Due to the wide dynamic range of measurement conditions occurring in processes, the ERT system must be as flexible as possible to allow it to be used on a number of different process applications. In order to overcome the problem associated with various process vessel sizes and differing conductivities of materials it is useful to have the facility to increase or decrease the amplitude of the injected current in order to optimize the signal-to-noise ratio (SNR) of the measured voltage outputs for specific applications. The P2000 has an injection current range of 0 to 75 mA which is divided into 3 broad bands (0-1.5, 1.5-15, 15-75) with 256 step changes possible.

Also, to accommodate a wide range of material conductivities and to improve the accuracy for slowly changing processes, a range of injected current frequencies is provided. The P2000 can operate within the frequency range 75 to 153.6 kHz (in 12 steps).

The measurement strategy or protocol for probing the conductivity distribution within the vessel via the electrodes arranged around the vessel boundary is of paramount importance. The following strategies are available with the P2000 system.

A. Normal Adjacent

This is the recommended measurement strategy for sensors with insulating boundaries with 16 electrodes arranged at equal intervals around the periphery of the sensor. As could be seen in Figure 6, current is applied through two neighboring electrodes (in this case electrodes 1 and 2) and the voltages are measured from the remaining pairs of neighboring electrodes (in this case electrodes 3 and 4). Current is then applied through the next pair of electrodes and the voltage measurements are repeated. The procedure is repeated until all the independent measurements have been made. The adjacent measurement strategy yields N^2 measurements, where N is the number of electrodes. However of these only $N(N-1)/2$ are independent. Furthermore, to avoid electrode/electrolyte contact impedance problems, the voltage

is not measured at a current-injecting electrode and therefore the total number of independent measurements *M* is reduced to *N(N-3)/2*. Therefore a 16-electrode sensor gives 104 independent measurements.

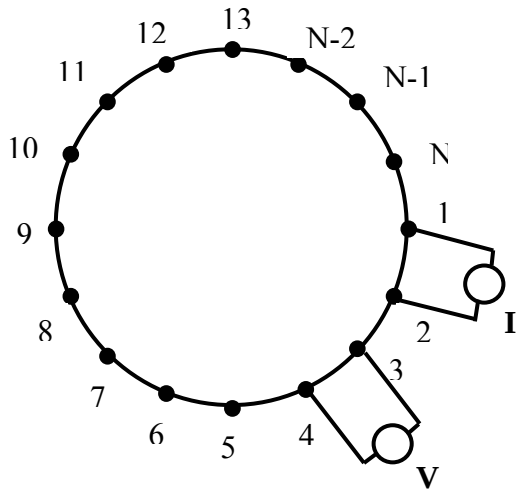

Figure 6 Arrangement of electrode in the type of adjacent measurement strategy.

3.5 Image reconstruction

Following the acquisition of data from the boundary of the object to be imaged it is necessary to process this data using an appropriate image reconstruction algorithm. For an ERT system the reconstructed image will contain information on the cross-sectional distribution of the electrical conductivity of the contents within the measurement plane. A square grid with 20 x 20 = 400 pixels represents the vessel interior cross-section. Some of these pixels will lie outside the vessel circumference as shown in Figure 7 and the image is therefore formed from the pixels inside the vessel. The circular image is constructed using 316 pixels from the 400 pixels square grid.

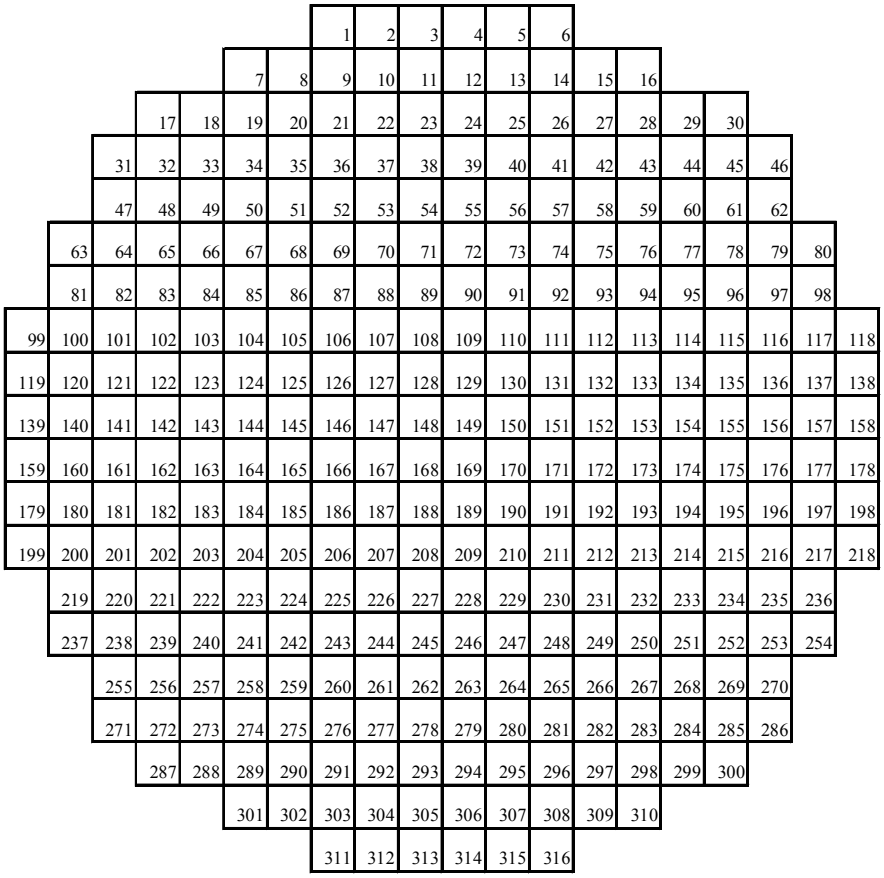

Figure 7 Image reconstruction grid**.**

It is well known that, for electrostatic fields, when current lines are encountered by an interface of different conductivities, the current lines will deflect. Therefore image reconstruction algorithms such as those for straight-ray transmission (*e.g.* X-ray, γ-ray) are inappropriate. In addition reconstruction algorithms developed for diffraction tomography such as ultrasonic and optical are unsuitable since the propagation of electromagnetic field lines and the distribution of electrostatic field lines are governed by different differential equations.

The choice of image reconstruction algorithm is a trade-off between accuracy of image and time required for reconstruction. There has been a demand for fast image reconstruction algorithms that could be used for the real time imaging of fast moving processes. Therefore, much effort has been focused on the development of image reconstruction algorithms, both non-iterative and iterative, for electrical

tomography. The P2000 system comes with a qualitative, non-iterative algorithm based on linear back-projection. An iterative algorithm based on Sensitivity Conjugate Gradient Methods has also been developed by ITS and is available as a separate software product.

The inverse problem in ERT is non-linear due to the equipotential lines curving in a way which depends on the spatial conductivity distribution. Before the inverse problem could be solved, it is necessary to solve the forward problem - forward because $\sigma(x,y)$ is known everywhere inside the sensor (*i.e.,* the task is to find the boundary voltage measurements, given the injection current I applied to the electrodes and the conductivity distribution $\sigma(x,y)$ at all points) - by the calculation of a sensitivity map which describes the behaviour of the sensor.

A. The forward problem – sensitivity map

The image reconstruction process involves determining the electrical conductivity of each pixel within the image from the set of electrical measurements. This is known as the inverse problem. However, these electrical measurements taken at the boundary of the process vessel or pipeline contain insufficient information to allow the inverse problem to be solved directly. First, it is necessary to solve the forward problem i.e. the changes in electrical measurements which will result when the electrical conductivity of one pixel only in the cross-section is changed by a known amount. This could be done in a number of ways including direct measurement although it is much more commonly performed by computation.

The model of a source free conducting inhomogeneous domain Γ, with a conductivity distribution $\sigma(x,y)$, into which a steady-state current is injected and the corresponding voltage $V(x,y)$ is measured is governed by Poisson's equation as follows:

$$\nabla\cdot\{\sigma(x,y)\nabla V(x,y)\} = 0 \qquad \text{in } \Gamma$$

For a unique solution to exist, sufficient boundary conditions must be specified. The P2000 has the following boundary conditions:

$V = 0$ at reference point (ground electrode)

$\int\sigma(\delta V/\delta n) = +I$ on source (input) electrode

$\int\sigma(\delta V/\delta n) = -I$ on sink (output) electrode

where I denotes the current applied to the electrodes and n denotes the outward unit normal to the sensor.

The finite element method (FEM) is used to solve Poisson's equation for electrical resistance tomography by reducing it to a series of simultaneous equations describing the behavior of each of the 316-pixels in Figure 8. For a 16-electrode sensor, there are 14 pairs of electrodes for current injection when the adjacent measurement strategy is used. Therefore, for the i^{th} current injection, the use of the FEM converts the solution to Poisson's equation to the following set of linear equations:

$$Av_{(i)} = b_{(i)} \qquad (i = 1, \ldots.., 14)$$

where A is the system's stiffness matrix of $N \times N$ entries and N is the number of nodes within the finite-element mesh, $v_{(i)}$ is a vector representing the N unknown nodal potentials and $b_{(i)}$ is a $N \times 1$ vector indicating the boundary conditions as described above.

ITS have computed these sensitivity maps for 8, 16 and 32 electrodes arranged around a circular section, 16 electrodes arranged around a square section and 16 electrodes arranged vertically in a line. Sensitivity maps for 8-electrode and 16-electrode circular and linear sensors are included within the software.

B. The inverse problem

The inverse problem is to determine the conductivity distribution $\sigma(x,y)$ from a finite number of boundary voltage measurements. The linear back-projection algorithm back projects the voltage measurements to conductivity values within the pixels for all possible injection and measurement combinations using the sensitivity map calculated by the FEM. The image is therefore reconstructed via a matrix/vector multiplication which could be performed rapidly on modern personal computers.

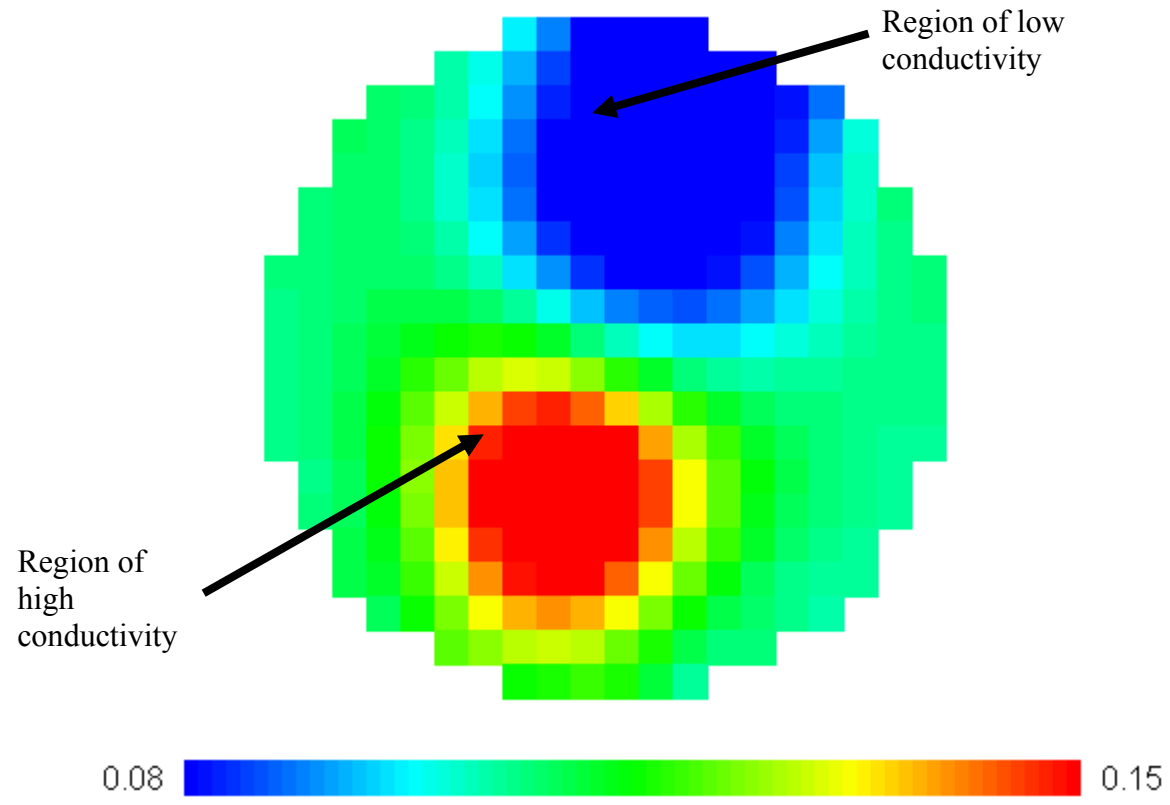

Figure 8 Tomogram showing region of high and low conductivity.

Source: ITS Tomography Toolsuite Users Manual Manchester, UK. Industrial Tomography Systems Ltd., 2004.

Figure 8 shows a typical tomographic image obtained from the linear back-projection algorithm. The image contains a region of high conductivity indicated by the color red and a region of low conductivity indicated by the color blue. The scale below the image relates color to conductivity. In this case the scale is between 0.08 and 0.15 *mS/cm*.

3.6 Replaying recorded measurement files

A. Standard Measurement files

Standard measurement files are opened for playback by selecting File/ Open and selecting the appropriate file. These measurement files have the extension .p2k. An ERT p2k typed example of the playback window, spilt in four, is shown in Figure 9. The window is split by selecting 'Window / Split'. By default the four windows display the tomographic image in the top left window, resistivity in the top right window, pixel values in the bottom left and the voltage measurements in graphical form in the bottom right window.

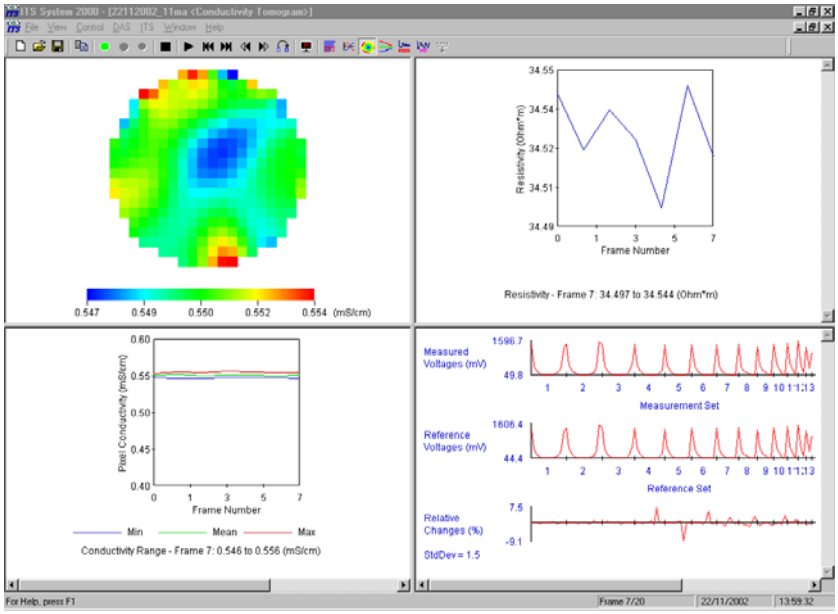

Figure 9 Playback Window.

A limited number of the basic configuration parameters could be changed during playback by selecting 'Control / Configuration'. These are: Background conductivity, Conductivity of objects, Conductivity – Concentration Conversion Expression, Sampling Time Interval, Notes. Any changes made to these parameters are temporary and if the measurement set is closed the values will remain as those used during data collection. This feature is particularly useful to view data that was collected with a large sampling time interval.

3.7 Mixing Statistics

A. Standard Mixing Index

The standard mixing index compares each pixel in a first tomogram with the same pixel in a second tomogram. The second tomogram could be from any other plane at a fixed time (measured in frame numbers) earlier than the first tomogram. Before viewing this function it is necessary to complete the Mixing Index Set-up window under Control. The mixing index σ or (ε) is calculated as follows:

$$\sigma(\%) = \left(1 - \frac{\sigma_2}{\sigma_1}\right) \times 100 \tag{13}$$

$$\sigma_1 = \sqrt{\sum_{i=1}^{N} \left(\frac{C_{1i}}{C_1} - 1\right)^2} \tag{14}$$

$$\sigma_2 = \sqrt{\sum_{i=1}^{N} \left(\frac{C_{2i}}{C_2} - 1\right)^2} \tag{15}$$

where C_{1i} = conductivity (permittivity) of pixel i in tomogram 1, C_1 = average conductivity (permittivity) of tomogram 1, C_{2i} = conductivity (permittivity) of pixel i in tomogram 2, C_2 = average conductivity (permittivity) of tomogram 2, N = the number of pixels in a tomogram.

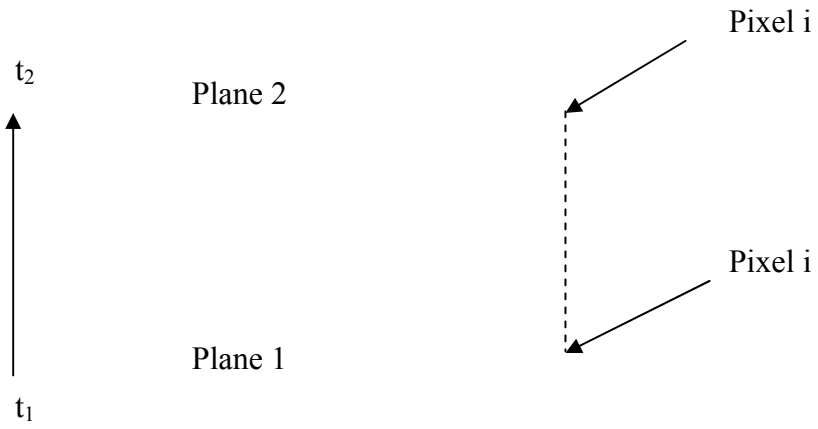

Figure 10 Standard mixing index profile.

For example,

No mixing $C_{1i} = C_{2i}$ $\sigma_1 = \sigma_2$ $\sigma = 0$

Perfect mixing $C_{2i} = C_2$ $\sigma_2 = 0$ $\sigma = 100$ or -100

B. Heterogeneity Index for pixel-based Tomograms (HIT) Statics

Tomographic images reveal the conductivity (permittivity) distribution across the measurement plane from which the distribution of components could be inferred. Therefore, the image provides visual evidence on the heterogeneity or otherwise of the image. The HIT statistic has been specifically designed for analysis of tomographic images and could be regarded as quantification of heterogeneity. It is investigated with reference to a mesh (or grouping of pixels). The selection of available regionisation schemes for circular and linear sensors is shown in Appendix A. The mesh is calculated to match the sensor geometry. The pixel values (conductivity values) are first ranked, so creating an index independent of scaling. An important consequence of using ranks rather than the individual pixel values is that the ranks are independent of the relative scale of the tomography image. The configuration of these ranked values within the image is utilized to derive the HIT statistic.

Homogenous flows contain well-mixed components throughout the cross-section under interrogation whereas heterogeneous flows contain regions of differing component concentration. Thus for homogenous flows pixel ranks will be uniformly distributed throughout the cross-section and for heterogeneous flows low ranks will dominate in some zones and high ranks will dominate in others. The HIT statistic has a small value when the flow through the sensor is homogeneous and increases for turbulent flows producing a heterogeneous cross-section.

It is possible to experiment with different mesh configurations and different numbers of zones to investigate the patterns within tomographic images. The selection of different meshes is dependent on the system of interest.

3.8 Concentration

These features convert conductivity data and the permittivity data to concentration. The software allows the use of three conductivity-concentration models for ERT data. These are:

A. Non-conductive phase

This calculates the concentration of a dispersed phase in a continuous background by using the Maxwell equation.

$$\alpha = \frac{2\sigma_1 + \sigma_2 - 2\sigma_{mc} - \frac{\sigma_{mc}\sigma_2}{\sigma_1}}{\sigma_{mc} - \frac{\sigma_2}{\sigma_1}\sigma_{mc} + 2(\sigma_1 - \sigma_2)} \tag{16}$$

where α is the volume fraction of the dispersed material; σ_1 is the conductivity of the continuous phase, *mS/cm*; σ_2 is the conductivity of the dispersed phase, *mS/cm*; σ_{mc} is the reconstructed measured conductivity, *mS/cm.*

4. Basics of Non-ideal Reactors (Fogler, 1953 & Levenspiel, 1999)

Generally, there are two types of flow patterns; there are plug flow and mixed flow. The flow behaviors of the two patterns are very different due to the size of reactor and distribution of products. In most cases, designing equipment to approach one or the other was the popular because one or the other often optimum no matter what there are designed for and these two patterns are simple to treat. However, real equipment always deviates from these ideals. There are three interrelated factors that make up the contacting or flow pattern consist of RTD or residence time distribution of material which is flowing through the reactor, the state of aggregation of flowing material and the earliness and lateness of mixing of material in the reactor. This work focused on the RTD. Then the detail of the RTD is as follows:

4.1 The residence time distribution, RTD

The residence time distribution (RTD) of a chemical reactor is a probability distribution function that describes the amount of time a fluid element could spend inside the reactor. Chemical engineers use the RTD to characterize the mixing and flow within reactors and to compare the behavior of real reactors to their ideal models. This is useful, not only for troubleshooting existing reactors, but also in estimating the yield of a given reaction and designing future reactors (MacMullin and Weber, 1935). The distribution of residence times is represented by an exit age distribution, $E(t)$, or the residence time distribution RTD of fluid, and Figure 11 shows this. It is convenient to represent the RTD in such a way that the area under the curve is unity. The function $E(t)$ has the units of time^{-1} and is defined such that

$$\int_0^\infty E(t)dt = 1 \tag{17}$$

the fraction of the fluid that spends a given duration, t inside the reactor is given by the value of $E(t)dt$. The fraction of the fluid that leaves the reactor with an age less than t_1 is

$$\int_0^{t_1} E(t)dt \tag{18}$$

The fraction of the fluid that leaves the reactor with an age greater that t_1 is

$$\int_{t_1}^{\infty} E(t)dt = 1 - \int_0^{t_1} E(t)dt \tag{19}$$

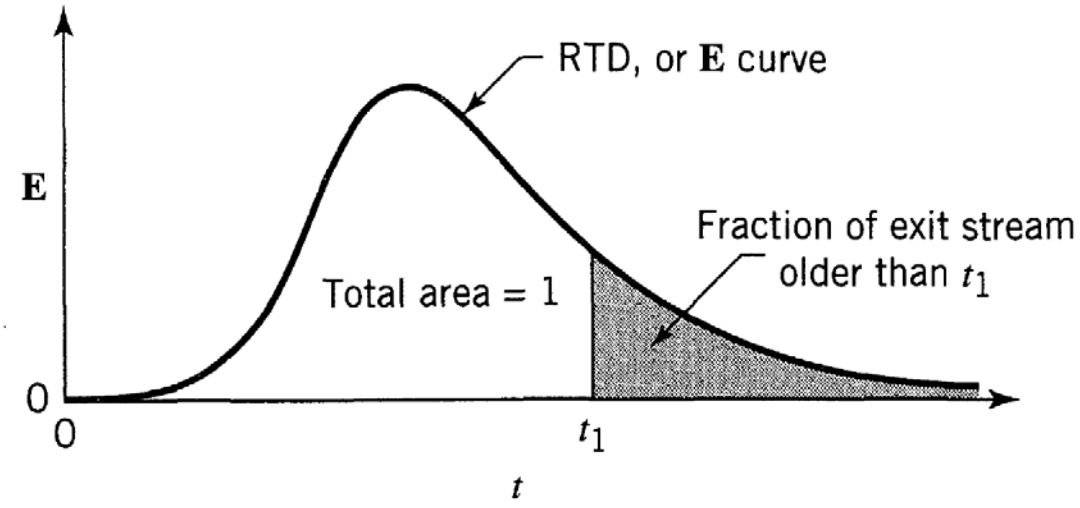

Figure 11 The exit age distribution curve *E* for fluid flowing through a vessel; also called the residence time distribution, or RTD.

One restriction on the *E-curve* that is the fluid only enters and only leaves the vessel one time. This means that there should be no flow or diffusion or upflow eddies at the entrance or at the vessel exit. This called the closed vessel boundary condition. Where elements of fluid can cross the vessel boundary more than one time could be called the open vessel boundary condition.

4.2 Tracer

A tracer is an identifiable substance that could be followed through the course of a process providing information on the pattern of events in the process or on the redistribution of the parts or elements involved. A tracer is a simulator. It must be similar in behavior to the substance which it has to trace, yet it must be sufficiently different to be identifiable. These are two contradictory conditions. The selection of a tracer is thus a search for a compromise. Tracers are often used in the oil industry to estimate residual oil saturation and volumetric sweep efficiency. In drilling, tracers are used to identify lost circulation zones. In hydraulic fracturing, tracers provide information on the location and orientation of fractures. During a multiple string well completion, tracers are used for orientation and depth correlation of perforators. Tracers are used in the identification of directional flow trends and delineation of flow barriers such as faults.

The use of tracers throughout the industry is diverse and widespread. In the management of geothermal reservoirs, tracers have become an important tool. They have provided valuable insight into the problem of short circuiting of waste water between reinjection and production wells. Tracer tests provide a method of evaluating the fractured nature of the system and thus the magnitude of the short circuiting problem.

In particular, the degradation of commonly used tracer materials as they pass through typical rock types at high temperatures is examined in a quantitative way. Tracers could be divided in to two general groups: (1) chemical tracers; and (2) radioactive tracers. Chemical tracers are those which could be identified and measured quantitatively by general an analytical method such as conductivity, refractive index and elemental spectrometry. Radioactive tracers are detected by their emitted radiation, usually beta or gamma. This work was concerned exclusively with the use of chemical tracers.

A. Selection of tracer

Accurate determination of RTD in a vessel requires proper selection and introduction of a tracer. Characteristics and examples of tracers will be considered. Ideally, a tracer should have the following characteristics:

1. The tracer should be stable and conserved, so that it could be accounted for by a material balance relating the response to the input; if the tracer decays (*e.g.,* a radio-labeled tracer), its half-life should be such that $t_{1/2}$ (tracer) > $25\bar{t}$ (fluid).

2. The analysis for tracer should be convenient, sensitive, and reproducible.

3. The tracer should be inexpensive and easy to handle; this is particularly important for a step input, in which relatively large quantities of tracer may be required

4. The tracer should not be adsorbed on or react with the surface of the vessel. Alternatively, the tracer should be chemically and physically similar to the fluid flowing, so that any adsorption (or diffusion) behavior may be replicated.

Examples of tracers are:

a). Gas-phase tracers such as He, Ne, and Ar used with thermal conductivity detectors.

b). pH indicators such as phenol red and methylene blue.

c). Electrolytes such as K^+ and Na^+ used with electrical conductivity detectors or specific-ion electrodes.

d). Dyes (*e.g.,* India ink) used with color intensity.

e). Radioactive isotopes such as 3H, 14C, 18O, 51 Cr-labeled red-blood cells used to investigated hepatic blood flow; isotopes of iodine, thallium, and technetium used to investigate cardiac blood flow.

f). Stereoisomers and structural analogs used for diffusion-limited processes (*e.g., f* vs *d*-glucose in biological systems).

B. Character of injecting tracer

Any material that could be detected and which does not disturb the flow pattern in the vessel could be used as tracer, and any type of input signal as shown in Figures 12-15 such as a random signal, a periodic signal, a step signal, or a pulse signal, etc. may be used.

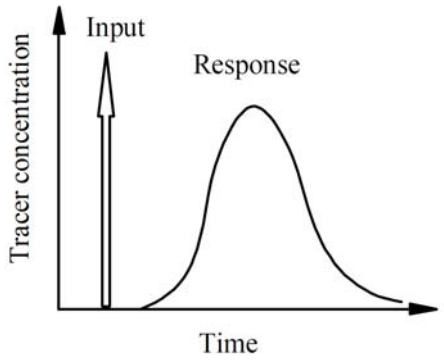

Figure 12 Commonly used stimulus-responses techniques in type of Pulse input signal.

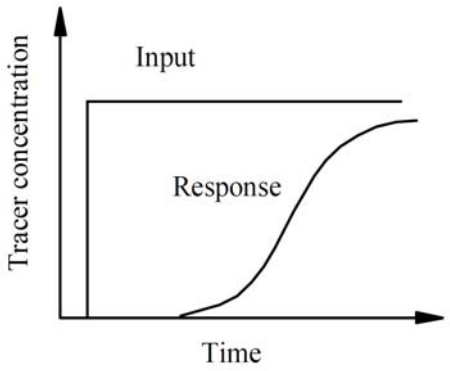

Figure 13 Commonly used stimulus-responses techniques type of Step input signal.

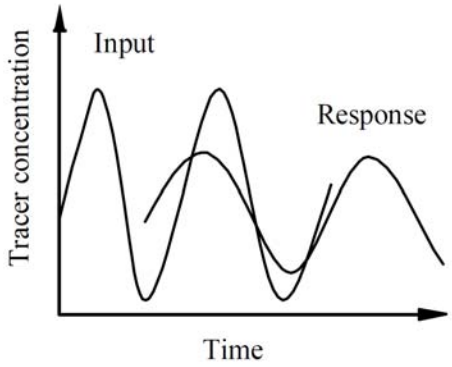

Figure 14 Commonly used stimulus-responses techniques type of Cyclic (or Periodic) input signal.

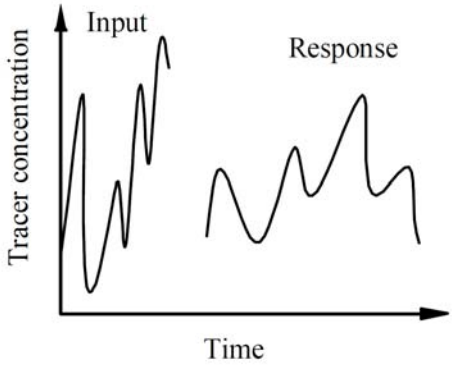

Figure 15 Commonly used stimulus-responses techniques type of Random input signal.

C. Experimental Methods (Nonchemical) for finding *E*

Residence time distributions are measured by introducing a non-reactive tracer into the system at the inlet. So, the simplest and most direct way of finding the *E-curve* uses a physical or non-reactive tracer. The concentration of the tracer is changed according to a known function and the response is found by measuring the concentration of the tracer at the out let. The selected tracer should not modify the physical characteristics of the fluid (equal density, equal viscosity) and the introduction of the tracer should not modify the hydrodynamic conditions. In general, the change in tracer concentration will either be a pulse or a step.

1. Pulse Input

In a pulse input, an amount of tracer is suddenly injected in one shot into the feed stream entering the reactor in as short time as possible. This method required the introduction of a very small volume of concentrated tracer at the inlet of the tracer. Although an infinitely short injection could not be produced, it could be made much smaller than the mean residence time of the vessel. The outlet concentration is then measured as a function of time. The effluent concentration-time curve is referred to as the *C-curve* in the RTD analysis. If a mass of tracer, M (*kg* or *moles*), is introduced into a vessel of volume V (m^3) through which flow v m^3/s of fluid and an expected residence time of τ, the resulting curve of $C_{pulse}(t)$ could be transformed into a dimensionless residence time distribution curve. From the material balance for the vessel could be found as the following relation:

(Area under the C_{pulse} curve): $$A = \int_0^\infty C dt \cong \sum_i C_i \Delta t_i = \frac{M}{v} \qquad \left[\frac{kg \cdot s}{m^3}\right] \tag{20}$$

(Mean of the C_{pulse} curve): $$\bar{t} = \frac{\int_0^\infty tCdt}{\int_0^\infty Cdt} \cong \frac{\sum_i t_i C_i \Delta t_i}{\sum_i C_i \Delta t_i} = \frac{V}{v} \qquad [s] \tag{21}$$

all this is shown in Figure 16.

To find the *E-curve* from the C_{pulse} curve simply change the concentration scale such that the area under the curve is unity. Thus, simply divide the concentration reading by M / v, as shown in Figure 17.

$$E(t) = \frac{C_{pulse}(t)}{\int_0^\infty C(t)dt} \tag{22}$$

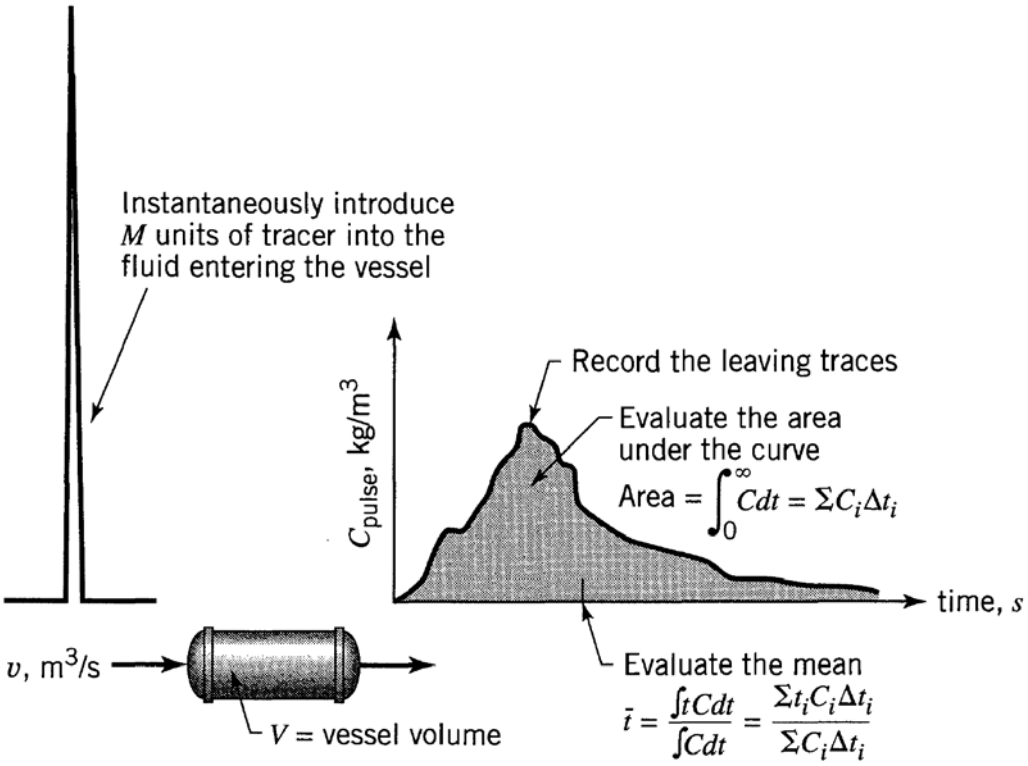

Figure 16 The useful information obtainable from the pulse tracer experiment.

The integral in the denominator is the area under the *C-curve*, Equation 22 could be rearranged into

$$E(t) = \frac{C_{pulse}(t)}{M / v} \tag{23}$$

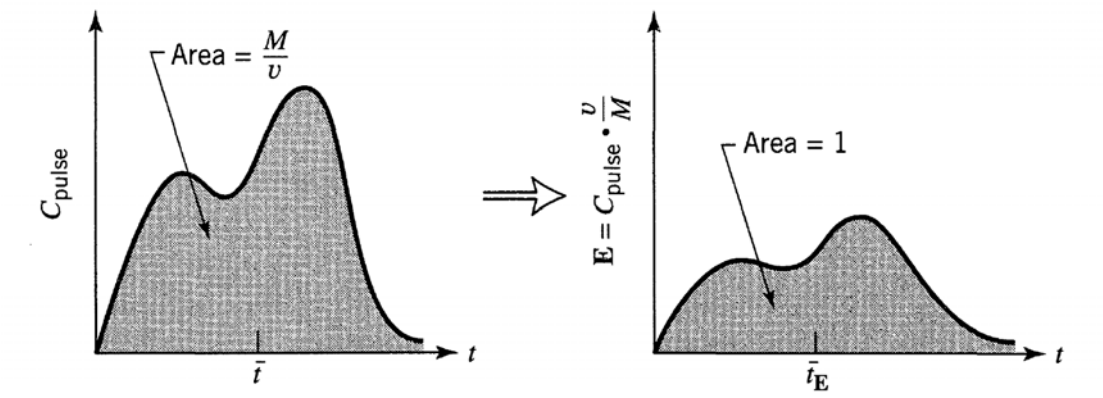

Figure 17 Transforming an experimental C_{pulse} curve into a *E-curve*.

Another RTD function is E_θ. Here time is measured in terms of mean residence time $\theta = t/\bar{t}$. Thus

$$E_\theta = \bar{t}E = \frac{V}{v} \cdot \frac{C_{pulse}}{M/v} = \frac{V}{M} C_{pulse} \tag{24}$$

E_θ is a useful measure when dealing with flow models. Figure 18 shows how to transform E to E_θ. One final reminder, the relationship between C_{pulse} and the *E-curve* only holds exactly for vessels with closed boundary conditions.

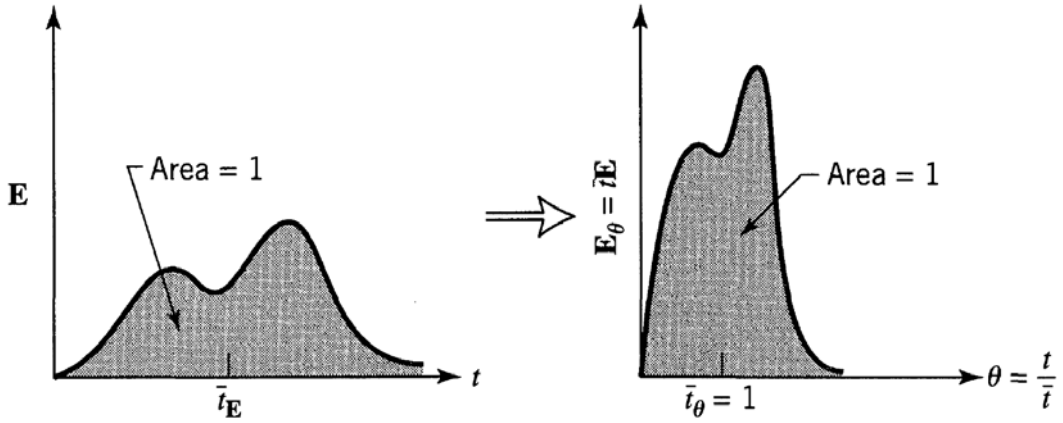

Figure 18 Transforming an *E-curve* into an $E_\theta - curve$.

4.3 Models for non-ideal flow

Many types of models could be used to characterize non-ideal flow presented within real bioreactor. One-parameter models such as the dispersion model and the tanks-in-series model are widely used in bioreaction engineering. The dispersion model is mainly used to design medium continuous sterilization processes or some enzyme catalytic reactions carried out within tubular reactors. For two-parameter model of CSTR with bypassing and dead space, by which some large scale stirred fermenters could be described properly.

A. The dispersion model

The dispersion model is also used to describe non-ideal tubular reactors. In this model, there is an axial dispersion of the material, which is governed by an analogy to Fick's law of diffusion, superimposed on the flow as shown in Figure 19. Some molecules will diffuse forward ahead of molar average velocity while others will lag behind.

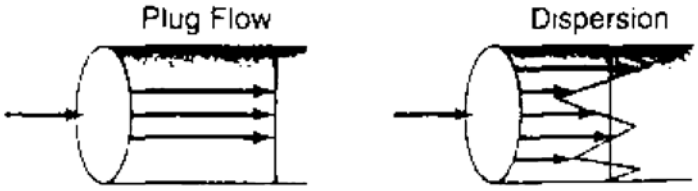

Figure 19 Concentration profiles (a) without and (b) with dispersion.

The dispersion coefficient D (m^2/s) represents this spreading process. Thus, large D means rapid spreading of the tracer curve, small D means slow spreading and $D = 0$ means no spreading, hence plug flow. Also (D/uL) is the dimensionless group characterizing the spread in the whole vessel, called the vessel dispersion number, and is the parameter that measures the extent of axial dispersion. Thus $(D/uL) \rightarrow 0$ is meaning of negligible dispersion, hence plug flow and $(D/uL) \rightarrow \infty$ is meaning of large dispersion, hence mixed flow. This model usually

represents quite satisfactorily flow that deviates not too greatly from plug flow, thus real packed beds, tubes (long ones if flow is streamline), laminar flow in long tubes, turbulent flow in pipes and shaft kilns.

Evaluate D or *(D/uL)* by recording the shape of the tracer curve as it passes the exit of the vessel. In particular, measured as *t* is time of passage, or when the curve passes by the exit σ^2 is variance, or a measure of the spread of the curve. These measures, $\bar{t}$ and σ^2, are directly linked by theory to D and *(D/uL)*. The mean, for continuous or discrete data, is defined as

$$\bar{t} = \frac{\int_0^\infty tCdt}{\int_0^\infty Cdt} = \frac{\Sigma t_i C_i \Delta t_i}{\Sigma C_i \Delta t_i} \tag{25}$$

The variance is defined as

$$\sigma^2 = \frac{\int_0^\infty \left(t_i - \bar{t}\right)^2 Cdt}{\int_0^\infty Cdt} = \frac{\int_0^\infty t^2 Cdt}{\int_0^\infty Cdt} - \bar{t}^2 \tag{26}$$

or in discrete form

$$\sigma^2 \cong \frac{\Sigma\left(t_i - \bar{t}\right)^2 C_i \Delta t_i}{\Sigma C_i \Delta t_i} = \frac{\Sigma t_i^2 C_i \Delta t_i}{\Sigma C_i \Delta t_i} - \bar{t}^2 \tag{27}$$

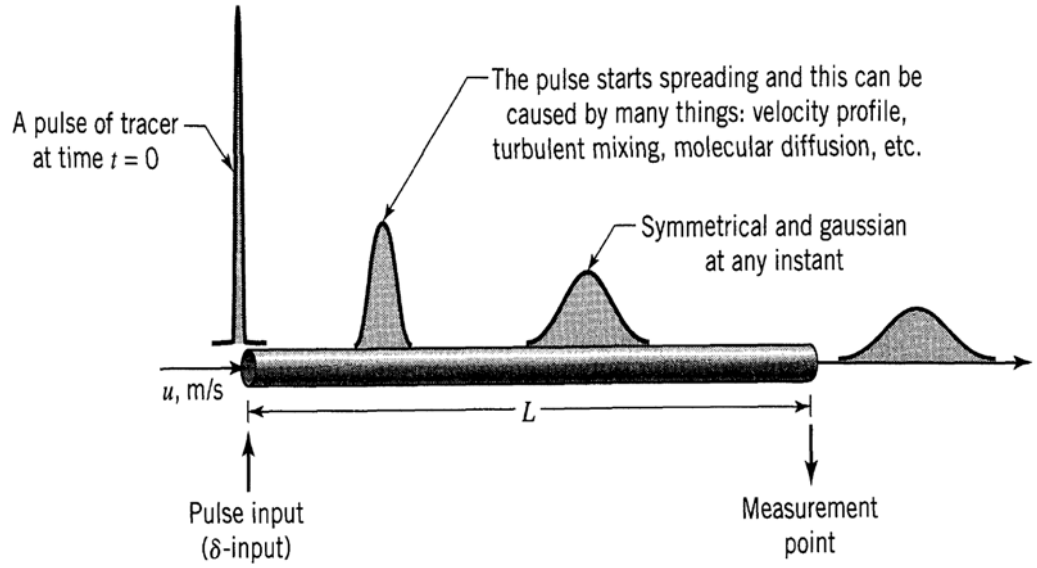

Figure 20 The spreading of tracer according to the dispersion model.

The dispersion model was fitted for small extents of dispersion, $(D/uL) < 0.01$. The spreading tracer curve does not significantly change in shape as it passes the measuring point (during the time it is being measured) as shown in Figure 20. The equations representing this family are in Equations 28-31.

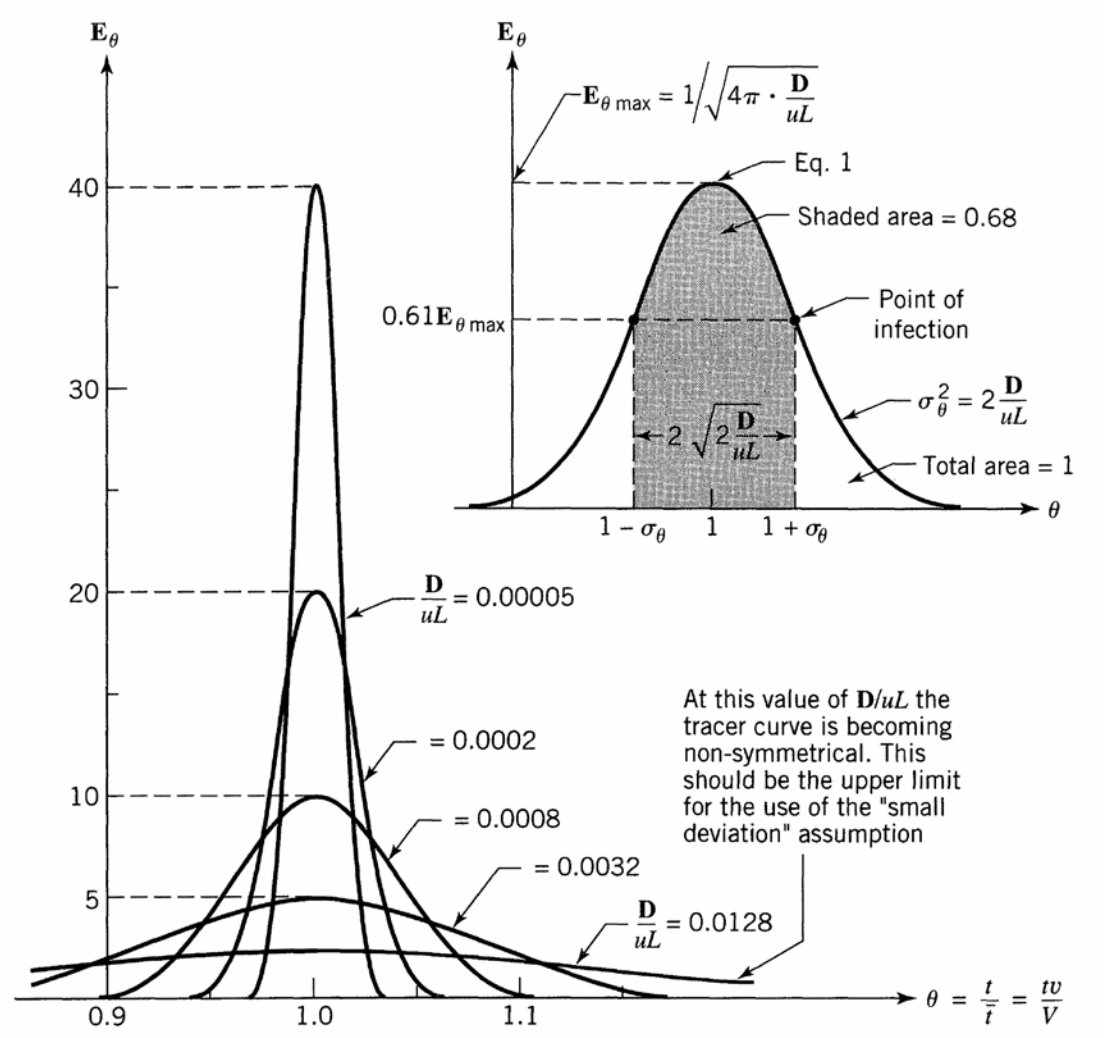

Figure 21 Relationship between D/uL and the dimensionless E_θ curve for small extents of dispersion.

$$E_\theta = \bar{t} \cdot E = \frac{1}{\sqrt{4\pi(D/uL)}} \exp\left[-\frac{(1-\theta)^2}{4(D/uL)}\right] \tag{28}$$

$$E = \sqrt{\frac{u^3}{4\pi DL}} \exp\left[-\frac{(L-ut)^2}{4DL/u}\right] \tag{29}$$

$$\bar{t}_E = \frac{V}{v} = \frac{L}{u} \qquad \text{or} \qquad \bar{\theta}_E = 1 \tag{30}$$

$$\sigma_\theta^2 = \frac{\sigma_t^2}{\bar{t}^2} = 2\left(\frac{D}{uL}\right) \qquad \text{or} \qquad \sigma^2 = 2\left(\frac{DL}{u^3}\right) \tag{31}$$

If large deviation from plug flow, $(D/uL) > 0.01$. The pulse response is broad and it passes the measurement point slowly enough that it changes shape. This leads to four combinations of boundary conditions, closed-closed, open-open, and mixed. Figure 22 illustrates the closed and open extremes, whose RTD curves are designed as E_{cc} and E_{oo}.

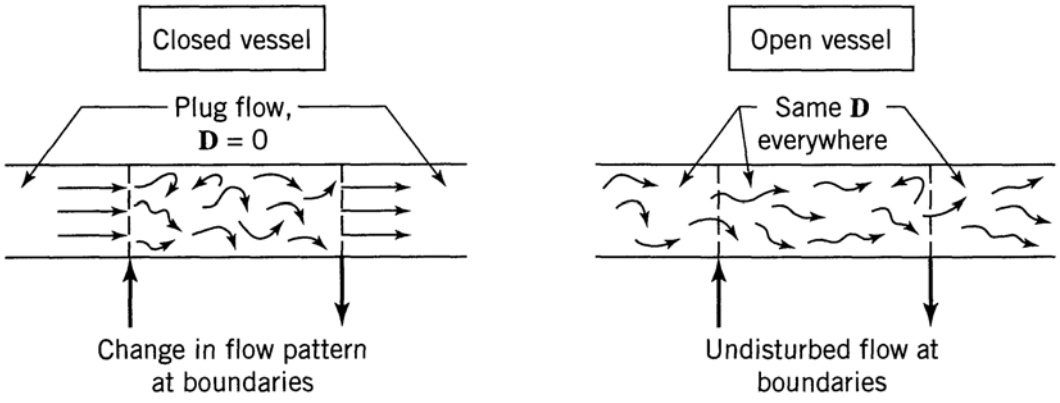

Figure 22 Various boundary conditions used with the dispersion model.

Closed vessel, could be constructed by numerical methods, see Figure 23 or evaluate its mean and variance exactly. Thus

$$\bar{t}_E = \bar{t} = \frac{V}{v} \qquad \text{or} \qquad \bar{\theta}_E = \frac{\bar{t}_E}{\bar{t}} = \frac{\bar{t}_E v}{V} = 1 \tag{32}$$

$$\sigma_\theta^2 = \frac{\sigma_t^2}{\bar{t}^2} = 2\left(\frac{D}{uL}\right) - 2\left(\frac{D}{uL}\right)^2\left[1 - e^{-uL/D}\right] \tag{33}$$

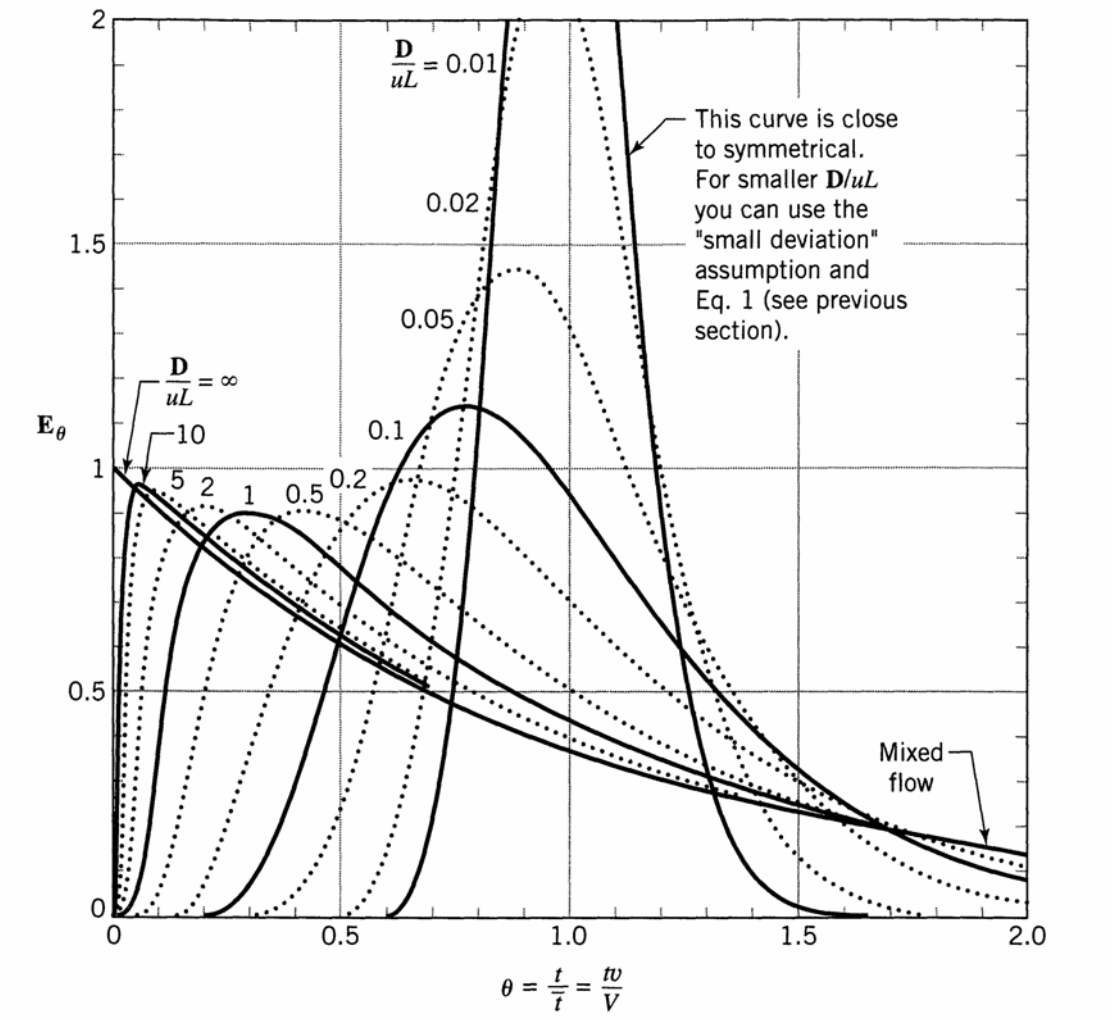

Figure 23 Tracer response curves for closed vessels and large deviations from plug flow.

Open vessel, this represents a convenient and commonly used experimental device, a section of long pipe as shown in Figure 24. The results are given by the response curves shown in Figure 25, and by following equations, first derived by Levenspiel and Smith (1957).

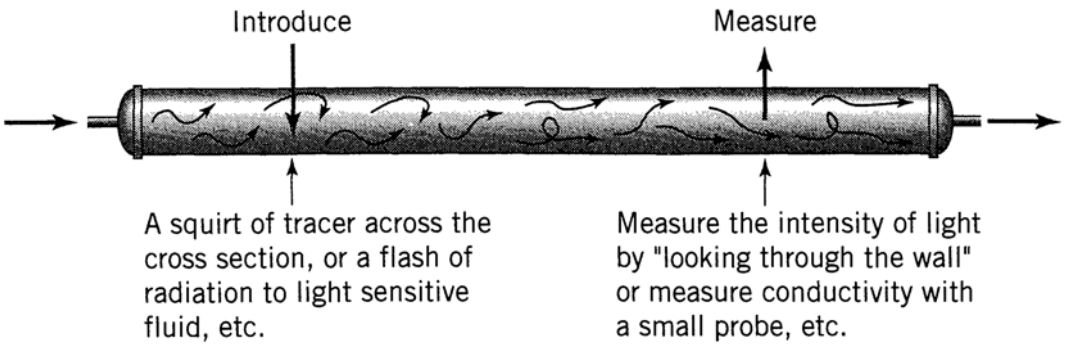

Figure 24 The open-open vessel boundary condition.

$$E_{\theta,oo} = \frac{1}{\sqrt{4\pi(D/uL)\theta}} exp\left[-\frac{(1-\theta)^2}{4\theta(D/uL)}\right] \tag{34}$$

$$E_{t,oo} = \frac{u}{\sqrt{4\pi Dt}} \exp\left[-\frac{(L-ut)^2}{4Dt}\right] \tag{35}$$

$$\overline{\theta}_{E,oo} = \frac{\bar{t}_{E,oo}}{\bar{t}} = 1 + 2\left(\frac{D}{uL}\right) \qquad \text{or} \qquad t_{E,oo} = \frac{V}{v}\left(1 + 2\frac{D}{uL}\right) \tag{36}$$

$$\sigma^2_{\theta,oo} = \frac{\sigma^2_{t,oo}}{\bar{t}^2} = 2\frac{D}{uL} + 8\left(\frac{D}{uL}\right)^2 \tag{37}$$

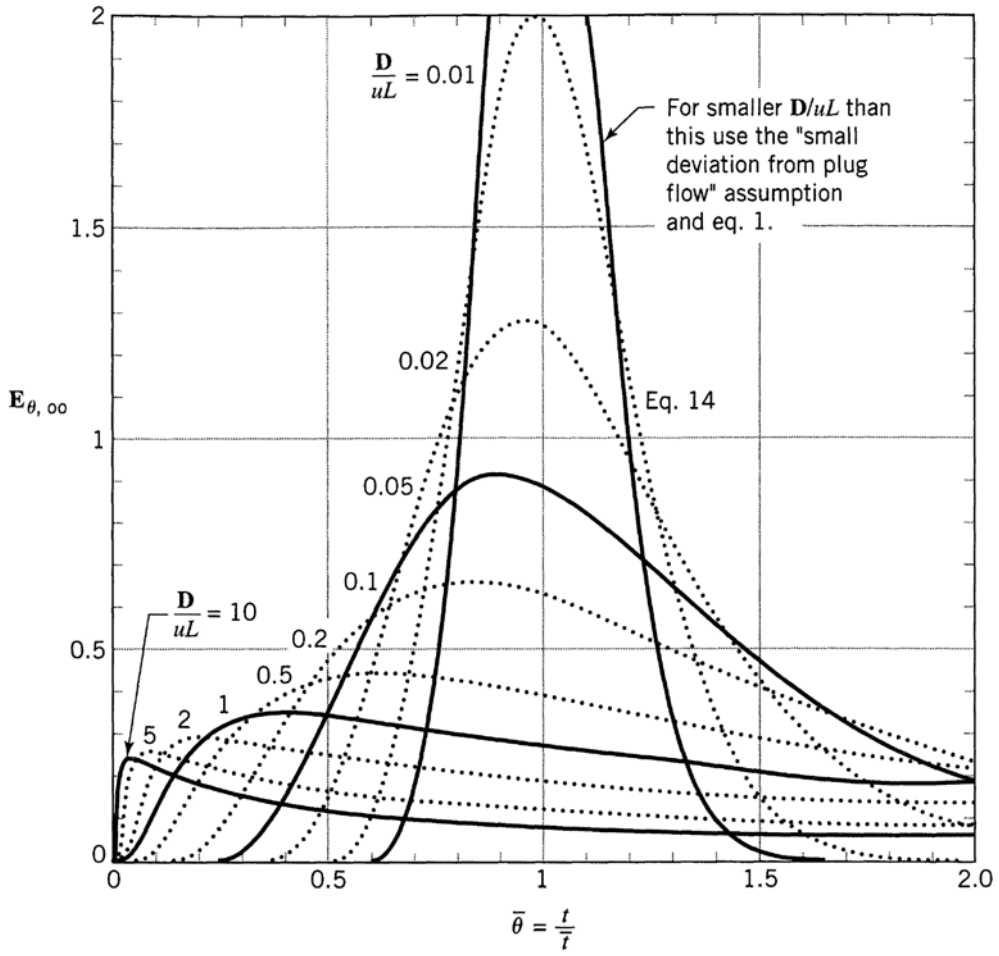

Figure 25 Tracer response curves for open vessels and large deviations from plug flow.

To find the *E-curve* from the C_{pulse} curve the concentration is simply changed such that the area under the curve is unity. Thus, the concentration is divided by area under curve ($\sum C\Delta t$). Here time is measured in terms of dimensionless time unit or mean residence time $\theta = t/\bar{t}$. Thus

$$E_\theta = \bar{t}E = \frac{\bar{t}C}{area\ under\ curve} = \frac{\bar{t}C}{\sum C\Delta t} \tag{38}$$

The relationship between C_{pulse} and the E_θ as shown in this equation (Equation 38) only holds exactly for vessels with closed boundary conditions. However, in this system the boundary conditions are opened boundary conditions. The axial dispersion model was chosen in this system by using the condition of large deviation from plug flow, $(D/uL) > 0.01$, whose RTD curves are designed as E_{oo} by the following equation, first derived by Levenspiel and Smith (1957).

$$E_{\theta,oo} = \frac{1}{\sqrt{4\pi(D/uL)\theta}} \exp\left[-\frac{(1-\theta)^2}{4\theta(D/uL)}\right] \tag{39}$$

The parameters, (D/uL) and $\bar{t}$ in Equation 39 are the unknown parameters that can be obtained by fitting the experimental E_θ curve with the axial dispersion model (Equation 39). (D/uL) and $\bar{t}$ in the Equation 39 are adjustable parameters. To evaluate (D/uL) and $\bar{t}$, the measured tracer curve has to be matched with the theoretical curve as following steps.

a). The dispersion parameter (D/uL) is firstly guessed.

b). The mean residence time, $\bar{t}$, is guessed.

c). Knowing (D/uL) and $\bar{t}$, the theoretical E_θ can be calculated by the axial dispersion model, Equation 39.

d). The calculated E_θ with the guessed $\bar{t}$ is converted to E_t by Equation 38.

e). The area under the concentration curve is assumed.

f). The calculated E_t with the guessed area under the C_t *-curve* is transformed into a concentration curve using Equation 38.

g). The area under the obtained from the concentration curve is compared with the guessed area under the curve. If they are not matched, a new area under the curve is guessed again. Then go to Step *F*. If they are matched, the corrected area under the curve will be obtained.

h). $\bar{t}$ can be obtained from the calculated concentration curve (from Step *F*) and is compared with the guessed $\bar{t}$ from Step *B*. If they are not matched, a new $\bar{t}$ is guessed again and then goes to Step *C*. If they are matched, the corrected $\bar{t}$ is obtained.

i). The calculated concentration curve from Step *F* is compared with the experimental concentration curve. If their shapes are not matched, a new value of (D/uL) is guessed. If they are matched, a corrected value of (D/uL) is obtained.

Figures 26 and 27 show the dimensionless exit age distribution $E(\theta)$-*curve* from the Equations 38 and 39 in the riser and downcomer, respectively at the superficial gas velocities in the riser of 6.14 cm/s and in the downcomer of 1.02 cm/s, respectively. In this case, $\bar{t}$ equals to 75.69 with *(D/uL)* of 1.04. It can be seen that *(D/uL)* is more than 0.01. Therefore $E(\theta)$-*curve* was implied that the fluid flow behavior in the riser large deviation from plug flow and more close to mixed flow.

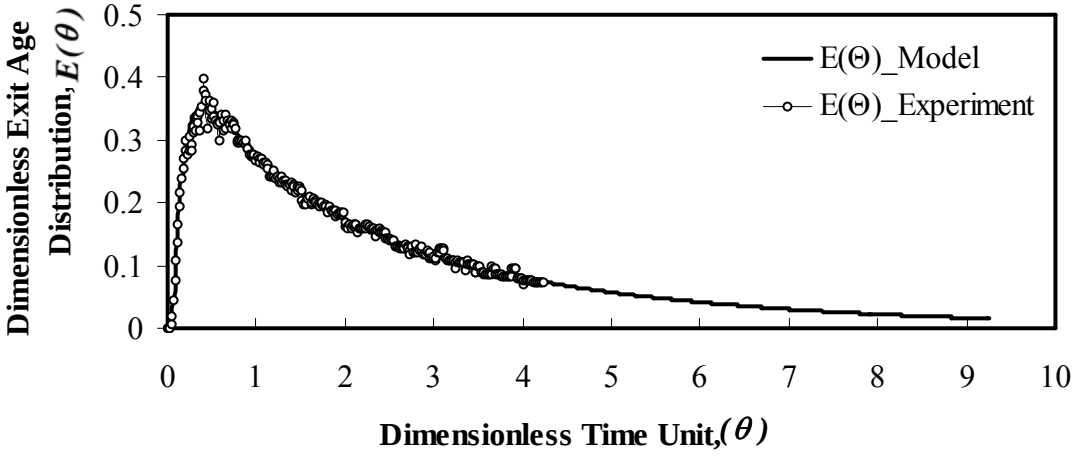

Figure 26 Comparison of the exit age distribution (RTD) based on the dimensionless time unit (θ) curves in the riser obtained from the experiments and models at the superficial gas velocities in the riser of 6.14 cm/s and in the downcomer of 1.02 cm/s.

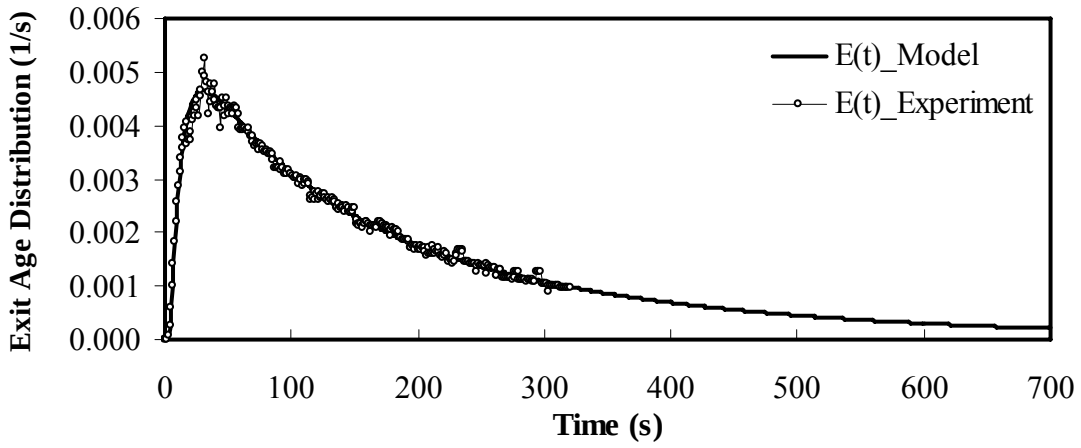

Figure 27 Comparison of exit age distribution (RTD) curve in the riser obtained from the experiments and models at the superficial gas velocities in the riser of 6.14 cm/s and in the downcomer of 1.02 cm/s.

MATERIALS AND METHODS

1. Experimental setup (ERT system)

1.1 External-loop gas lift facility

Figure 28 shows the schematic diagram of the external-loop gas lift facility used in this study. The external-loop gas lift reactor consists of three main parts: riser, downcomer and gas-liquid separator. All sections are made of transparent Perspex acrylic. The riser and downcomer with an inner diameter is 14.4 cm. A height in riser and downcomer are 154 cm and 179 cm, respectively and, the last part a gas-liquid separator with an inner diameter of 26.9 cm. The gas-liquid separator is located at the top of the riser to separate out the gas from the gas and liquid flow. The two gas spargers were located at the bottom of both columns. The gas spargers were perforated plates with the diameter of 0.1 cm. The flow rates of inlet gases for the riser and downcomer were measured by two flow meters (Cole Parmer) that connect to the air compressor (1 hp). The hydrodynamics in an external-loop gas lift reactor was studied. The experiments are divided into 3 parts. The local gas holdup distributions in the riser and downcomer in an external-loop gas lift reactor were measured by ERT. In addition, the diameters of bubbles in the reactor were investigated by a camera. Finally, the residence time distribution (RTD) was evaluated by using a stimulus-response tracer technique. All experiments were carried out at room temperature and atmospheric pressure. Air and tap water were used as the gas, liquid phases, respectively because air and tap water is not expensive. The total volume of the liquid phase was kept 73 *L* at the beginning. Calibration measurements both of systems (ERT system and stimulus-response tracer technique) were required before experimental measurements in the reactor were carried out. The superficial gas velocities in the riser are 1.02-2.05 cm/s, 4.09-6.14 cm/s and 8.19-10.23 cm/s in the bubble, transient and turbulent regimes, respectively. The superficial gas velocities in the downcomer are 0-3.07 cm/s.

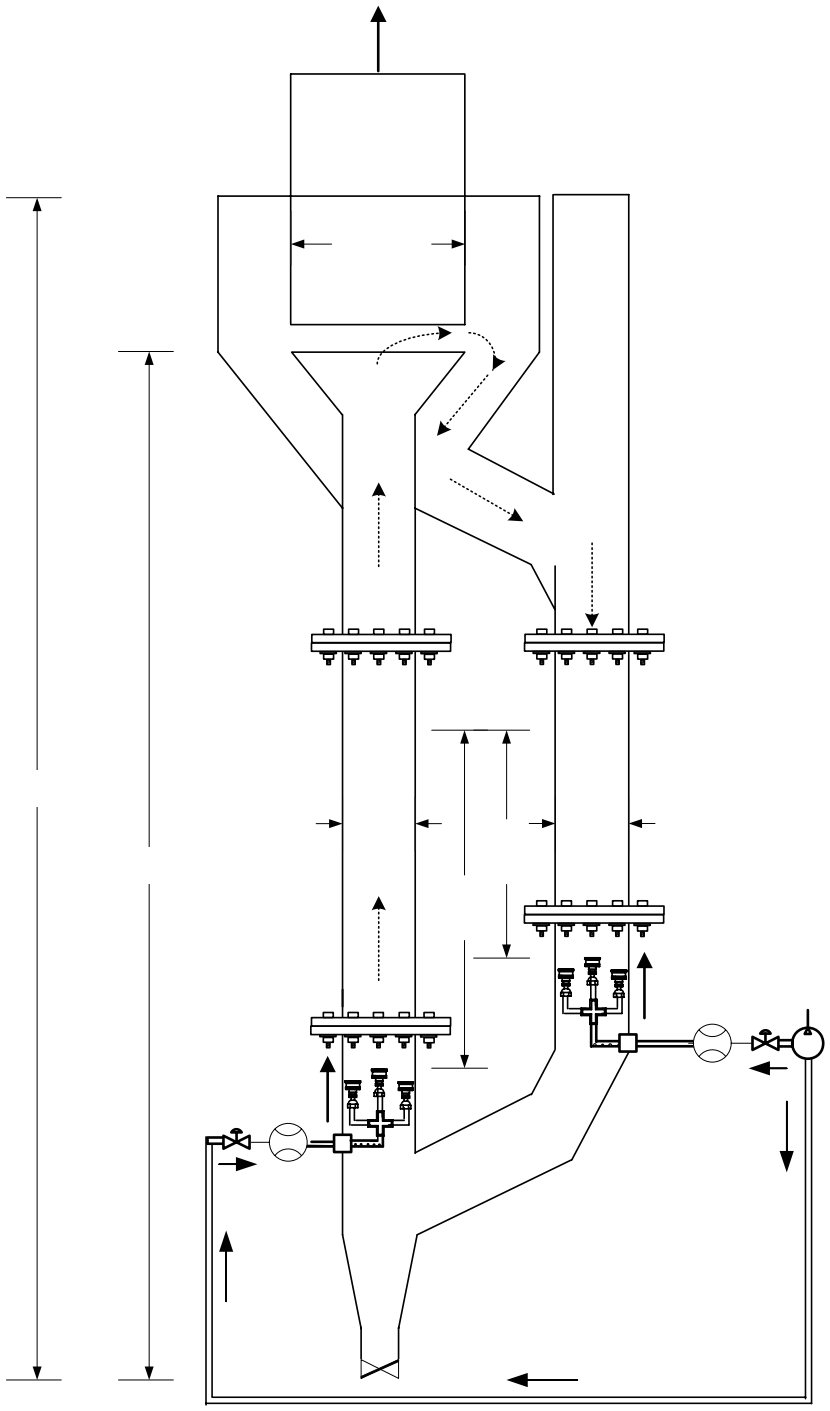

Figure 28 Schematic diagram of the external-loop gas lift circulating facility.

These range of the superficial gas velocities for studying of the hydrodynamic behavior in the range of bubbling regime to the turbulent regime.

1.2 Electrical Resistance Tomography (ERT) facility

A. ERT system

An electrical resistance tomography (ERT) system is one of non-invasive techniques that produce a time-averaged cross-sectional image showing the distribution of electrical conductivity of the contents of the fluids in the vessel from measurements taken at the boundary of the vessel. Multiple electrodes are arranged around the boundary of the vessel at fixed locations in such a way that they make electrical contact with the fluid inside the vessel but do not disturb the flow or movement of materials. The electrodes are connected to the data acquisition system by co-axial cables. The data acquisition system (DAS) is responsible for obtaining the quantitative data describing the state of the conductivity distributions inside the pipeline. The data must be collected quickly and accurately in order to track small changes in measurement of the true conductivity distributions.

The conductivity data obtained by ERT were converted to gas holdup. The gas holdup or dispersed phase gas in continuous background water can be calculated by the Maxwell's equation (Jin *et al.,* 2007) as follows:

$$\alpha = \frac{2\sigma_1 + \sigma_2 - 2\sigma_{mc} - \frac{\sigma_{mc}\sigma_2}{\sigma_1}}{\sigma_{mc} - \frac{\sigma_2}{\sigma_1}\sigma_{mc} + 2(\sigma_1 - \sigma_2)} \tag{40}$$

where α is the volume fraction of the dispersed material; σ_1 is the conductivity of the continuous phase, mS/cm; σ_2 is the conductivity of the dispersed phase, mS/cm; σ_{mc} is the reconstructed measured conductivity, mS/cm.

B. ERT measurement

Figure 29 shows the schematic diagram of the measurement principle in the ERT system. The system comprises an ERT sensor, a data acquisition unit plus a personal computer for data storage, processing and display. The electrical-model tomography system connecting with the personal computer, and ERT sensor mode was required in this system. The ERT system used in the present study was manufactured by ITS. In this work, two sets of signal cables (16 cables plus 1 ground cable per set) were used. The inner diameter of the sensor section is built equal to the inner diameter of the riser. Thus the sensors can be lined up with the riser. In the part of downcomer, the system is the same in riser. Two rings of ERT sensor, each ring composed of 16 rectangular electrodes, were mounted on the inner wall of the columns. The electrodes were made of stainless steel with a contact area of 12 mm *(w)* by 12 mm *(h)*. The ERT sensor rings of riser and downcomer were located 43 cm and 28 cm above the gas sparger, respectively. The details of the column configuration are shown in Figure 30.

The ERT sensor supports two planes (plane1&2) of electrodes. Sixteen electrodes equally spaced on the two planes provide the voltage signals for reconstructing phase distributions. The voltages measured at the periphery of the sensor were reconstructed to a tomogram representing the electrical conductivity of material flowing within the sensor. The adjacent electrode pair strategy was adopted using 8 mA injection current at 10 kHz for parameter measurement. Data collection rates for plane 1 and plane 2 were 100 ms per frame. 250 images per experiment were acquired.

Calibration measurements with tap water in both of the riser and downcomer columns were required before experimental measurements in the reactor were carried out. The flow rates of inlet gases for the riser and downcomer were measured by two flow meters. The sets of the superficial gas velocity of the system as below:

Table 3 The superficial gas velocities both of columns.

Downcomer *(L/min)*	Riser *(L/min)*
0	5, 10, 20, 40, 60, 80, 100
1	20, 40, 60, 80, 100
20	40, 60, 80,100
30	40, 60, 80,100

The data were imported from ITS Tomography program. The results comprise of time-averaged cross-sectional local gas holdup distribution images, radial gas holdup profiles and mixing index distributions.

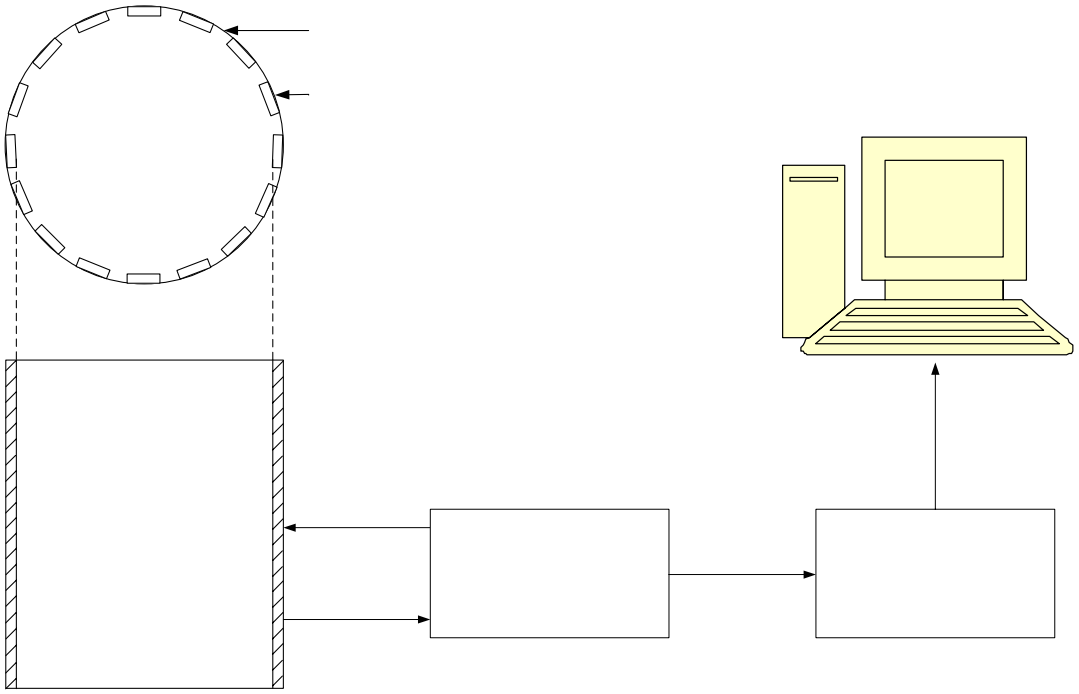

Figure 29 Schematic diagram of the measurement principle in the ERT system.

Figure 30 Schematic diagram of the ERT sensors.

2. Experimental setup (RTD system)

2.1 A stimulus-response tracer technique facility

A. A stimulus-response tracer technique

A stimulus-response technique was used for measuring residence time distributions of the liquid phase. The evaluation of experiments depended on the type of stimulus input signals and kinds of tracer. This system uses stimulus-responses techniques in type of pulse input signal with chemical tracer (KCl) 3 ml. Potassium chloride is the chemical tracer that can easy to dissociate in the water, and the volume of 3 ml is not disturbing the flow inside the reactor. Two sensor probes of the riser and the downcomer columns were located 73 cm and 33 cm above the gas sparger, respectively. The axial height between the injecting point and sensor probe of the riser is 53 cm. In a pulse input, an amount of tracer is suddenly injected in one shot into the feed stream entering the reactor in as short of time as possible. This method

required the introduction of a very small volume of concentrated tracer at the inlet of the tracer. The outlet concentration is then measured as a function of time. The concentration-time curve is referred to as the *C-curve* in the residence time distribution analysis. Therefore, the simplest and most direct way to finding $E(t)-curve$ or $E(\theta)-curve$ uses a physical or non-reactive tracer. The conductivity of the tracer in the reactor is changed according to a known function of the concentration. The selected tracer should not modify the physical characteristics of the fluid (equal density, equal viscosity).

One type of model that is used to characterize non-ideal flow in the reactor is the dispersion model. The dispersion model is mainly used to design medium continuous sterilization processes or some enzyme catalytic reactions carried out within tubular reactors (Levenspiel, 1999). Therefore, this model was chosen in this study. The dispersion coefficient D (m^2/s) represents this spreading process. Thus, large D means rapid spreading of the tracer curve, small D means slow spreading and D =0 means no spreading, hence plug flow. Also, *(D/uL)* is the dimensionless group characterizing the spread in the whole vessel, called the vessel dispersion number, and is the parameter that measures the extent of axial dispersion. Thus, $(D/uL) \rightarrow 0$ is meaning of negligible dispersion, hence plug flow and $(D/uL) \rightarrow \infty$ is meaning of large dispersion, hence mixed flow.

B. RTD measurement

Figure 31 shows the schematic diagram of the measurement principle of a stimulus-response tracer technique. The system is comprised of two sensor probes, transmitter, analog to digital unit, a data acquisition unit (USB 6008), plus a personal computer for data storage, processing and display. Two probes were made of small stainless steel tubes (outer diameter of 2 mm) as illustrated in Figure 32. Two cables inside of the tube were made of copper, and head of the sensor probe was emerged at the distance of 1 cm. Figure 33 shows the circuit board connecting to the data acquisition unit.

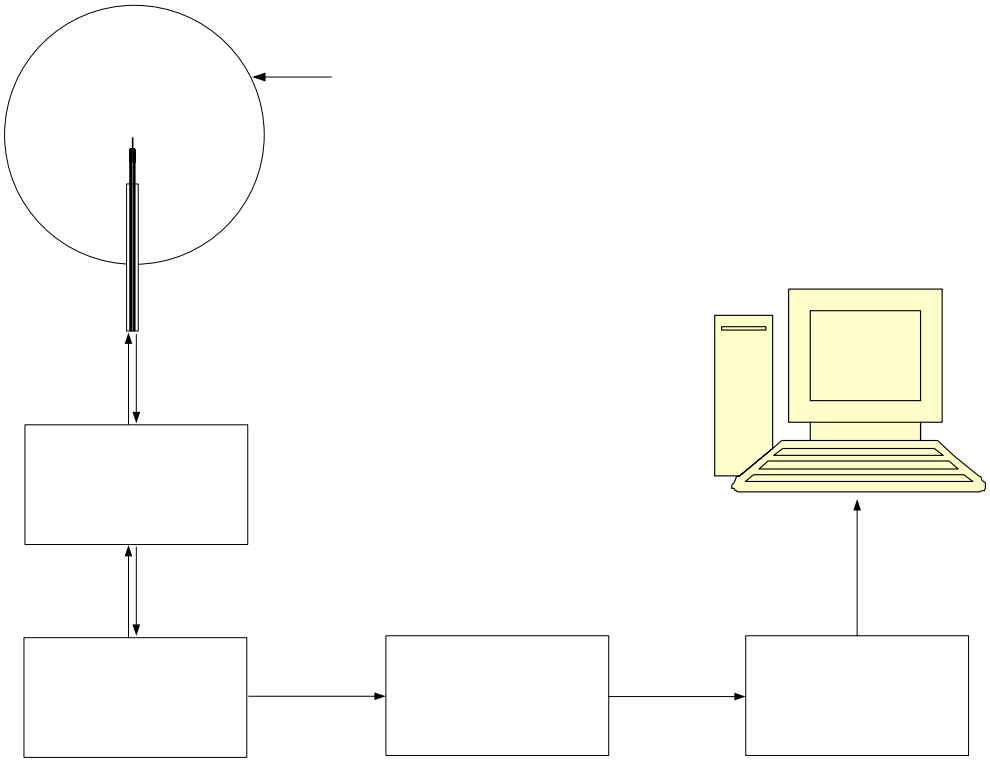

Figure 31 Schematic diagram of the measurement principle of a stimulus-response tracer technique.

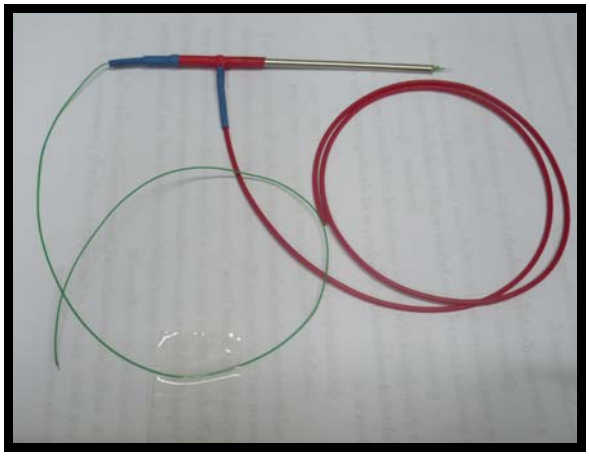

Figure 32 Sensor probe for measuring the conductivity value of solution in the reactor.

Alternating Current Signal

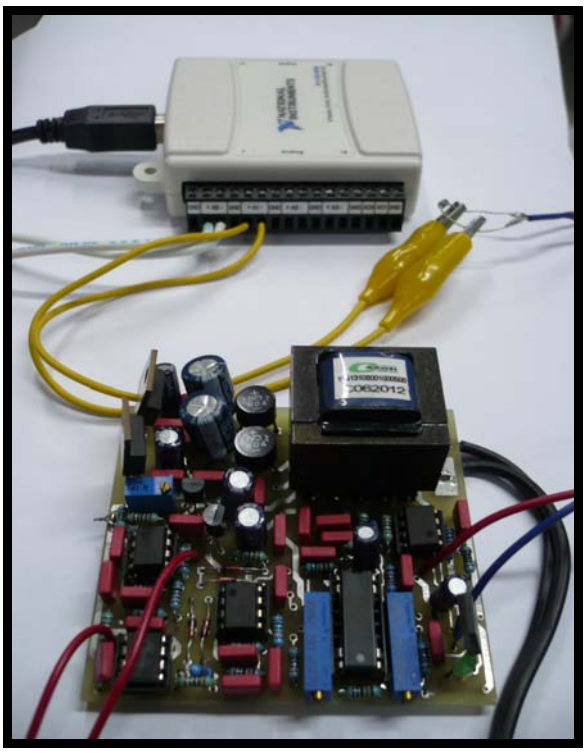

Figure 33 Experimental setup of circuit board connecting to the data acquisition unit.

The procedure of the system begins with the oscillator which is inside the transmitter. The oscillator was sent alternating current (AC) to the sensor probe by the one cable. When the sensor probe was immersed into the fluid which the resistance was changed, the back-signal of alternating current was turn-back to another cable. Inside of the Transmitter was the Amplifier, for amplify alternating current signal. Afterwards, the signal went to the Rectifier which the alternating current (AC) was changed to direct current (DC). Furthermore, volt to current (V to I) was inside the transmitter, for adjusting the voltage to current. Direct current was sent from the transmitter to resistor board, thus the current was changed to voltage. Thereafter, was sent analog to digital (A/D) for converting of analog signal into digital signal. The final part, the CPU received digital signal from A/D.

LabVIEW Program version 8.5 was used in this system for changing voltage value into conductivity value by data acquisition unit (USB 6008) with NI-DAQmx version 8.6. The default value of conductivity is 4-20 mA range from the

minimum conductivity to maximum conductivity of solution. The values between these default values were interpolated from the equations. Then, the results were sent to the computer monitor later. The value was read at every 1 second time interval.

Calibration conductivity value with concentration curves at different superficial gas velocities was required before experimental measurements in the reactor were carried out. The flow rates of inlet gases for the riser and downcomer were measured by two flow meters. The sets of the superficial gas velocities of the system are the same in ERT system.

RESULTS AND DISCUSSION

The hydrodynamics in an external-loop gas lift reactor was studied. The experiments were divided into 2 parts. The local gas holdup distributions in the riser and downcomer in an external-loop gas lift reactor were measured by ERT. In addition, the residence time distribution (RTD) was evaluated by using a stimulus-response tracer technique.

1. Electrical resistance tomography system (ERT)

1.1 Gas holdup in the riser and downcomer

1.1.1 Cross-sectional gas holdup distributions in the riser and downcomer

Figures 34 and 35 show the cross-sectional gas holdup distributions in the riser and downcomer, respectively at the middle sections of the column lengths. The superficial gas velocities at the riser and downcomer are 6.14 cm/s and 1.02 cm/s, respectively. The shade scales represent various values of local gas holdup ranging from the low local gas holdup (in black) to high local gas holdup (in white). It was apparent that gas holdup was not uniform in the riser and downcomer. The cross-sectional gas holdup in the riser was more approximately axis-symmetric than that in the downcomer, and in both columns was decreased from the center to the wall all the time. Last images of Figures 34 and 35 show that the time-averaged conductivity in the riser and downcomer is in the range of 0-0.25 mS/cm. The conductivity values of pure gas and pure tap water are 0 and 0.25 mS/cm, respectively. The conductivity value was decreased from the wall to the center in the riser and downcomer. It was apparent that time-averaged conductivity was not uniform in both columns. Uncertainty exists in the regions close to the column wall where some measurement and reconstruction error were presented. The gas holdup in the riser is always higher than that in the downcomer. Time-averaged gas holdup in the riser and downcomer are in the ranges of 0-0.337 and 0-0.236, respectively.

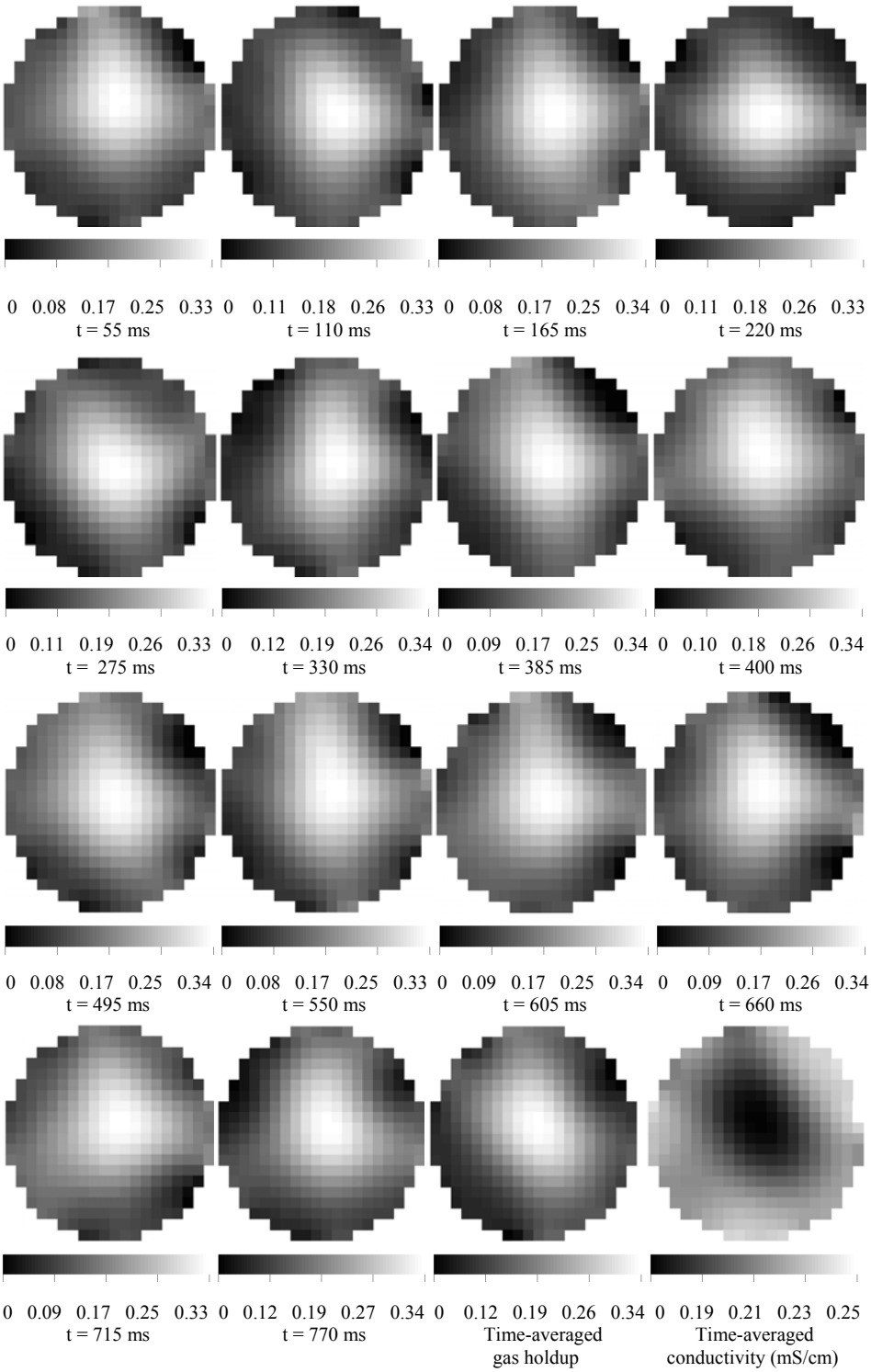

Figure 34 Cross-sectional gas holdup distributions in the riser at the superficial gas velocities in the riser of 6.14 cm/s and in the downcomer of 1.02 cm/s.

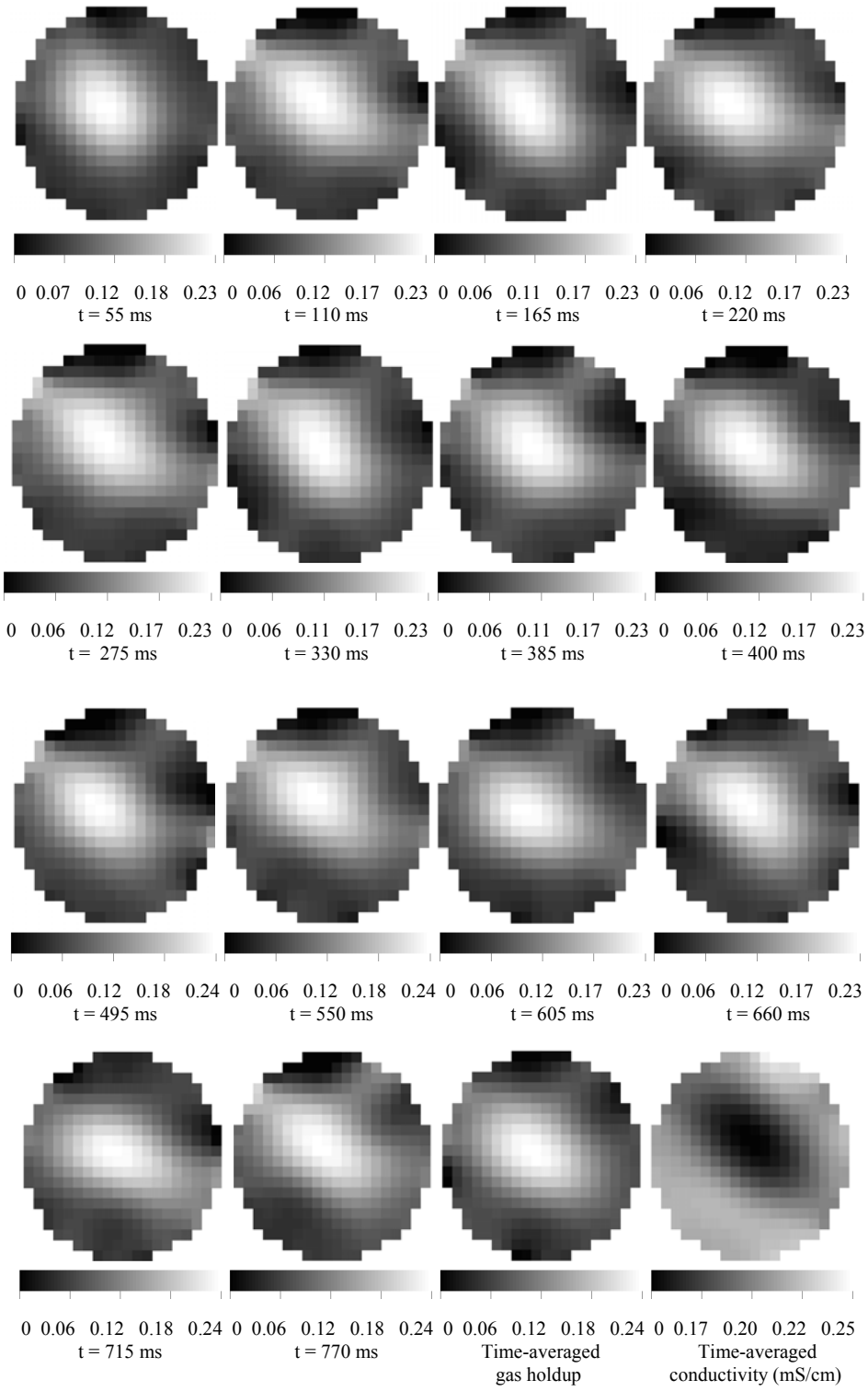

Figure 35 Cross-sectional gas holdup distributions in the downcomer at the superficial gas velocities in the riser of 6.14 cm/s and in the

downcomer of 1.02 cm/s.

1.1.2 Radial gas holdup profiles in the riser and downcomer

Figure 36 shows the azimuthally averaged gas holdups which is time averaged in the riser and downcomer as a function of radial position. The radial gas holdup profiles in both systems are similar. At the center of the columns the gas holdup was maximum and decreased along with the radial distance from the center to the wall. The gas holdup in the riser is clearly higher than that in the downcomer due to higher gas velocity in the riser.

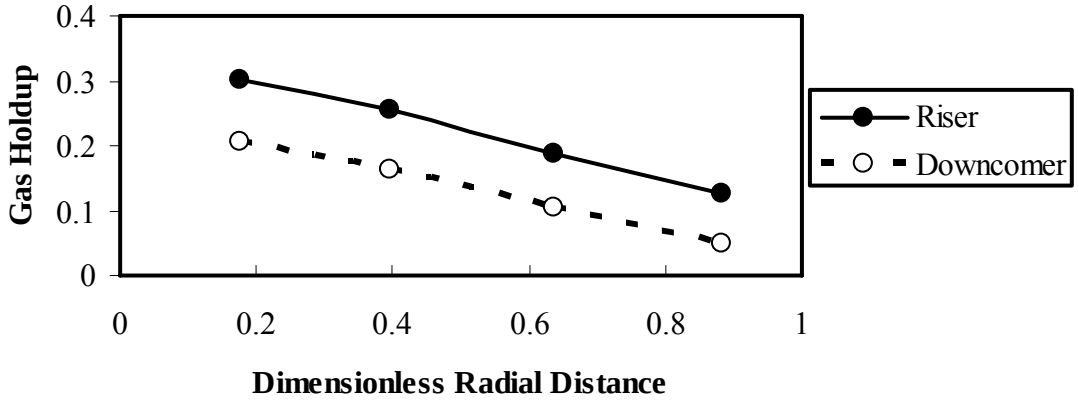

Figure 36 Azimuthally averaged gas holdup profile obtained by ERT at the superficial gas velocities in the riser of 6.14 cm/s and in the downcomer of 1.02 cm/s.

1.2 The superficial gas velocities in the riser and downcomer on the gas holdup in the riser and downcomer

1.2.1 Effect of the superficial gas velocities in the riser on the time-averaged cross-sectional gas holdup distributions of the riser and downcomer

Figures 37 and 38 show the time-averaged cross-sectional gas holdup distributions in the riser and downcomer, respectively at different superficial gas velocities of the riser for different superficial gas velocities in the downcomer.

The superficial gas velocities at the riser and downcomer are in the ranges of 1.02-10.23 cm/s and 0-3.07 cm/s, respectively.

Figure 37 shows the results in the riser. It was found that the gas holdup was increased with increasing of the superficial gas velocity in the riser. The gas holdup was dependent with the volumetric flow rate of gas inlet. Moreover, the gas holdup distribution was nearly axis symmetrical but not uniform across the sectional area for all superficial gas velocities in the riser. Figure 38 shows the results in the downcomer. It was found that the span of value of the gas holdup was increased with increasing of the superficial gas velocity in the riser. Furthermore, the gas holdup distribution was not uniform with less symmetry for all superficial gas velocities in the riser. The superficial gas velocity of the riser affects the gas holdup in both columns. At the center of both columns, the gas holdup was the maximum and was decreased from the center to the wall at all the superficial gas velocities. The pattern of the gas holdup distributions in the riser was more symmetrical than that in the downcomer.

1.2.2 Effect of the superficial gas velocities in the downcomer on the time-averaged cross-sectional gas holdup distributions of the riser and downcomer

Figures 39 and 40 show the time-averaged cross-sectional gas holdup distributions in the riser and downcomer, respectively at different superficial gas velocities of the downcomer. The superficial gas velocities in the downcomer are in the range of 0-3.07 cm/s with the superificial gas velocities in the riser of 4.09-8.19 cm/s.

Figure 39 showed that the scale value of the gas holdup distribution in the riser was increased with increasing of the superficial gas velocities in the downcomer. At high inlet gas flow rate of the downcomer, the gas and liquid circulated from the riser into the downcomer are impeded by up flow of high gas velocity in the downcomer. Therefore, the gas holdup in riser was increased at higher superficial gas velocity in the downcomer.

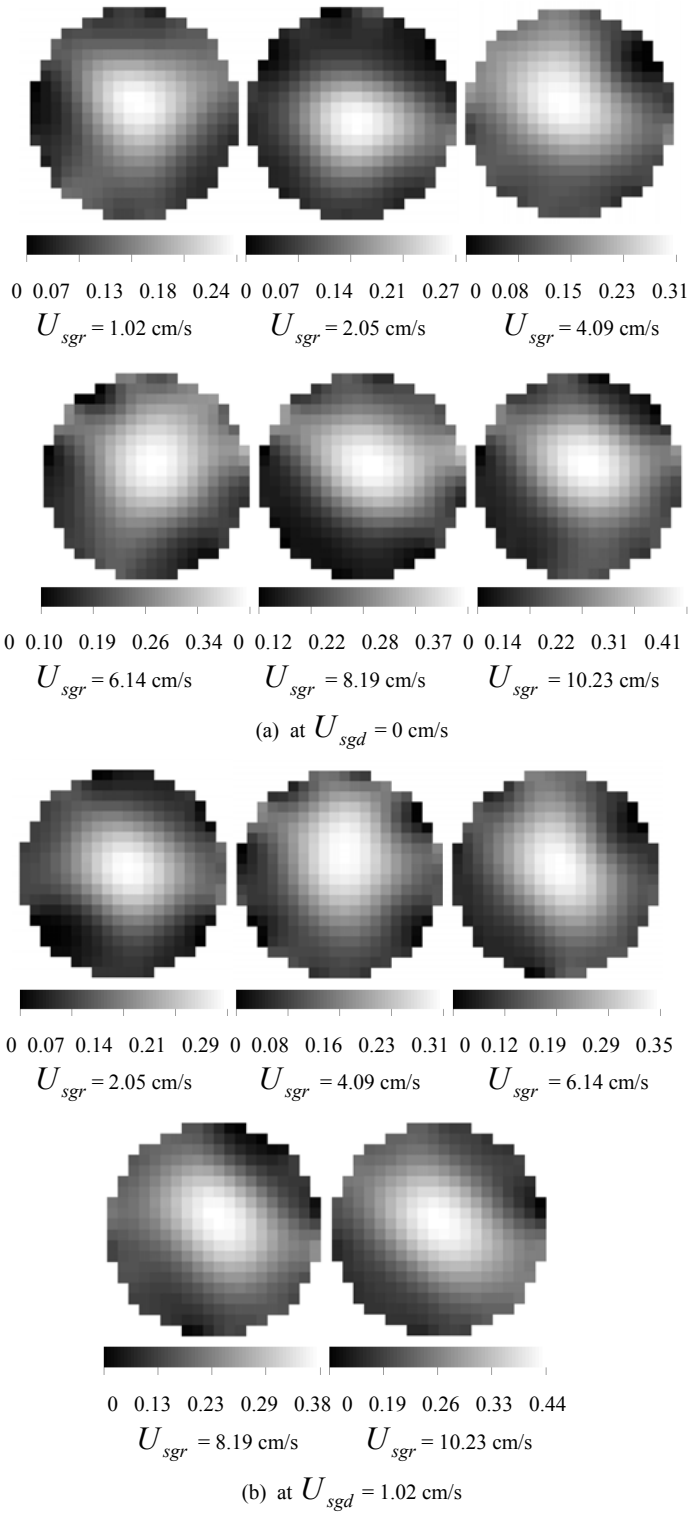

Figure 37 Time-averaged cross-sectional gas holdup distributions in the riser at the superficial gas velocities of the downcomer (a) U_{sgd} = 0 cm/s (b) U_{sgd} = 1.02 cm/s (c) U_{sgd} = 2.05 cm/s (d) U_{sgd} = 3.07 cm/s.

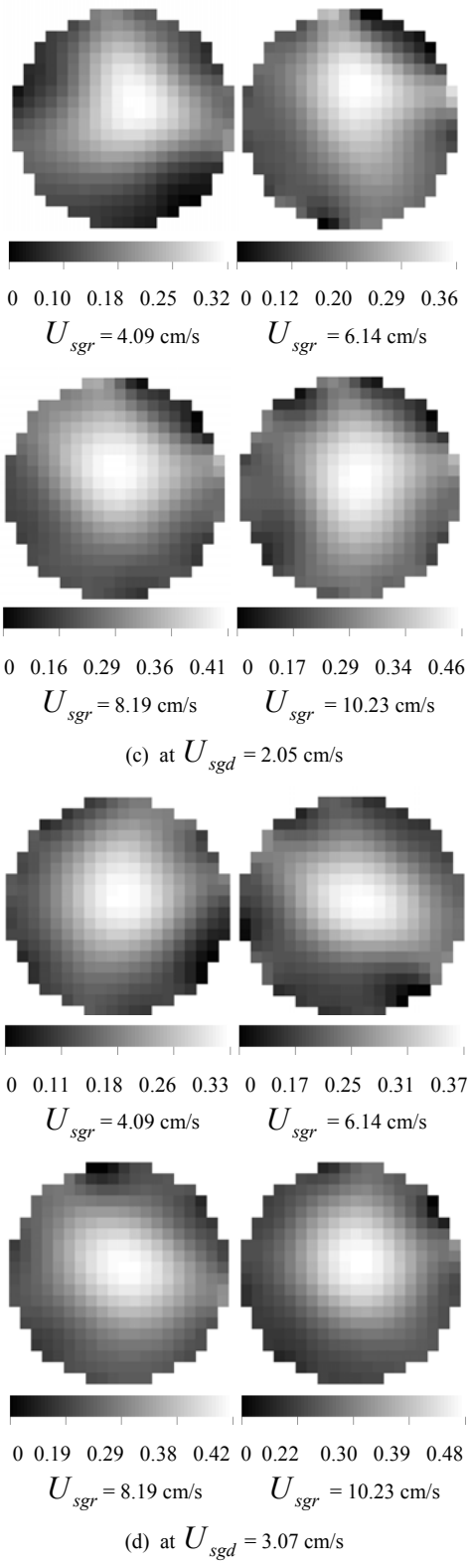

Figure 37 (continued).

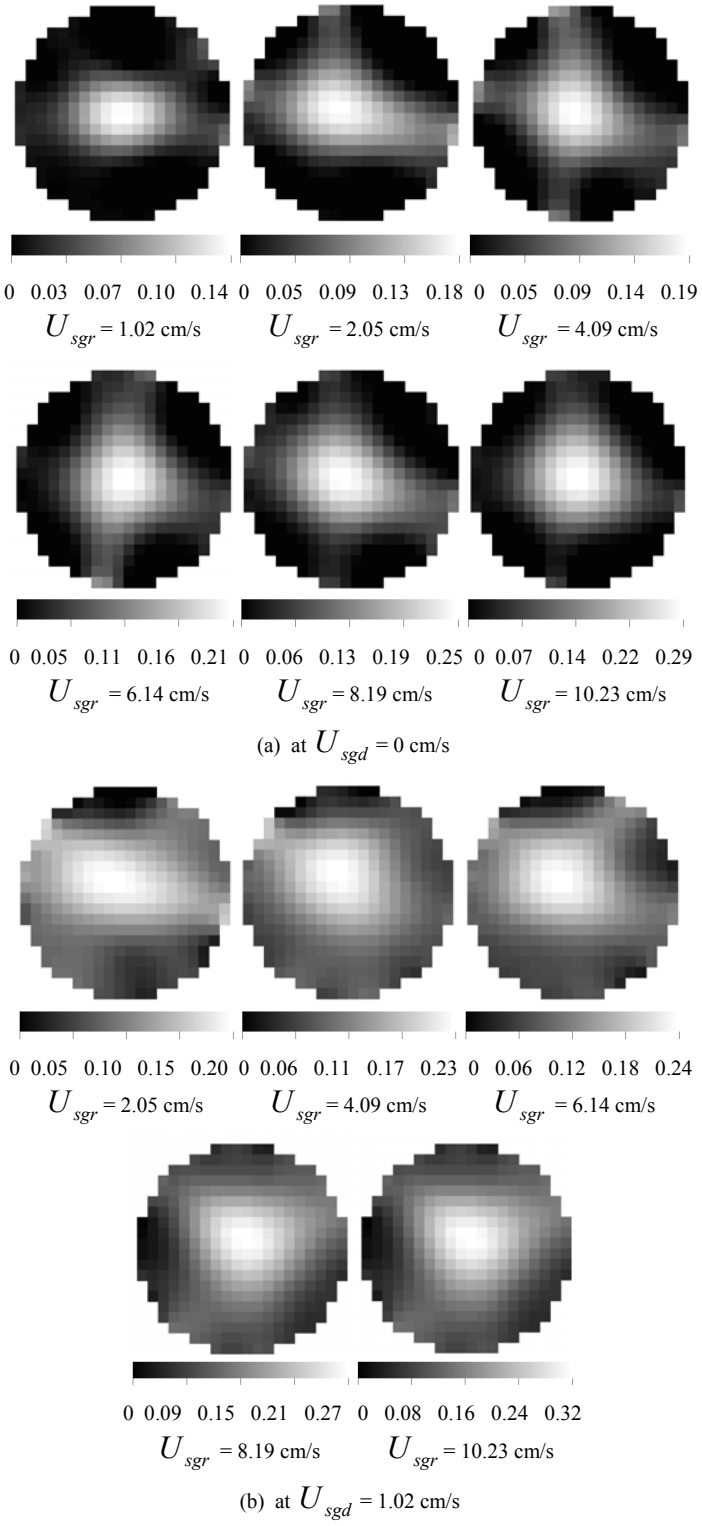

Figure 38 Time-averaged cross-sectional gas holdup distributions in the downcomer at the superficial gas velocity of the downcomer (a) U_{sgd} = 0 cm/s (b) U_{sgd} = 1.02 cm/s (c) U_{sgd} = 2.05 (d) U_{sgd} = 3.07 cm.

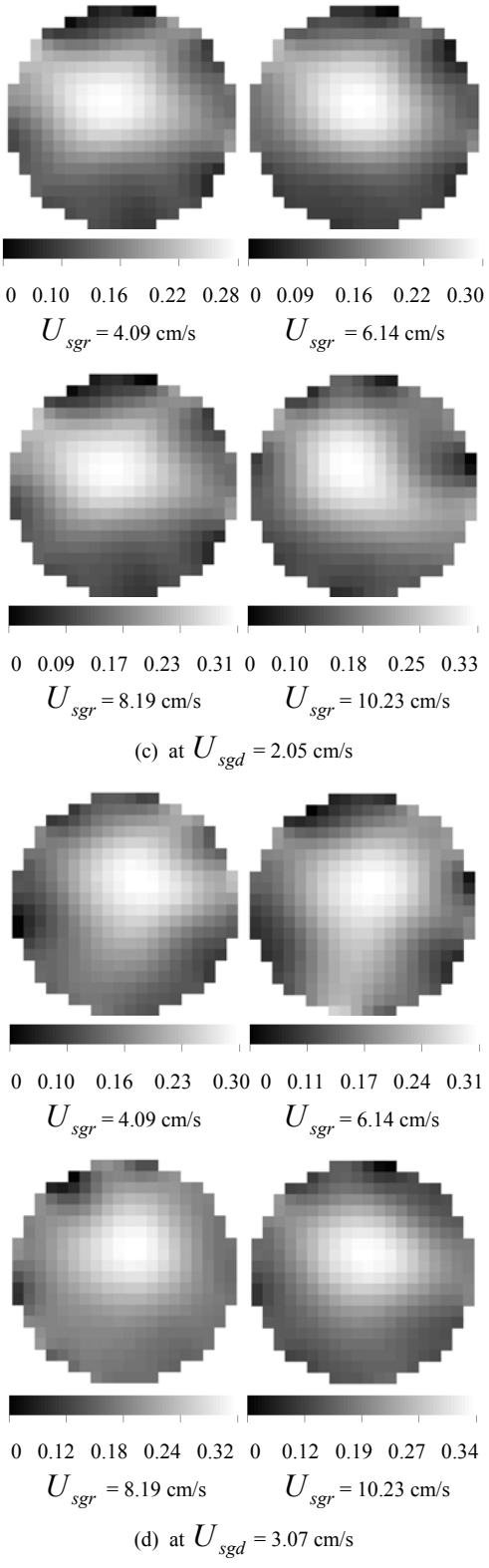

Figure 38 (continued).

At all superficial gas velocities in the downcomer, the gas holdup distribution was not uniform along with the radial distance. Figure 40 showed that the gas holdup in the downcomer was increased with increasing of the superficial gas velocity in the downcomer. At no inlet gas of the downcomer, the gas holdup still existed because the gas bubbles from the riser were induced by the circulated liquid to the downcomer when the gas inlet in the riser was higher than that in the downcomer. However, the gas holdup in the downcomer at this condition was relatively low. In addition, the gas holdup distribution was not uniform across the sectional area at all superficial gas velocities. In both columns, it was found that the superficial gas velocity of the downcomer increased, the time-averaged cross-sectional gas holdup in both columns was increased. Furthermore, the gas holdup distribution in riser was more axis-symmetrical than that in the downcomer.

1.2.3 Effect of the superficial gas velocity of the riser and downcomer on the radial gas holdup distributions

Figures 41 - 44 show the azimuthally averaged gas holdup as a function of radial distance in the riser and downcomer at the superficial gas velocities in the riser of 0.51-10.23 cm/s and in the downcomer of 0-3.07 cm/s. The gas holdup in both columns was increased with increasing of the superficial gas velocities of both columns. At the center of the columns the gas holdup was the maximum and was decreased along with the radial distance from the center to the wall. In the turbulent flow regime ($U_{sgr} = 8.09 - 10.23$ cm/s), the radial gas holdup profiles in both columns are less flat than those in the bubble and transient regimes ($U_{sgr} = 0.51 - 6.14$ cm/s). In the riser, the gas holdup was higher than that in the dowmcomer because the inlet gas flow rate in the riser was more than that in the downcomer.

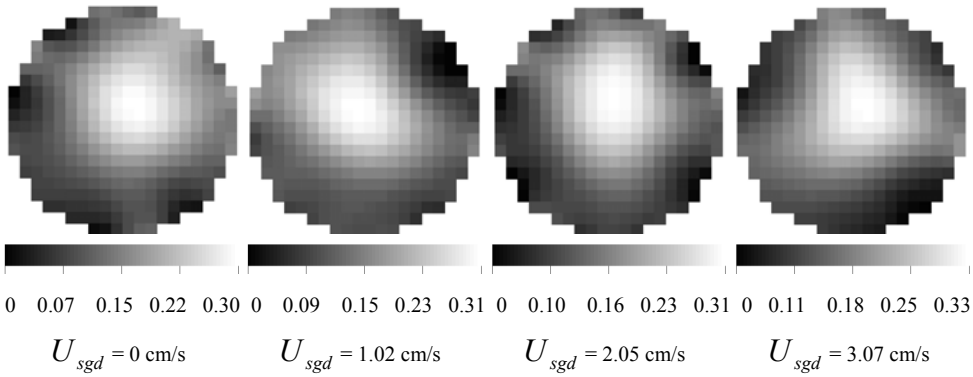

(a) at U_{sgr} = 4.09 cm/s

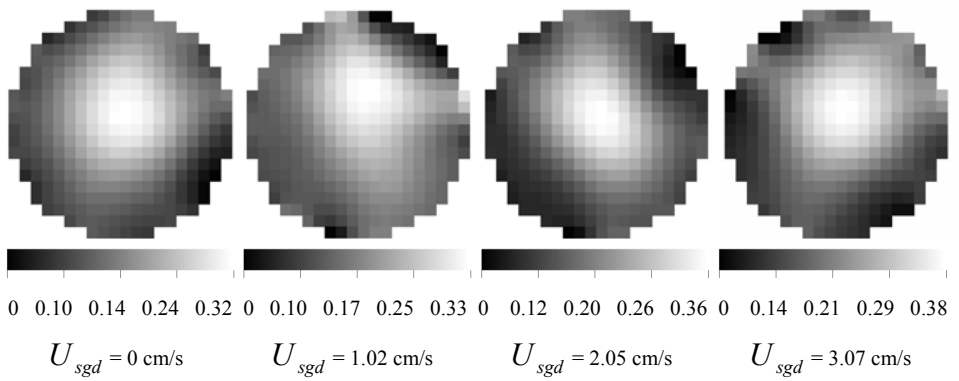

(b) at U_{sgr} = 6.14 cm/s

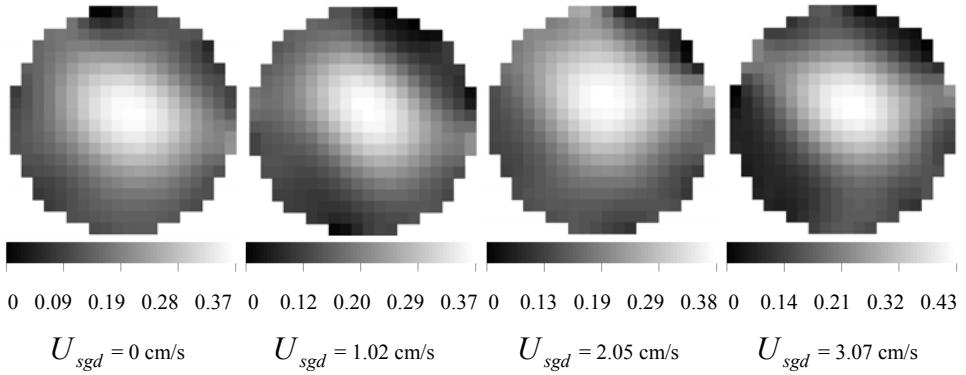

(c) at U_{sgr} = 8.19 cm/s

Figure 39 Time-averaged cross-sectional gas holdup distributions in the riser at the superficial gas velocities of the riser (a) U_{sgr} = 4.09 cm/s (b) U_{sgr} = 6.14 cm/s (c) U_{sgr} = 8.19 cm/s.

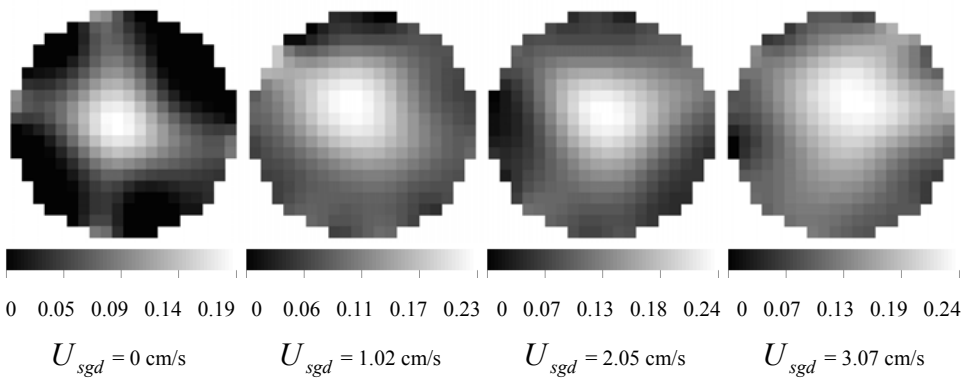

(a) at U_{sgr} = 4.09 cm/s

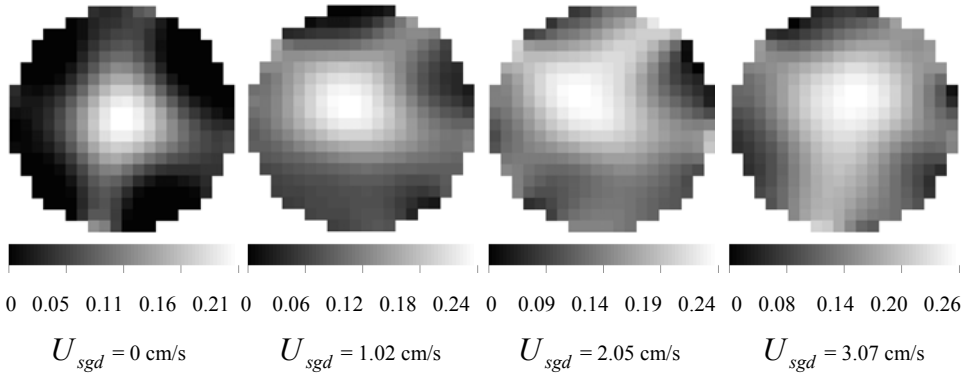

(b) at U_{sgr} = 6.14 cm/s

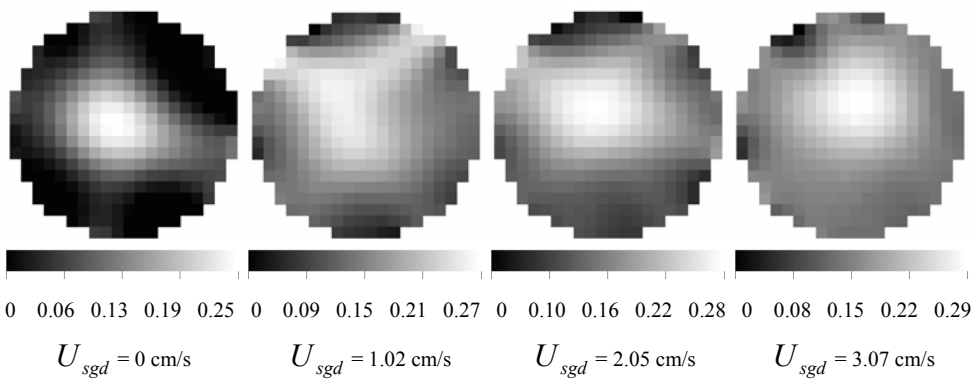

(c) at U_{sgr} = 8.19 cm/s

Figure 40 Time-averaged cross-sectional gas holdup distributions in the downcomer at the superficial gas velocities of the riser (a) U_{sgr} = 4.09 cm/s (b) U_{sgr} = 6.14 cm/s (c) U_{sgr} = 8.19 cm/s.

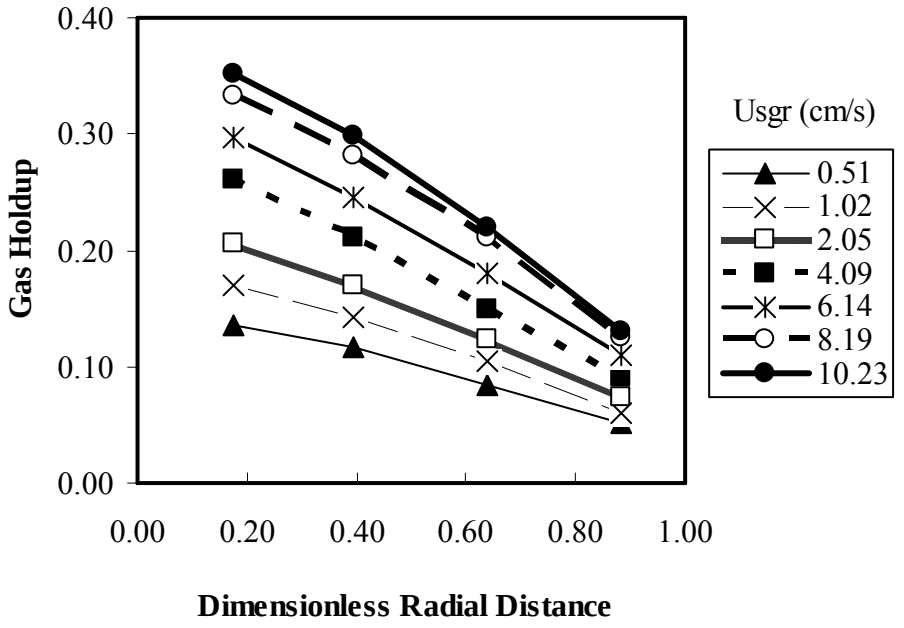

(a) Riser

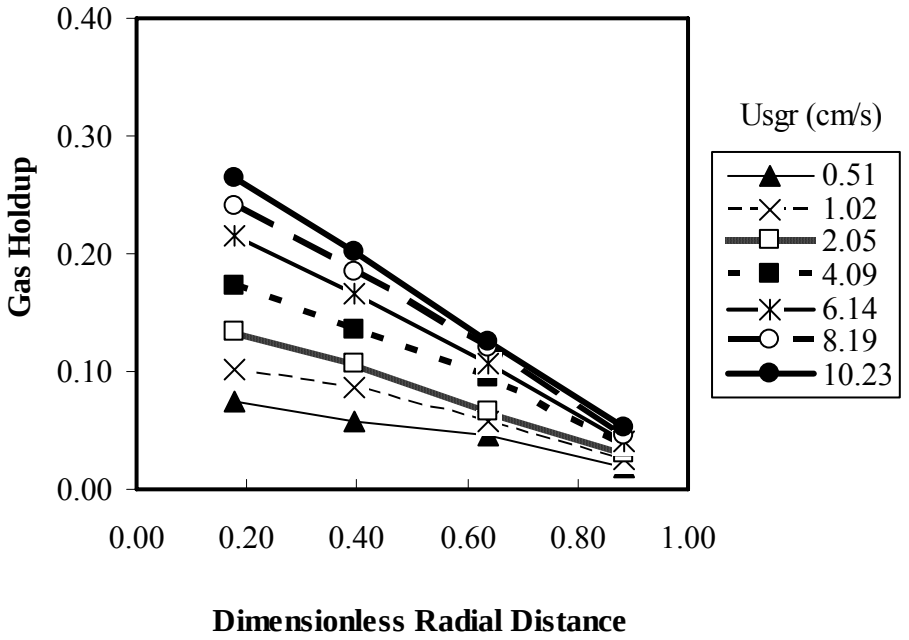

(b) Downcomer

Figure 41 Radial gas holdup profiles in the riser and in the downcomer obtained by ERT system at the superficial gas velocities in the riser of 0.51-10.23 cm/s and in the downcomer of 0 cm/s (a) in the riser (b) in the downcomer.

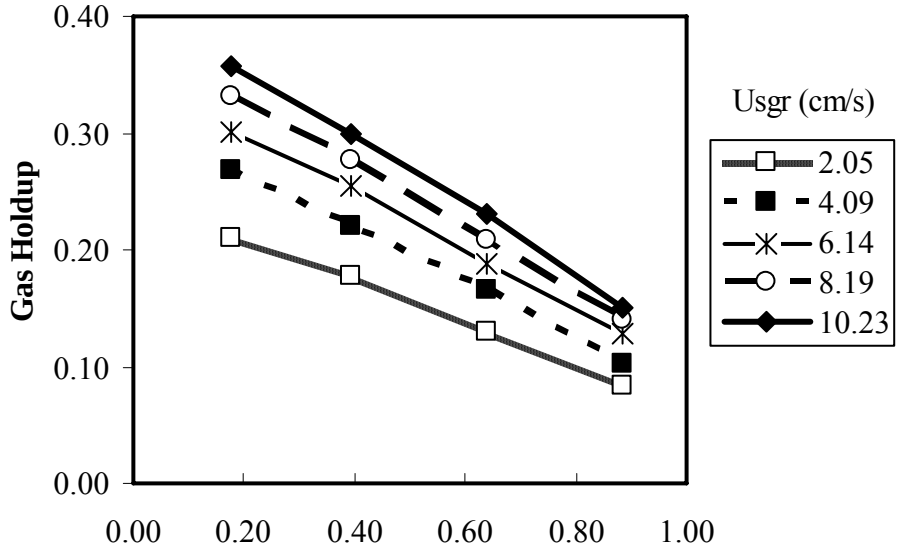

(a) Riser

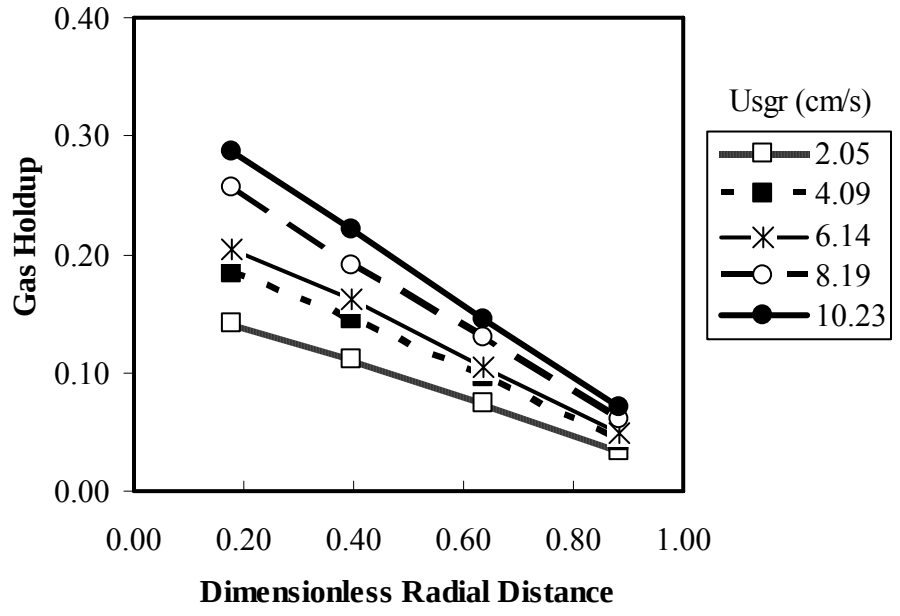

(b) Downcomer

Figure 42 Radial gas holdup profiles in the riser and in the downcomer obtained by ERT system at the superficial gas velocities in the riser of 2.05-10.23 cm/s and in the downcomer of 1.02 cm/s (a) in the riser (b) in the downcomer.

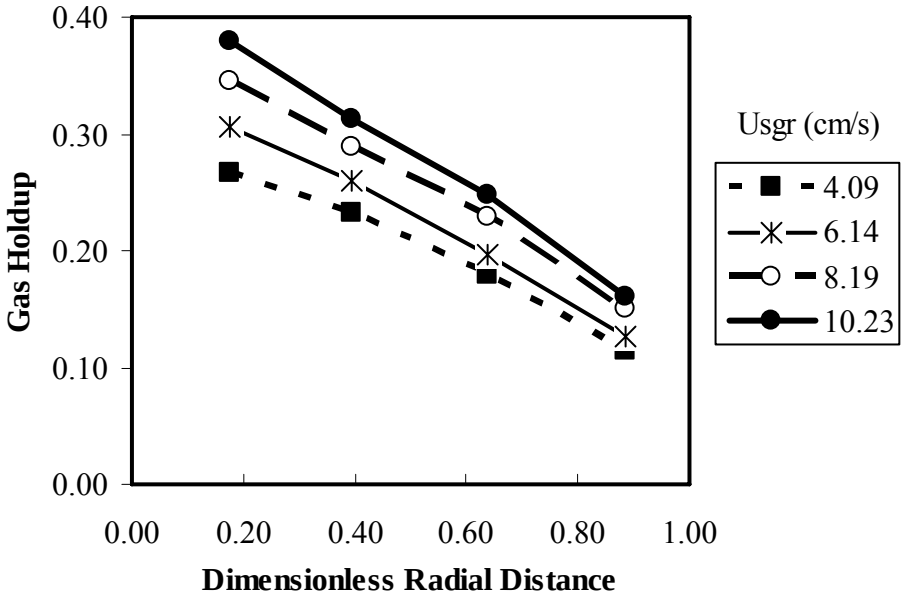

(a) Riser

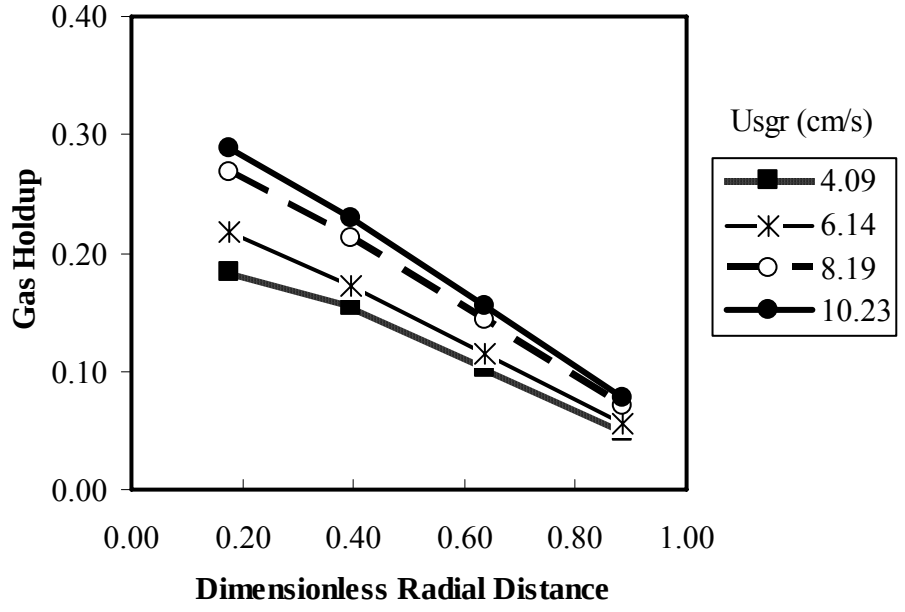

(b) Downcomer

Figure 43 Radial gas holdup profiles in the riser and in the downcomer obtained by ERT system at the superficial gas velocities in the riser of 4.09-10.23 cm/s and in the downcomer of 2.05 cm/s (a) in the riser (b) in the downcomer.

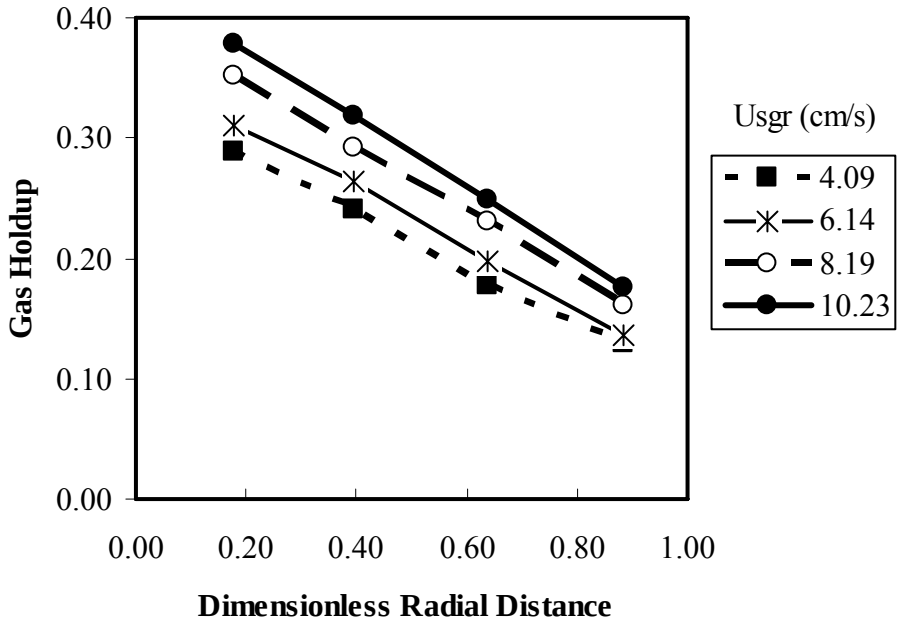

(a) Riser

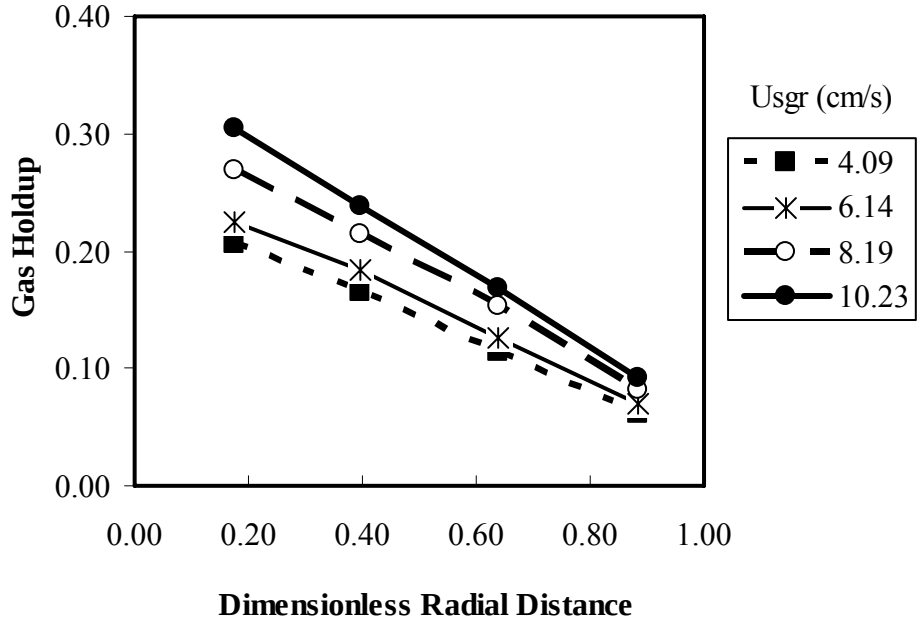

(b) Downcomer

Figure 44 Radial gas holdup profiles in the riser and in the downcomer obtained by ERT system at the superficial gas velocities in the riser of 4.09-10.23 cm/s and in the downcomer of 3.07 cm/s (a) in the riser (b) in the downcomer.

1.2.4 Effect of the superficial gas velocities of the riser and downcomer on the cross-sectional averaged gas holdup in the riser and downcomer

Figures 45 and 46 show the cross-sectional averaged gas holdups in the riser and downcomer, respectively at different superficial gas velocities of the riser and downcomer. It was found that the superficial gas velocity in the riser affects the cross-sectional averaged gas holdup in the riser and downcomer. At the superficial gas velocities in the riser of 0.51-10.23 cm/s with no gas inlet in the downcomer, the cross-sectional averaged gas holdups on the riser and downcomer are in the ranges of 0.079-0.204 and 0.038-0.117, respectively. At higher gas inlet in the downcomer (at 1.02 cm/s), the cross-sectional averaged gas holdup values in the riser and downcomer are higher and in the ranges of 0.123-0.216 and 0.067-0.136, respectively. It was found that at high gas velocity in the downcomer, the gas holdups in the riser and downcomer were increased. In addition, at higher gas velocities in the downcomer (2.05 and 3.07 cm/s), the gas holdup values in the riser are higher, in the ranges of 0.166-0.230 and 0.175-0.240; respectively, while the gas holdup in the downcomer are 0.094-0.143 and 0.106-0.157, respectively.

Figures 45 and 46 show that the dependency of gas holdup on the superficial gas velocities in both the riser and downcomer is the same for all gas velocities in the downcomer. The gas holdup in both columns was increased with increasing of the superficial gas velocities. In the case of no gas inlet in the downcomer, the cross-sectional averaged gas holdup still existed, because the gas was induced from the riser into the downcomer. In both columns, the gas holdup in the riser was higher than that in the dowmcomer because the inlet gas in the riser was more than that in the downcomer. The difference of the gas holdup in the downcomer at different superficial gas velocities of the downcomer was greater than that in the riser, since the superficial gas velocity of the downcomer directly affects the gas holdup in the downcomer.

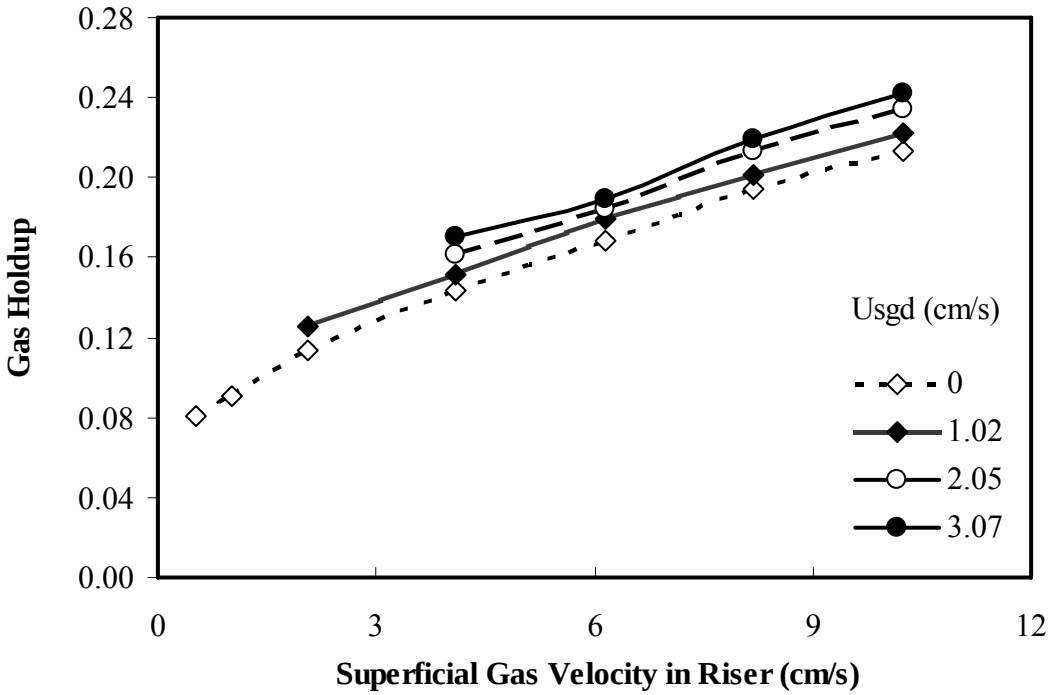

Figure 45 Cross-sectional averaged gas holdup in the riser at the superficial gas velocities in the riser of 0.51-10.23 cm/s and in the downcomer of 0-3.07 cm/s.

Figure 47 shows the comparison of gas holdup in the riser and downcomer at different superficial gas velocities of the downcomer. The gas holdup in the riser is always higher than that in the downcomer. In bubbly flow regime, at low superficial gas velocities in the riser (U_{sgr} = 0.51-2.05 cm/s), the difference of gas holdup in the riser and downcomer was less. With low superficial gas velocity in the riser, less gas was injected into the riser. In addition, the gas velocity in the downcomer is always low in this study. Therefore, the gas holdup difference in both columns is less in this regime.

However, in the transition flow regime and turbulent flow regime, at medium and high superficial gas velocities in the riser (U_{sgr} = 4.09 -6.14 cm/s and U_{sgr} = 8.19-10.23 cm/s), respectively with the superficial gas velocities at the downcomer of 0-3.07 cm/s, the gas holdups in the riser and downcomer were

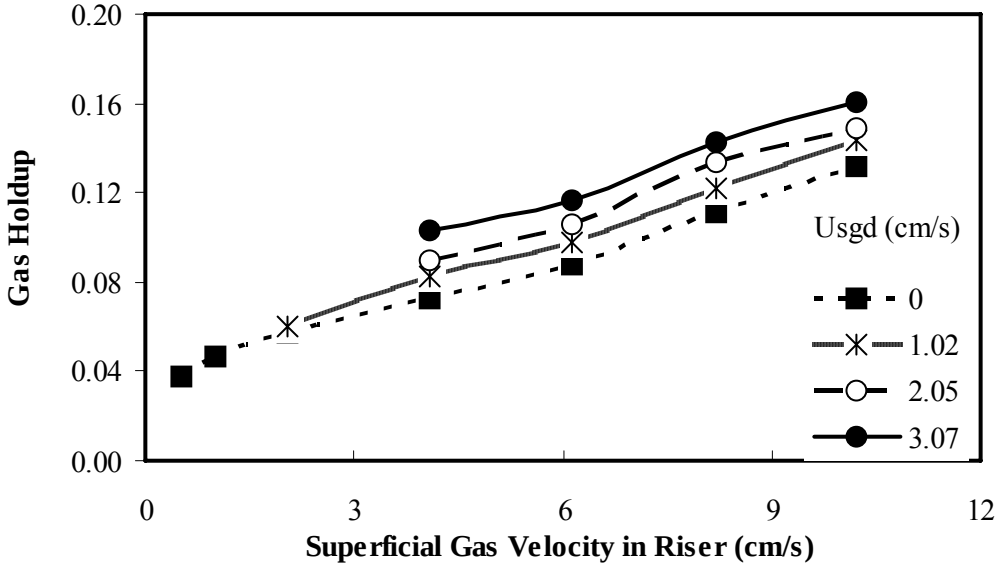

Figure 46 Cross-sectional averaged gas holdup in the downcomer at the superficial gas velocities in the riser of 0.51-10.23 cm/s and in the downcomer of 0-3.07 cm/s.

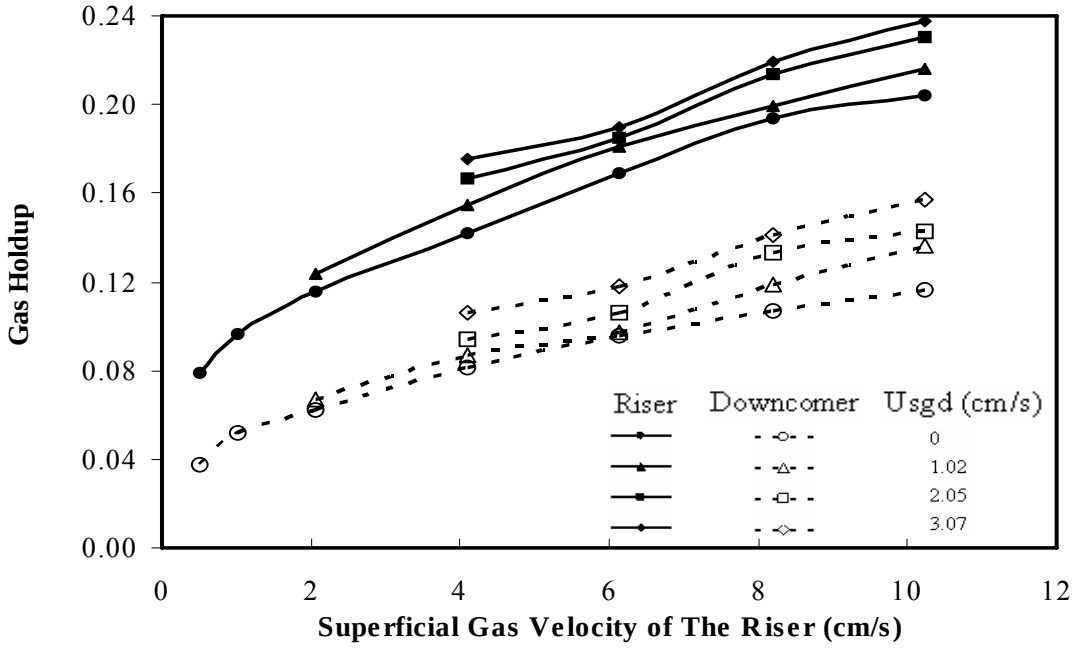

Figure 47 Comparison of cross-sectional averaged gas holdup in the riser and downcomer at the superficial gas velocities in the riser of 0.51-10.23 cm/s and in the downcomer of 0-3.07 cm/s.

significantly different due to more difference in inlet velocities in both columns. At high velocity of inlet gas in the downcomer (at 3.07 cm/s) the down flow bubbles from the riser were impeded by high velocity of inlet gas in the downcomer. Therefore, high gas holdup in the riser was found. Gas holdup in the downcomer is high due to high feed gas in the downcomer.

1.3 Empirical models of gas holdup

1.3.1 Radial gas holdup

The model equations for radial gas holdup profiles obtained from the experiments were developed by fitting the radial gas holdup with the important variables, i.e., superficial gas velocities of the riser and downcomer. They can be written in the form of Equation 41. The fitted equations for both columns are shown in Tables 4 and 5, respectively.

$$\varepsilon_{local} = (aU_{sgr}{}^{m})(1 - b\left(\frac{r}{R}\right)^{cU_{sgr}{}^{-n}}) \tag{41}$$

The empirical models of gas holdups in the riser and downcomer in Tables 4 and 5 show that the coefficient *a* in both columns slightly increases with an increasing of the superficial gas velocity in the downcomer, while the coefficients *b* in both columns were decreased with increasing of the superficial gas velocity in the downcomer. The coefficient *c* indicates the radial gas holdup profile flattening. The coefficient *c* in the riser was decreased while that in the downcomer was increased with increasing of the superficial gas velocity in the downcomer. Furthermore, parameters *m, n* were fixed as constants for both columns in this study.

Figures 48-51 show the comparison of the radial gas holdup profiles obtained from ERT system experiments and empirical models at the superficial gas velocities in the riser of 0.51-10.23 cm/s for the superficial gas velocities in the

downcomer of 0, 1.02, 2.05, and 3.07 cm/s; respectively. It was found that the fitted gas holdups obtained from the experiment and model was well fitted.

Table 4 Equations of radial gas holdup in the riser obtained from fitting of experimental data at the superficial gas velocities in the riser of 0.51-10.23 cm/s and in the downcomer of 0-3.07 cm/s.

.

Conditions	The fitted models for radial gas holdup in the riser	
U_{sgr} = 0.51 – 10.23 cm/s with U_{sgd} = 0 cm/s	$\varepsilon_{local\_r} = 0.168 U_{sgr}^{0.36}\left(1 - 0.77\left(\frac{r}{R}\right)^{1.37 U_{sgr}^{-0.05}}\right)$	(42)
U_{sgr} = 2.05 – 10.23 cm/s with U_{sgd} = 1.02 cm/s	$\varepsilon_{local\_r} = 0.174 U_{sgr}^{0.36}\left(1 - 0.74\left(\frac{r}{R}\right)^{1.30 U_{sgr}^{-0.05}}\right)$	(43)
U_{sgr} = 4.09 – 10.23 cm/s with U_{sgd} = 2.05 cm/s	$\varepsilon_{local\_r} = 0.182 U_{sgr}^{0.36}\left(1 - 0.71\left(\frac{r}{R}\right)^{1.21 U_{sgr}^{-0.05}}\right)$	(44)
U_{sgr} = 4.09 – 10.23 cm/s with U_{sgd} = 3.07 cm/s	$\varepsilon_{local\_r} = 0.185 U_{sgr}^{0.36}\left(1 - 0.68\left(\frac{r}{R}\right)^{1.13 U_{sgr}^{-0.05}}\right)$	(45)

The important variables are dimensionless radial distance $\left(\frac{r}{R}\right)$ and the superficial gas velocities of the riser and downcomer $\left(U_{sgr}, U_{sgd}(cm/s)\right)$. The coefficients in the model equations of the riser and downcomer (a,b,c) are obtained by fitting as a function of the superficial gas velocities of the downcomer as follows:

$$a_r = 0.17 e^{0.03 U_{sgd}} \tag{46}$$

$$a_d = 0.1e^{0.03U_{sgd}} \tag{47}$$

$$b_r = 0.77e^{-0.04U_{sgd}} \tag{48}$$

$$b_d = 0.95e^{-0.04U_{sgd}} \tag{49}$$

$$c_r = 1.38e^{-0.06U_{sgd}} \tag{50}$$

$$c_d = 1.05e^{0.03U_{sgd}} \tag{51}$$

Table 5 Equations of radial gas holdup in the downcomer obtained from fitting of experimental data at the superficial gas velocities in the riser of 0.51-10.23 cm/s and in the downcomer of 0-3.07 cm/s.

Conditions	The fitted models for radial gas holdup in the downcomer	
U_{sgr} = 0.51 – 10.23 cm/s with U_{sgd} = 0 cm/s	$\varepsilon_{local\_d} = 0.105U_{sgr}^{0.47}\left(1-0.95\left(\frac{r}{R}\right)^{1.05U_{sgr}^{-0.02}}\right)$	(52)
U_{sgr} = 2.05 – 10.23 cm/s with U_{sgd} = 1.02 cm/s	$\varepsilon_{local\_d} = 0.108U_{sgr}^{0.47}\left(1-0.91\left(\frac{r}{R}\right)^{1.09U_{sgr}^{-0.02}}\right)$	(53)
U_{sgr} = 4.09 – 10.23 cm/s with U_{sgd} = 2.05 cm/s	$\varepsilon_{local\_d} = 0.110U_{sgr}^{0.47}\left(1-0.88\left(\frac{r}{R}\right)^{1.12U_{sgr}^{-0.02}}\right)$	(54)
U_{sgr} = 4.09 – 10.23 cm/s with U_{sgd} = 3.07 cm/s	$\varepsilon_{local\_d} = 0.114U_{sgr}^{0.47}\left(1-0.85\left(\frac{r}{R}\right)^{1.16U_{sgr}^{-0.02}}\right)$	(55)

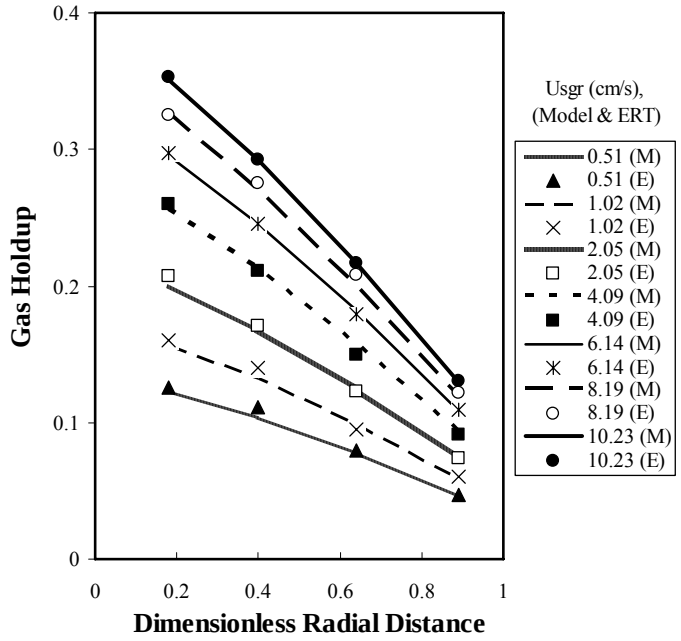

(a) Riser

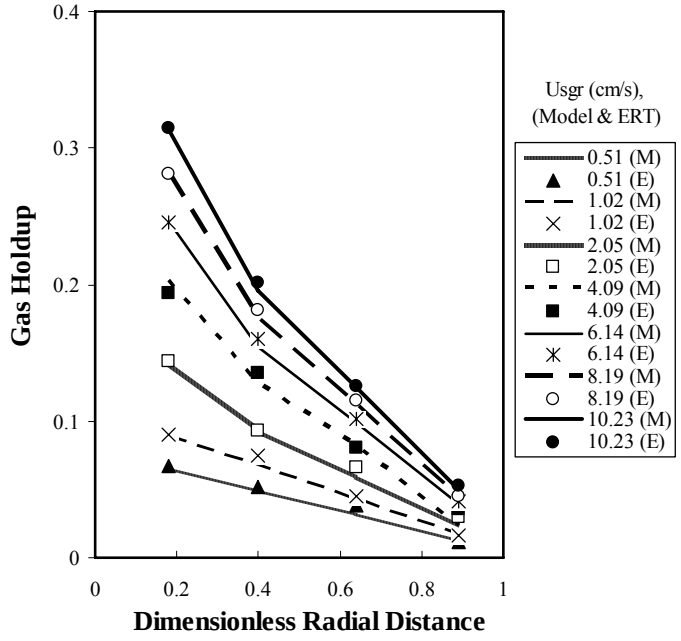

(b) Downcomer

Figure 48 Comparison of radial gas holdup profile obtained from the model and the experiments at the superficial gas velocities in the riser of 0.51-10.23 cm/s and in the downcomer of 0 cm/s (a) in the riser (b) in the downcomer.

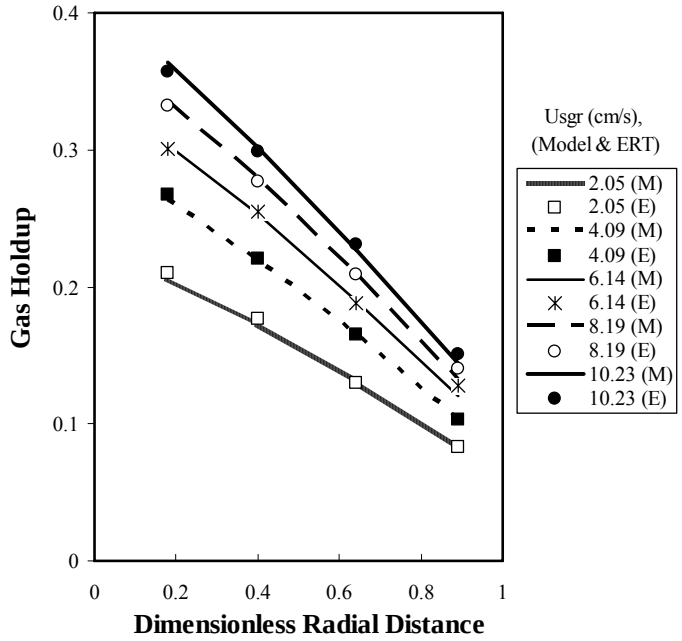

(a) Riser

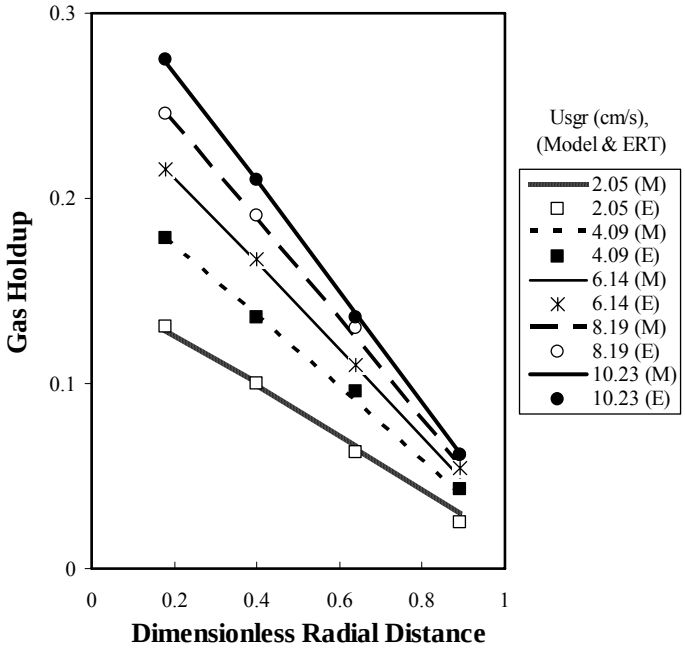

(b) Downcomer

Figure 49 Comparison of radial gas holdup profile obtained from the model and the experiments at the superficial gas velocities in the riser of 2.05-10.23 cm/s and in the downcomer of 1.02 cm/s (a) in the riser (b) in the downcomer.

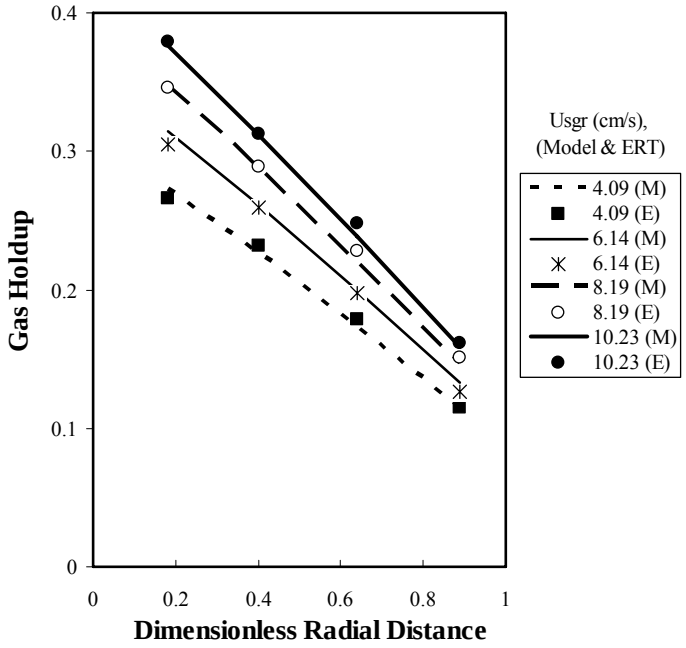

(a) Riser

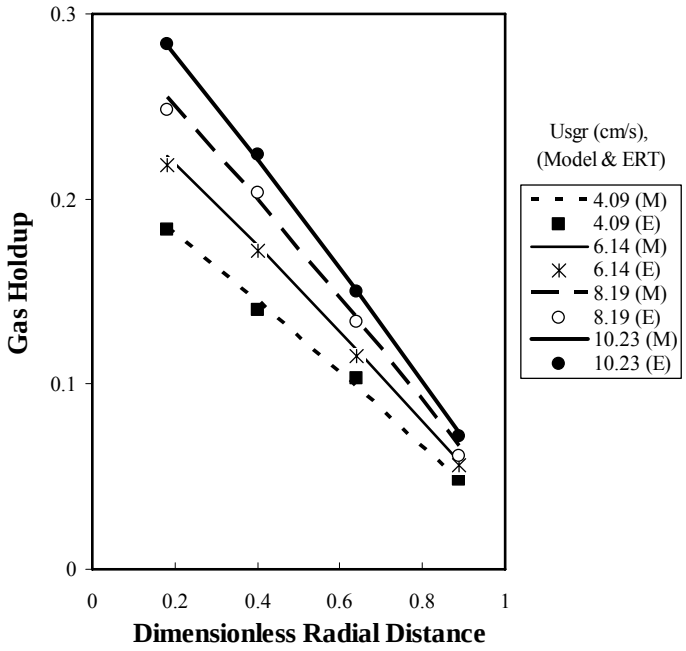

(b) Downcomer

Figure 50 Comparison of radial gas holdup profile obtained from the model and the experiments at the superficial gas velocities in the riser of 4.09-10.23 cm/s and in the downcomer of 2.05 cm/s (a) in the riser (b) in the downcomer.

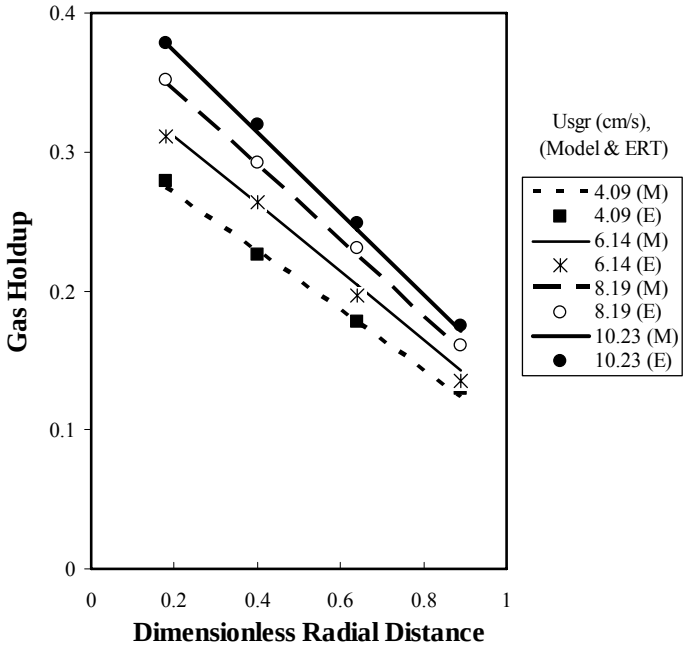

(a) Riser

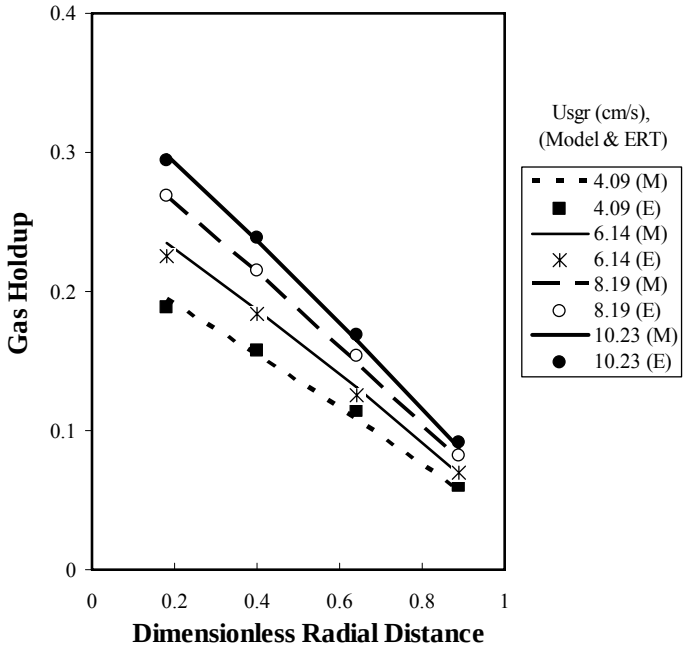

(b) Downcomer

Figure 51 Comparison of radial gas holdup profile obtained from the model and the experiments at the superficial gas velocities in the riser of 4.09-10.23 cm/s and in the downcomer of 3.07 cm/s (a) in the riser (b) in the downcomer.

1.3.2 Cross-sectional averaged gas holdup

The model equations for cross-sectional averaged gas holdup were obtained from the experiments by fitting the important variable, i.e., superficial gas velocities of the riser and downcomer. They can be written in the form of Equation 56.

$$\bar{\varepsilon}_{avg} = A U_{sgr}^{\ N} \tag{56}$$

where the coefficient A for the riser and downcomer can be written as a function of the superficial gas velocity of the downcomer.

$$A_r = 0.09 e^{0.05 U_{sgd}} \tag{57}$$

$$A_d = 0.04 e^{0.08 U_{sgd}} \tag{58}$$

The parameter N was fitted as a constant for both columns in this study. The cross-sectional averaged gas holdups for the riser and downcomer are written as,

$$\bar{\varepsilon}_r = 0.09 e^{0.05 U_{sgd}} U_{sgr}^{\ 0.36} \tag{59}$$

$$\bar{\varepsilon}_d = 0.04 e^{0.08 U_{sgd}} U_{sgr}^{\ 0.47} \tag{60}$$

1.4 Mixing index distributions in the riser and downcomer

The mixing index is defined to be one minus deviation of the conductivity value between each pixel and average value of all pixels in first tomogram divided by deviation of the conductivity value between each pixel and average value of all pixels in second tomogram. The values of mixing index have two ranges. The first range is 0 to100 and the second range is 0 to -100.

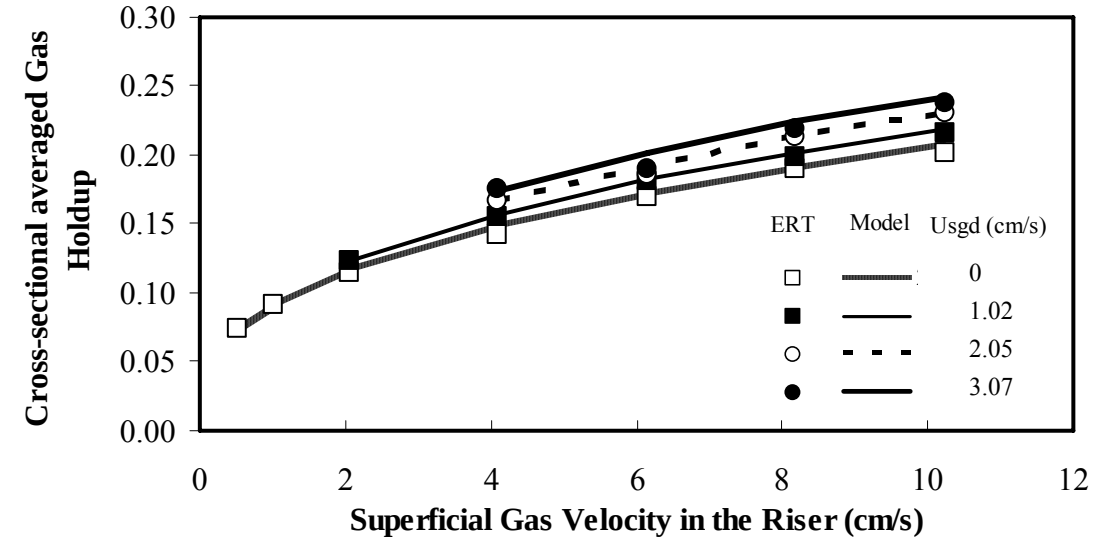

(a) Riser

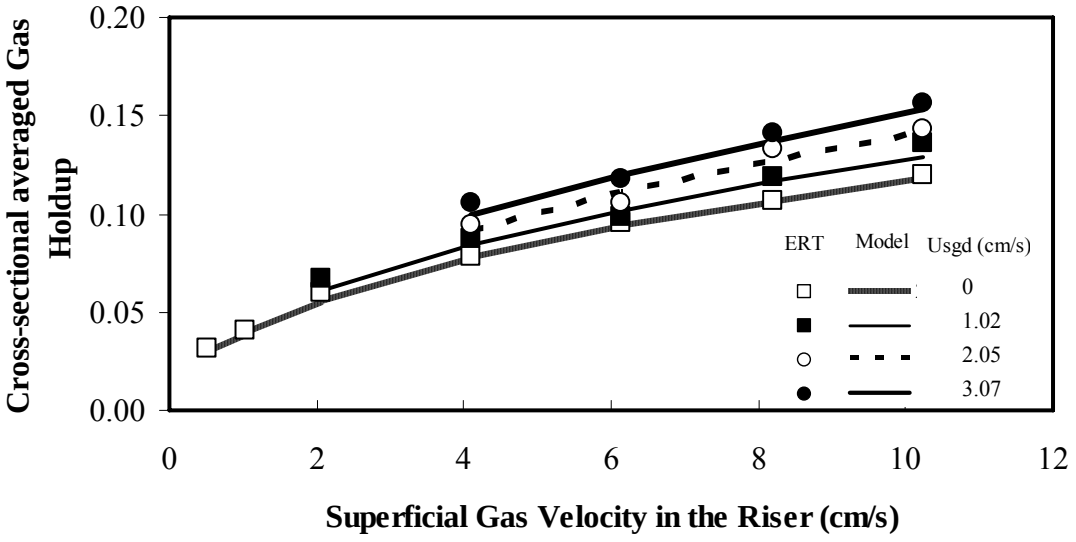

(b) Downcomer

Figure 52 Comparison of cross-sectional gas holdup profile obtained from the model and the experiments at the superficial gas velocities in the riser of 0.51-10.23 cm/s and in the downcomer of 0-3.07 cm/s (a) in the riser (b) in the downcomer.

If no mixing, the mixing index is equal to 0 because the conductivity does not change with time. However, if there is perfect mixing, the mixing index is equal to 100 or -100. Mixing index indicates the comparison of the deviation of conductivity of one tomogram to another tomogram's. If the first tomogram has more deviation of conductivity with the average conductivity of its tomogram than the second tomogram, then the mixing index is equal to a positive value. On the other hand, if the first tomogram has less deviation of conductivity value with the average conductivity of its tomogram than the second tomogram then the mixing index is equal to a negative value. The mixing index (σ) is calculated as follows (Industrial Tomography Systems Ltd, 2004):

$$\sigma(\%) = \left(1 - \frac{\sigma_2}{\sigma_1}\right) \times 100 \tag{61}$$

$$\sigma_1 = \sqrt{\sum_{i=1}^{N} \left(\frac{C_{1i}}{C_1} - 1\right)^2} \tag{62}$$

$$\sigma_2 = \sqrt{\sum_{i=1}^{N} \left(\frac{C_{2i}}{C_2} - 1\right)^2} \tag{63}$$

where C_{1i} = conductivity of pixel i in Tomogram 1; C_1 = average conductivity in Tomogram 1; C_{2i} = conductivity of pixel i in Tomogram 2; C_2 = average conductivity in Tomogram 2; N = the number of pixels in a Tomogram (316 pixels per each Tomogram)

Furthermore, the mixing index is one index that can be told about characteristic of mixing distributions of the fluid as shown in Figures 53-60. Table 6 shows the mean values of mixing index in the riser and downcomer at different superficial gas velocities of both columns. The absolute mean values of mixing index in the riser and downcomer are in the ranges of 0.156-0.280 and 0.119-0.235, respectively. It was apparent that the mean value of mixing index was increased with

increasing of the superficial gas velocities in the riser. High gas velocity in the riser induces more gas holdup in the riser leading to more mixing.

In addition, at high gas velocity in the riser the fluctuation of mixing index is higher as shown in Figures 53-60 because the flow is in the turbulent regime. However, the mixing index in the riser was decreased with increasing of the superficial gas velocity in the downcomer. Gas flow with high velocity in the downcomer impedes the flow circulated from the riser to the downcomer. Thus, the fluid was less fluctuated in the riser. Therefore, the fluid in the riser has less mixing at higher superficial gas velocity in the downcomer.

The results of mixing index in the downcomer are shown in Figures 53-60. It was found that the mean value and the fluctuation of mixing index were increased with increasing of the superficial gas velocities of both columns. Comparing the mixing in both columns, the mixing index distribution in the downcomer has less fluctuation than that in the riser due to less feed gas velocity in the downcomer leading to less turbulence. Therefore, the flow behavior in the riser has more mixing than that in the downcomer. Moreover, it was found that the average mixing indexes were close to 0. In the system used only tap water; the only one variable that affected the conductivity value was the superficial gas velocity. The conductivity value was increased with increasing of the superficial gas velocities of both columns.

1.5 Gas holdup by pressure drop measurements

Figure 61 shows the overall gas holdups in the system obtained by measuring the different levels of fluid in the riser and downcomer at different superficial gas velocities of both columns. Calculation of these values was obtained from the ratio between volume of gas divided by volume of both gas-liquid (Hossein *et al.,* 2005) as follows:

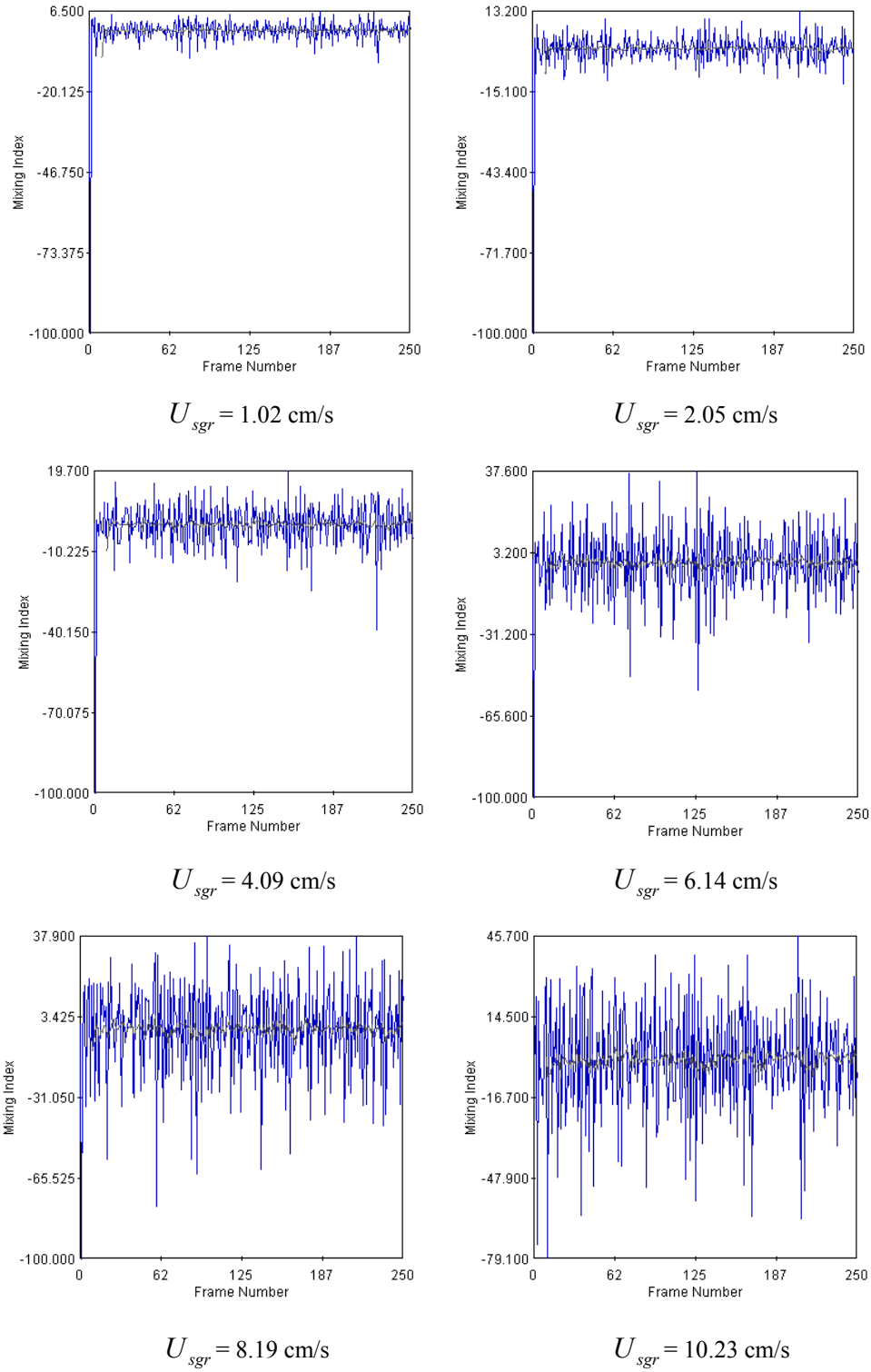

U_{sgr} = 1.02 cm/s

U_{sgr} = 2.05 cm/s

U_{sgr} = 4.09 cm/s

U_{sgr} = 6.14 cm/s

U_{sgr} = 8.19 cm/s

U_{sgr} = 10.23 cm/s

Figure 53 Mixing index in the riser at the superficial gas velocities in the riser of 1.02-10.23 cm/s and in the downcomer of 0 cm/s.

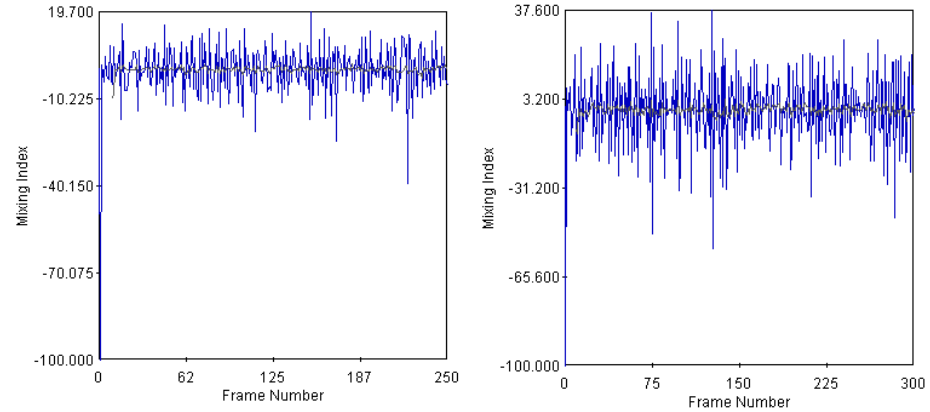

U_{sgr} = 2.05 cm/s

U_{sgr} = 4.09 cm/s

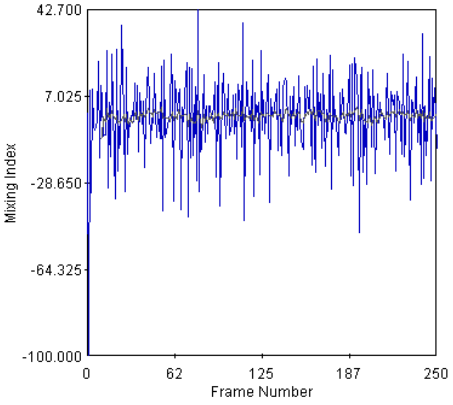

U_{sgr} = 6.14 cm/s

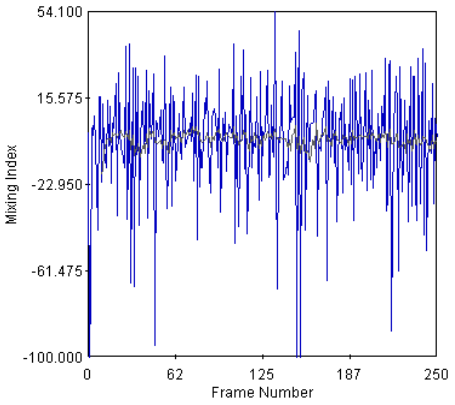

U_{sgr} = 8.19 cm/s

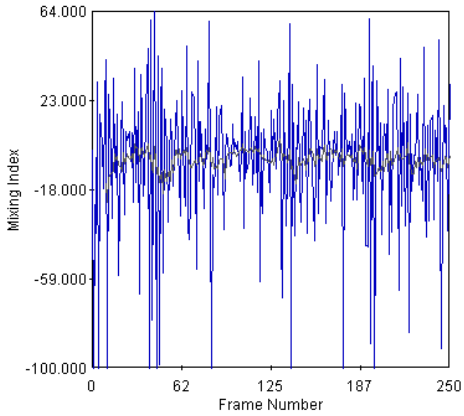

U_{sgr} = 10.23 cm/s

Figure 54 Mixing index in the riser at the superficial gas velocities in the riser of 2.05-10.23 cm/s and in the downcomer of 1.02 cm/s.

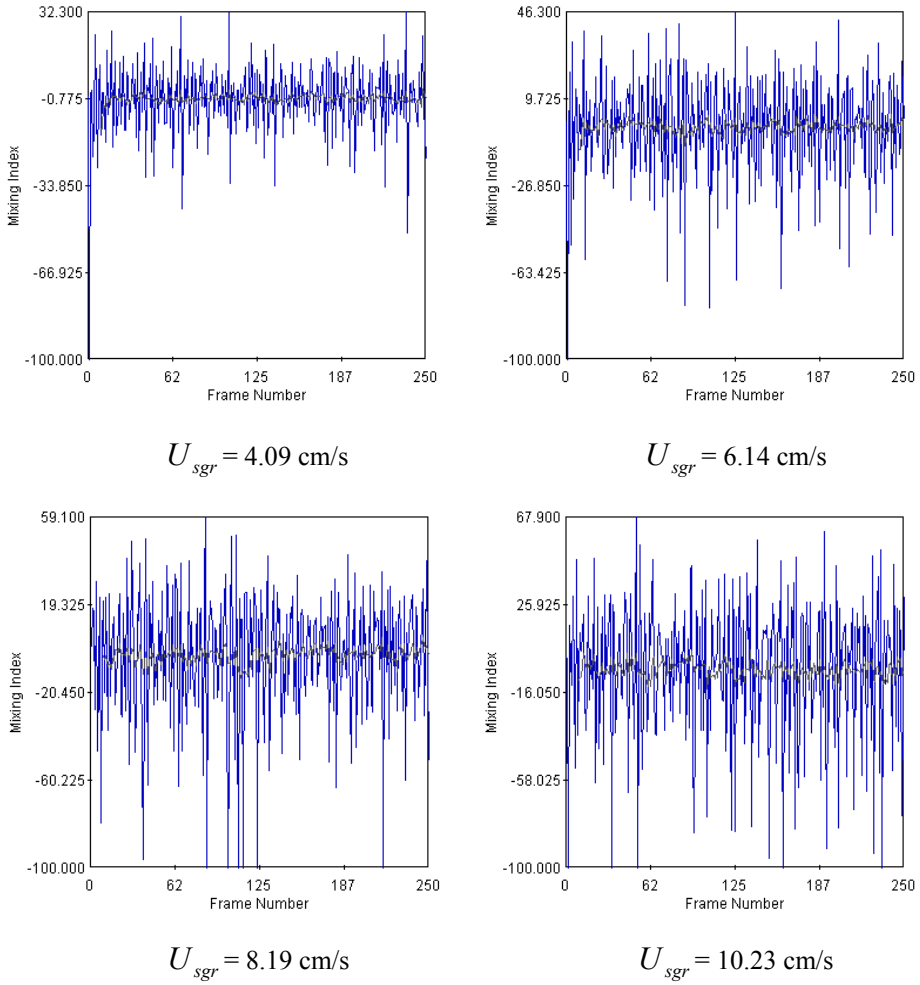

U_{sgr} = 4.09 cm/s

U_{sgr} = 6.14 cm/s

U_{sgr} = 8.19 cm/s

U_{sgr} = 10.23 cm/s

Figure 55 Mixing index in the riser at the superficial gas velocities in the riser of 4.09-10.23 cm/s and in the downcomer of 2.05 cm/s.

$$\varepsilon_{overall} = \frac{V_G}{V_G + V_L} \tag{64}$$

where V_G is volume of gas in the system; V_L is volume of liquid in the system. In this system, the volume of liquid at the beginning was 73 L. The details in calculating were shown in Appendix D.

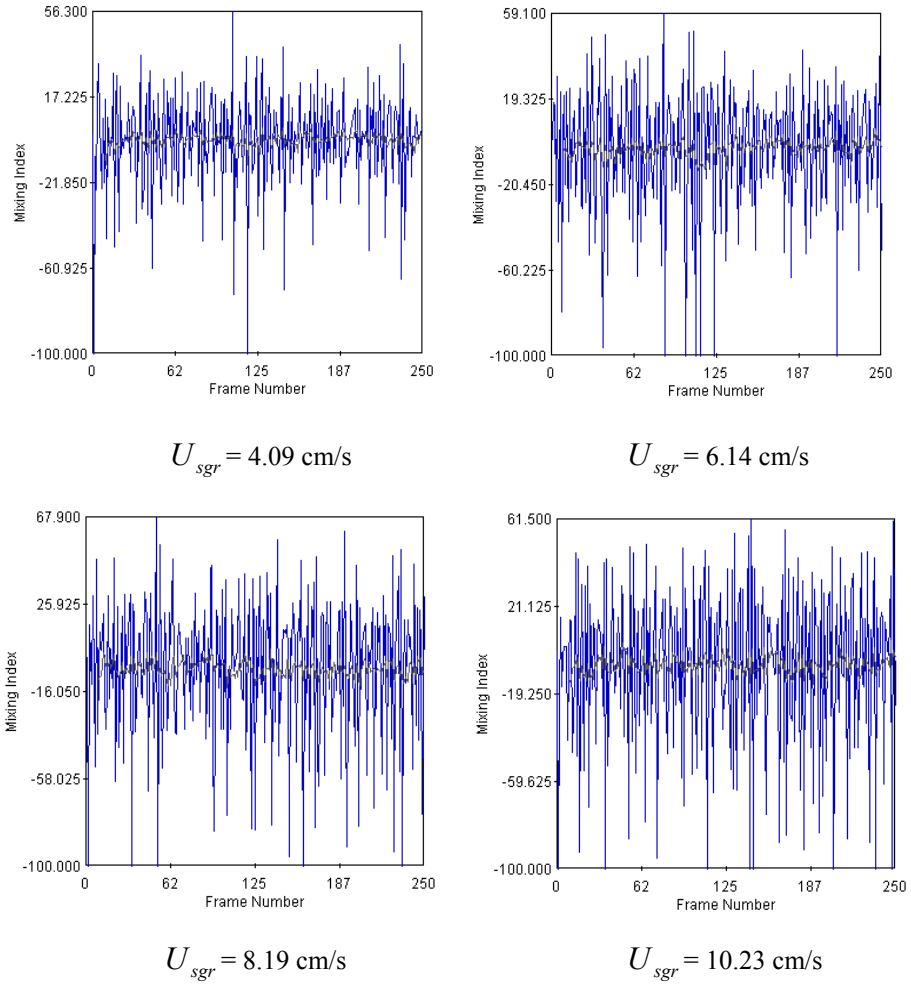

U_{sgr} = 4.09 cm/s

U_{sgr} = 6.14 cm/s

U_{sgr} = 8.19 cm/s

U_{sgr} = 10.23 cm/s

Figure 56 Mixing index in the riser at the superficial gas velocities in the riser of 4.09-10.23 cm/s and in the downcomer of 3.07 cm/s.

The overall gas holdup in the system was increased with increasing of the superficial gas velocities in both columns. Table 7 shows the comparison of overall gas holdup obtained by level measurements and gas holdups in the middle sections of the riser and downcomer by ERT system. It was found that the overall gas holdup obtained by level measurements is higher than the gas holdup in the downcomer but is lower than that in the riser obtained by ERT. The gas holdup values in the riser and downcomer obtained by ERT system are local cross-sectional averaged values in the riser and downcomer at the middle sections of both columns (at height of 47 and 27 cm from the spargers). However, the overall gas holdup obtained by level

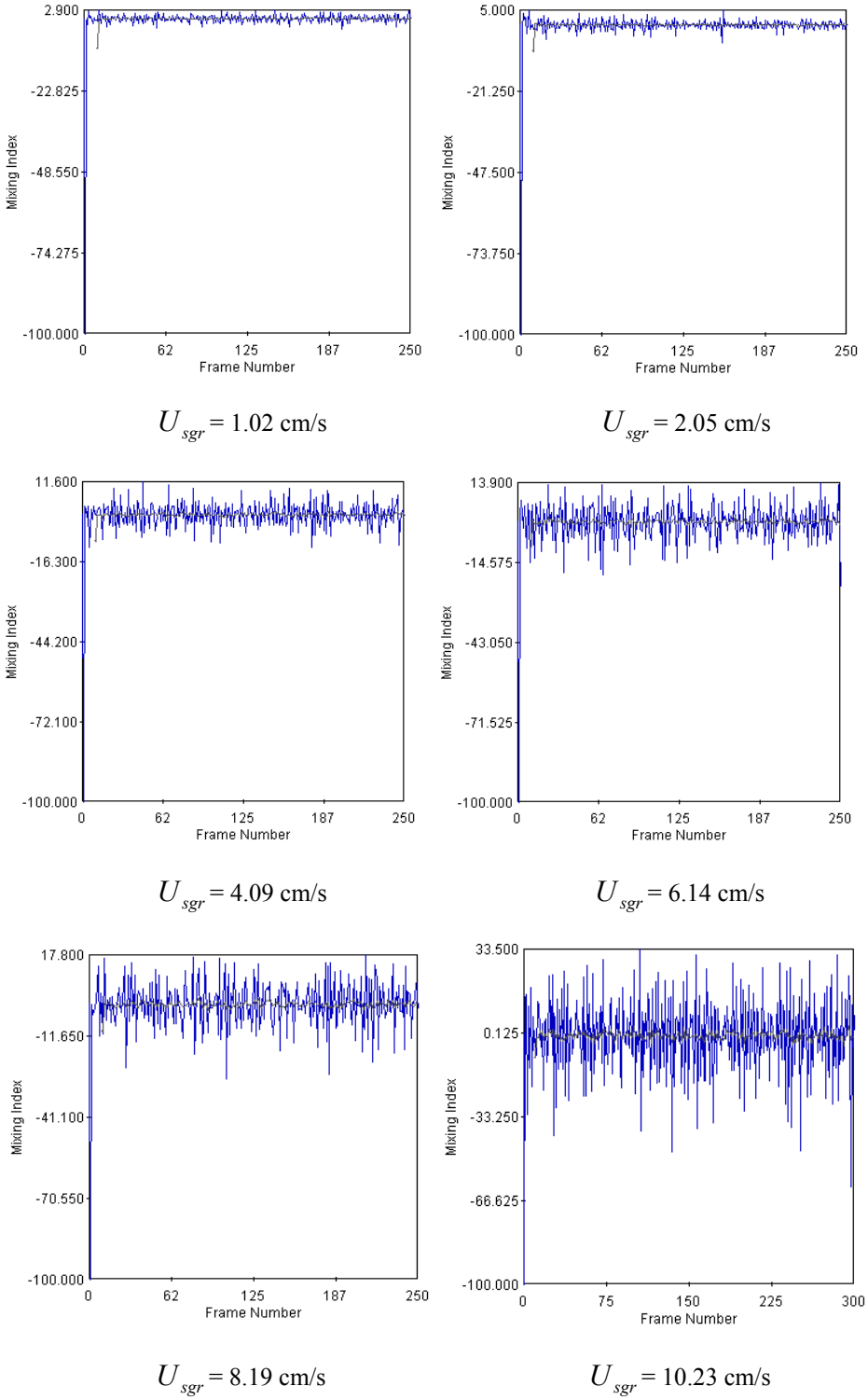

U_{sgr} = 1.02 cm/s

U_{sgr} = 2.05 cm/s

U_{sgr} = 4.09 cm/s

U_{sgr} = 6.14 cm/s

U_{sgr} = 8.19 cm/s

U_{sgr} = 10.23 cm/s

Figure 57 Mixing index in the downcomer at the superficial gas velocities in the riser of 1.02-10.23 cm/s and in the downcomer of 0 cm/s.

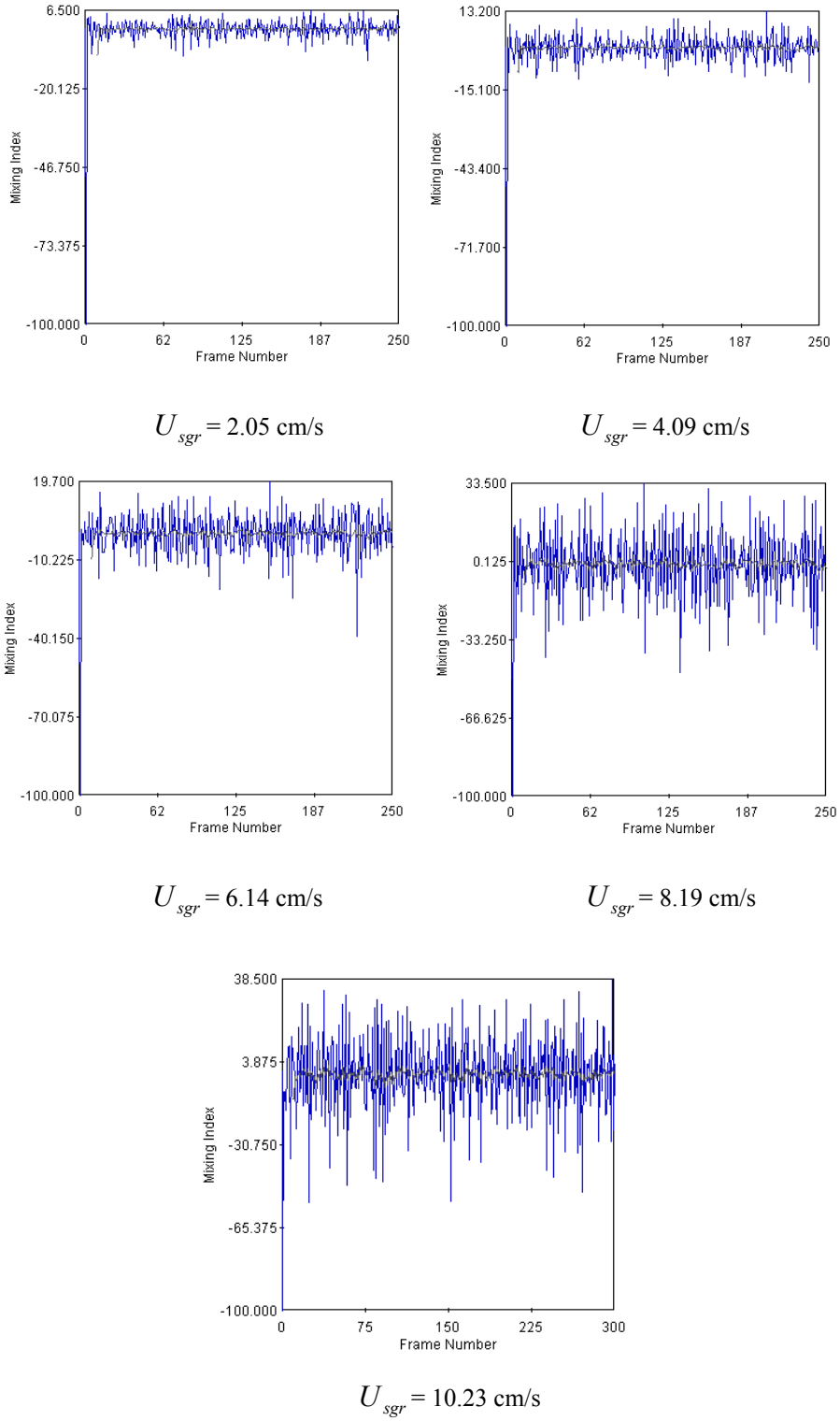

Figure 58 Mixing index in the downcomer at the superficial gas velocities in the riser of 2.05-10.23 cm/s and in the downcomer of 1.02 cm/s.

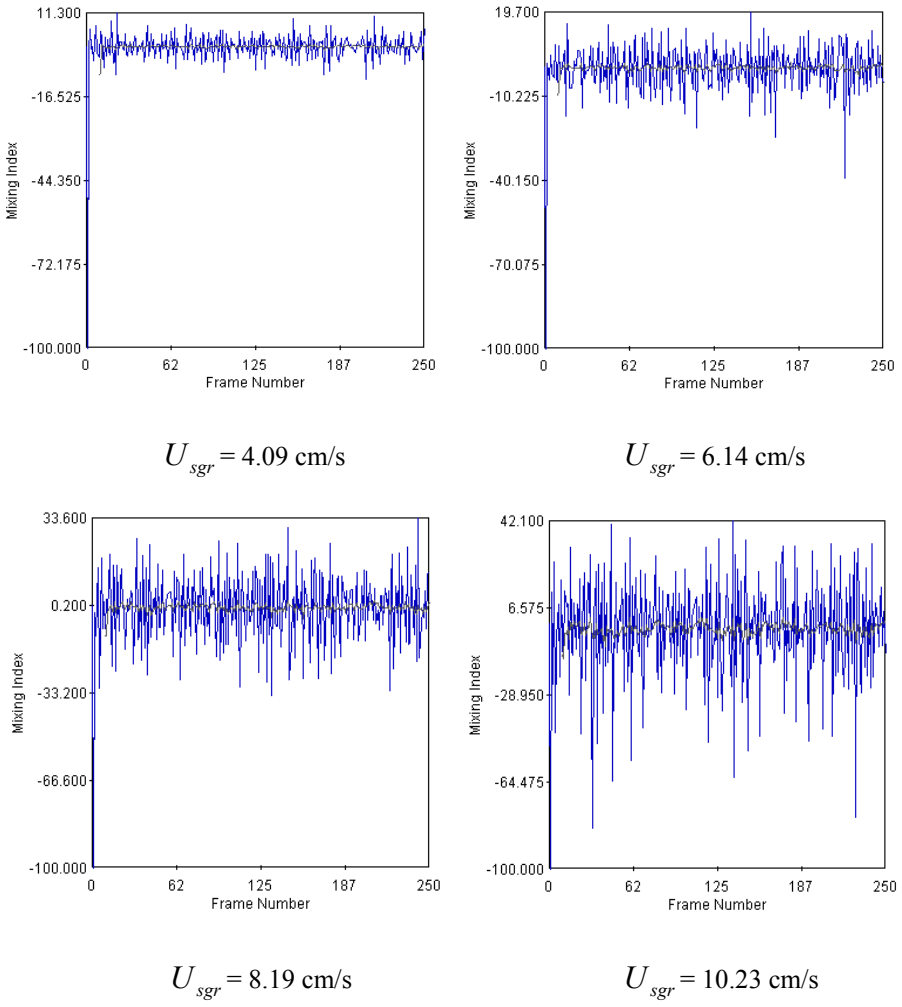

U_{sgr} = 4.09 cm/s

U_{sgr} = 6.14 cm/s

U_{sgr} = 8.19 cm/s

U_{sgr} = 10.23 cm/s

Figure 59 Mixing index in the downcomer at the superficial gas velocities in the riser of 4.09-10.23 cm/s and in the downcomer of 2.05 cm/s.

measurements is axially averaged value in the system. The difference of gas holdup values in both methods was increased with increasing of the superficial gas velocities of both columns.

Figures 62-65 show the gas holdup in the riser and downcomer using pressure drop measurement. This method measures the pressure difference (ΔP) between the two levels along the column length (Kaustubha *et al.,* 2006). The gas holdup is related to the pressure drop by:

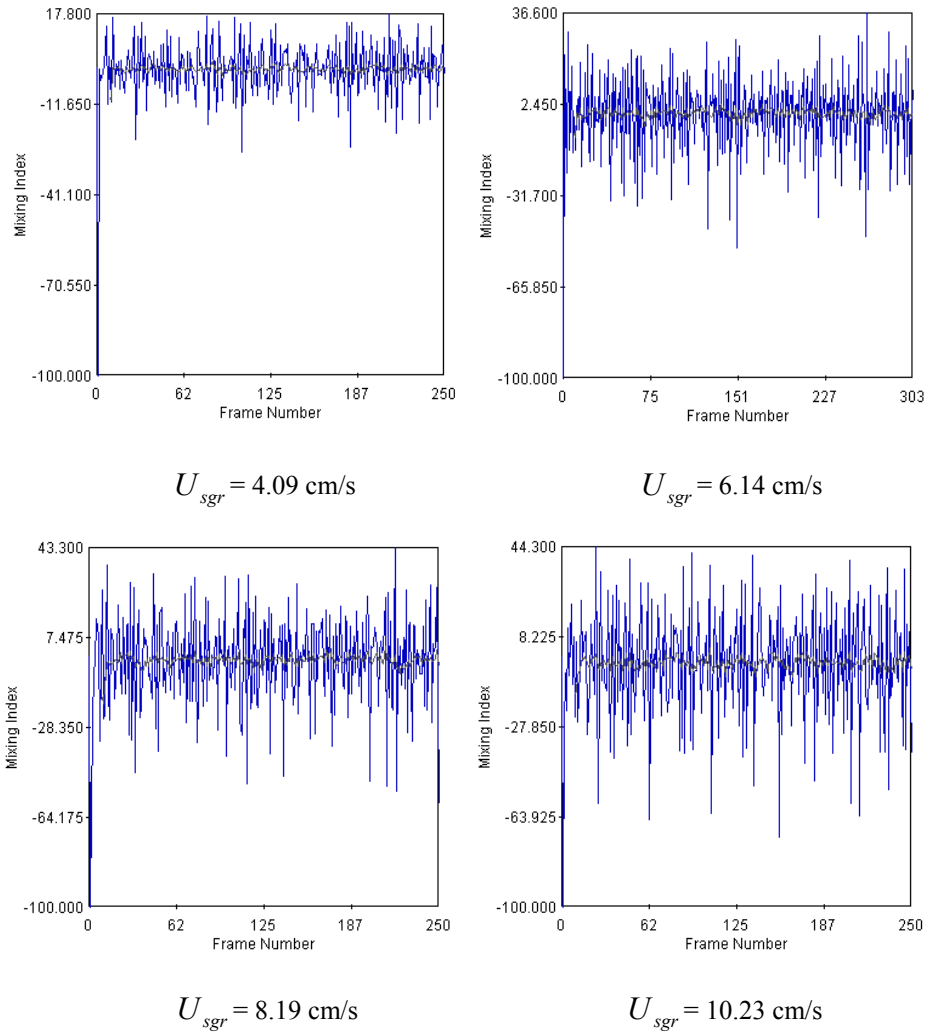

U_{sgr} = 4.09 cm/s

U_{sgr} = 6.14 cm/s

U_{sgr} = 8.19 cm/s

U_{sgr} = 10.23 cm/s

Figure 60 Mixing index in the downcomer at the superficial gas velocities in the riser of 4.09-10.23 cm/s and in the downcomer of 3.07 cm/s.

$$\Delta P = \left(1 - \varepsilon_g\right)\rho_L g \Delta z \tag{65}$$

Measurements of local pressure drop along the column height of the riser and downcomer provide the cross-sectional averaged gas holdup at fixed axial positions. Figures 62-65 show the gas holdup in the riser and downcomer at the superficial gas velocities in the riser and downcomer in the ranges of 0.51-10.23 cm/s and 0-3.07 cm/s, respectively. It was found that the gas holdup in the riser was increased with increasing of the superficial gas velocities of both columns.

Table 6 Mean value of mixing index of the riser and downcomer at different superficial gas velocities of both columns.

U_r, (cm/s)	U_d, (cm/s)	Mean value of mixing index (riser)	Mean value of mixing index (downcomer)
1.02	0	-0.156	-0.119
2.05		0.229	-0.124
4.09		0.249	-0.135
6.14		0.253	0.148
8.19		0.265	-0.159
10.23		-0.280	0.167
2.05	1.02	-0.197	-0.137
4.09		0.215	0.155
6.14		0.231	-0.168
8.19		0.257	0.181
10.23		-0.269	-0.193
4.09	2.05	-0.192	-0.175
6.14		0.219	0.187
8.19		-0.244	0.205
10.23		-0.257	-0.216
4.09	3.07	-0.173	-0.188
6.14		-0.205	-0.196
8.19		-0.235	-0.219
10.23		-0.248	0.235

Furthermore, the gas holdup was decreased along the height in the riser. The gas holdup in the downcomer was decreased along the height of the downcomer. It was increased with increasing of the superficial gas velocities of both columns. In both columns, it was apparent that the gas holdup in the riser is higher than that in the downcomer, because the gas inlet in the riser is higher than that in the downcomer. The gas holdup in both columns was the maximum at the bottom of the columns and was gradually decreased along with the axial distance from the bottom to the top of

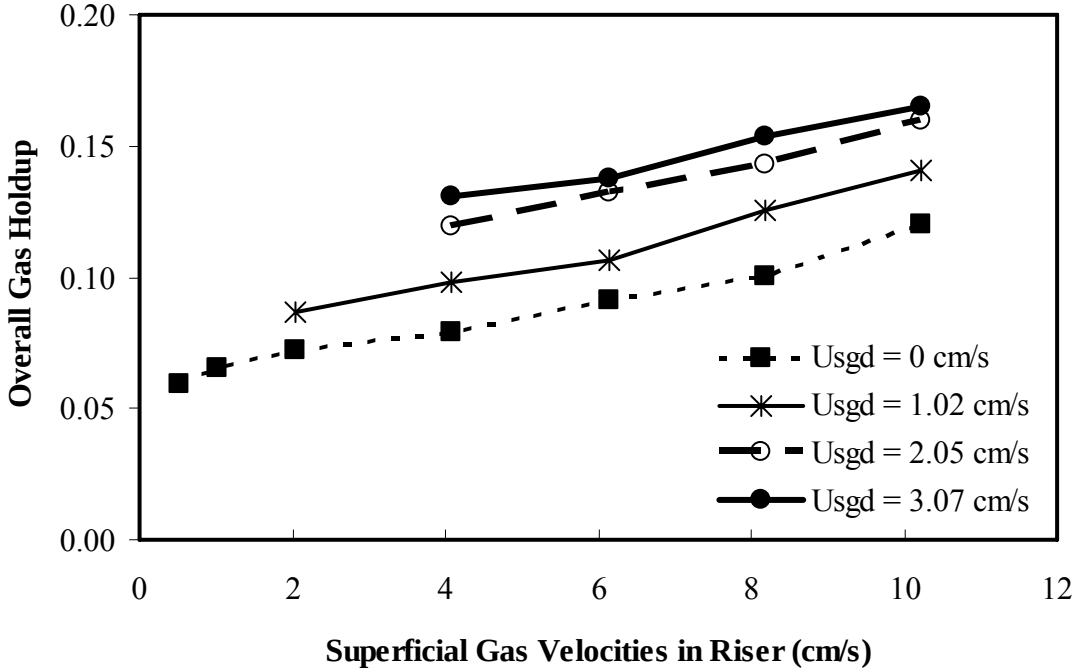

Figure 61 Overall gas holdup in the system at the superficial gas velocities in the riser of 0.51-10.23 cm/s and in the downcomer of 0-3.07 cm/s.

the column, because the spargers were located near the bottom sections. The gas holdup was influenced by the superficial gas velocities. It was increased with increasing of the superficial gas velocities in all sections.

Figure 66 shows the gas holdup in the riser and downcomer obtained by pressure drop measurement and ERT. The gas holdup in the riser and downcomer from ERT system obtained at the middle sections of the columns (at height of 47 and 27 cm from the spargers). The gas holdup from pressure drop measurement in the riser and downcomer obtained at the axial lengths of 25-65 cm and 25-45 cm, respectively. The averaged gas holdup values obtained from both methods in the riser are in a good agreement, especially at low superficial gas velocity in the riser (0.51-4.09 cm/s). However, the gas holdup from pressure drop measurement has slightly higher than the gas holdup from the ERT, because the position of ERT measurement was located slightly above the middle position of pressure drop measurements.

Table 7 Comparison of overall gas holdup obtained by ERT and level measurements.

U_r (cm/s)	U_d (cm/s)	Overall gas holdup by level measurements	Cross-sectional gas holdup in the riser at the middle section by ERT	Cross-sectional gas holdup in the downcomer at the middle section by ERT
0.51	0	0.059	0.079	0.037
1.02		0.066	0.097	0.052
2.05		0.073	0.115	0.062
4.09		0.079	0.142	0.081
6.14		0.091	0.169	0.096
8.19		0.101	0.194	0.107
10.23		0.120	0.204	0.117
2.05	1.02	0.087	0.123	0.067
4.09		0.098	0.155	0.087
6.14		0.106	0.181	0.098
8.19		0.125	0.199	0.119
10.23		0.141	0.216	0.136
4.09	2.05	0.119	0.166	0.094
6.14		0.132	0.185	0.106
8.19		0.143	0.213	0.133
10.23		0.160	0.230	0.143
4.09	3.07	0.130	0.175	0.106
6.14		0.138	0.190	0.118
8.19		0.154	0.219	0.141
10.23		0.165	0.238	0.159

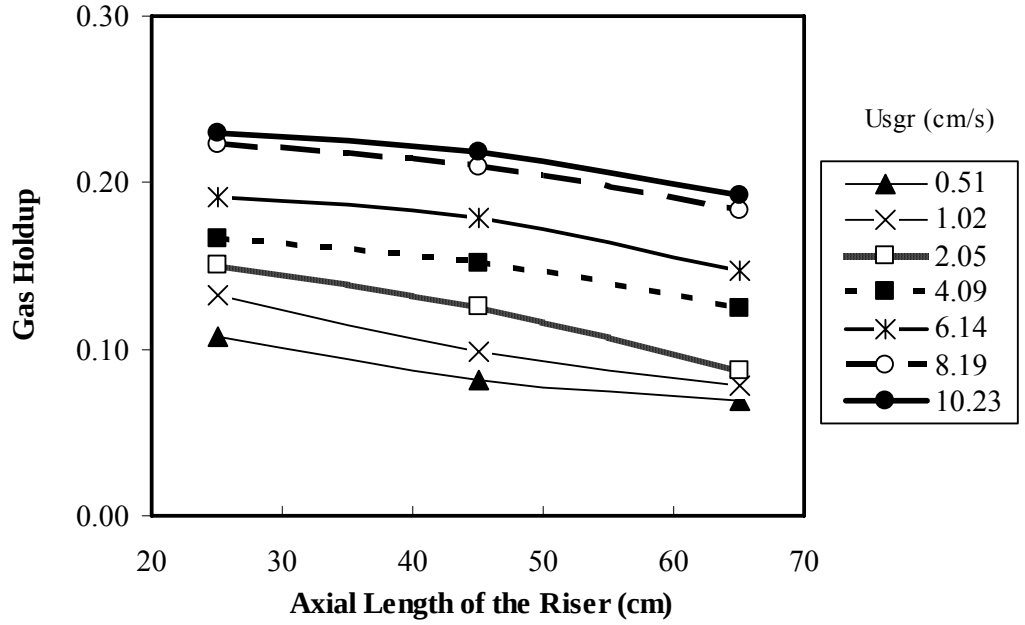

(a) Riser

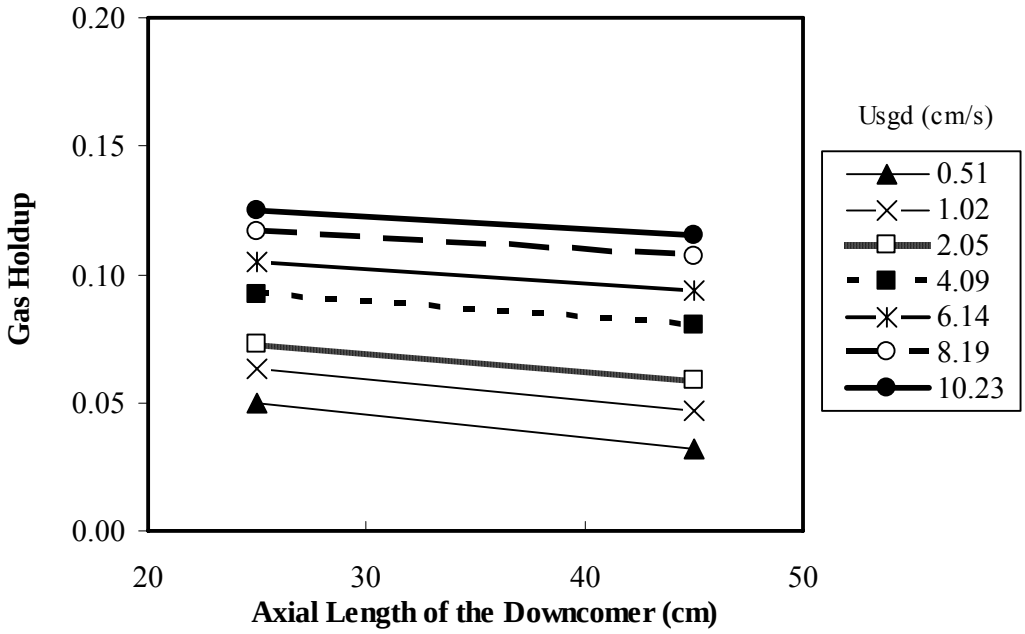

(b) Downcomer

Figure 62 Gas holdup along the different axial distances in the riser and downcomer obtained by pressure drop at the superficial gas velocities in the riser of 0.51-10.23 cm/s and in the downcomer of 0 cm/s (a) in the riser (b) in the downcomer.

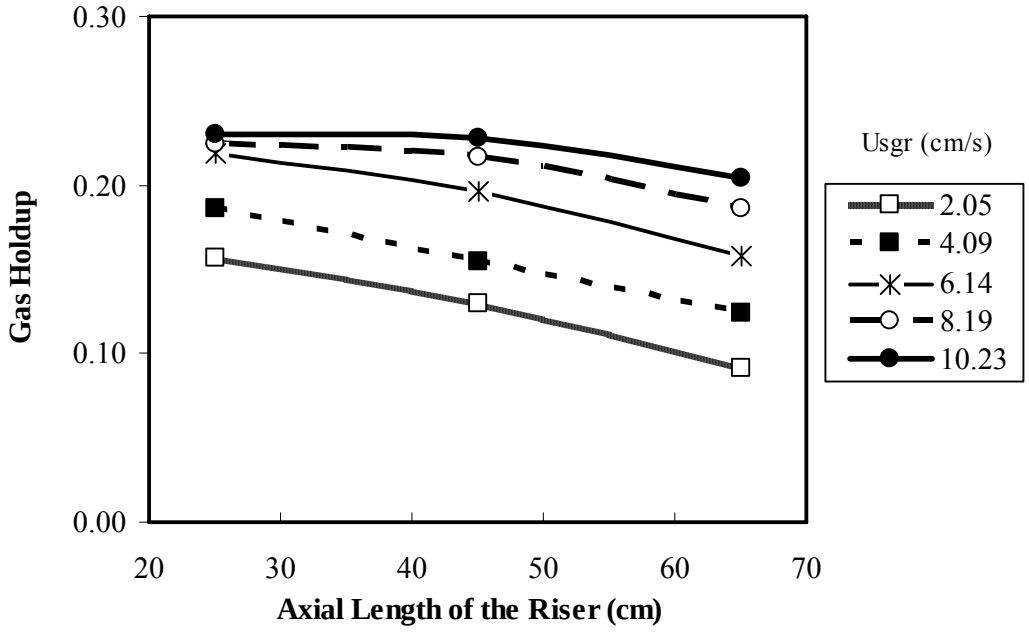

(a) Riser

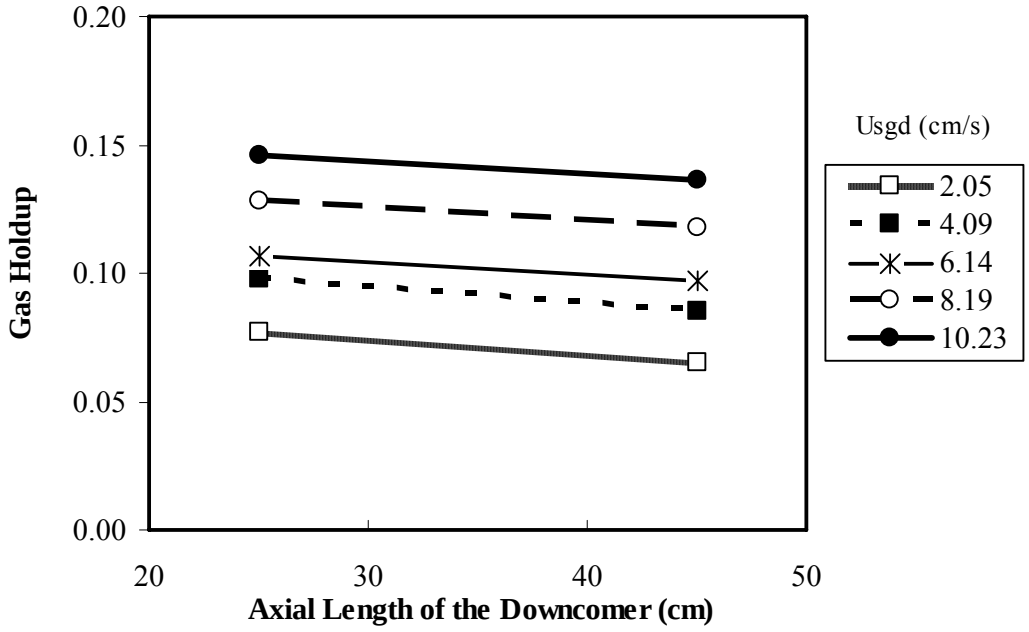

(b) Downcomer

Figure 63 Gas holdup along the different axial distances in the riser and downcomer obtained by pressure drop at the superficial gas velocities in the riser of 2.05-10.23 cm/s and in the downcomer of 1.02 cm/s (a) in the riser (b) in the downcomer.

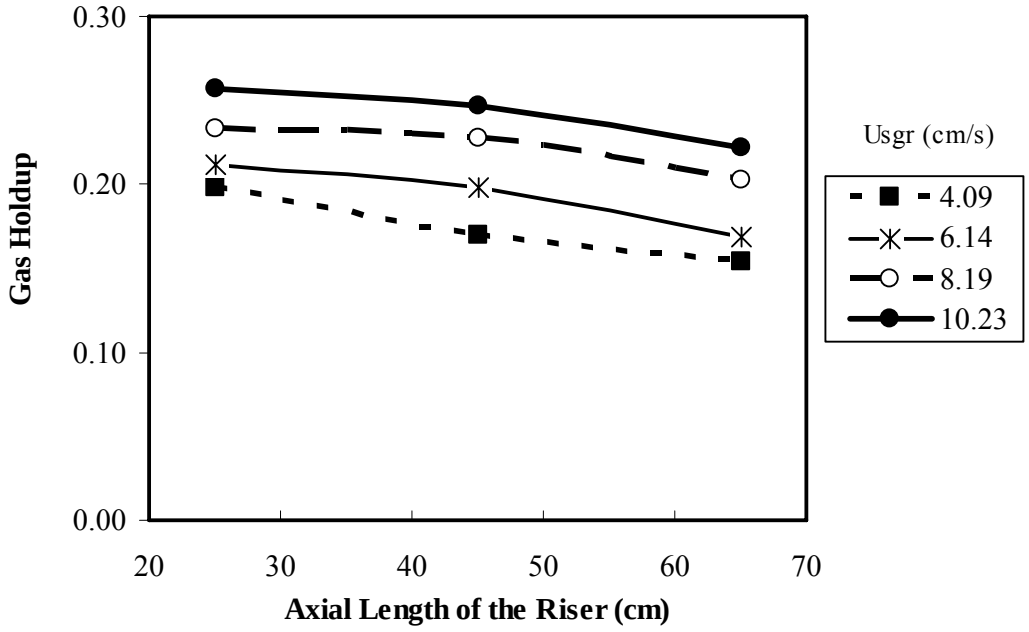

(a) Riser

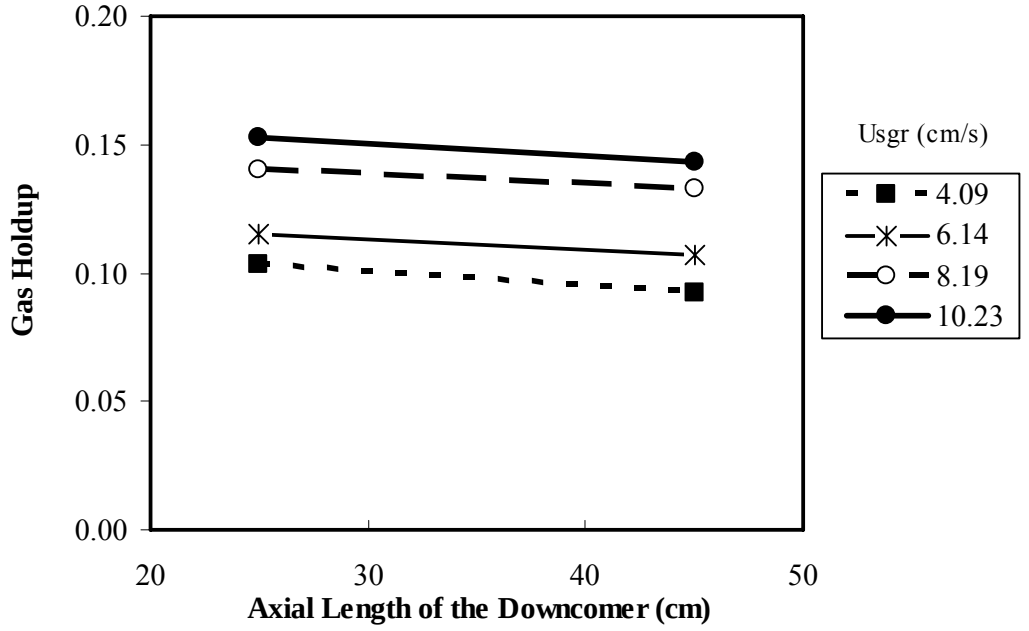

(b) Downcomer

Figure 64 Gas holdup along the different axial distances in the riser and downcomer obtained by pressure drop at the superficial gas velocities in the riser of 4.09-10.23 cm/s and in the downcomer of 2.05 cm/s (a) in the riser (b) in the downcomer.

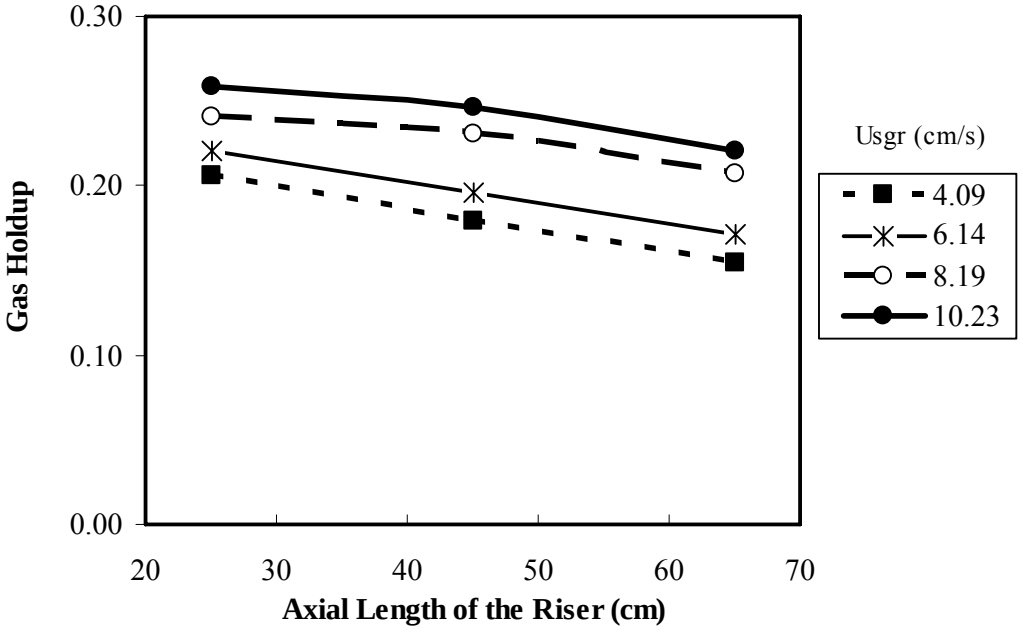

(a) Riser

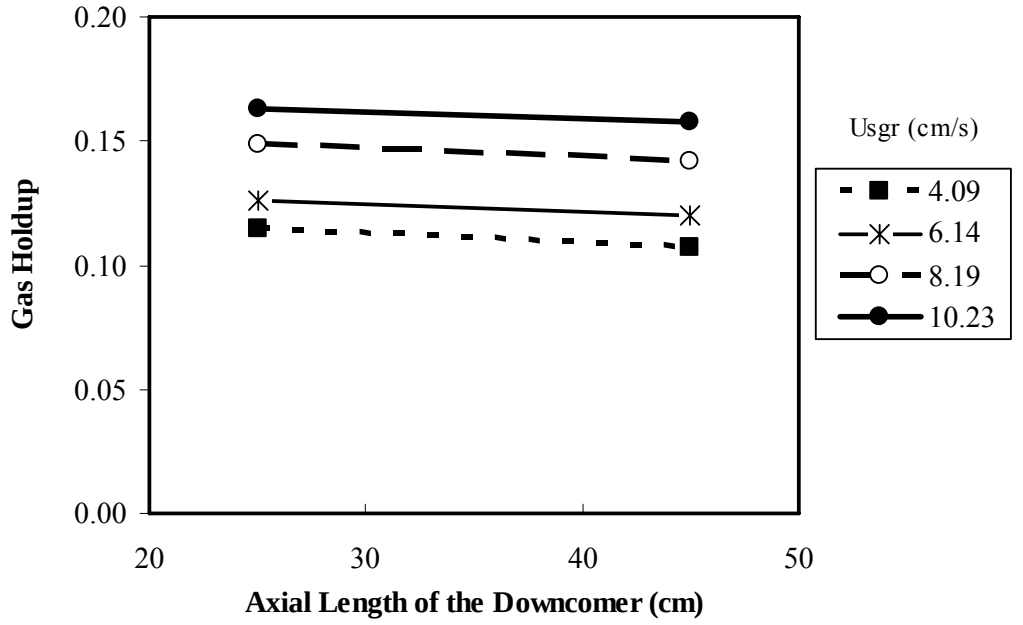

(b) Downcomer

Figure 65 Gas holdup along the different axial distances in the riser and downcomer obtained by pressure drop at the superficial gas velocities in the riser of 4.09-10.23 cm/s and in the downcomer of 3.07 cm/s (a) in the riser (b) in the downcomer.

Without inlet gas in the downcomer, the gas holdup still existed because the gas bubbles from the riser were induced to the downcomer. Moreover, the gas holdup obtained by pressure drop is slightly higher than that obtained by ERT for all cases. This is due to the gas holdup measured by ERT is a slice value while the gas holdup measured by a pressure drop measurement is a value for an axial section.

1.6 Bubble diameters in the riser and downcomer

Figures 67 and 68 show the average bubble diameters in the riser and downcomer, respectively. The superficial gas velocities in the riser and downcomer are 6.14 cm/s and 1.02 cm/s, respectively. In the riser, the size of bubble diameters was increased along the bed height. This result corresponds to the axial gas holdup profile. The gas holdup decreased along with the bed height. The size of bubble diameters was increased with decreasing of the gas holdup. Furthermore, the bubble diameters at the top of the column (at 90-105 cm) were reduced, since the pressure drop dramatically changed at the surface of the fluid. In the downcomer, it was found that the size of bubbles were fluctuated along with the axial distance of the downcomer, because the size of bubbles was influenced by the circulated downflow from the riser and the up flow from the feed gas in the downcomer.

Table 8 shows the relation between gas holdups along with the axial length of columns and bubble diameters in the riser and downcomer. It can be seen that the size of bubble diameters was increased with increasing along with the axial distance from the bottom to the top of the columns. The average bubble diameter in the riser and downcomer are 2.8 and 3.6 mm, respectively as shown in Figure 69. From the previous results, the average bubble diameter in the riser is less than that in the downcomer because the average gas holdup in the riser is more than that in the downcomer. Furthermore, the gas holdup was decreased with increasing along the axial distance of both columns.

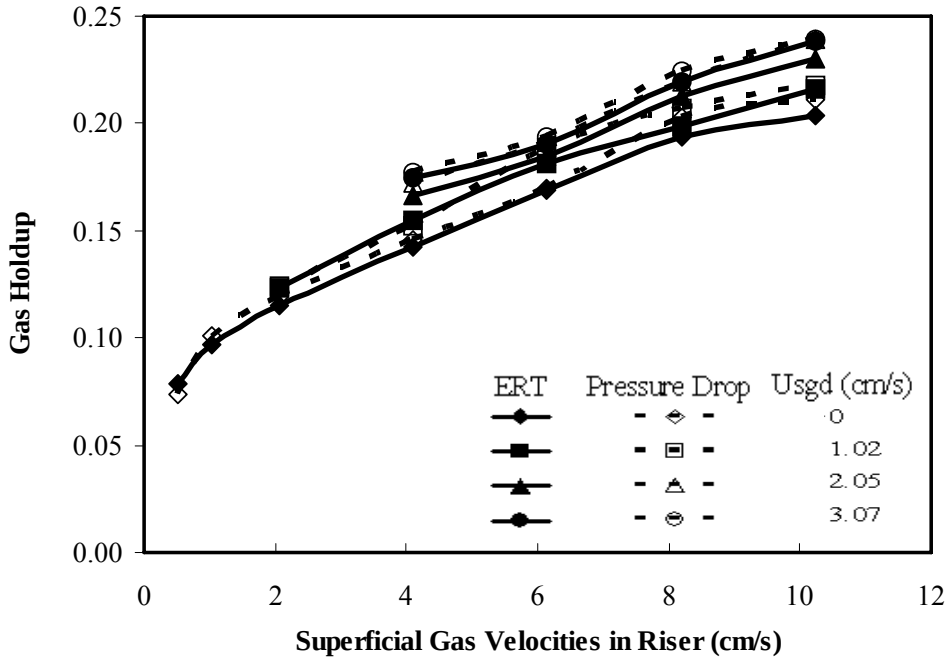

(a) Riser

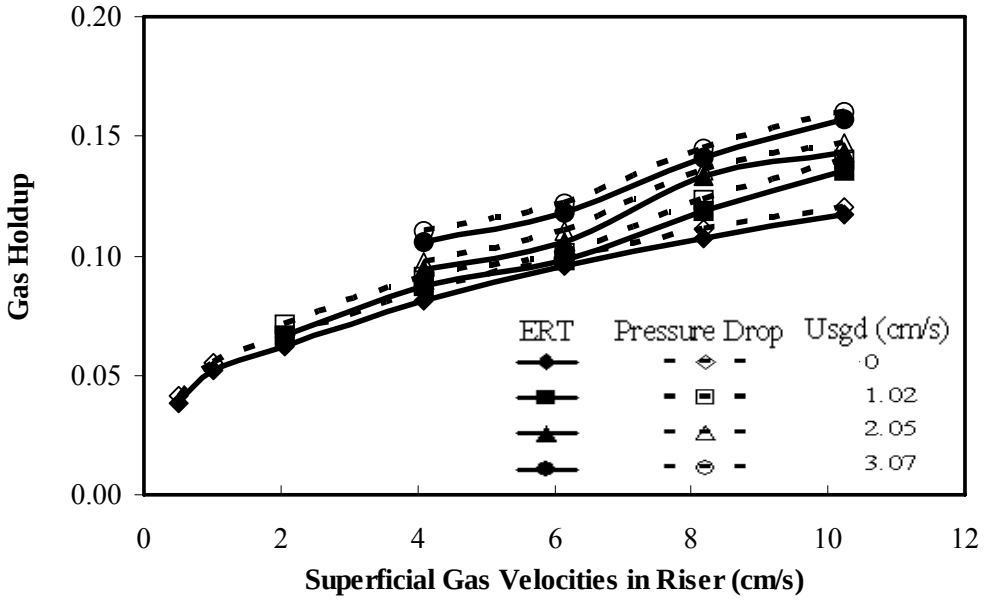

(b) Downcomer

Figure 66 Comparison of gas holdup profiles obtained by the pressure drop measurements and ERT system at the superficial gas velocities in the riser of 0.51-10.23 cm/s and in the downcomer of 0-3.07 cm/s (a) in the riser (b) in the downcomer.

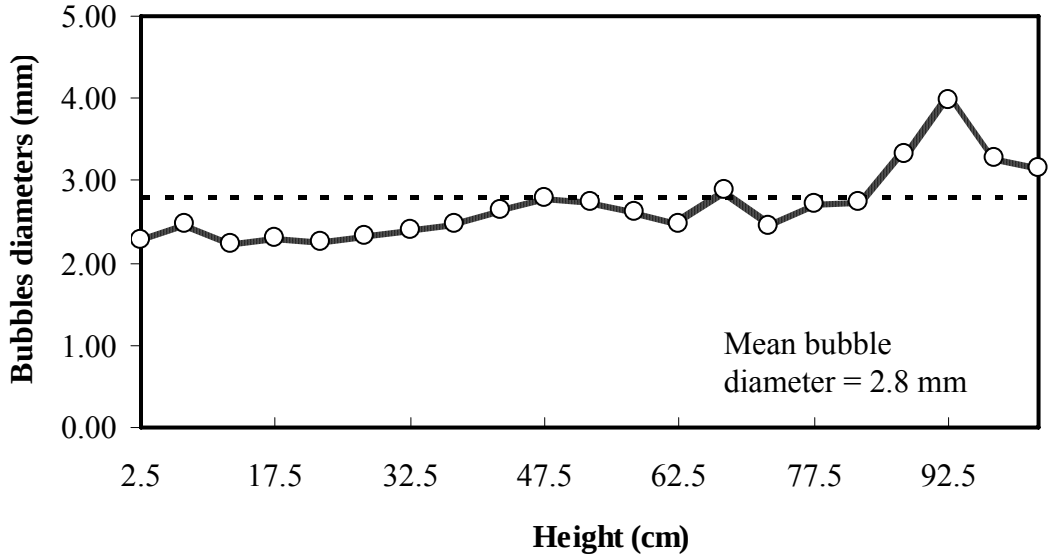

Figure 67 Bubble diameters along the bed height of the riser measured by a camera at the superficial gas velocities in the riser of 6.14 cm/s and in the downcomer of 1.02 cm/s.

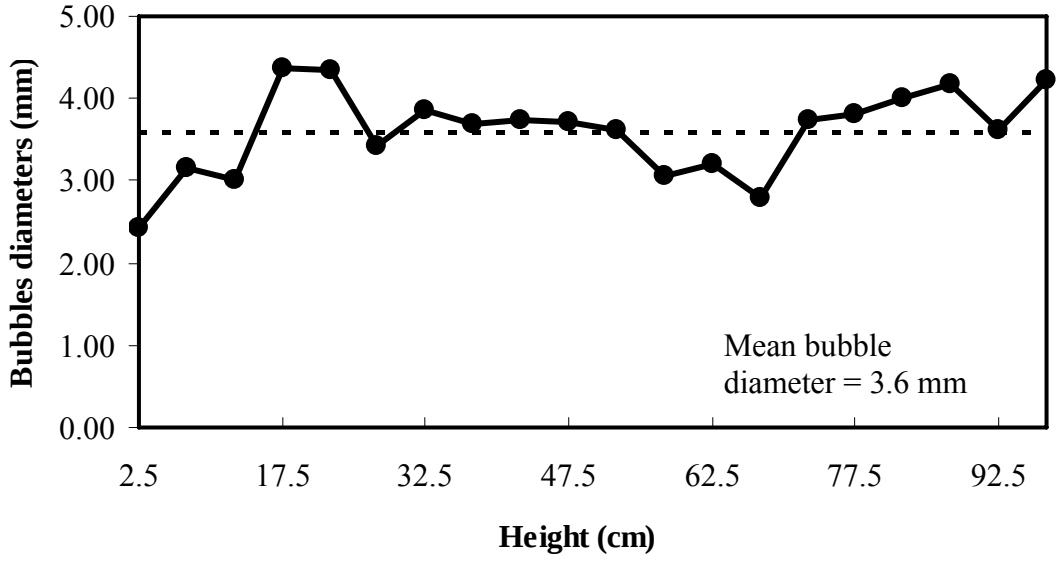

Figure 68 Bubble diameters along the bed height of the downcomer measured by a camera at the superficial gas velocities in the riser of 6.14 cm/s and in the downcomer of 1.02 cm/s.

Table 8 Gas holdup and averaged bubble diameters along the bed height in the riser and downcomer.

Parameters \ Height (cm) (bottom to top)	H_r = 25 cm	H_r = 45 cm	H_r = 65 cm	H_d = 25 cm	H_d = 45 cm
ε_{riser}	0.219	-	-	-	-
ε_{riser}	-	0.196	-	-	-
ε_{riser}	-	-	0.158	-	-
d_{B_riser} (mm)	2.4	-	-	-	-
d_{B_riser} (mm)	-	2.5	-	-	-
d_{B_riser} (mm)	-	-	2.6	-	-
ε_{down}	-	-	-	0.107	-
ε_{down}	-	-	-	-	0.097
d_{B_down} (mm)	-	-	-	3.7	-
d_{B_down} (mm)	-	-	-	-	4.0

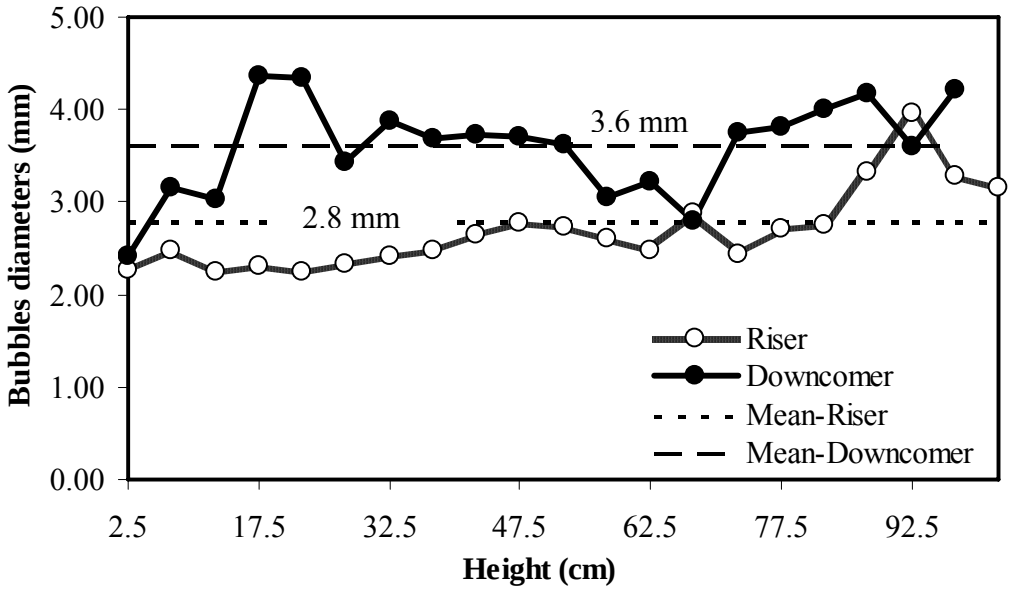

Figure 69 Bubble diameters along the bed height of the columns measured by a camera at the superficial gas velocities in the riser of 6.14 cm/s and in the downcomer of 1.02 cm/s.

2. Residence time distribution (RTD)

2.1 RTD analysis method and axial dispersion model

Pulse input was used in this study. This method requires a very small volume of tracer at the inlet of the tracer. The outlet concentration is then measured as a function of time. The effluent concentration-time curve is referred as the *C-curve* in the RTD analysis. To find the *E-curve* from the C_{pulse} curve the concentration is simply changed such that the area under the curve is unity. Thus, the concentration is divided by area under curve ($\sum C\Delta t$). The residence time distribution based on the dimensionless time unit ($\theta = t/\bar{t}$) is written as:

$$E_\theta = \bar{t}E = \frac{\bar{t}C}{area\ under\ curve} = \frac{\bar{t}C}{\sum C\Delta t} \tag{66}$$

In this system the boundary conditions are open-open boundary conditions. The axial dispersion model was chosen in this system to evaluate the mixing parameters. The condition of large deviation from plug flow, $(D/uL) > 0.01$ is applied. In addition, the tracer injection and response measurement methods in this work provide the information based on open-open conditions. Therefore, the residence time distribution derived by Levenspiel and Smith (1957) is written as a function of the dispersion parameter, (D/uL).

$$E_\theta = \frac{1}{\sqrt{4\pi(D/uL)\theta}} exp\left[-\frac{(1-\theta)^2}{4\theta(D/uL)}\right] \tag{67}$$

(D/uL) is the dimensionless group characterizing the spread in the whole vessel, called the vessel dispersion number, and is the parameter that measures the extent of axial dispersion. Thus $(D/uL) \to 0$ is meaning of negligible dispersion, hence plug flow and $(D/uL) \to \infty$ is meaning of large dispersion, hence mixed flow.

The pulse response is broad and it passes the measurement point slowly enough that it changes shape.

The parameters, (D/uL) and $\bar{t}$ in Equation 67 are the unknown parameters that can be obtained by fitting the experimental E_θ curve with the axial dispersion model (Equation 67). (D/uL) and $\bar{t}$ in the Equation 67 are adjustable parameters. To evaluate (D/uL) and $\bar{t}$, the measured tracer curve has to be matched with the theoretical curve as following steps.

a). The dispersion parameter (D/uL) is firstly guessed.

b). The mean residence time, $\bar{t}$, is guessed.

c). Knowing (D/uL) and $\bar{t}$, the theoretical E_θ can be calculated by the axial dispersion model, Equation 67.

d). The calculated E_θ with the guessed $\bar{t}$ is converted to E_t by Equation 66.

e). The area under the concentration curve is assumed.

f). The calculated E_t with the guessed area under the C_t *-curve* is transformed into a concentration curve using Equation 66.

g). The area under the obtained from the concentration curve is compared with the guessed area under the curve. If they are not matched, a new area under the curve is guessed again. Then go to Step *F*. If they are matched, the corrected area under the curve will be obtained.

h). $\bar{t}$ can be obtained from the calculated concentration curve (from Step *F*) and is compared with the guessed $\bar{t}$ from Step *B*. If they are not matched, a new $\bar{t}$ is guessed again and then goes to Step *C*. If they are matched, the corrected $\bar{t}$ is obtained.

i). The calculated concentration curve from Step *F* is compared with the experimental concentration curve. If their shapes are not matched, a new value of (D/uL) is guessed. If they are matched, a corrected value of (D/uL) is obtained.

Figures 70-72 show the concentration-time curve obtained from the tracer measurement at the superficial gas velocity in the riser of 6.14 cm/s and in the downcomer of 1.02 cm/s.

The adjustable parameters, (D/uL) of 1 and $\bar{t}$ of 75.09 s obtained from a trial and error search provide the calculated concentration curve as shown in Figure 72. Figure 73 shows a good fit of the calculated and experimental concentration curves. The experimental concentration-time curve can be converted to E_t and E_θ curves. Figures 74 and 75 show the E_t and E_θ curves obtained from the experiments and calculations. In this case, the parameters in the axial dispersion model, (D/uL) of 1 and $\bar{t}$ of 75.09 s are obtained. (D/uL) more than 0.01 implies that the fluid flow behavior in the riser was large deviation from a plug flow and more close to mixed flow.

Figure 76 shows the fitting of the exit age distribution $E(\theta)-curves$ obtained from the experiments and axial dispersion model (Equation 67) at various superficial gas velocities of the riser and no gas inlet of the downcomer. The vessel dispersion number (D/uL) was increased from 0.23 to 1.3 with increasing of the superficial gas velocities in the riser from 0.51-8.19 cm/s. However, the mean residence time $\bar{t}$ was decreased from 85.51 to 68.09 s with increasing of the superficial gas velocities in the riser. This indicates that at high gas velocity in the riser, the flow behavior approaches more mixing.

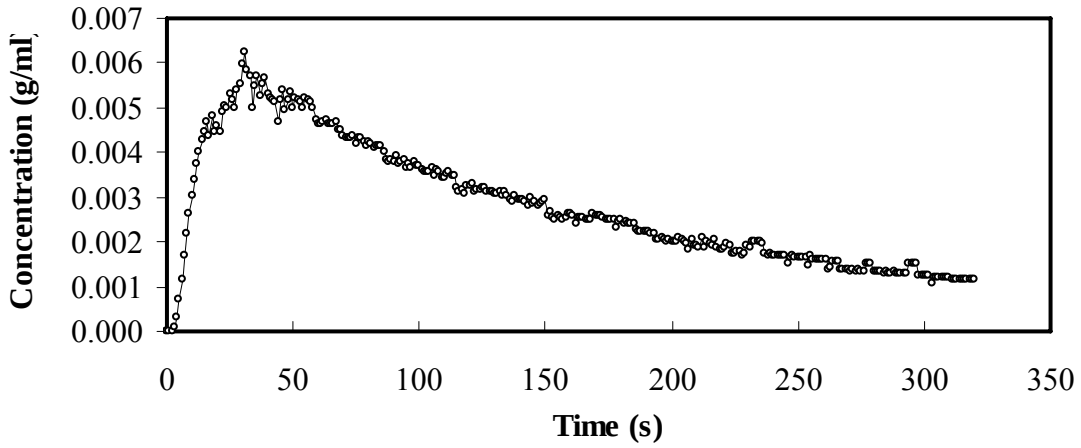

Figure 70 Concentration-time value *C(t)* in the riser obtained by a stimulus-response tracer technique at the superficial gas velocities in the riser of 6.14 cm/s and in the downcomer of 1.02 cm/s.

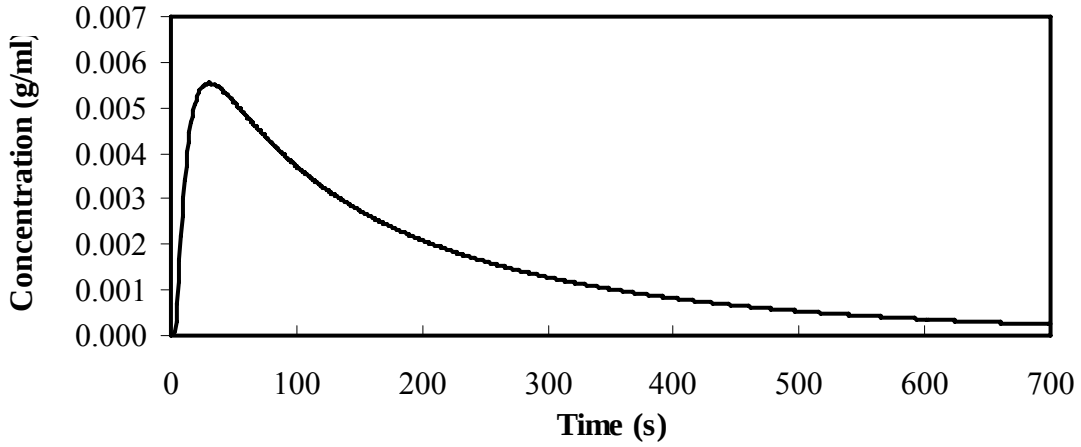

Figure 71 Concentration-time value *C(t)* in the riser calculated from Equation 66 and Equation 67 with (D/uL) of 1 and $\bar{t}$ of 75.09 s at the superficial gas velocities in the riser of 6.14 cm/s and in the downcomer of 1.02 cm/s.

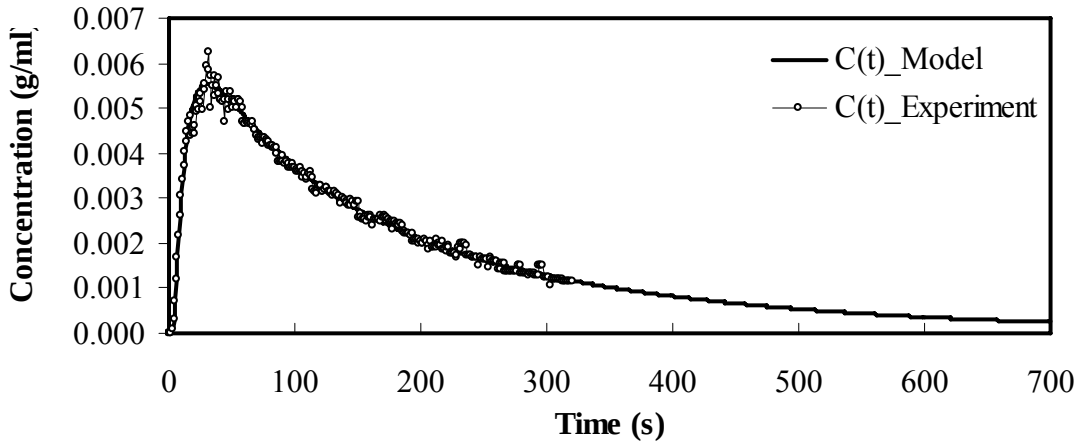

Figure 72 Comparison of concentration-time curves in the riser obtained from the experiments and models at the superficial gas velocities in the riser of 6.14 cm/s and in the downcomer of 1.02 cm/s.

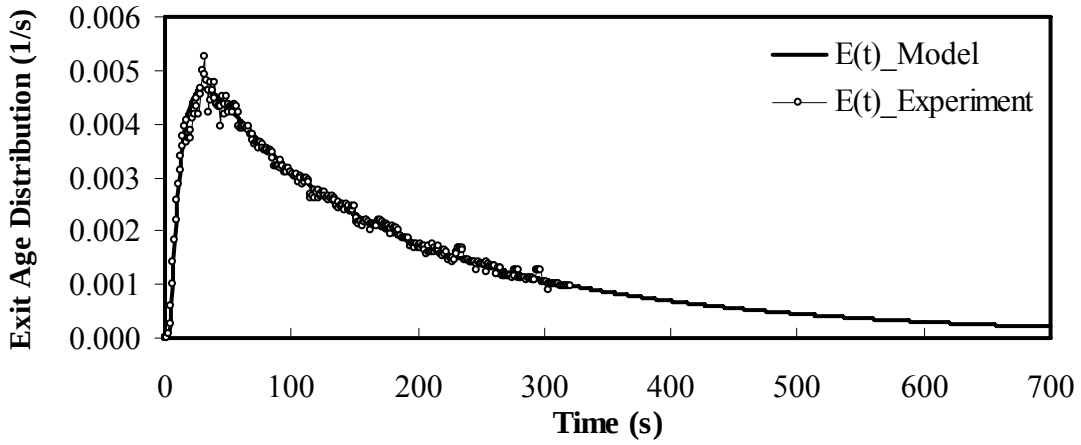

Figure 73 Comparison of exit age distribution (RTD) curve in the riser obtained from the experiments and models at the superficial gas velocities in the riser of 6.14 cm/s and in the downcomer of 1.02 cm/s.

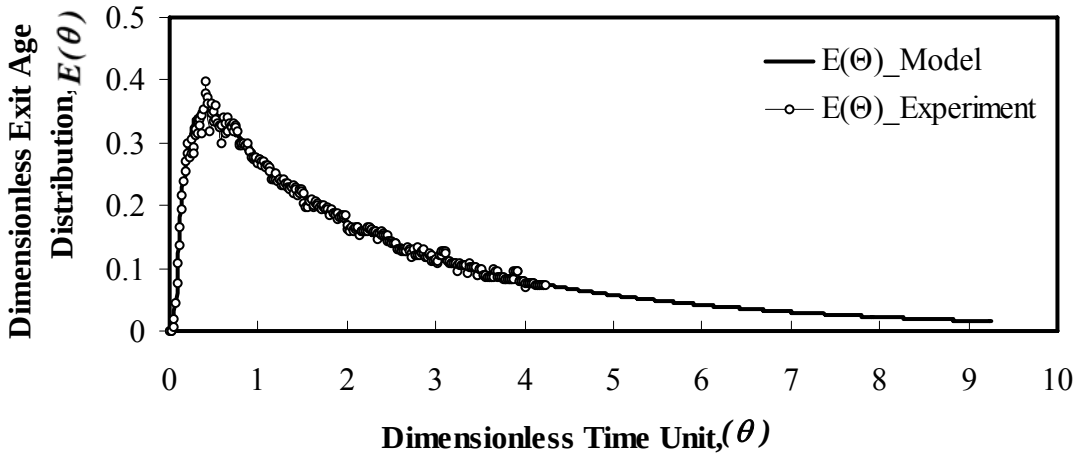

Figure 74 Comparison of the exit age distribution (RTD) based on the dimensionless time unit (θ) curves in the riser obtained from the experiments and models at the superficial gas velocities in the riser of 6.14 cm/s and in the downcomer of 1.02 cm/s.

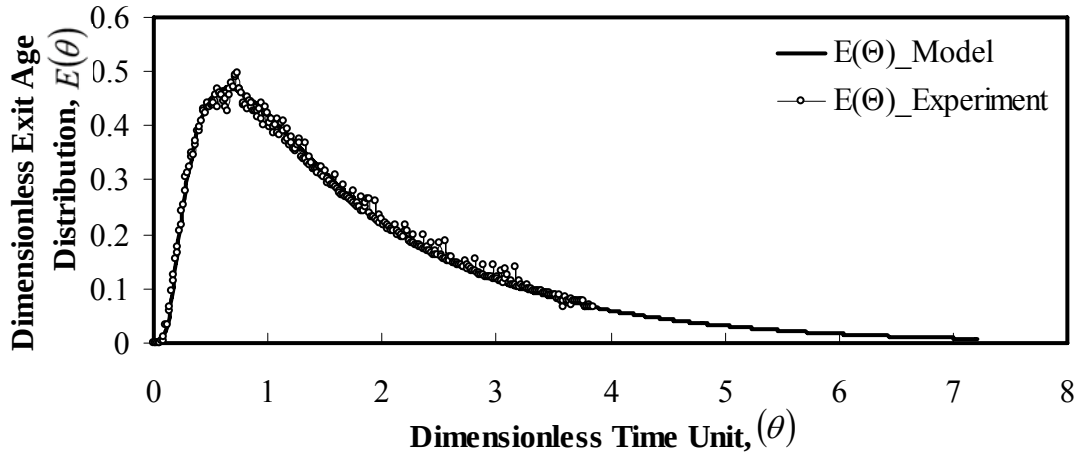

Figure 75 Comparison of the exit age distribution (RTD) based on the dimensionless time unit (θ) curves in the downcomer obtained from the experiments and models at the superficial gas velocities in the riser of 6.14 cm/s and in the downcomer of 1.02 cm/s.

2.2 The effect of the superficial gas velocities in the riser on the dimensionless exit age distribution $E(\theta)$ of the riser and downcomer

Figures 77 a and b show the dimensionless exit age distribution $E(\theta)$-*curves* converted from the response concentration curves and obtained from the axial dispersion models in the riser at different superficial gas velocities in the riser. The superficial gas velocities in the riser are in the range of 0.51-10.23 cm/s with no gas inlet to the downcomer. Figures 78 a and b show the dimensionless exit age distribution $E(\theta)$ -*curves* converted from the response concentration curves and obtained from the axial dispersion models in the downcomer. The vessel dispersion number values (D/uL) in the riser and downcomer corresponds to the axial dispersion models are in the ranges of 0.23-1.51 and 0.08-0.55, respectively as shown in Table 9. The mean residence time values are in the ranges of 64.30-85.51 s and 82.82-96.08 s. It was found that the superficial gas velocity in the riser affects the fluid flow behavior in the riser and downcomer. The vessel dispersion number (D/uL) in both columns was increased with increasing of the superficial gas velocity in the riser (see Table 9 and Figure 81). The fluid flow behavior was a large deviation from a plug flow. The fluid flow behavior in the riser was close to a mixed flow and has more mixing than that in the downcomer. The exit age distribution curve for the downcomer approaches a Gaussian curve more. Therefore the flow behavior in the downcomer has less mixing compared to that in the riser.

In both columns, at high superficial gas velocity in the riser, the fluid flow behavior in the system has more churn-turbulent of the gas-liquid than at low superficial gas velocity. Therefore the fluid flow behaviors in both columns were more close to a mixed flow than a plug flow, when the superficial gas velocity in the riser increased. Furthermore, in the riser the fluid flow behavior was more close to a mixed flow than that in the downcomer because there was gas inlet only in the riser without gas inlet in the downcomer. In the downcomer, although there was no gas inlet gas holdup still existed. When the liquid was circulated from the riser to the downcomer, the gas in the riser was induced to the downcomer. The mixed flow

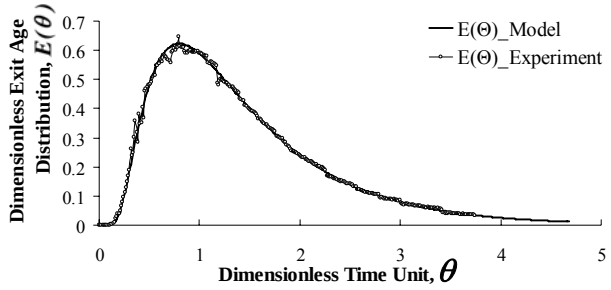

(a) U_{sgr} = 0.51 cm/s, U_{sgd} = 0 cm/s

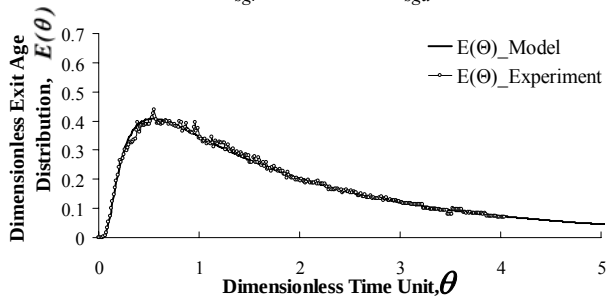

(b) U_{sgr} = 2.05 cm/s, U_{sgd} = 0 cm/s

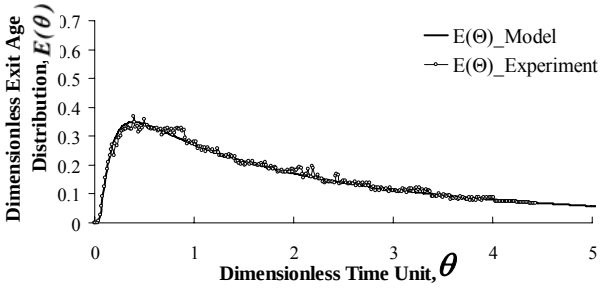

(c) U_{sgr} = 6.14 cm/s, U_{sgd} = 0 cm/s

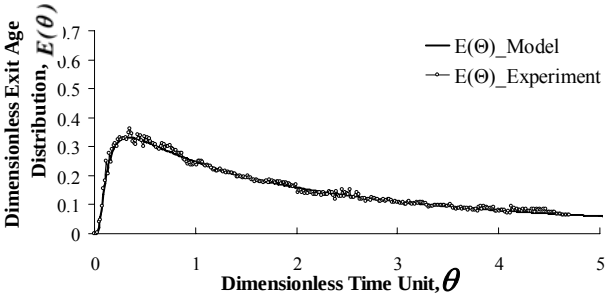

(d) U_{sgr} = 8.19 cm/s, U_{sgd} = 0 cm/s

Figure 76 Comparison of the exit age distribution (RTD) based on the dimensionless time unit (θ) curves in the riser obtained from the experiments and models without gas feeding in the downcomer and at the superficial gas velocities in the riser (a) U_{sgr} = 0.51 cm/s (b) U_{sgr} = 2.05 cm/s (c) U_{sgr} = 6.14 cm/s (d) U_{sgr} = 8.19 cm/s.

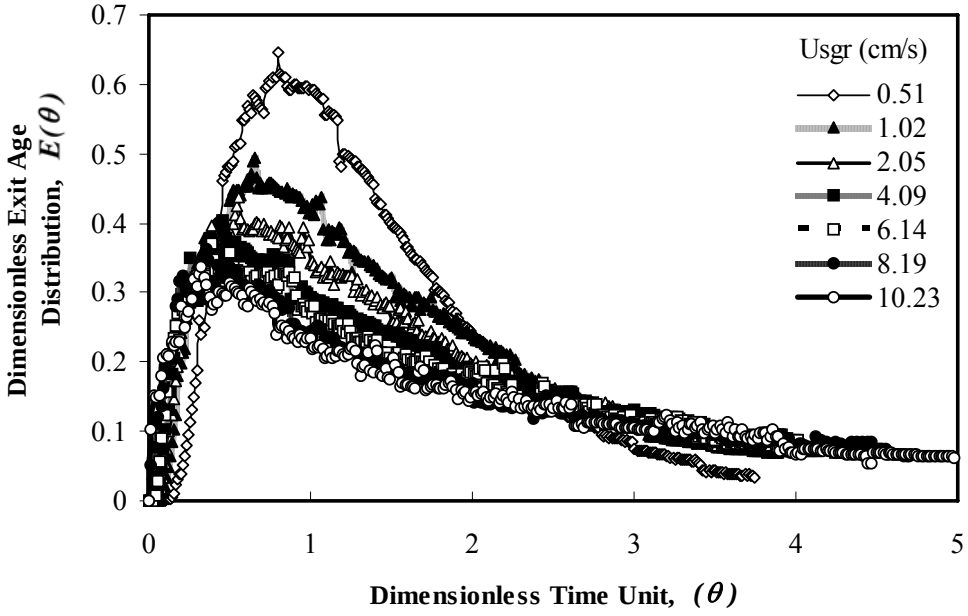

(a) Experiment

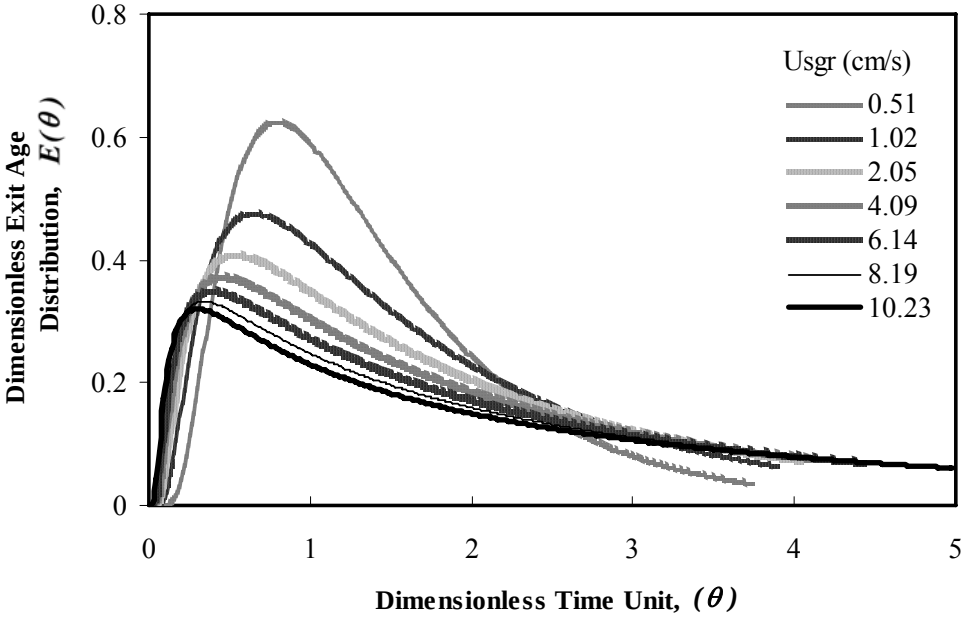

(b) Axial Dispersion Model

Figure 77 Dimensionless exit age distribution $E(\theta)$ in the riser at various superficial gas velocities in the riser and without gas inlet in the downcomer (a) obtained from the experiments (b) obtained from the axial dispersion model (Equation 67).

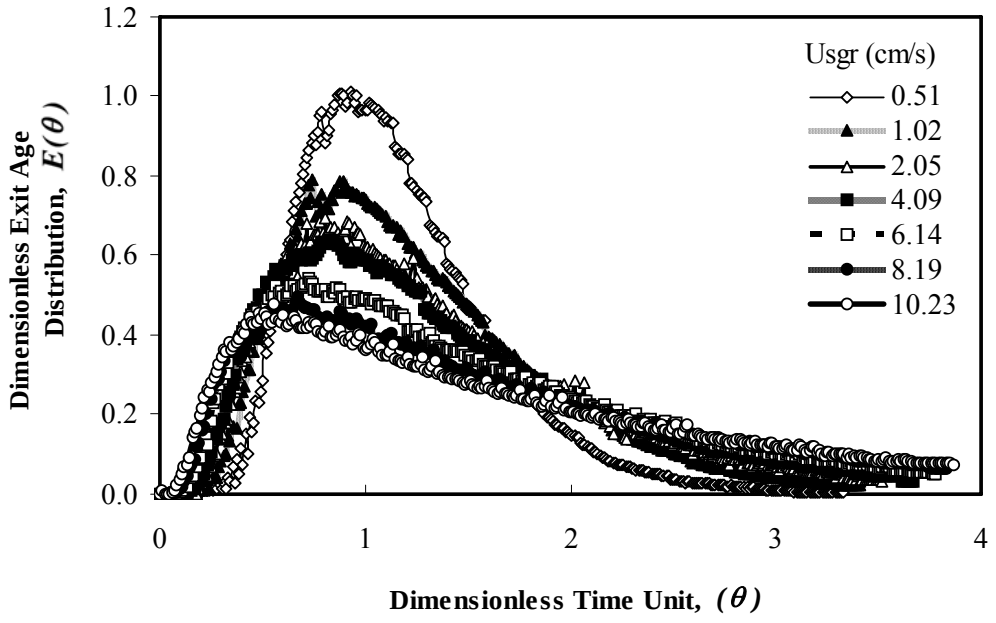

(a) Experiment

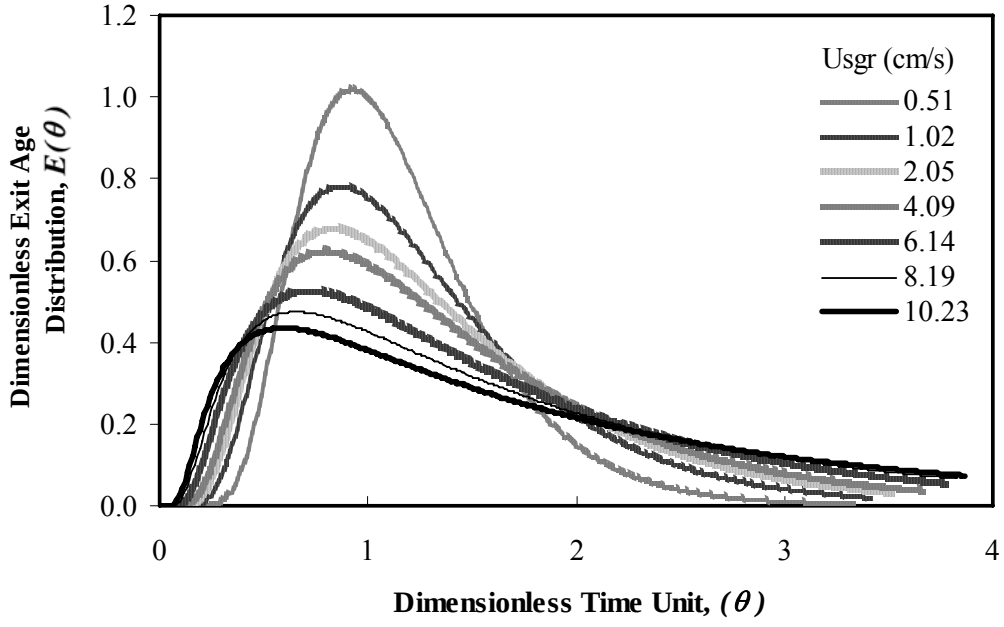

(b) Axial Dispersion Model

Figure 78 Dimensionless exit age distribution $E(\theta)$ in the downcomer at various superficial gas velocities in the riser and without gas inlet in the downcomer (a) obtained from the experiments (b) obtained from the axial dispersion model (Equation 67).

behavior in the riser is always higher than that in the downcomer, especially at very high superficial gas velocity in the riser. Table 9 shows that the mean residence time ($\bar{t}$) in both columns at different superficial gas velocities of the riser. The effect of the feed gas velocity in the riser on the mean residence time showed that the mean residence time ($\bar{t}$) in the riser and downcomer were decreased with increasing of the superficial gas velocities in the riser. This indicates that the fluid flows resides shorter when increasing of the superficial gas velocity in the riser. In addition, ($\bar{t}$) was not linearly decreased with increasing of the superficial gas velocities in the riser as shown in Table 9.

More results of the exit age distribution for different superficial gas velocities in the riser and downcomer obtained from the experiments and axial dispersion models can be seen in Appendix F. Table 9 and Figure 81 show the vessel dispersion number for all cases.

2.3 The effect of the superficial gas velocities in the downcomer on the dimensionless exit age distribution $E(\theta)$ of the riser and downcomer

Figures 79 and 80 show the dimensionless exit age distribution $E(\theta)-curves$ obtained from experiment and the axial dispersion models in the riser and in the downcomer at different superficial gas velocities in the downcomer and at the superficial gas velocities in the riser of 8.19 cm/s. More results for all conditions can be seen in Appendix F. The vessel dispersion number (D/uL) in the riser was slightly decreased with increasing of the superficial gas velocity in the downcomer. Due to the gas in the downcomer impedes the flow circulated from the riser into the downcomer. Therefore, the mixed flow behavior in the riser was decreased when increasing of the superficial gas velocity in the downcomer. On the other hand, the vessel dispersion number (D/uL) in the downcomer was slightly increased with increasing of the superficial gas velocity in the downcomer due to the direct effect of the inlet feed gas in the downcomer induced more mixing in the downcomer at higher inlet gas velocity. The effect of the feed gas velocity in the downcomer on the mean

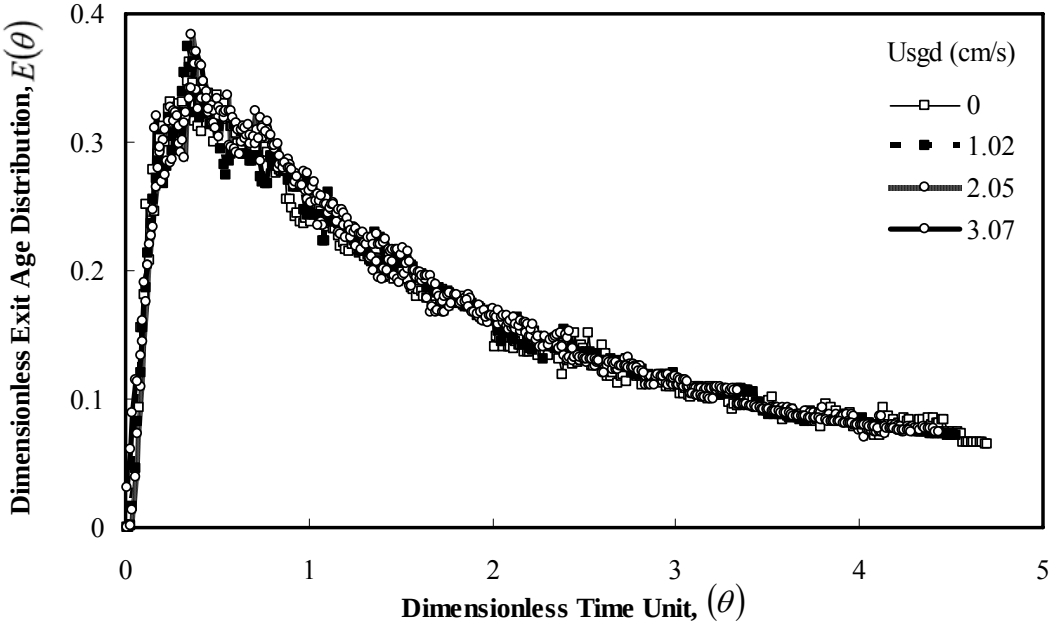

(a) Experiment

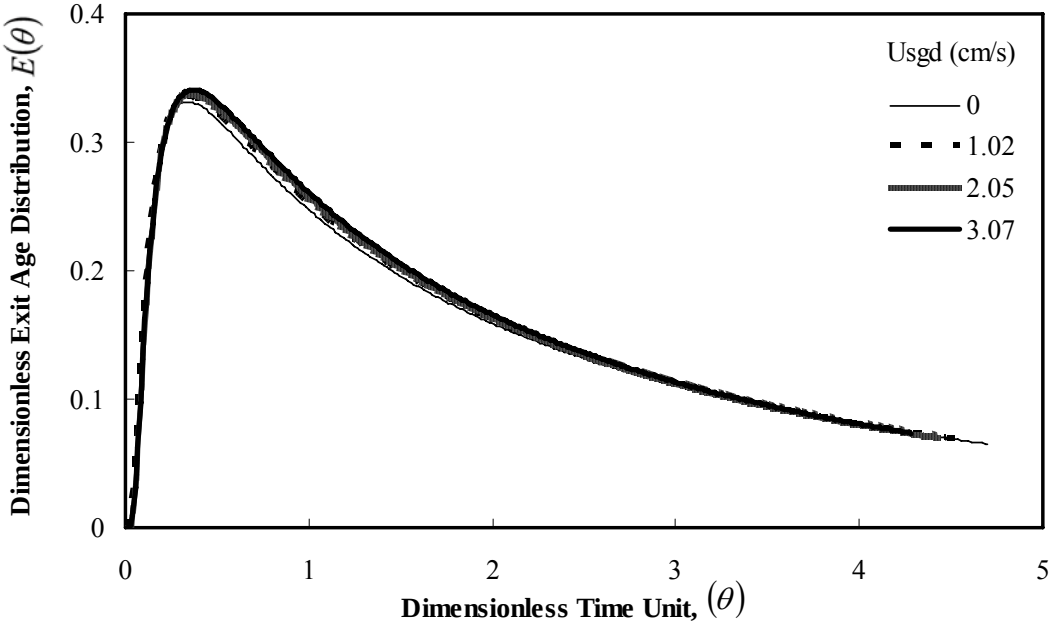

(b) Axial Dispersion Model

Figure 79 Dimensionless exit age distribution $E(\theta)$ in the riser at various superficial gas velocities in the downcomer and the gas inlet in the riser of 8.19 cm/s (a) obtained from the experiments (b) obtained from the axial dispersion model (Equation 67).

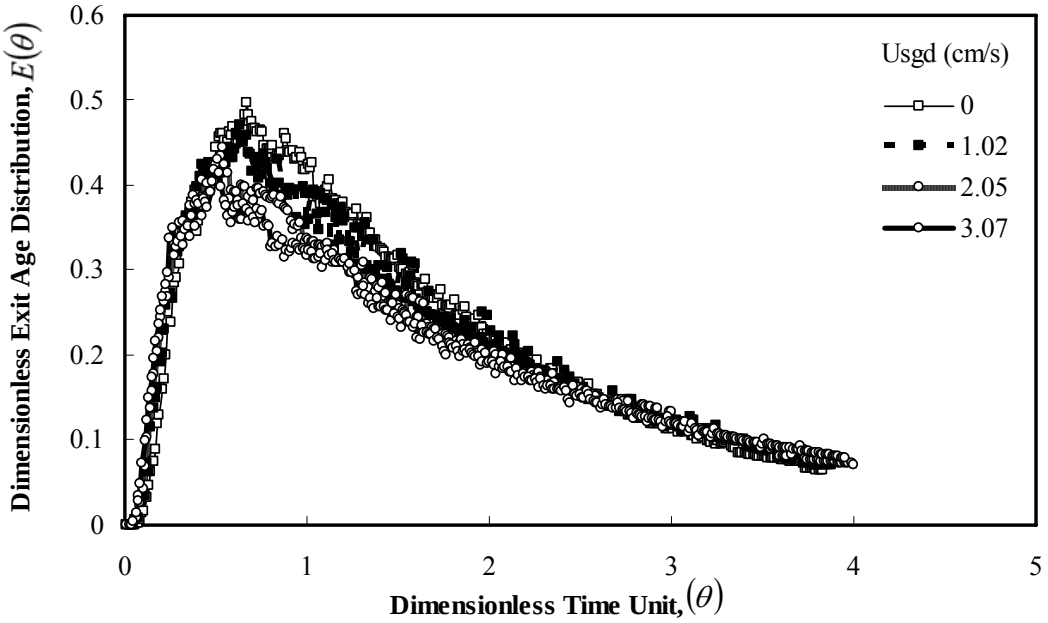

(a) Experiment

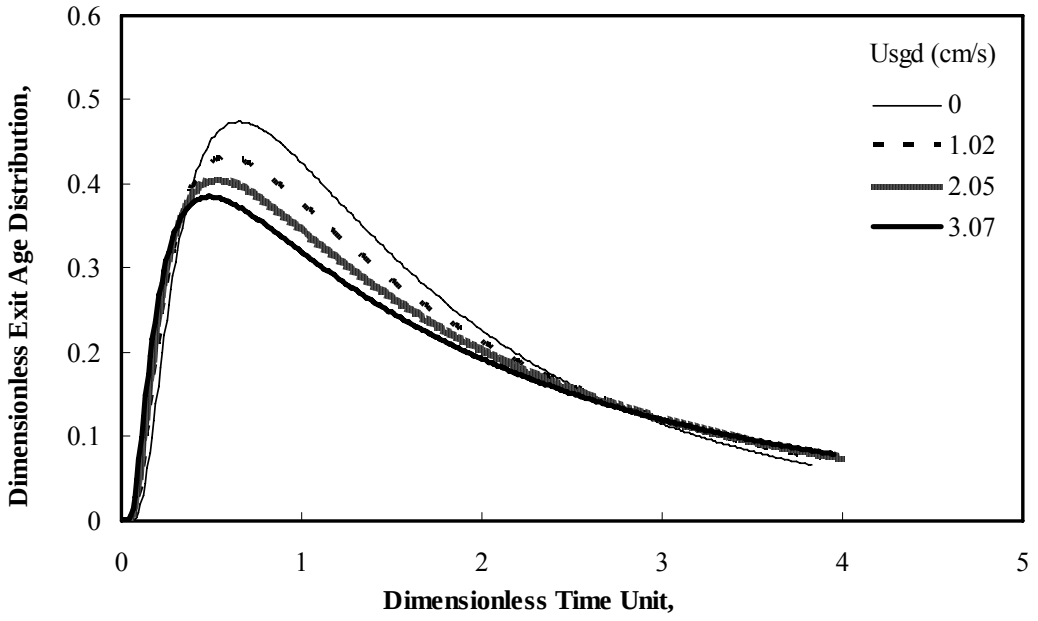

(b) Axial Dispersion Model

Figure 80 Dimensionless exit age distribution $E(\theta)$ in the downcomer at various superficial gas velocities in the downcomer and the gas inlet in the riser of 8.19 cm/s (a) obtained from the experiments (b) obtained from the axial dispersion model (Equation 67).

residence time can be seen in Table 9. The mean residence time ($\bar{t}$) in the riser slightly increased with increasing of the superficial gas velocities in the downcomer but that in the downcomer slightly decreased with the superficial gas velocities in the downcomer. This corresponds to slower liquid flows upwards in the riser at higher superficial gas velocity in the downcomer due to flow impeded by high velocity in the downcomer. Thus, at high superficial gas velocity in the downcomer the fluid flow in the riser resides longer than at low superficial gas velocity.

2.4 The effect of the superficial gas velocities on the Peclect number (Pe) of the riser and downcomer

The dispersion model takes the form of the one-dimension diffusion equation with a convection term. The relation between mean (plug flow) velocity and mixing dispersion coefficient is defined in the term of Peclect number (Pe). The Peclect number (Pe) is related to reactor length (L), superficial fluid velocity (V_l), and fluid dispersion coefficient (D) by

$$Pe = \frac{LV_l}{D} \tag{68}$$

It is seen that the dispersion model can represent mixing behavior ranging for complete mixed $(Pe \to 0)$ to plug flow $(Pe \to \infty)$. The parameter, which is used to identify the reactor behavior in the dispersion model, is (Pe). Table 9 shows the value of liquid phase Peclect number (Pe) is converted from the vessel dispersion number in the axial dispersion model. The Peclect number (Pe) in the riser was decreased with increasing of the superficial gas velocities in the riser; it was increased with increasing of the superficial gas velocities in the downcomer. Gas flow with high velocity in the downcomer impedes the flow circulated from the riser to the downcomer. Thus, the fluid was less fluctuated in the riser. In this study, the Peclect number (Pe) is near zero. That means the fluid behavior in the system more

approaches a mixed flow. However, at no inlet gas of the downcomer the Peclect number (Pe) in the downcomer is higher. It implies that the fluid in the downcomer has less mixing and behaves near plug flow more.

2.5 Empirical models of the vessel dispersion number

The model equations for vessel dispersion number (D/uL) obtained from the experiments were developed by fitting the vessel dispersion number with the superficial gas velocities of the riser and downcomer. They can be written in the form of Equation 69. The fitted equations for both columns are shown in Figure 81.

$$\left(\frac{D}{uL}\right) = BU_{sgr}{}^{M} \tag{69}$$

where the coefficient *B* for the riser and downcomer can be written as a function of the superficial gas velocity of the downcomer.

$$B_r = 0.376e^{-0.034U_{sgd}} \tag{70}$$

$$B_d = 0.119e^{0.258U_{sgd}} \tag{71}$$

The parameter *M* was fitted as a constant for both columns in this study. The vessel dispersion number value for the riser and downcomer are written as,

$$\left(\frac{D}{uL}\right)_r = 0.376e^{-0.034U_{sgd}}U_{sgr}{}^{0.626} \tag{72}$$

$$\left(\frac{D}{uL}\right)_d = 0.119e^{0.258U_{sgd}}U_{sgr}{}^{0.573} \tag{73}$$

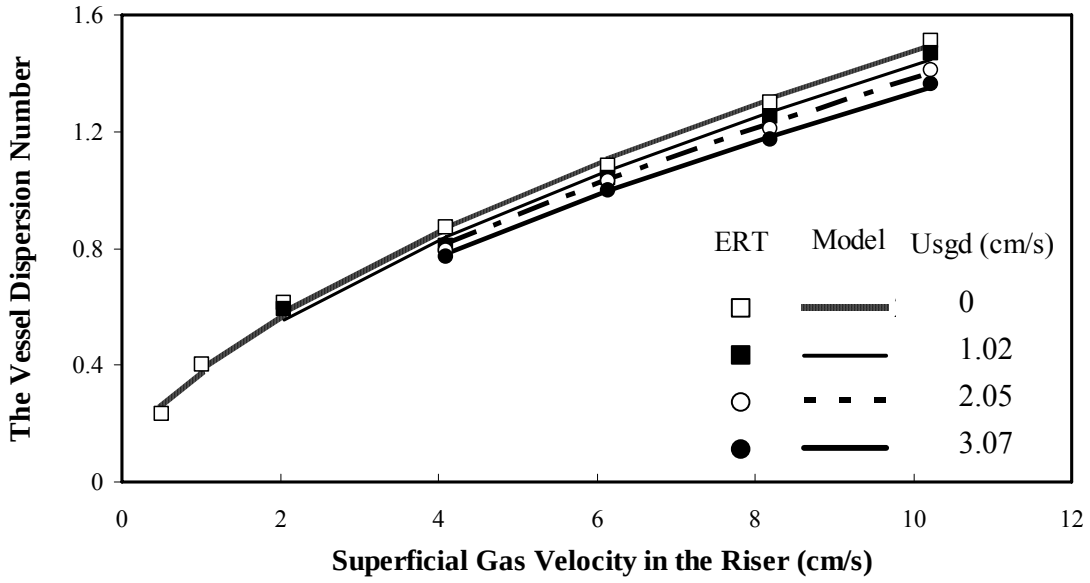

(a) Riser

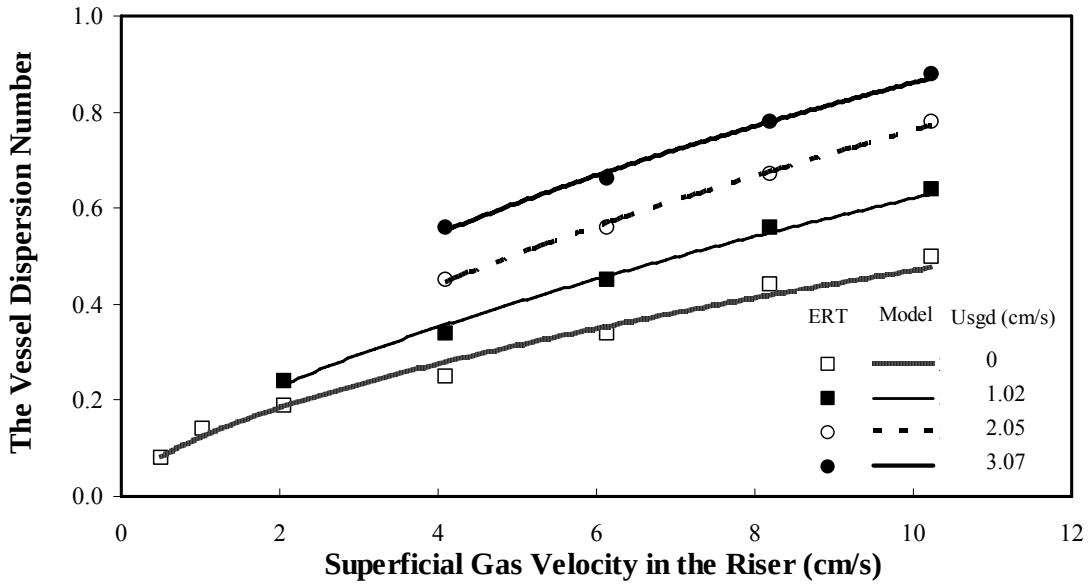

(b) Downcomcer

Figure 81 Comparison of the vessel dispersion number (D/uL) obtained from the model and the experiments at the superficial gas velocities in the riser of 0.51-10.23 and in the downcomer of 0-3.07 cm/s (a) in the riser (b) in the downcomer.

Table 9 The vessel dispersion number (D/uL) mean residence time ($\bar{t}$), and Peclect number (Pe) obtained from the dispersion model in the riser and downcomer.

		Riser			Downcomer		
U_r (cm/s)	U_d (cm/s)	(D/uL)	(Pe)	$(\bar{t})$	(D/uL)	(Pe)	$(\bar{t})$
0.51		0.23	4.256	85.51	0.08	12.449	96.08
1.02		0.44	2.253	82.21	0.14	7.013	93.87
2.05		0.66	1.523	79.14	0.19	5.354	90.90
4.09	0	0.87	1.155	76.99	0.23	4.330	87.14
6.14		1.08	0.926	72.28	0.34	2.982	84.67
8.19		1.30	0.772	68.09	0.44	2.263	83.50
10.23		1.51	0.661	64.30	0.55	1.824	82.82
2.05		0.59	1.699	82.36	0.24	4.220	85.00
4.09		0.81	1.233	79.82	0.34	2.912	84.10
6.14	1.02	1.00	1.000	75.09	0.45	2.223	83.19
8.19		1.25	0.798	70.71	0.56	1.791	82.55
10.23		1.47	0.680	67.23	0.67	1.495	80.03
4.09		0.77	1.304	82.54	0.45	2.223	83.19
6.14	2.05	1.03	0.967	78.92	0.56	1.785	82.45
8.19		1.21	0.826	72.26	0.67	1.495	80.03
10.23		1.43	0.700	68.04	0.78	1.277	78.10
4.09		0.72	1.383	85.08	0.56	1.798	86.42
6.14	3.07	1.03	0.969	81.88	0.67	1.495	82.05
8.19		1.17	0.856	74.68	0.78	1.283	80.88
10.23		1.39	0.721	70.39	0.90	1.116	70.39

CONCLUSIONS

Electrical resistance tomography (ERT) and a stimulus-response tracer technique can provide the hydrodynamic behavior in an external-loop gas lift reactor with the conclusions as follows:

1. The cross-sectional gas holdup distributions in the riser and downcomer are non uniform and nearly axial-symmetric. At the center of both columns, the gas holdup was the maximum and was decreased along with the radial distance from the center to the wall at all the superficial gas velocities.

2. The gas holdup in the riser is clearly higher than that in the downcomer due to higher gas velocity in the riser.

3. The gas holdup in both columns was increased with increasing of the superficial gas velocity of both columns.

4. The mean value of mixing index was increased with increasing of the superficial gas velocities of both columns. At high gas velocity in the riser in which the flow is in the turbulent regime, the fluctuation of mixing index is higher.

5. The residence time distributions in the riser and downcomer indicate that the flows in the riser and downcomer approach a mixed flow.

6. The vessel dispersion number obtained from the axial dispersion model was increased with an increase in the superficial gas velocity in the riser. The mixed flow behavior in the riser is always higher than that in the downcomer, especially at very high superficial gas velocity.

7. The results from both methods (Electrical Resistance Tomography (ERT) system and Stimulus-Response Tracer Technique) lead to the conclusions that the

fluid flow in the riser approaches a mixed flow and the mixing is higher than that in the downcomer. Increasing superficial gas velocities increases the mixing in both columns.

LITERATURE CITED

Al-Dahhan, M.H., J.J. Lerou., L. Han., M.P. Dudukovic., P. Gupta., P.L. Mills and T.M. Leib. 2006. Liquid-phase tracer response in a cold-flow counter trayed bubble column from conductivity probe measurements. **Chem. Eng. Process.** 45: 945-953.

Bolton, G.T., C.W. Hooper., E.H. Stitt and R. Mann. 2004. Flow distribution and velocity measurement in a radial flow fixed bed reactor using electrical resistance tomography. **Chem. Eng. Sci.** 59: 1989-1997.

Chisrt, M.Y. 1989. **Airlift Bioreactor.** n.d. n.p.

Chisti, Y., Moo-Chisti, Y., and Moo-Young, M. 1986. Disruption of microbial cells for intracellular products. **Enzym Microb Tech.** 8: 194-204.

Cho, H., C.H. Chung., G.R. Ahn., G.Y. Han and J.S. Kong. 2000. Axial gas dispersion in a fluidized bed of polyethylene particles. **Korean J. Chem. Eng.** 17(3): 292-298.

Forret, A., D. Schweich., J-M. Schweitzer., R. Krishna and T. Gauthier. 2003. Influence of scale on the hydrodynamics of bubble column reactors: an experimental study in columns of 0.1, 0.4 and 1 m diameters. **Chem. Eng. Sci.** 58: 719-724.

Fradette, L., Giguere, R., Mignon, D., Tanguy, P.A. 2008. ERT algorithms for quantitative concentration measurement of multiphase flows. **Chem. Eng. J.** 141: 305-317.

Guo, H., F. Dong., B. Yan., J. Hu and M. Wu. 2005. Gas/liquid two-phase flow regime identification in horizontal pipe using support vector machines. **International Conference on Machine Learning and Cybernetics,** Tianjin University, China.

Hoppe, S., C. Detrez and F. Pla. 2002. Modeling of a cokneader for the manufacturing of composite materials having absorbent properties at ultra-high-frequency waves. Part I: modeling of flow from residence time distribution investigations. **Polymer Eng. and Sci.**

Hua, S and F. Dong. 2006. Flowrate measurement with characteristic value cross-correlation by ERT two-phase vertical pipe flows. **International Conference on Machine Learning and Cybernetics,** Tianjin University, China.

Industrial Tomography System Ltd. 2004. **ITS Tomography Toolsuite Users Manual.** Manchester, UK.

Inglezakis, V.J and S.G. Poulopoulos. **Dispersion coefficients in fixed beds packed with irregular-shaped particles.** National Technical University of Athens, Greece.

Jin, H., Wang, M and Williams, R.A. 2007. Analysis of bubble behaviors in bubble columns using electrical resistance tomography. **Chem. Eng. J.** 130: 179-185.

Klein, J., A.A. Vicente and J.A. Teixeira**. Residence time of tagged magnetic particle in an internal-loop airlift reactor with an enlarged dual separator.** Centro de Engenharia Biologica-IBQF, Universidade do Minho, Portugal.

Lee, S., S. Chung and S. Park. 2007. Chemical tracer method for measurement of flow rates in closed conduits. **J. of Nuclear Sci. and Tech.** 44(11): 1467-1473.

Limtrakul, S., Chen, J., Ramachandran, P.A., Dudukovic, and M.P. 2005**.** Solids motion and holdup profiles in liquid fluidized beds. **Chem. Eng. Sci.** 60: 1889-1900.

Minsker, L.K., E. Joannet and A. Renken. 2004. Loop reactor staged with structured fibrous catalytic layers for liquid-phase hydrogenations. **Chem. Eng. Sci.** 59: 4919-4925.

Nadeau, P., D. Berk and R.J. Munz. 1996. Measurment of residence time distribution by tracer absorption spectroscopy. **Chem. Eng. Sci.** 51: 2607-2612.

Nie, D., Q. Liu., W. Shen., X. Wang and Z. Zhang. 2006. Flow mixing model of liquid phase in an internal airlift loop reactor. **J. of Shanghai University** 10(2): 185-188.

Pakzad, L., F.E. Mozaffari and P. Chan. 2008. Using electrical resistance tomography and computational fluid dynamics modeling to study the formation of cavern in the mixing of pseudoplastic fluids possessing yield stress. **Chem. Eng. Sci.** 63: 2508-2522.

Pramparo, L., A. Fabregat., A. Fortuny., C. Bengoa., F. Stuber., J. Font., J. Legrand., J. Pruvost and P. Legentilhomme. 2008. Mixing and hydrodynamics investigation using CFD in a square-sectioned torus reactor in batch and continuous regimes**.** **Chem. Eng. J.** 137: 386-395.

Razzak, S.A., J.X. Zhu., S. Barghi and Y. Mi. 2009**.** Phase holdup measurement in a gas-liquid-solid circulating fluidized bed (GLSCFB) riser using electrical resistance tomography and optical fibre probe. **Chem. Eng. J.** 147: 210-218.

Vereechen, H., Daily, W.D., Binley, A.M., LaBrecque, D.L., Ramirez, A.L., 1996. ERT monitoring of environmental remediation processes. **Measurement Sci. Technol.** 7: 375-383.

Wang, M., Man, R and Dickin, F.J. 1999. Electrical resistance tomographic sensing systems for industrial applications. **Chem. Eng. Comm.** 175: 49-70.

Wang, M., A. Dorward., D. Vlaev and R. Mann. 1999. **Measurements of gas-liquid mixing in a stirred vessel using electrical resistance tomography (ERT).** Virtual Centre for Industrial Process Tomography, Manchester, UK.

APPENDICES

Appendix A

ERT data

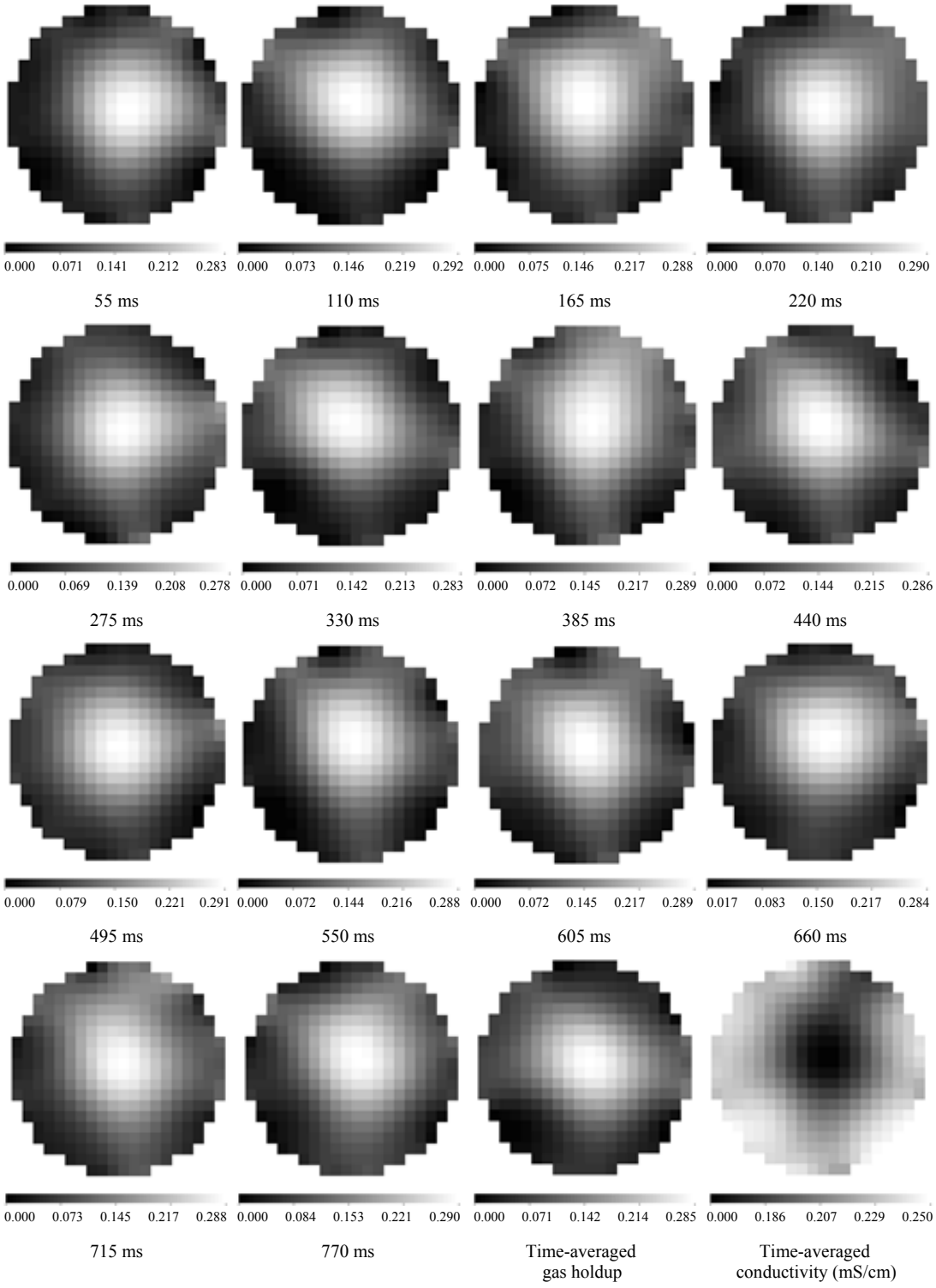

Appendix Figure A1 Cross-sectional gas holdup distributions in the riser at the superficial gas velocity in the riser of 2.05 cm/s and in the downcomer of 1.02 cm/s.

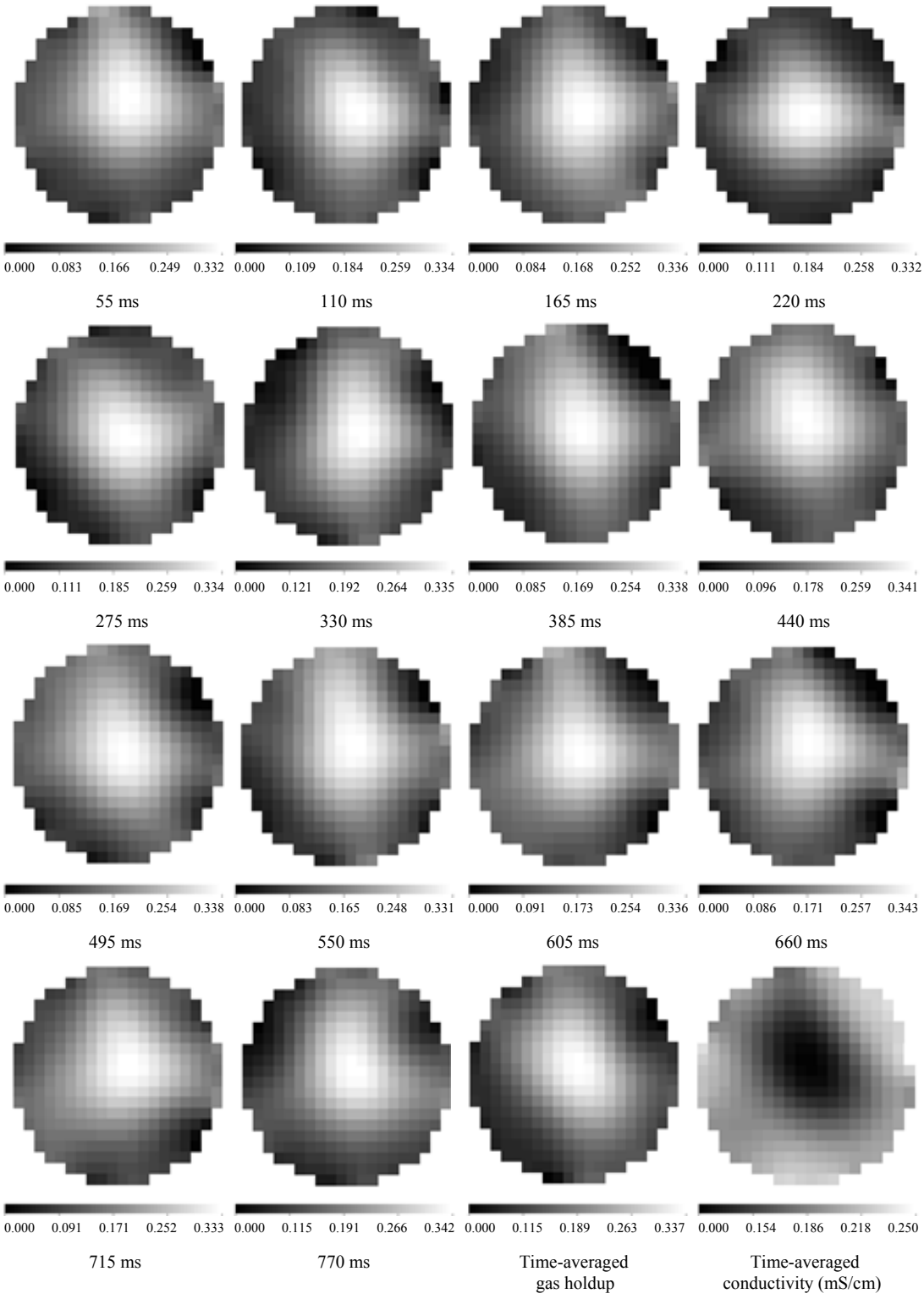

Appendix Figure A2 Cross-sectional gas holdup distributions in the riser at the superficial gas velocity in the riser of 10.23 cm/s and in the downcomer of 1.02 cm/s.

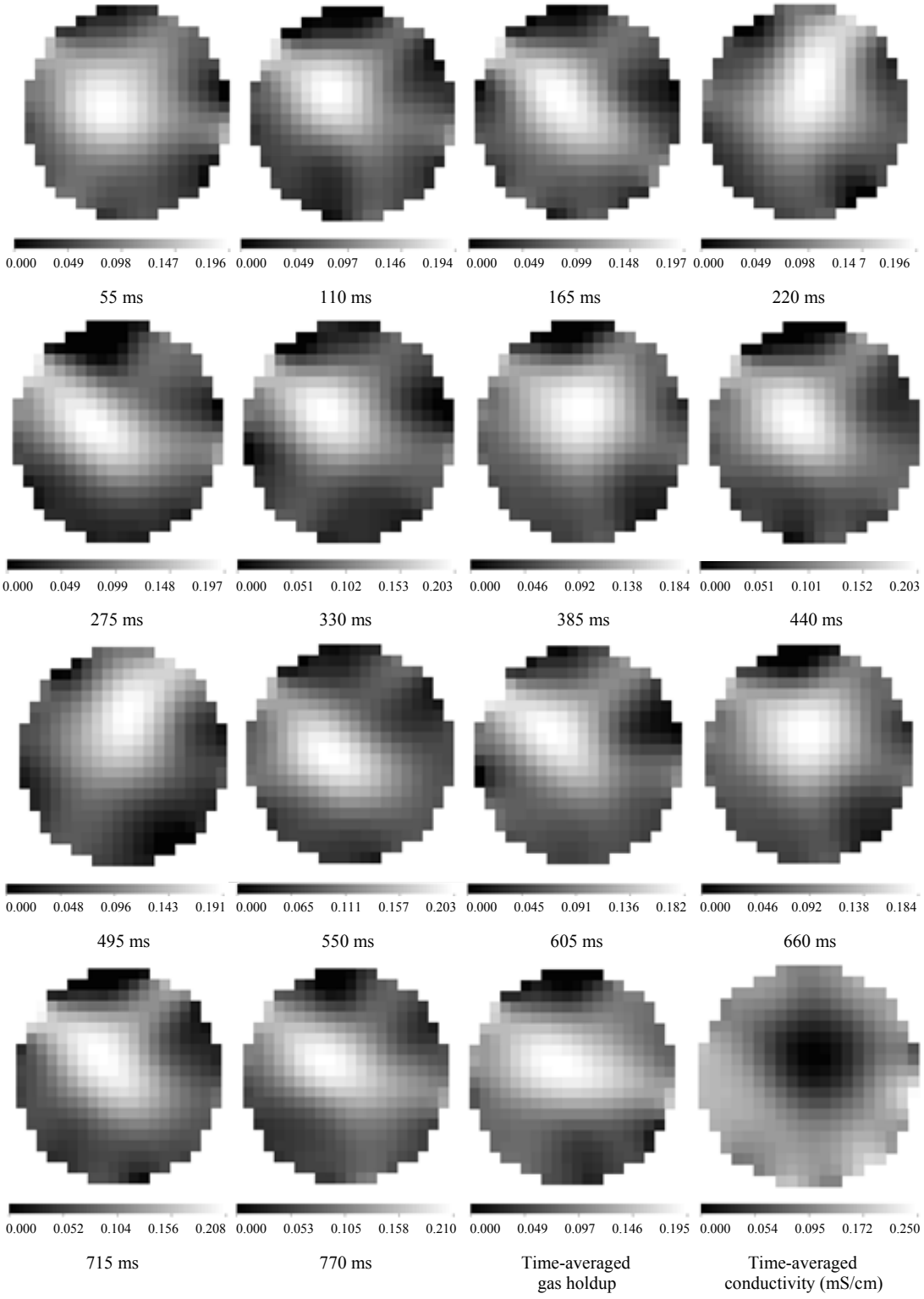

Appendix Figure A3 Cross-sectional gas holdup distributions in the downcomer at the superficial gas velocity in the riser of 2.05 cm/s and in the downcomer of 1.02 cm/s.

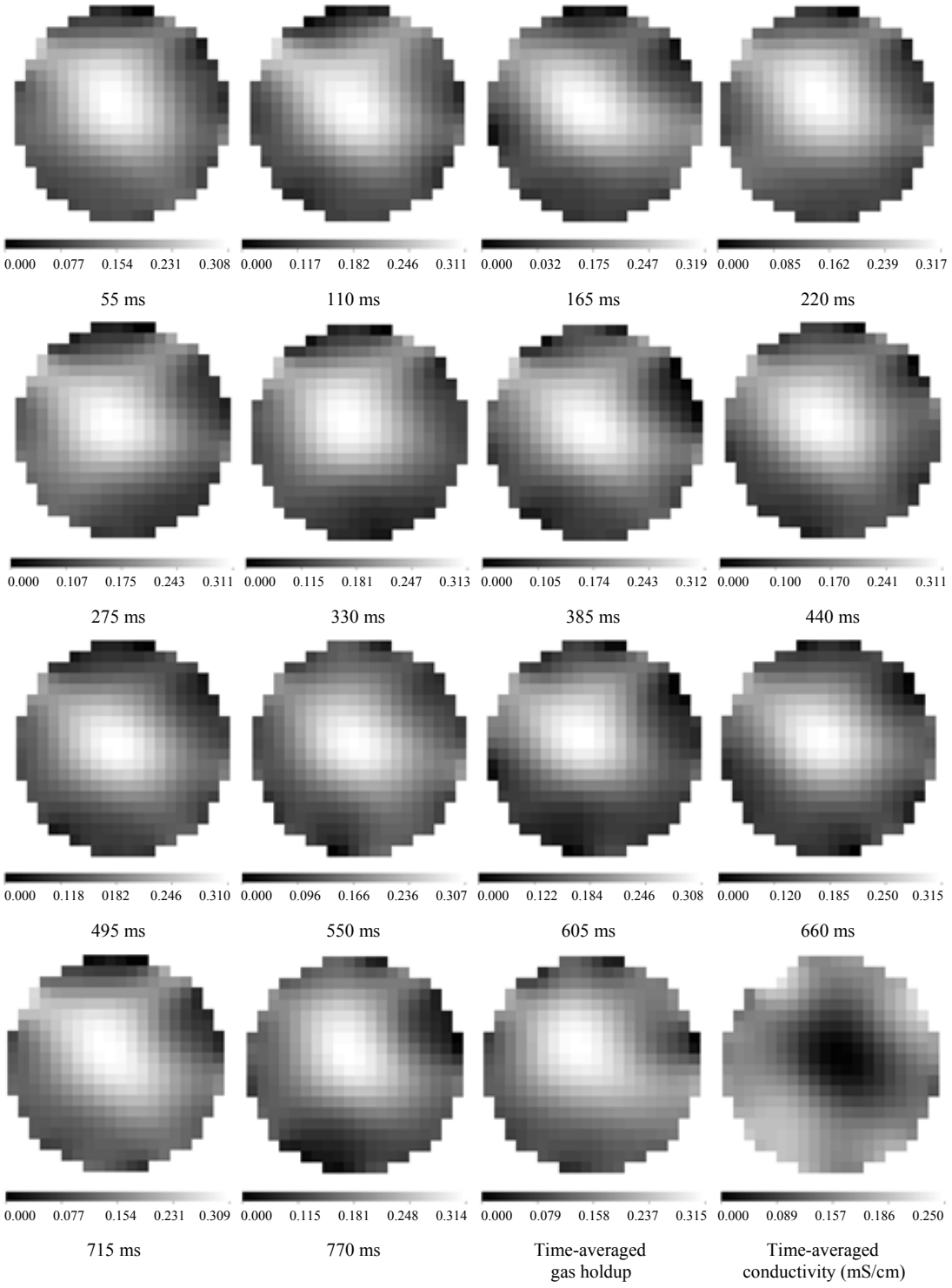

Appendix Figure A4 Cross-sectional gas holdup distributions in the downcomer at the superficial gas velocity in the riser of 10.23 cm/s and in the downcomer of 1.02 cm/s.

Appendix Table A1 Gas holdup in the riser by ERT measurements at the superficial gas velocity in the riser of 0.51-10.23 cm/s and in the downcomer of 0-3.07 cm/s.

U_r (cm/s)	U_d (cm/s)	ε_r at $\left(\frac{r}{R}\right)=$ 0.177	ε_r at $\left(\frac{r}{R}\right)=$ 0.395	ε_r at $\left(\frac{r}{R}\right)=$ 0.637	ε_r at $\left(\frac{r}{R}\right)=$ 0.884	$\bar{\varepsilon}_{avg\_r}$
0.51	0	0.126	0.112	0.079	0.047	0.074
1.02		0.160	0.140	0.095	0.060	0.092
2.05		0.207	0.170	0.123	0.074	0.115
4.09		0.260	0.211	0.149	0.091	0.142
6.14		0.297	0.246	0.180	0.109	0.169
8.19		0.325	0.276	0.208	0.122	0.190
10.23		0.353	0.293	0.217	0.130	0.202
2.05	1.02	0.210	0.177	0.130	0.083	0.123
4.09		0.268	0.221	0.165	0.103	0.155
6.14		0.301	0.255	0.188	0.127	0.181
8.19		0.332	0.277	0.209	0.140	0.199
10.23		0.357	0.299	0.231	0.151	0.216
4.09	2.05	0.266	0.232	0.179	0.115	0.166
6.14		0.305	0.260	0.197	0.127	0.185
8.19		0.345	0.289	0.228	0.151	0.213
10.23		0.379	0.312	0.248	0.161	0.230
4.09	3.07	0.279	0.226	0.178	0.129	0.175
6.14		0.311	0.264	0.197	0.136	0.190
8.19		0.352	0.292	0.230	0.161	0.219
10.23		0.379	0.319	0.249	0.175	0.238

Appendix Table A2 Gas holdup in the downcomer by ERT measurements at the superficial gas velocity in the riser of 0.51-10.23 cm/s and in the downcomer of 0-3.07 cm/s.

U_r (cm/s)	U_d (cm/s)	ε_d at $\left(\frac{r}{R}\right)=$ 0.177	ε_d at $\left(\frac{r}{R}\right)=$ 0.395	ε_d at $\left(\frac{r}{R}\right)=$ 0.637	ε_d at $\left(\frac{r}{R}\right)=$ 0.884	$\bar{\varepsilon}_{avg\_d}$
0.51	0	0.067	0.051	0.038	0.011	0.031
1.02		0.090	0.075	0.045	0.017	0.041
2.05		0.144	0.093	0.066	0.030	0.060
4.09		0.194	0.135	0.080	0.035	0.078
6.14		0.246	0.161	0.101	0.041	0.095
8.19		0.281	0.181	0.115	0.046	0.107
10.23		0.315	0.202	0.125	0.053	0.120
2.05	1.02	0.131	0.100	0.063	0.025	0.067
4.09		0.179	0.136	0.096	0.043	0.087
6.14		0.216	0.167	0.110	0.054	0.098
8.19		0.246	0.190	0.130	0.061	0.119
10.23		0.275	0.210	0.136	0.061	0.136
4.09	2.05	0.184	0.140	0.103	0.048	0.094
6.14		0.218	0.172	0.115	0.056	0.106
8.19		0.248	0.203	0.134	0.061	0.133
10.23		0.284	0.224	0.150	0.072	0.143
4.09	3.07	0.188	0.158	0.114	0.061	0.106
6.14		0.225	0.184	0.126	0.070	0.118
8.19		0.269	0.215	0.154	0.082	0.141
10.23		0.294	0.239	0.169	0.092	0.156

Appendix Table A3 Gas holdup in the riser by fitted model at the superficial gas velocity in the riser of 0.51-10.23 cm/s and in the downcomer of 0-3.07 cm/s.

U_r (cm/s)	U_d (cm/s)	ε_r at $\left(\frac{r}{R}\right)=$ 0.177	ε_r at $\left(\frac{r}{R}\right)=$ 0.395	ε_r at $\left(\frac{r}{R}\right)=$ 0.637	ε_r at $\left(\frac{r}{R}\right)=$ 0.884	$\bar{\varepsilon}_{avg\_r}$
0.51	0	0.123	0.104	0.078	0.046	0.071
1.02		0.157	0.132	0.099	0.058	0.091
2.05		0.201	0.168	0.125	0.074	0.117
4.09		0.256	0.213	0.158	0.094	0.149
6.14		0.295	0.245	0.182	0.109	0.173
8.19		0.327	0.271	0.201	0.120	0.192
10.23		0.351	0.292	0.217	0.130	0.208
2.05	1.02	0.206	0.173	0.131	0.082	0.123
4.09		0.263	0.220	0.166	0.104	0.157
6.14		0.304	0.253	0.190	0.120	0.182
8.19		0.336	0.279	0.210	0.133	0.202
10.23		0.364	0.302	0.227	0.144	0.219
4.09	2.05	0.276	0.230	0.176	0.116	0.166
6.14		0.305	0.253	0.194	0.129	0.192
8.19		0.350	0.291	0.222	0.148	0.213
10.23		0.377	0.313	0.243	0.163	0.230
4.09	3.07	0.284	0.237	0.184	0.128	0.174
6.14		0.308	0.257	0.199	0.139	0.202
8.19		0.351	0.292	0.227	0.159	0.224
10.23		0.380	0.315	0.245	0.172	0.242

Appendix Table A4 Gas holdup in the downcomer by fitted model at the superficial gas velocity in the riser of 0.51-10.23 cm/s and in the downcomer of 0-3.07 cm/s.

U_r (cm/s)	U_d (cm/s)	ε_d at $\left(\frac{r}{R}\right)=$ 0.177	ε_d at $\left(\frac{r}{R}\right)=$ 0.395	ε_d at $\left(\frac{r}{R}\right)=$ 0.637	ε_d at $\left(\frac{r}{R}\right)=$ 0.884	$\bar{\varepsilon}_{avg\_d}$
0.51	0	0.065	0.049	0.031	0.013	0.029
1.02		0.089	0.068	0.043	0.017	0.040
2.05		0.143	0.093	0.060	0.024	0.056
4.09		0.203	0.128	0.082	0.024	0.078
6.14		0.246	0.155	0.099	0.039	0.094
8.19		0.282	0.177	0.112	0.045	0.107
10.23		0.313	0.196	0.125	0.050	0.119
2.05	1.02	0.130	0.100	0.066	0.030	0.061
4.09		0.179	0.137	0.091	0.041	0.084
6.14		0.216	0.166	0.109	0.049	0.102
8.19		0.247	0.189	0.125	0.056	0.117
10.23		0.273	0.210	0.138	0.062	0.129
4.09	2.05	0.185	0.145	0.099	0.049	0.091
6.14		0.223	0.175	0.119	0.059	0.111
8.19		0.255	0.200	0.136	0.067	0.127
10.23		0.283	0.221	0.150	0.074	0.141
4.09	3.07	0.194	0.155	0.108	0.057	0.099
6.14		0.235	0.187	0.131	0.069	0.120
8.19		0.268	0.214	0.149	0.079	0.137
10.23		0.298	0.237	0.166	0.088	0.153

1. Calculation of cross-sectional averaged gas holdup in both columns ($r = 14.4cm$) by ERT system.

At the superficial gas velocity in the riser of 0.51 cm/s and no inlet gas of the downcomer.

$$\bar{\varepsilon}_{avg\_r} = \frac{A_1\varepsilon_1 + A_2\varepsilon_2 + A_3\varepsilon_3 + A_4\varepsilon_4}{A_1 + A_2 + A_3 + A_4}$$

$$= \frac{(10.179)(0.126) + (30.536)(0.112) + (50.894)(0.079) + (71.251)(0.047)}{(10.179) + (30.536) + (50.894) + (71.251)}$$

$$= 0.074$$

2. Calculation of cross-sectional averaged gas holdup in both columns ($r = 14.4cm$) by fitted model.

NLREG program was used to fit the model, this condition at the superficial gas velocity in the riser of 0.51 cm/s and no inlet gas of the downcomer.

$$\bar{\varepsilon}_{avg\_r} = 0.09e^{0.05U_{sgd}}U_{sgr}^{0.36}$$

$$\bar{\varepsilon}_{avg\_r} = 0.09e^{0.05(0)}(0.51)^{0.36}$$

$$= 0.071$$

$$\bar{\varepsilon}_{avg\_d} = 0.04e^{0.08U_{sgd}}U_{sgr}^{0.47}$$

$$\bar{\varepsilon}_{avg\_d} = 0.04e^{0.08(0)}(0.51)^{0.47}$$

$$= 0.029$$

with a regression coefficient of 0.95-0.99 and in the range of the superficial gas velocities in the riser of 0.51-10.23 cm/s and in the downcomer of 0-3.07 cm/s.

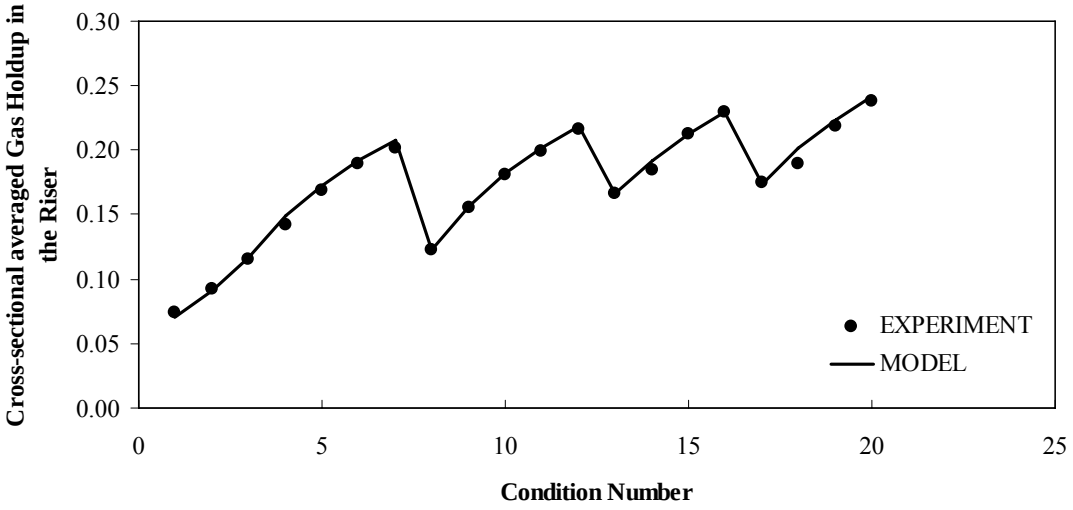

(a) Riser

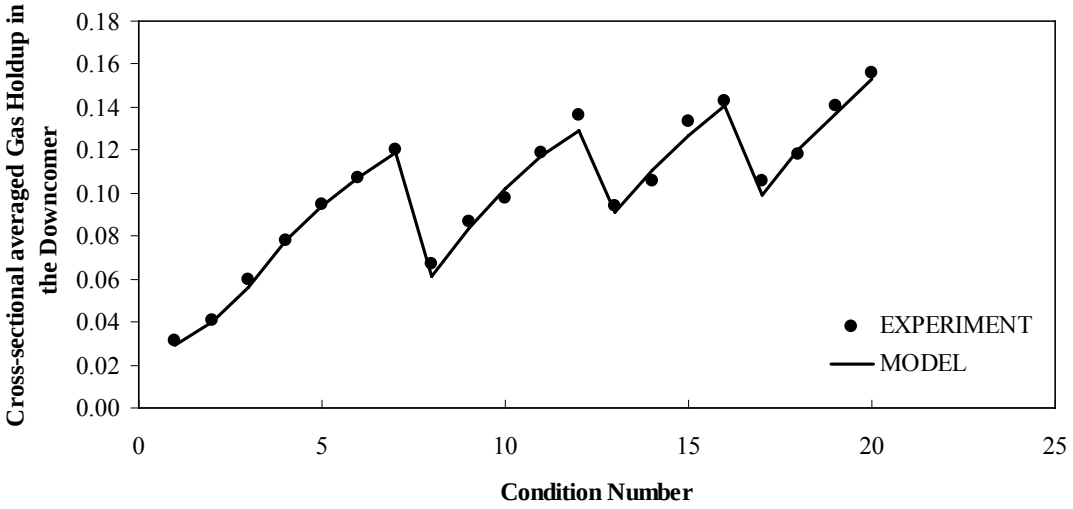

(b) Downcomer

Appendix Figure A5 Cross-sectional averaged gas holdup distributions in the riser and downcomer at the superficial gas velocity in the riser of 0.51-10.23 cm/s and in the downcomer of 0-3.07 cm/s.

Appendix B

Calculation of the inlet superficial gas velocities

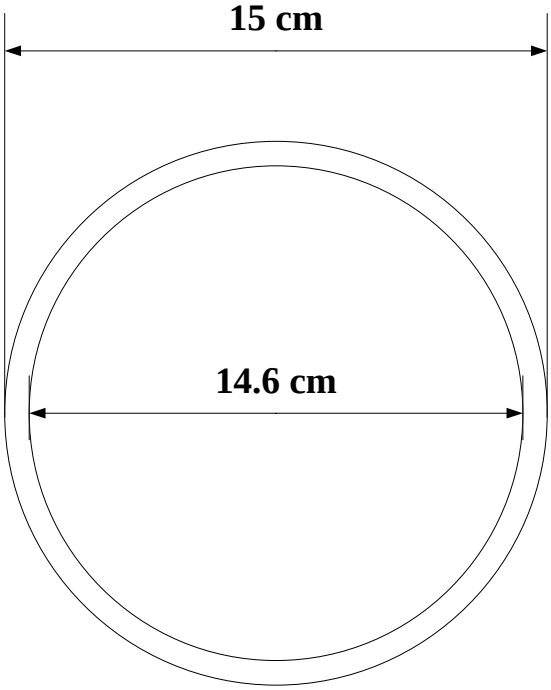

Appendix Figure B1 Cross-sectional gas holdup in the riser and in the downcomer.

Cross-sectional area $= \frac{\pi D^2}{4} = \frac{\pi(14.6)^2}{4} = 164.415\ cm^2$

The superficial gas velocities of the inlets gas in the riser and in the downcomer.

At the superficial gas velocity in the riser of 5 l/min

$$= \left(\frac{5l}{\min}\right)\left(\frac{1}{164.415cm^2}\right)\left(\frac{1000cm^3}{1l}\right)\left(\frac{1\min}{60\sec}\right)$$

$= 0.51\ \ cm/s$

At the superficial gas velocity in the riser of 10 l/min

$$= \left(\frac{10l}{\min}\right)\left(\frac{1}{164.415cm^2}\right)\left(\frac{1000cm^3}{1l}\right)\left(\frac{1\min}{60\sec}\right)$$

$= 1.02\ \ cm/s$

At the superficial gas velocity in the riser of 20 l/min

$$= \left(\frac{20l}{\min}\right)\left(\frac{1}{164.415cm^2}\right)\left(\frac{1000cm^3}{1l}\right)\left(\frac{1\min}{60\sec}\right)$$

$$= 2.05 \ \ cm/s$$

At the superficial gas velocity in the riser of 40 l/min

$$= \left(\frac{40l}{\min}\right)\left(\frac{1}{164.415cm^2}\right)\left(\frac{1000cm^3}{1l}\right)\left(\frac{1\min}{60\sec}\right)$$

$$= 4.09 \ \ cm/s$$

At the superficial gas velocity in the riser of 60 l/min

$$= \left(\frac{60l}{\min}\right)\left(\frac{1}{164.415cm^2}\right)\left(\frac{1000cm^3}{1l}\right)\left(\frac{1\min}{60\sec}\right)$$

$$= 6.14 \ \ cm/s$$

At the superficial gas velocity in the riser of 80 l/min

$$= \left(\frac{80l}{\min}\right)\left(\frac{1}{164.415cm^2}\right)\left(\frac{1000cm^3}{1l}\right)\left(\frac{1\min}{60\sec}\right)$$

$$= 8.19 \ \ cm/s$$

At the superficial gas velocity in the riser of 100 l/min

$$= \left(\frac{100l}{\min}\right)\left(\frac{1}{164.415cm^2}\right)\left(\frac{1000cm^3}{1l}\right)\left(\frac{1\min}{60\sec}\right)$$

$$= 10.23 \ \ cm/s$$

At the superficial gas velocity in the downcomer of 10 l/min

$$= \left(\frac{10l}{\min}\right)\left(\frac{1}{164.415cm^2}\right)\left(\frac{1000cm^3}{1l}\right)\left(\frac{1\min}{60\sec}\right)$$

$$= 1.02 \ \ cm/s$$

At the superficial gas velocity in the downcomer of 20 l/min

$$= \left(\frac{20l}{\min}\right)\left(\frac{1}{164.415cm^2}\right)\left(\frac{1000cm^3}{1l}\right)\left(\frac{1\min}{60\sec}\right)$$

$$= 2.05 \ \ cm/s$$

At the superficial gas velocity in the downcomer of 30 l/min

$$= \left(\frac{30l}{\min}\right)\left(\frac{1}{164.415cm^2}\right)\left(\frac{1000cm^3}{1l}\right)\left(\frac{1\min}{60\sec}\right)$$

$$= 3.07 \ \ cm/s$$

Appendix C

Model data

Appendix Table C1 Equations of cross-sectional averaged gas holdup in the riser obtained from fitting of experimental data at the superficial gas velocities in the riser of 0.51-10.23 cm/s and in the downcomer of 0-3.07 cm/s.

.

Conditions	The fitted models for cross-sectional averaged gas holdup in the riser	
U_{sgr} = 0.51 – 10.23 cm/s with U_{sgd} = 0 cm/s	$\bar{\varepsilon}_r = 0.088U_r^{0.47}$	(1)
U_{sgr} = 2.05 – 10.23 cm/s with U_{sgd} = 1.02 cm/s	$\bar{\varepsilon}_r = 0.094U_r^{0.47}$	(2)
U_{sgr} = 4.09 – 10.23 cm/s with U_{sgd} = 2.05 cm/s	$\bar{\varepsilon}_r = 0.099U_r^{0.47}$	(3)
U_{sgr} = 4.09 – 10.23 cm/s with U_{sgd} = 3.07 cm/s	$\bar{\varepsilon}_r = 0.10U_r^{0.47}$	(4)

Appendix Table C2 Equations of cross-sectional averaged gas holdup in the downcomer obtained from fitting of experimental data at the superficial gas velocities in the riser of 0.51-10.23 cm/s and in the downcomer of 0-3.07 cm/s.

.

Conditions	The fitted models for cross-sectional averaged gas holdup in the downcomer	
U_{sgr} = 0.51 – 10.23 cm/s with U_{sgd} = 0 cm/s	$\bar{\varepsilon}_d = 0.040 U_r^{0.47}$	(1)
U_{sgr} = 2.05 – 10.23 cm/s with U_{sgd} = 1.02 cm/s	$\bar{\varepsilon}_d = 0.043 U_r^{0.47}$	(2)
U_{sgr} = 4.09 – 10.23 cm/s with U_{sgd} = 2.05 cm/s	$\bar{\varepsilon}_d = 0.046 U_r^{0.47}$	(3)
U_{sgr} = 4.09 – 10.23 cm/s with U_{sgd} = 3.07 cm/s	$\bar{\varepsilon}_d = 0.052 U_r^{0.47}$	(4)

Appendix D

Level measurements and pressure drop measurements data

Calculation of the overall gas holdup in the system

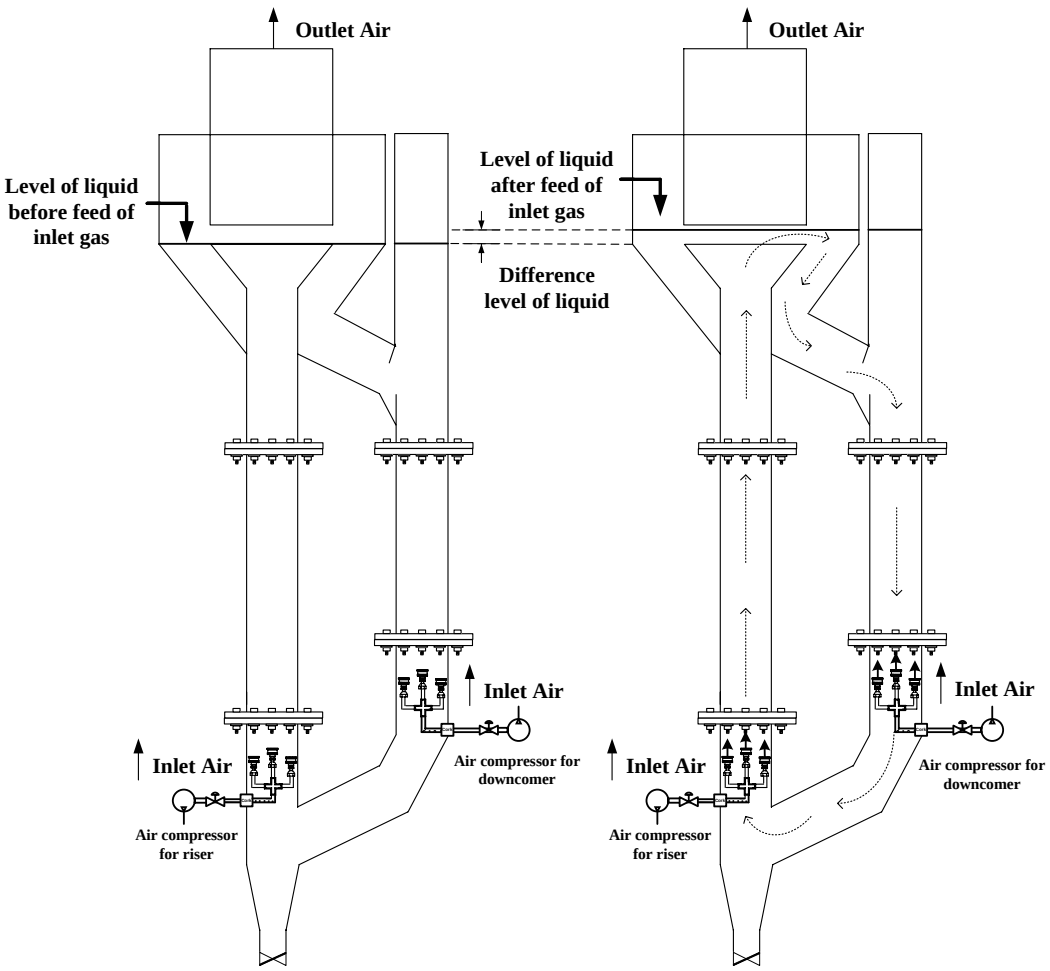

Appendix Figure D1 Level of liquid water that was increased with feeding of the inlet gas into the system.

One method for calculating of the gas holdup in the system at different gas flow rates as follow by: (Hossein *et al.,* 2005);

$$\varepsilon_{overall} = \frac{V_G}{V_G + V_L} \tag{1}$$

where V_G is volume of gas in the system; V_L is volume of liquid in the system.

$V_L = 73\ L$ or $73 \cdot 1000\ cm^3$ at the beginning

$$V_G = \Delta H_r \cdot \pi \cdot \left(\frac{51.1}{2}\right)^2 + \Delta H_d \cdot \pi \cdot \left(\frac{14.4}{2}\right)^2$$

So, overall gas holdup of the system could be calculated from

$$\varepsilon_{overall} = \frac{\Delta H_r \cdot \pi \cdot \left(\frac{51.1}{4}\right)^2 + \Delta H_d \cdot \pi \cdot \left(\frac{14.4}{2}\right)^2}{\left(\Delta H_r \cdot \pi \cdot \left(\frac{51.1}{4}\right)^2 + \Delta H_d \cdot \pi \cdot \left(\frac{14.4}{2}\right)^2 + (73 \cdot 1000)\right)}$$

At $U_{sgr} = 6.14$ cm/s, $U_{sgd} = 3.07$ cm/s

$$\varepsilon_{overall} = \frac{18.8 \cdot \pi \cdot \left(\frac{51.1}{4}\right)^2 + 12.43 \cdot \pi \cdot \left(\frac{14.4}{2}\right)^2}{\left(18.8 \cdot \pi \cdot \left(\frac{51.1}{4}\right)^2 + 12.43 \cdot \pi \cdot \left(\frac{14.4}{2}\right)^2 + (73 \cdot 1000)\right)}$$

$$\varepsilon_{overall} = 0.138$$

Calculation of the gas holdup both in the riser and downcomer.

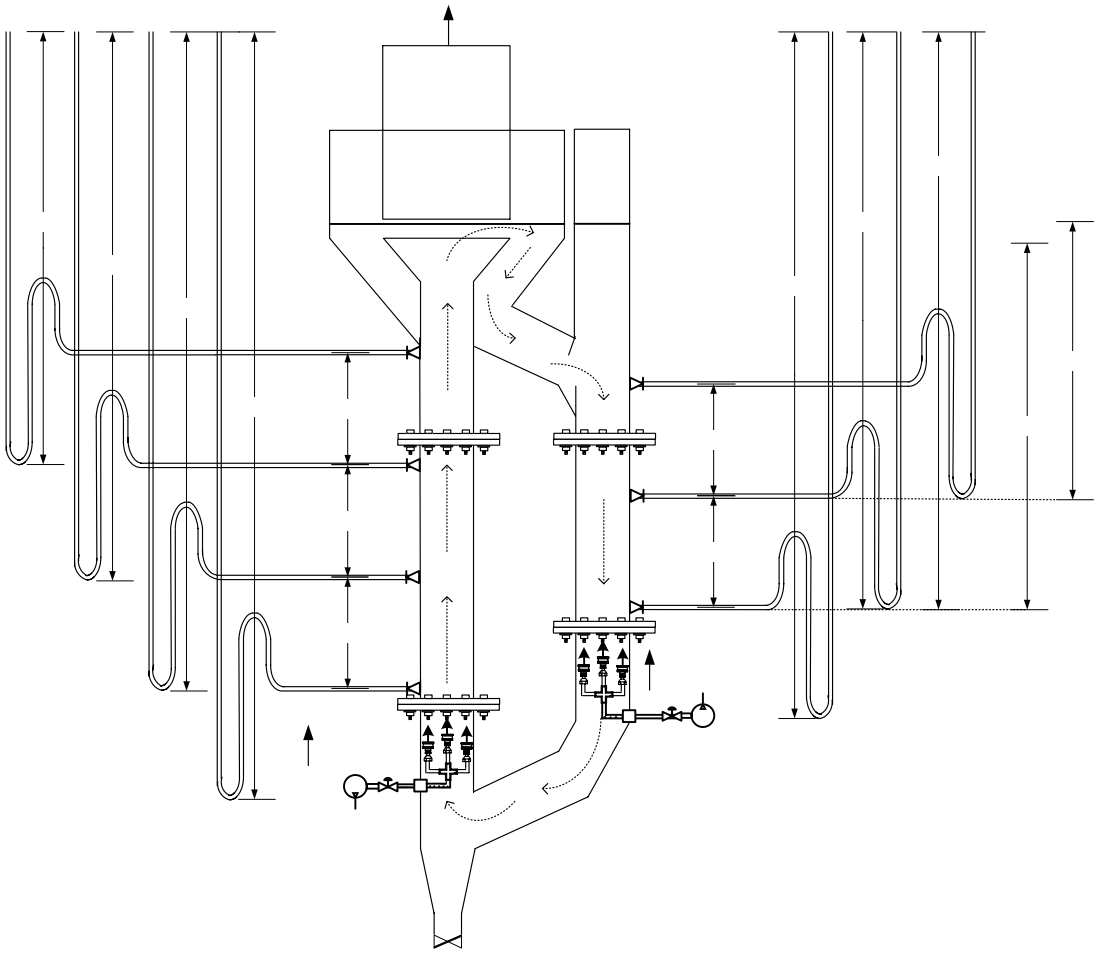

Appendix Figure D2 Different level of liquid water in U-tubes both in riser and downcomer columns when feeding of the inlet gas into the system.

Another method for calculating of the gas holdup could be measured by the usual manometric method. The method measures the pressure difference ΔP between the two levels of the column (Kaustubha *et al., 2006*). The gas holdup is related to the pressure drop by

$$\Delta P = \varepsilon_l \rho_l g h \tag{3}$$

$$\varepsilon_l = \frac{\Delta P}{\rho_l g h} \tag{4}$$

$$\varepsilon_l = \left(\frac{h_a - h_b}{h_L} \right) \tag{5}$$

$$\varepsilon_{gas} = 1 - \varepsilon_l \tag{6}$$

$$\varepsilon_{gas} = 1 - \left(\frac{h_a - h_b}{h_L} \right) \tag{7}$$

where h_a, h_b, h_L are the level of water at Appendix Figure D2

Gas holdup in riser at the superficial gas velocity of the riser is 0.51 cm/s without inlet gas of the downcomer

Distance from riser 2 to riser 3: 20 cm at the middle part of the riser

$$\varepsilon_{riser\,2-3} = 1 - \left(\frac{h_{riser\,2} - h_{riser\,3}}{20} \right)$$

$$\varepsilon_{riser\,2-3} = 1 - \left(\frac{91.10 - 68.74}{20} \right)$$

$$\varepsilon_{rise\,2-3} = 0.081$$

Appendix Table D1 Overall gas holdup in the reactor by measuring of the different level of water in the riser and in the downcomer.

U_r, (cm/s)	U_d (cm/s)	ΔH (cm) of the riser	ΔH (cm) of the downcomer	Overall gas holdup
0.51		7.92	3.24	0.059
1.02		8.61	4.35	0.066
2.05		9.31	5.76	0.073
4.09	0	10	6.87	0.079
6.14		11.99	7.08	0.091
8.19		13.03	9.1	0.101
10.23		16.18	10.42	0.120
2.05		11.2	7.29	0.087
4.09		12.9	8.34	0.098
6.14	1.02	13.91	9.41	0.106
8.19		17	10.61	0.125
10.23		19.49	11.93	0.141
4.09		15.84	10.86	0.119
6.14		17.85	11.97	0.132
8.19	2.05	19.56	13.16	0.143
10.23		22.43	14.47	0.160
4.09		11.77	7.33	0.130
6.14		12.80	8.43	0.138
8.19	3.07	14.52	9.61	0.154
10.23		17.38	10.92	0.165

Appendix Table D2 Level of water in 4 U-tubes along with axial distance from the bottom to the top with equally space 20 cm, for calculating gas holdup in the riser.

U_r, (cm/s)	U_d (cm/s)	H_{riser1} (cm)	H_{riser2} (cm)	H_{riser3} (cm)	H_{riser4} (cm)
0.51	0	111.70	91.10	68.74	48.14
1.02		112.59	91.93	69.29	48.63
2.05		113.50	92.77	69.85	49.12
4.09		114.40	93.60	70.40	49.60
6.14		116.99	95.99	71.99	50.99
8.19		118.34	97.24	72.82	51.72
10.23		122.43	101.02	75.34	53.93
2.05	1.02	114.66	93.84	70.56	49.74
4.09		116.87	95.88	71.92	50.93
6.14		118.18	97.09	72.73	51.64
8.19		120.38	99.12	74.08	52.82
10.23		124.14	102.59	76.39	54.84
4.09	2.05	118.09	97.01	72.67	51.59
6.14		119.41	98.22	73.48	52.30
8.19		121.63	100.27	74.85	53.49
10.23		125.36	103.72	77.14	55.50
4.09	3.07	119.30	98.12	73.42	52.24
6.14		120.64	99.36	74.24	52.96
8.19		122.88	101.42	75.62	54.16
10.23		126.59	104.86	77.90	56.17

Appendix Table D3 Gas holdup in the riser by using the pressure drop measurement. The method measures the pressure drop (ΔP) between the two levels of the column which is separated into 3 parts (top, middle, bottom) .

U_r (cm/s)	U_d (cm/s)	$\varepsilon_{riser1-2}$	$\varepsilon_{riser2-3}$	$\varepsilon_{riser3-4}$	Average $\varepsilon_{riser1-4}$	$\varepsilon_{riser1-4}$
0.51		0.069	0.081	0.107	0.086	0.074
1.02		0.078	0.098	0.133	0.103	0.101
2.05		0.087	0.126	0.151	0.121	0.119
4.09	0	0.125	0.152	0.166	0.148	0.146
6.14		0.147	0.179	0.191	0.172	0.170
8.19		0.183	0.210	0.223	0.205	0.203
10.23		0.192	0.218	0.230	0.213	0.211
2.05		0.091	0.130	0.157	0.126	0.124
4.09		0.124	0.154	0.186	0.155	0.152
6.14	1.02	0.158	0.196	0.219	0.191	0.189
8.19		0.186	0.217	0.225	0.210	0.207
10.23		0.204	0.228	0.230	0.221	0.218
4.09		0.154	0.170	0.198	0.174	0.172
6.14	2.05	0.169	0.198	0.212	0.193	0.191
8.19		0.203	0.228	0.233	0.221	0.219
10.23		0.222	0.247	0.257	0.242	0.239
4.09		0.154	0.179	0.206	0.179	0.177
6.14	3.07	0.171	0.196	0.221	0.196	0.194
8.19		0.207	0.231	0.241	0.226	0.224
10.23		0.220	0.246	0.259	0.242	0.239

Appendix Table D4 Level of water in 4 U-tubes along with the axial distance from the top to the bottom with equally space 20 cm, for calculating gas holdup in the downcomer.

U_r (cm/s)	U_d (cm/s)	H_{down1}(cm)	H_{down2}(cm)	H_{down3}(cm)
0.51	0	96.91	76.24	55.79
1.02		98.36	77.35	56.68
2.05		100.19	78.76	57.81
4.09		101.63	79.87	58.70
6.14		101.90	80.08	58.86
8.19		104.53	82.10	60.48
10.23		106.25	83.42	61.54
2.05	1.02	100.88	79.29	58.23
4.09		102.24	80.34	59.07
6.14		103.63	81.41	59.93
8.19		105.19	82.61	60.89
10.23		106.91	83.93	61.94
4.09	2.05	102.92	80.86	59.49
6.14		104.36	81.97	60.38
8.19		105.91	83.16	61.33
10.23		107.61	84.47	62.38
4.09	3.07	103.53	81.33	59.86
6.14		104.96	82.43	60.74
8.19		106.49	83.61	61.69
10.23		108.20	84.92	62.74

Appendix Table D5 Gas holdup in the downcomer by using the pressure drop measurement. The method measures the pressure drop (ΔP) between the two levels of the column which is separated into 2 parts (top, bottom) .

U_r (cm/s)	U_d (cm/s)	$\varepsilon_{down1-2}$	$\varepsilon_{down2-3}$	Average $\varepsilon_{down1-3}$	$\varepsilon_{down1-3}$
0.51		0.032	0.050	0.041	0.041
1.02		0.047	0.063	0.055	0.055
2.05		0.059	0.073	0.066	0.066
4.09	0	0.080	0.092	0.086	0.085
6.14		0.094	0.105	0.100	0.099
8.19		0.107	0.117	0.112	0.111
10.23		0.115	0.125	0.120	0.120
2.05		0.065	0.077	0.071	0.071
4.09		0.085	0.098	0.092	0.091
6.14	1.02	0.097	0.107	0.102	0.101
8.19		0.118	0.128	0.123	0.123
10.23		0.136	0.146	0.141	0.140
4.09		0.092	0.103	0.097	0.097
6.14	2.05	0.107	0.115	0.111	0.110
8.19		0.133	0.140	0.136	0.136
10.23		0.143	0.153	0.148	0.147
4.09		0.107	0.115	0.111	0.110
6.14	3.07	0.120	0.126	0.123	0.122
8.19		0.142	0.149	0.146	0.145
10.23		0.158	0.163	0.161	0.160

Appendix E

Calculation of the average bubble diameter

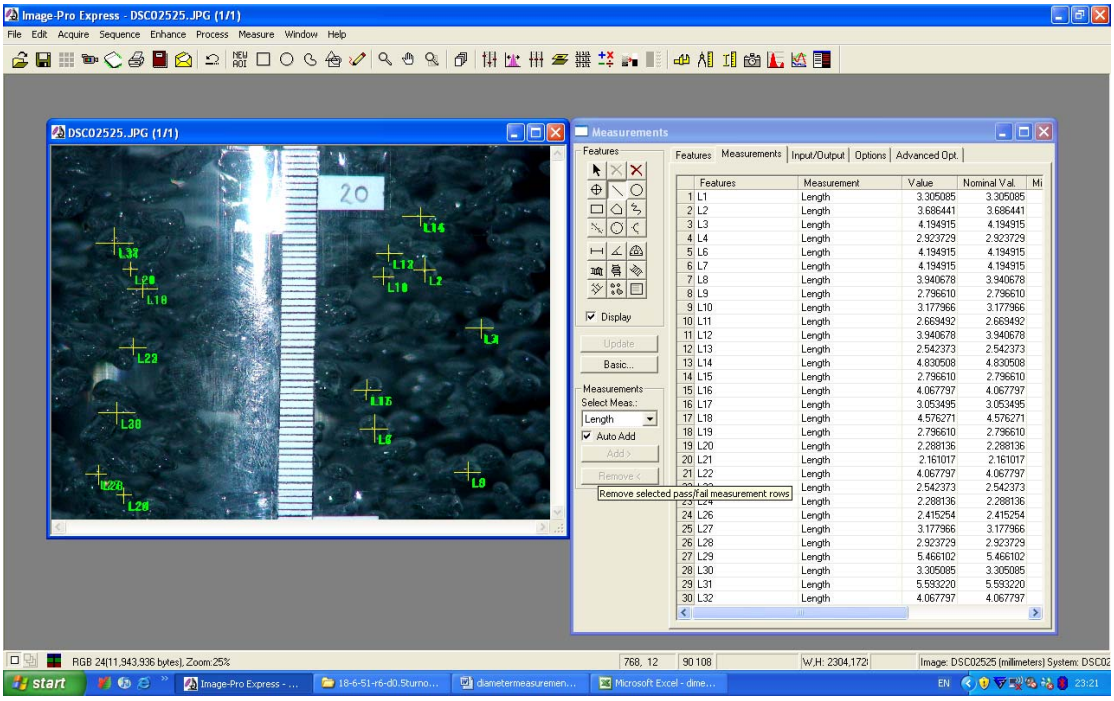

Appendix Figure E1 Calculation of the average bubbles diameters at the distance of 15-20 cm, from the bottom to the top of the downcomer by using the Image-Pro Plus Program at the superficial gas velocity in the riser of 6.14 cm/s and in the downcomer of 1.02 cm/s

The average Sauter mean diameter has the condition and the correlation as follow:

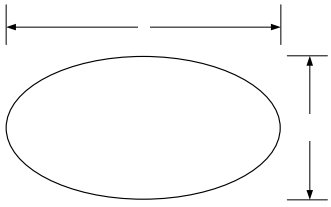

$$dbm = (x^2 y)^{(1/3)} \qquad (1)$$

$$dbs = \frac{\sum dbm^3}{\sum dbm^2} \quad (2)$$

Appendix Table E1 Calculation of the average Sauter mean diameter at the distance of 5-20 cms, from the bottom to the top of the downcomer by using the Image-Pro Plus Program at the superficial gas velocity in the riser of 6.14 cm/s and in the downcomer of 1.02 cm/s

No.	Features	*x*	*y*	*dbm*	dbm^2	dbm^3	*dbs (mm)*
1	L1	3.3051	3.6864	3.4276	11.7485	40.2692	
2	L2	4.1949	2.9237	3.7193	13.8332	51.4498	
3	L3	4.1949	4.1949	4.1949	17.5973	73.8192	
4	L4	3.9407	2.7966	3.5150	12.3552	43.4284	
5	L5	3.1780	2.6695	2.9985	8.9912	26.9604	
6	L6	3.9407	2.5424	3.4051	11.5946	39.4804	
7	L7	4.8305	2.7966	4.0260	16.2086	65.2556	
8	L8	4.0678	3.0535	3.6969	13.6671	50.5261	
9	L9	4.5763	2.7966	3.8835	15.0812	58.5673	
10	L10	2.2881	2.1610	2.2450	5.0398	11.3141	
11	L11	4.0678	2.5424	3.4779	12.0959	42.0686	
12	L12	2.2881	2.4153	2.3297	5.4277	12.6452	
13	L13	3.1780	2.9237	3.0909	9.5534	29.5281	
14	L14	5.4661	3.3051	4.6222	21.3645	98.7502	
15	L15	5.5932	4.0678	5.0299	25.3001	127.2574	
					212.7816	761.2238	**3.5775**

Appendix F

RTD data

The conductivity value was converted from the concentration value.

Appendix Table F1 Relation between concentration (g/ml) and conductivity (mS/cm) in the riser at the superficial gas velocities in the riser of 0.51-10.23 cm/s and in the downcomer of 0 cm/s.

U_r, U_d (cm/s) / Concentration	Conductivity (mS/cm)						
	0.51,0	1.02,0	2.05,0	4.09,0	6.14,0	8.19,0	10.2,0
0.00000	0.284	0.297	0.325	0.333	0.343	0.358	0.370
0.00001	0.313	0.326	0.360	0.371	0.383	0.403	0.413
0.00002	0.329	0.376	0.381	0.390	0.405	0.425	0.439
0.00003	0.350	0.387	0.407	0.421	0.429	0.454	0.485
0.00004	0.359	0.375	0.373	0.434	0.451	0.461	0.476
0.00005	0.385	0.398	0.422	0.459	0.482	0.466	0.479
0.00006	0.399	0.439	0.454	0.478	0.440	0.468	0.473
0.00007	0.426	0.441	0.438	0.508	0.472	0.486	0.491
0.00008	0.447	0.463	0.473	0.492	0.467	0.512	0.547
0.00009	0.456	0.486	0.499	0.499	0.482	0.517	0.510
0.00010	0.487	0.495	0.512	0.509	0.502	0.535	0.541
0.00011	0.503	0.508	0.507	0.526	0.528	0.546	0.573
0.00012	0.530	0.533	0.531	0.549	0.569	0.596	0.605
0.00013	0.556	0.555	0.569	0.569	0.578	0.586	0.618
0.00014	0.578	0.567	0.566	0.578	0.586	0.610	0.649

Appendix Table F2 Relation between concentration (g/ml) and conductivity (mS/cm) in the downcomer at the superficial gas velocities in the riser of 0.51-10.23 cm/s and in the downcomer of 0 cm/s.

U_r, U_d (cm/s) / Concentration	Conductivity (mS/cm)						
	0.51,0	1.02,0	2.05,0	4.09,0	6.14,0	8.19,0	10.2,0
0.00000	0.280	0.279	0.281	0.282	0.294	0.302	0.299
0.00001	0.311	0.318	0.314	0.314	0.328	0.333	0.332
0.00002	0.325	0.348	0.328	0.341	0.347	0.349	0.354
0.00003	0.350	0.353	0.363	0.368	0.371	0.378	0.400
0.00004	0.360	0.412	0.367	0.375	0.390	0.415	0.458
0.00005	0.392	0.408	0.380	0.382	0.386	0.390	0.390
0.00006	0.410	0.410	0.391	0.392	0.395	0.399	0.405
0.00007	0.407	0.409	0.410	0.410	0.411	0.431	0.439
0.00008	0.429	0.432	0.433	0.433	0.434	0.454	0.464
0.00009	0.442	0.443	0.444	0.445	0.445	0.463	0.470
0.00010	0.470	0.470	0.471	0.471	0.462	0.490	0.503
0.00011	0.488	0.489	0.490	0.491	0.492	0.510	0.510
0.00012	0.534	0.544	0.513	0.514	0.516	0.517	0.515
0.00013	0.534	0.536	0.536	0.537	0.538	0.538	0.577
0.00014	0.550	0.551	0.552	0.554	0.555	0.577	0.588

Appendix Table F3 Equations between concentration (g/ml) = x and conductivity (mS/cm) = y in both columns at the superficial gas velocities in the riser of 0.51-10.23 cm/s and in the downcomer of 0-3.07 cm/s.

U_r (cm/s)	U_d (cm/s)	Equation in the riser	Equation in the downcomer
0.51	0	$y = 2035.8x + 0.2843$	$y = 2075.9x + 0.2843$
2.05	1.02	$y = 1807.8x + 0.3297$	$y = 1852x + 0.2861$
4.09	2.05	$y = 1885.3x + 0.3285$	$y = 1838.6x + 0.2865$
4.09	3.07	$y = 2143.6x + 0.3006$	$y = 1863.7x + 0.2842$

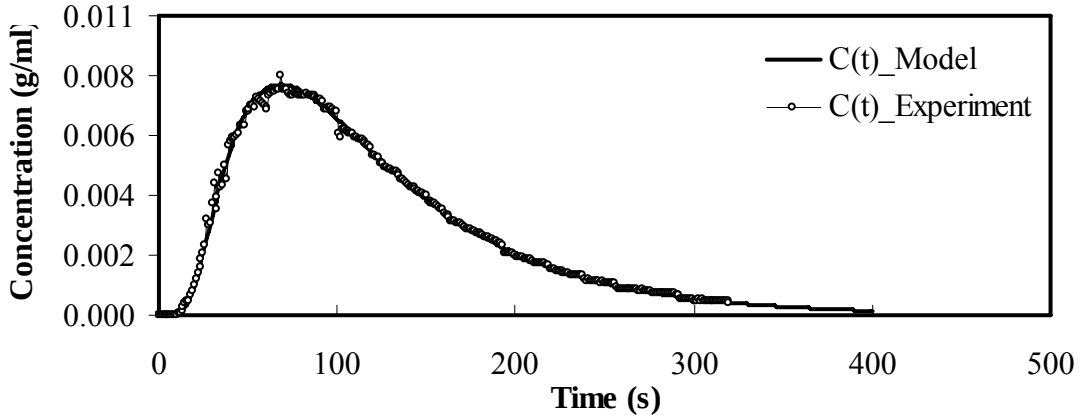

Appendix Figure F1 Relation of $C(t)-curve$ that were obtained from the experiment and dispersion model in the riser at the superficial gas velocity in the riser of 0.51 cm/s and in the downcomer of 0 cm/s

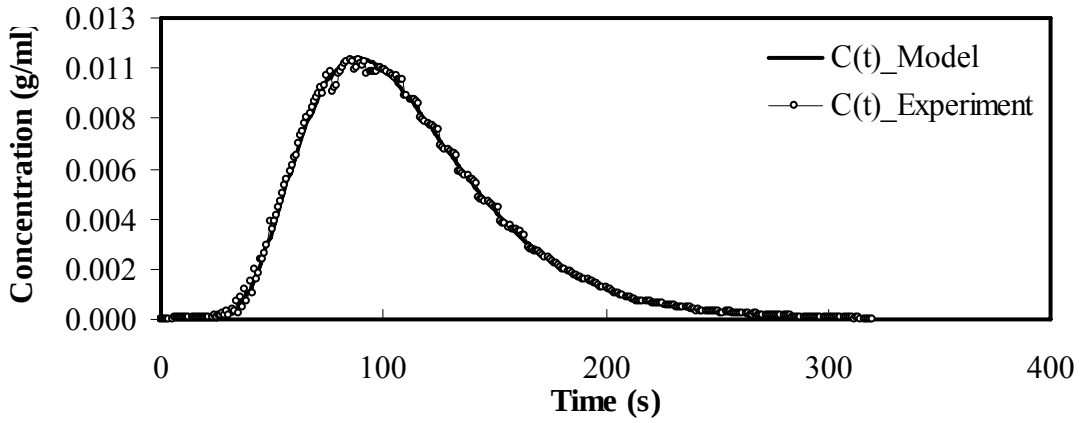

Appendix Figure F2 Relation of $C(t)-curve$ that were obtained from the experiment and dispersion model in the downcomer at the superficial gas velocity in the riser of 0.51 cm/s and in the downcomer of 0 cm/s

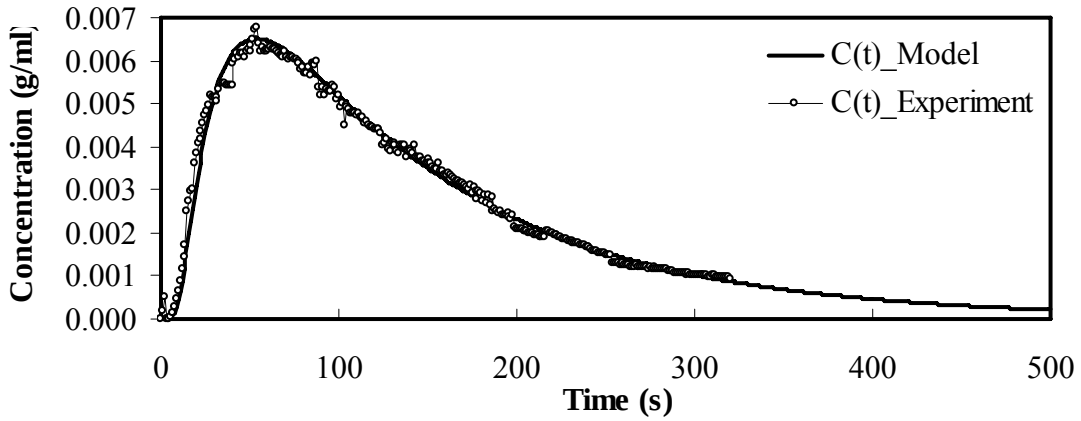

Appendix Figure F3 Relation of $C(t)-curve$ that were obtained from the experiment and dispersion model in the riser at the superficial gas velocity in the riser of 1.02 cm/s and in the downcomer of 0 cm/s

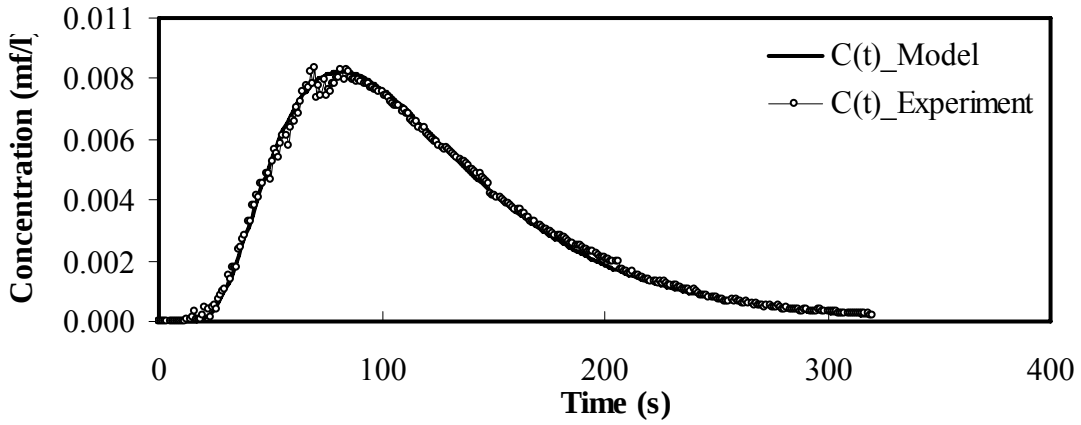

Appendix Figure F4 Relation of $C(t)-curve$ that were obtained from the experiment and dispersion model in the downcomer at the superficial gas velocity in the riser of 1.02 cm/s and in the downcomer of 0 cm/s

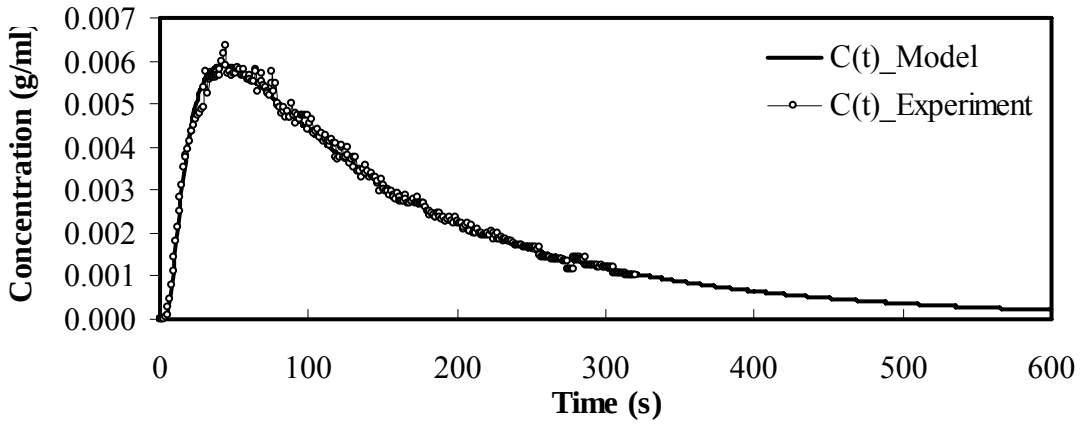

Appendix Figure F5 Relation of $C(t)-curve$ that were obtained from the experiment and dispersion model in the riser at the superficial gas velocity in the riser of 2.05 cm/s and in the downcomer of 0 cm/s

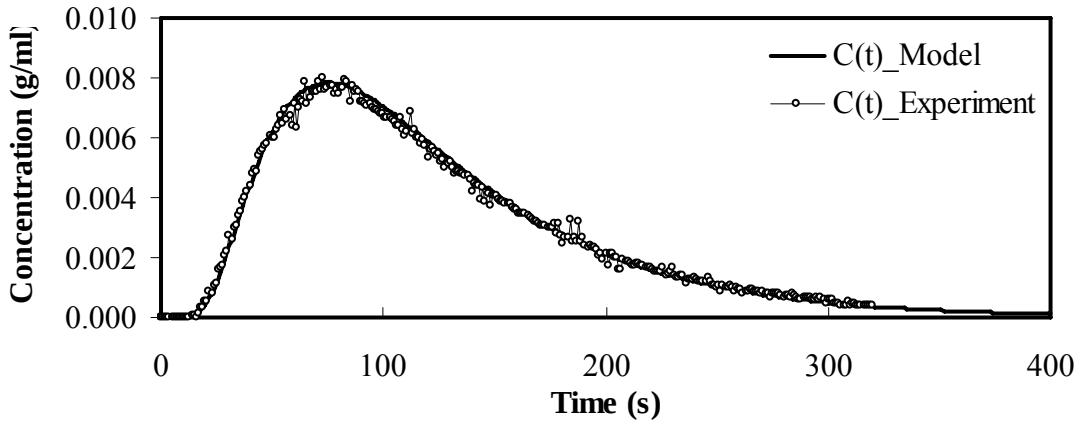

Appendix Figure F6 Relation of $C(t)-curve$ that were obtained from the experiment and dispersion model in the downcomer at the superficial gas velocity in the riser of 2.05 cm/s and in the downcomer of 0 cm/s

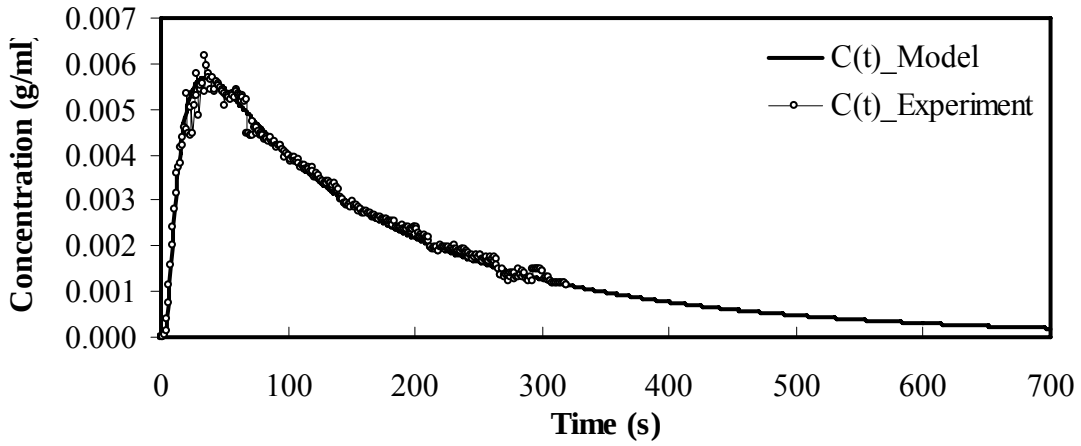

Appendix Figure F7 Relation of $C(t)-curve$ that were obtained from the experiment and dispersion model in the riser at the superficial gas velocity in the riser of 4.09 cm/s and in the downcomer of 0 cm/s

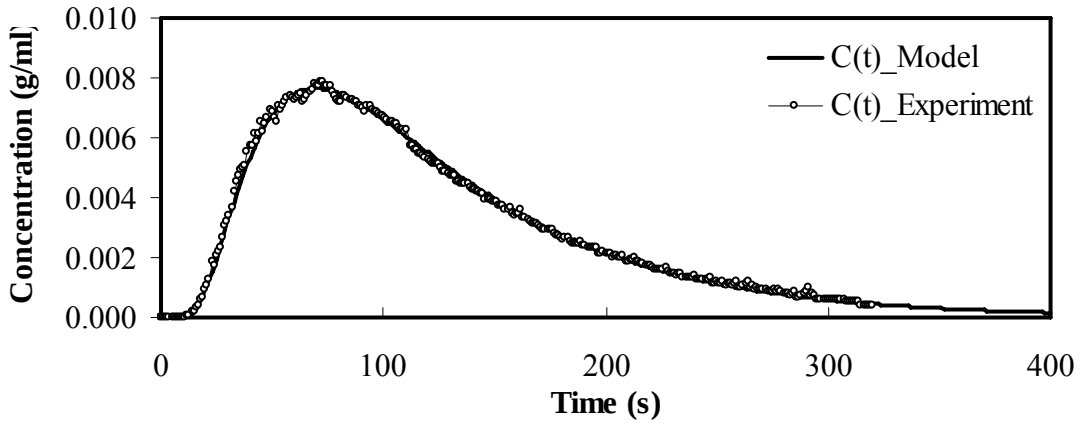

Appendix Figure F8 Relation of $C(t)-curve$ that were obtained from the experiment and dispersion model in the downcomer at the superficial gas velocity in the riser of 4.09 cm/s and in the downcomer of 0 cm/s

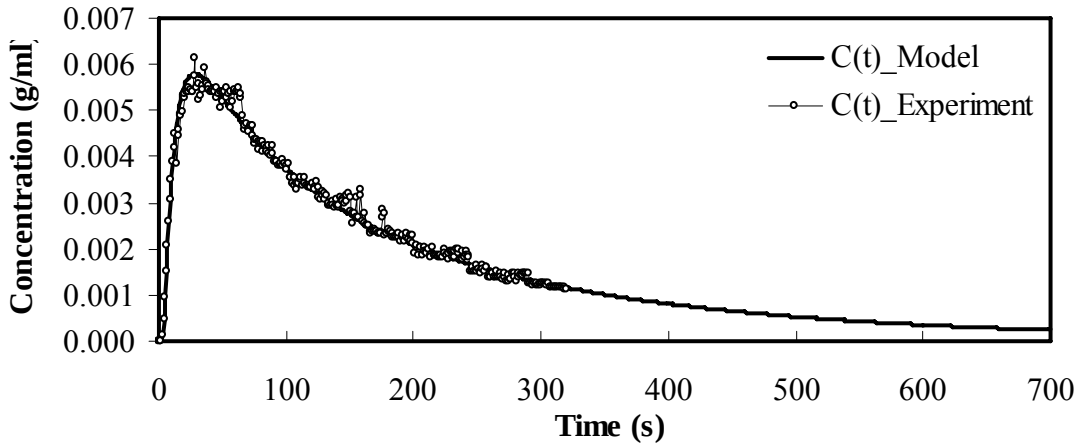

Appendix Figure F9 Relation of $C(t)-curve$ that were obtained from the experiment and dispersion model in the riser at the superficial gas velocity in the riser of 6.14cm/s and in the downcomer of 0 cm/s

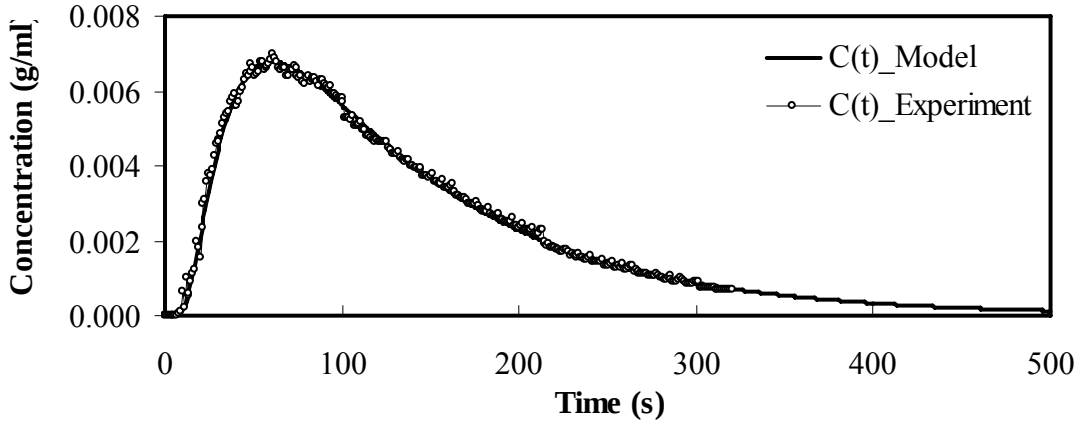

Appendix Figure F10 Relation of $C(t)-curve$ that were obtained from the experiment and dispersion model in the downcomer at the superficial gas velocity in the riser of 6.14cm/s and in the downcomer of 0 cm/s

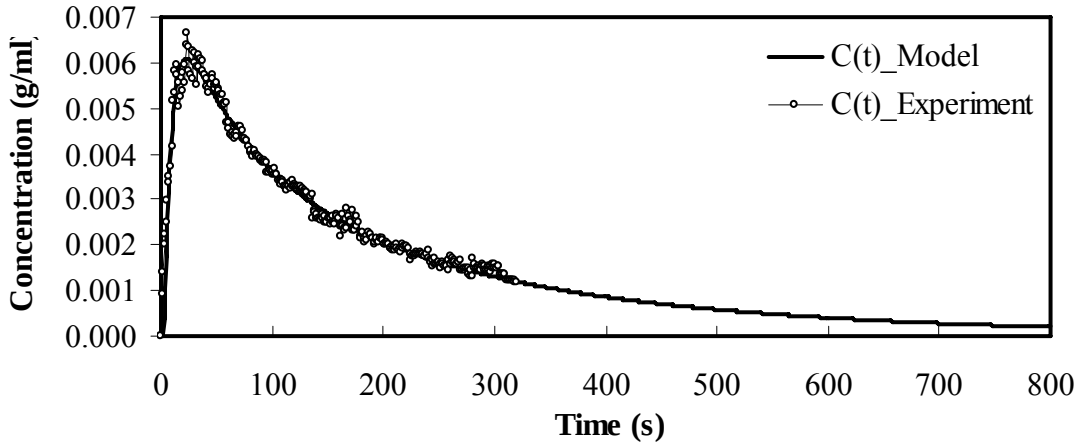

Appendix Figure F11 Relation of $C(t)-curve$ that were obtained from the experiment and dispersion model in the riser at the superficial gas velocity in the riser of 8.19 cm/s and in the downcomer of 0 cm/s

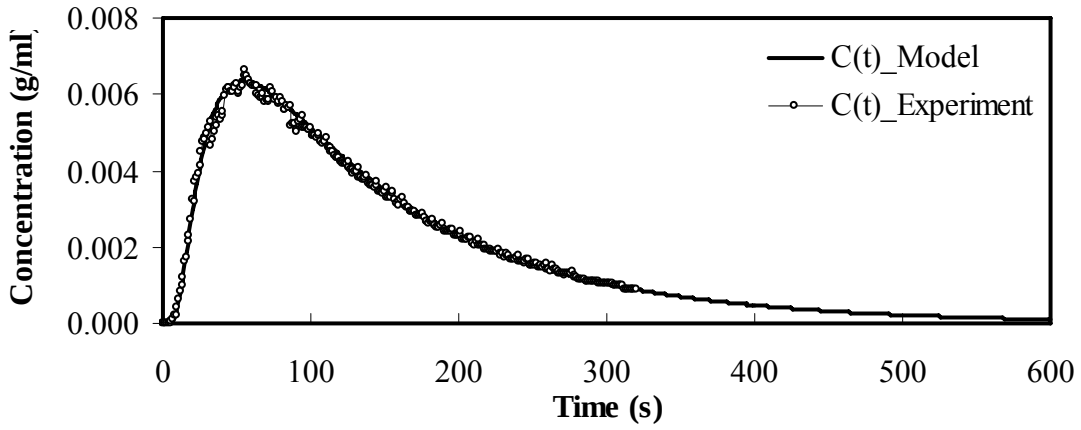

Appendix Figure F12 Relation of $C(t)-curve$ that were obtained from the experiment and dispersion model in the downcomer at the superficial gas velocity in the riser of 8.19 cm/s and in the downcomer of 0 cm/s

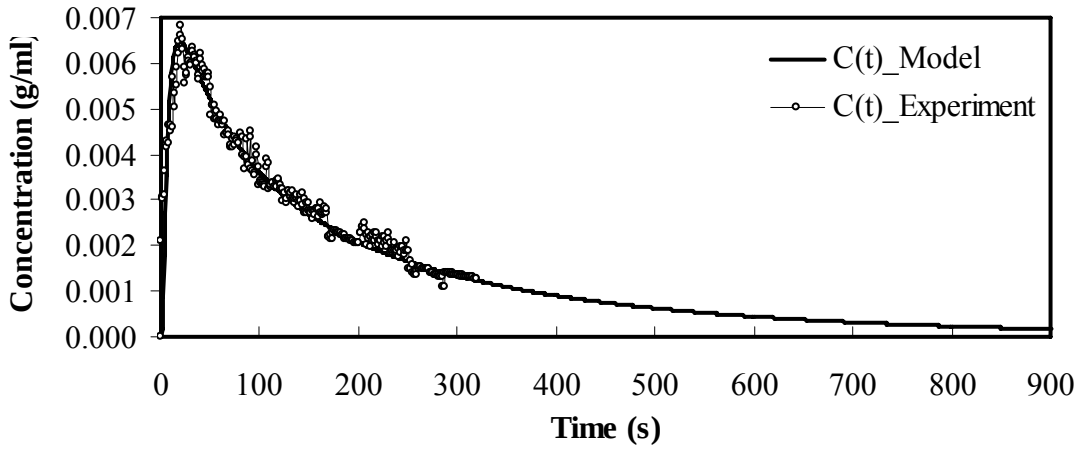

Appendix Figure F13 Relation of $C(t)-curve$ that were obtained from the experiment and dispersion model in the riser at the superficial gas velocity in the riser of 10.23 cm/s and in the downcomer of 0 cm/s

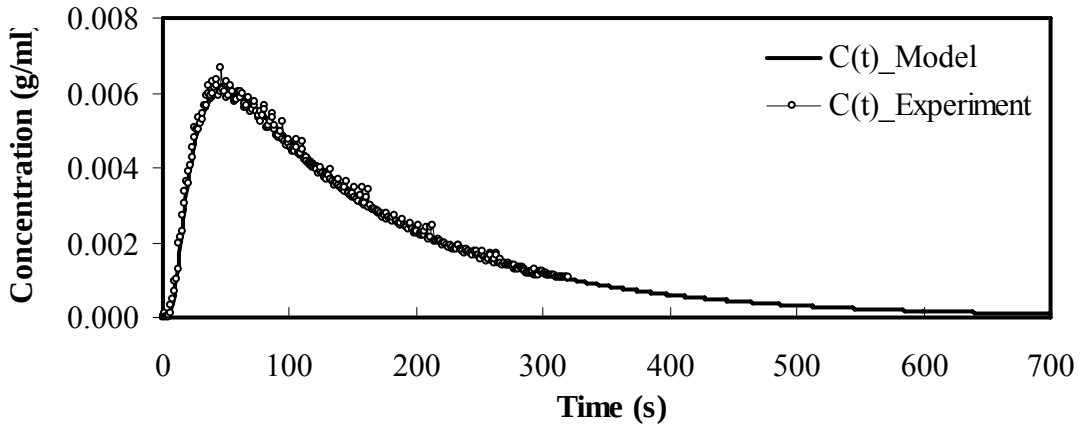

Appendix Figure F14 Relation of $C(t)-curve$ that were obtained from the experiment and dispersion model in the downcomer at the superficial gas velocity in the riser of 10.23 cm/s and in the downcomer of 0 cm/s

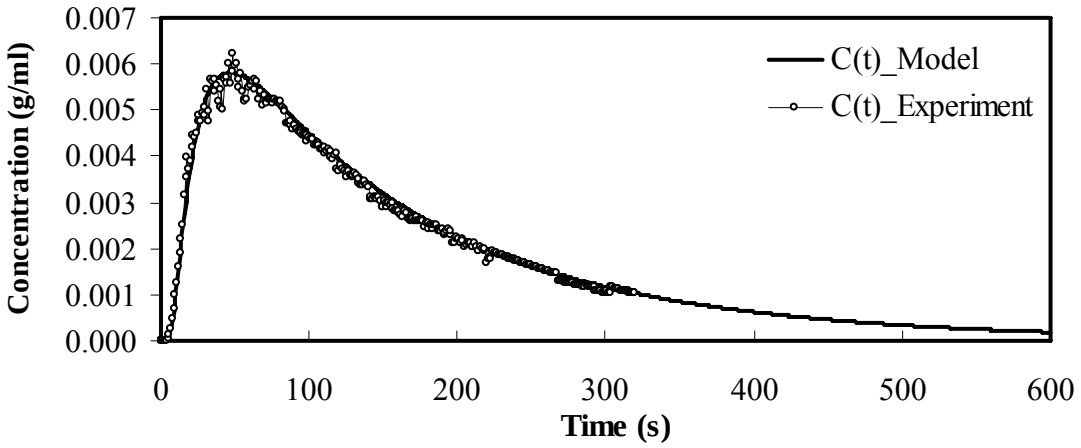

Appendix Figure F15 Relation of $C(t)-curve$ that were obtained from the experiment and dispersion model in the riser at the superficial gas velocity in the riser of 2.05 cm/s and in the downcomer of 1.02 cm/s

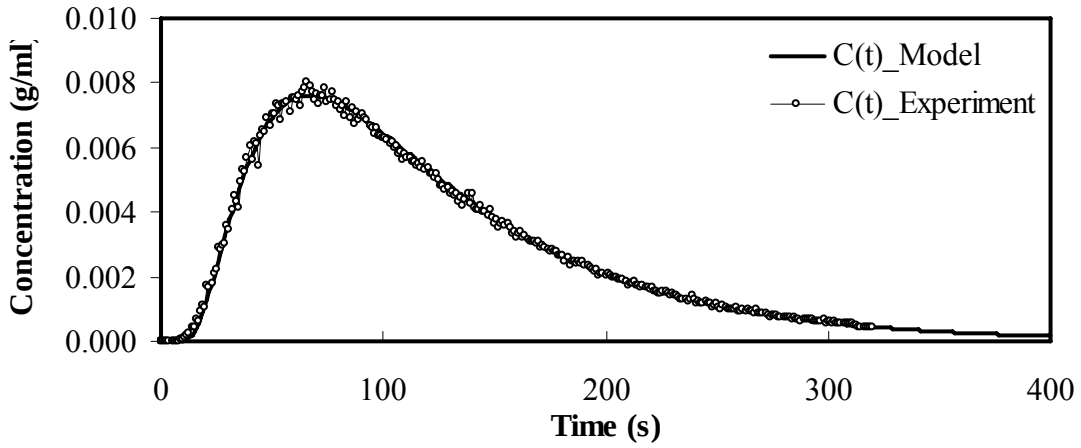

Appendix Figure F16 Relation of $C(t)-curve$ that were obtained from the experiment and dispersion model in the dowcomer at the superficial gas velocity in the riser of 2.05 cm/s and in the downcomer of 1.02 cm/s

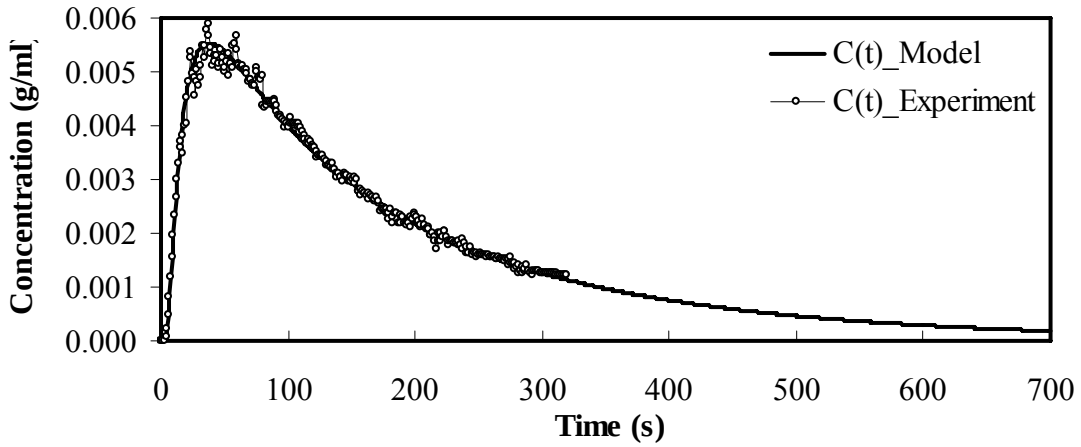

Appendix Figure F17 Relation of $C(t)-curve$ that were obtained from the experiment and dispersion model in the riser at the superficial gas velocity in the riser of 4.09 cm/s and in the downcomer of 1.02 cm/s

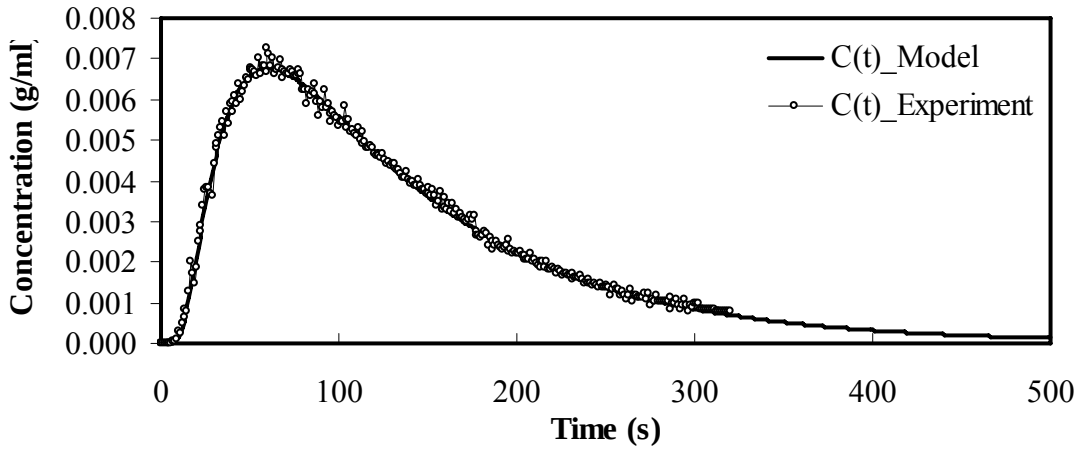

Appendix Figure F18 Relation of $C(t)-curve$ that were obtained from the experiment and dispersion model in the downcomer at the superficial gas velocity in the riser of 4.09 cm/s and in the downcomer of 1.02 cm/s

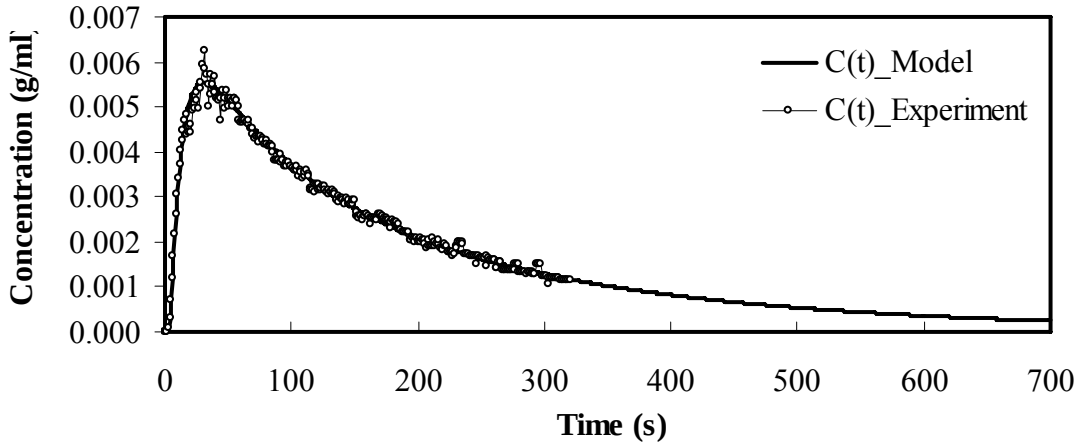

Appendix Figure F19 Relation of $C(t)-curve$ that were obtained from the experiment and dispersion model in the riser at the superficial gas velocity in the riser of 6.14 cm/s and in the downcomer of 1.02 cm/s

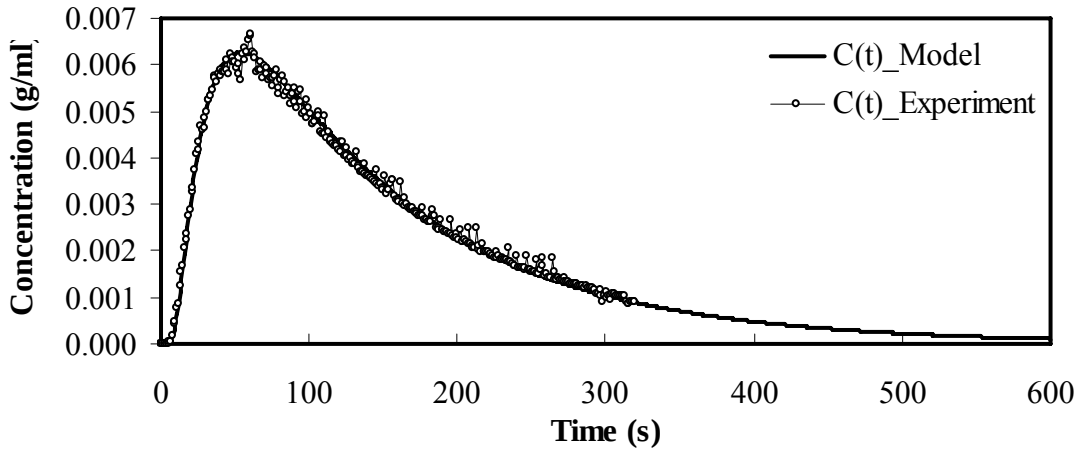

Appendix Figure F20 Relation of $C(t)-curve$ that were obtained from the experiment and dispersion model in the downcomer at the superficial gas velocity in the riser of 6.14 cm/s and in the downcomer of 1.02 cm/s

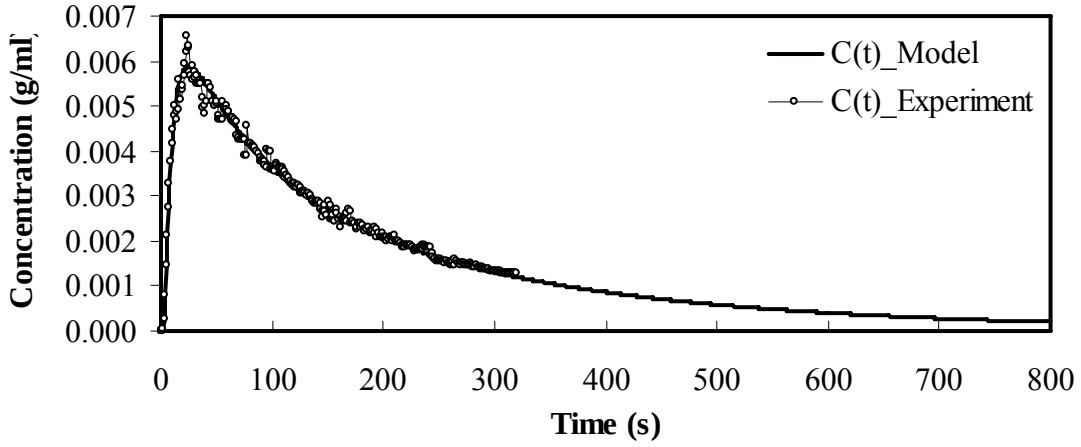

Appendix Figure F21 Relation of $C(t)-curve$ that were obtained from the experiment and dispersion model in the riser at the superficial gas velocity in the riser of 8.19 cm/s and in the downcomer of 1.02 cm/s

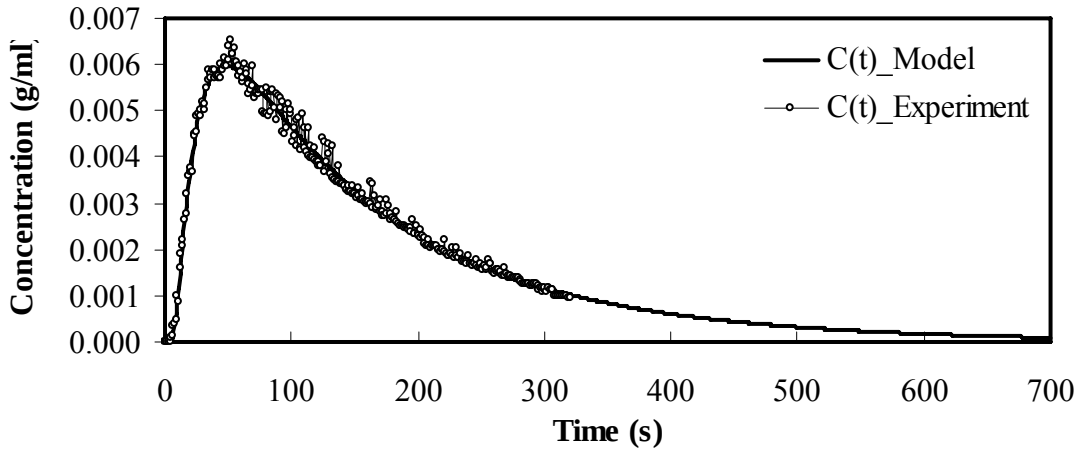

Appendix Figure F22 Relation of $C(t)-curve$ that were obtained from the experiment and dispersion model in the downcomer at the superficial gas velocity in the riser of 8.19 cm/s and in the downcomer of 1.02 cm/s

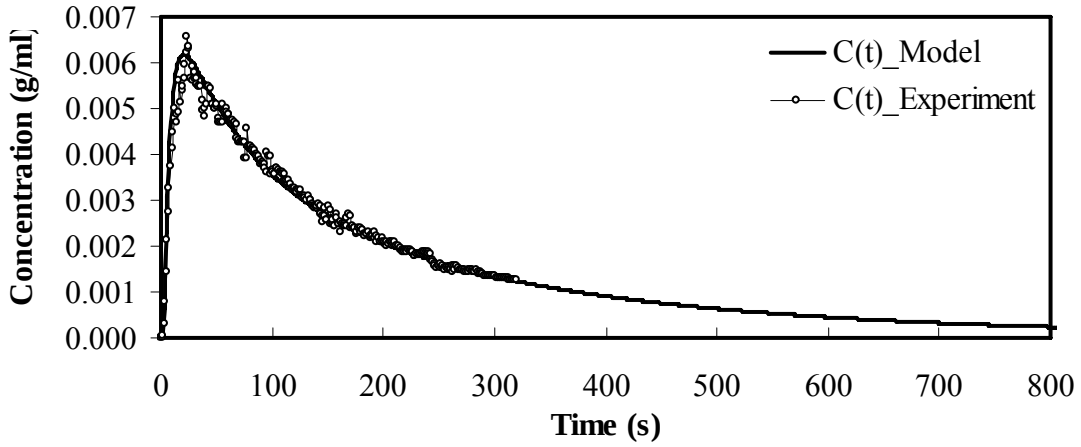

Appendix Figure F23 Relation of $C(t)-curve$ that were obtained from the experiment and dispersion model in the riser at the superficial gas velocity in the riser of 10.23 cm/s and in the downcomer of 1.02 cm/s

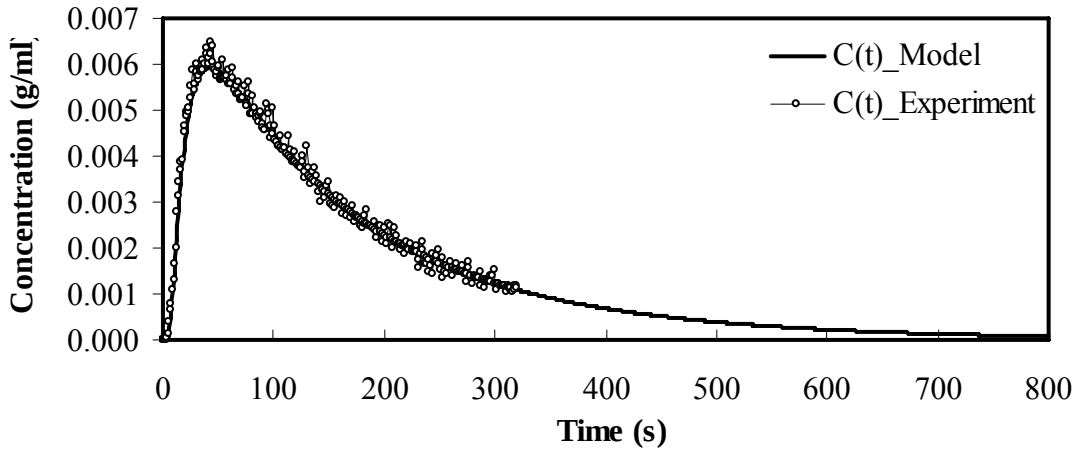

Appendix Figure F24 Relation of $C(t)-curve$ that were obtained from the experiment and dispersion model in the downcomer at the superficial gas velocity in the riser of 10.23 cm/s and in the downcomer of 1.02 cm/s

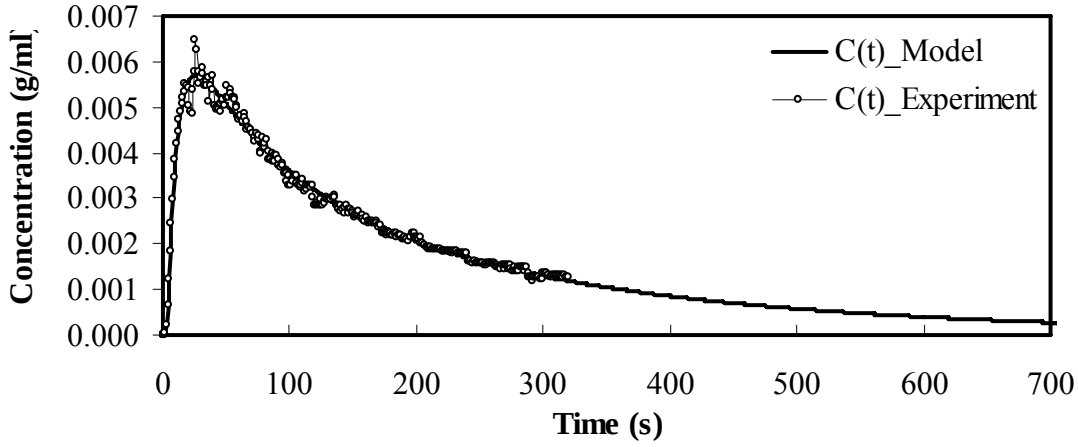

Appendix Figure F25 Relation of $C(t)-curve$ that were obtained from the experiment and dispersion model in the riser at the superficial gas velocity in the riser of 4.09 cm/s and in the downcomer of 2.05 cm/s

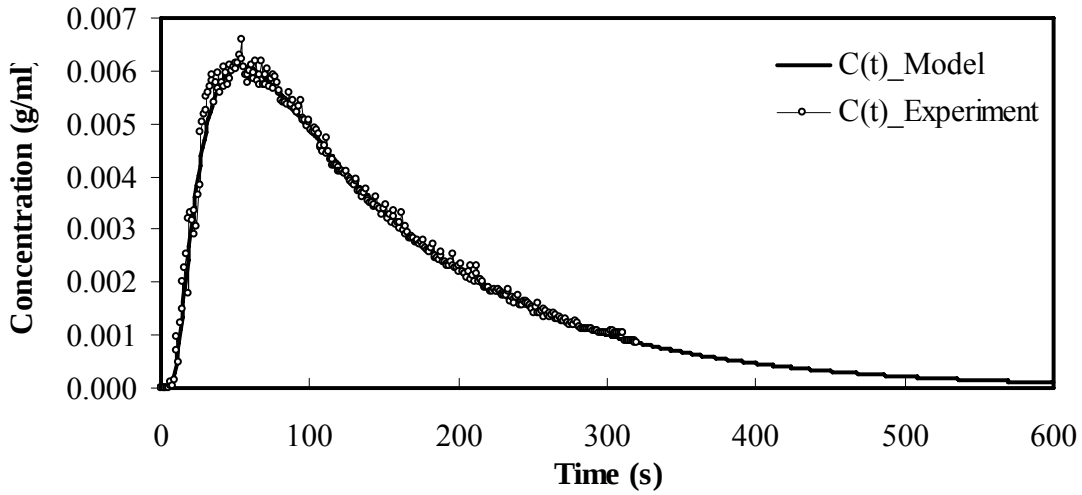

Appendix Figure F26 Relation of $C(t)-curve$ that were obtained from the experiment and dispersion model in the downcomer at the superficial gas velocity in the riser of 4.09 cm/s and in the downcomer of 2.05 cm/s

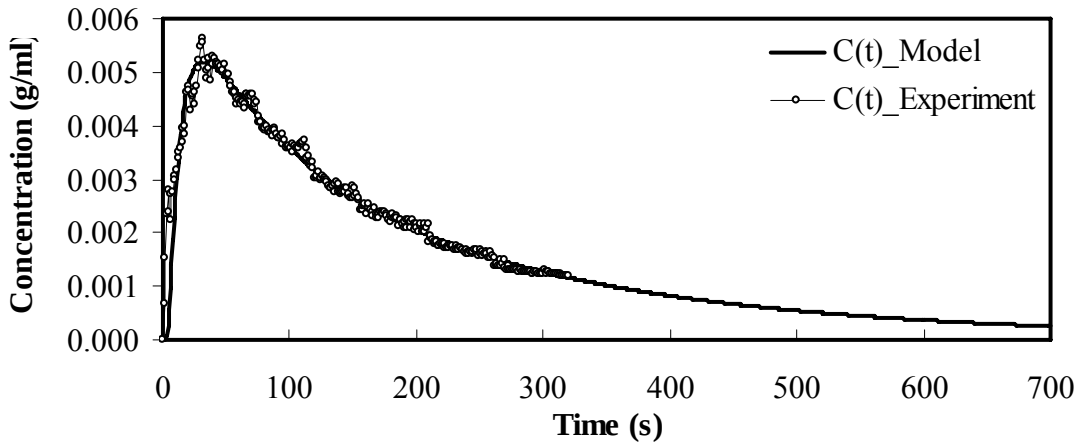

Appendix Figure F27 Relation of $C(t)-curve$ that were obtained from the experiment and dispersion model in the riser at the superficial gas velocity in the riser of 6.14 cm/s and in the downcomer of 2.05 cm/s

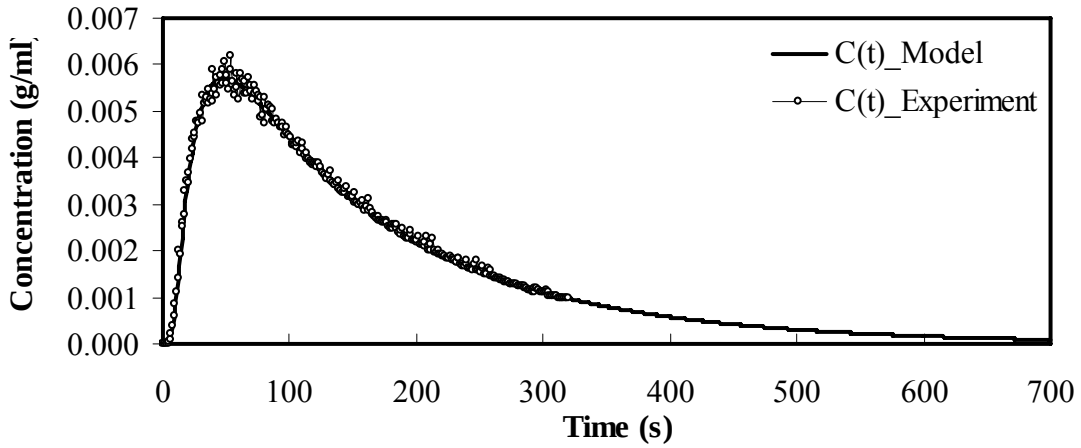

Appendix Figure F28 Relation of $C(t)-curve$ that were obtained from the experiment and dispersion model in the downcomer at the superficial gas velocity in the riser of 6.14 cm/s and in the downcomer of 2.05 cm/s

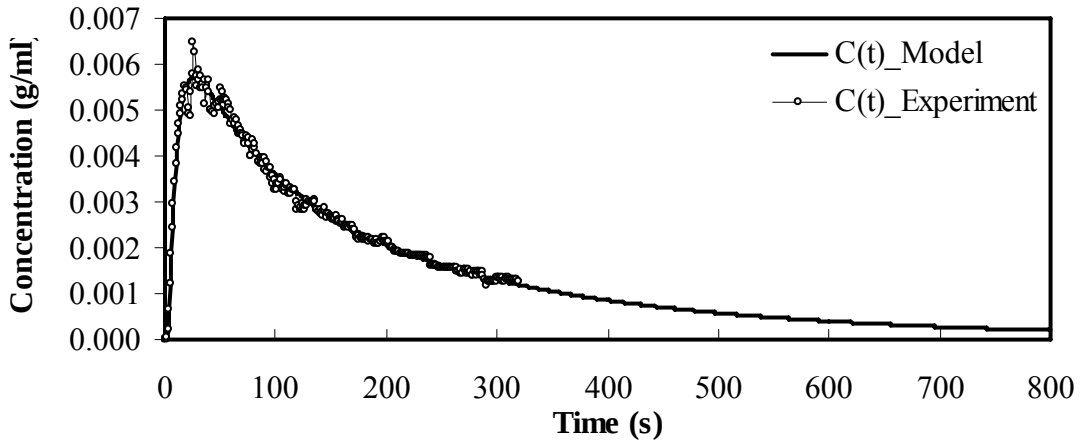

Appendix Figure F29 Relation of $C(t)-curve$ that were obtained from the experiment and dispersion model in the riser at the superficial gas velocity in the riser of 8.19 cm/s and in the downcomer of 2.05 cm/s

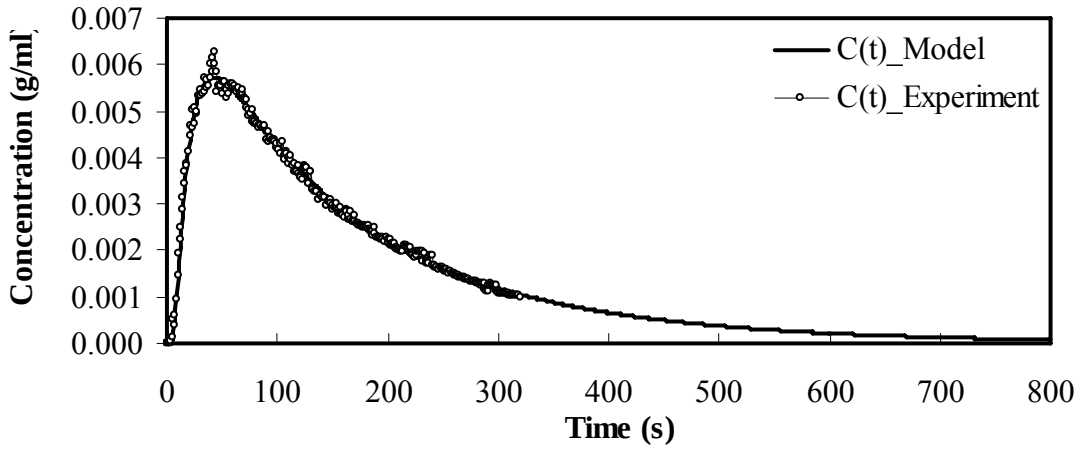

Appendix Figure F30 Relation of $C(t)-curve$ that were obtained from the experiment and dispersion model in the downcomer at the superficial gas velocity in the riser of 8.19 cm/s and in the downcomer of 2.05 cm/s

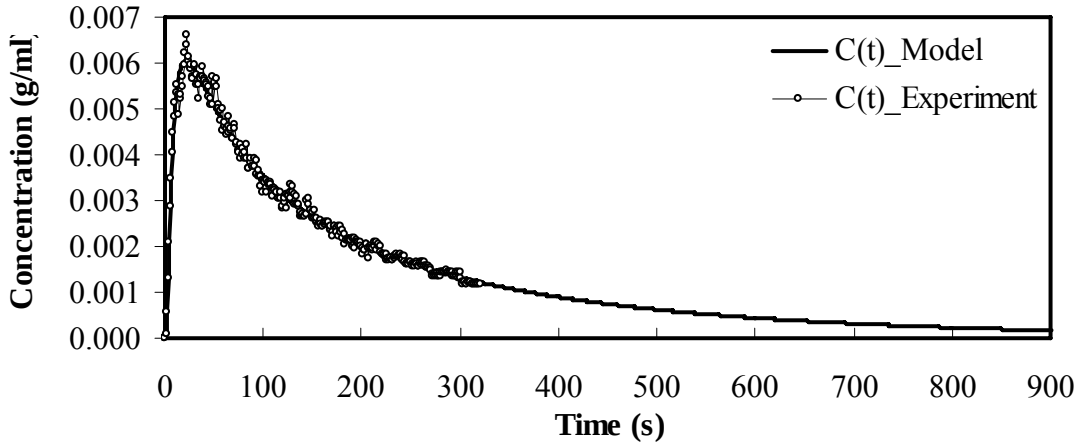

Appendix Figure F31 Relation of $C(t)-curve$ that were obtained from the experiment and dispersion model in the riser at the superficial gas velocity in the riser of 10.23 cm/s and in the downcomer of 2.05 cm/s

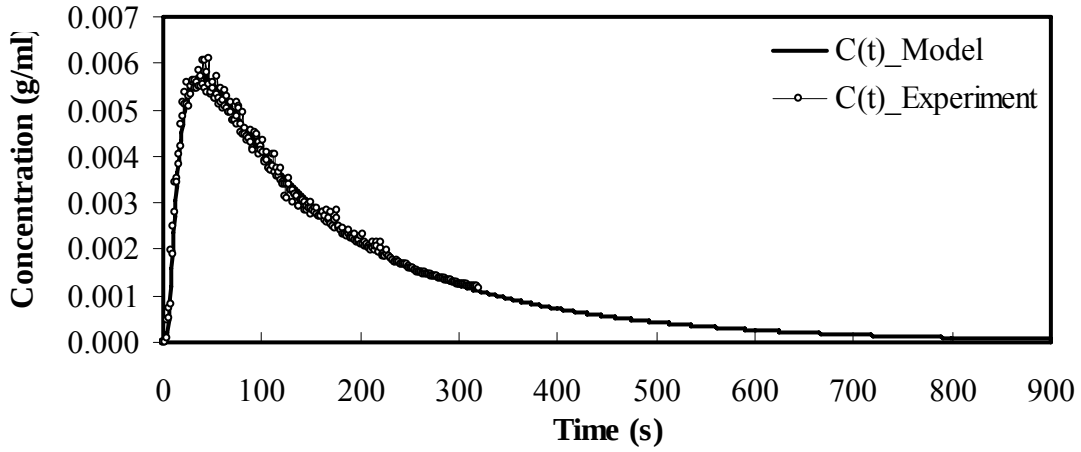

Appendix Figure F32 Relation of $C(t)-curve$ that were obtained from the experiment and dispersion model in the downcomer at the superficial gas velocity in the riser of 10.23 cm/s and in the downcomer of 2.05 cm/s

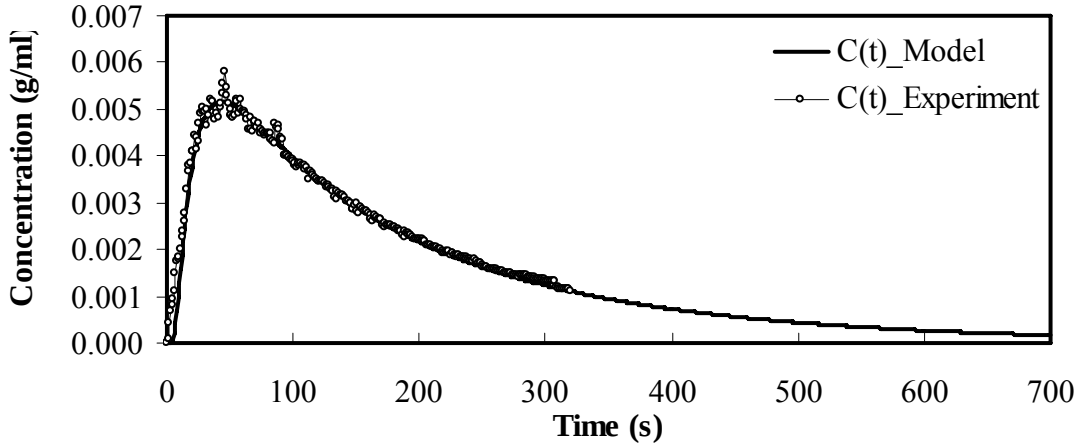

Appendix Figure F33 Relation of $C(t)-curve$ that were obtained from the experiment and dispersion model in the riser at the superficial gas velocity in the riser of 4.09 cm/s and in the downcomer of 3.07 cm/s

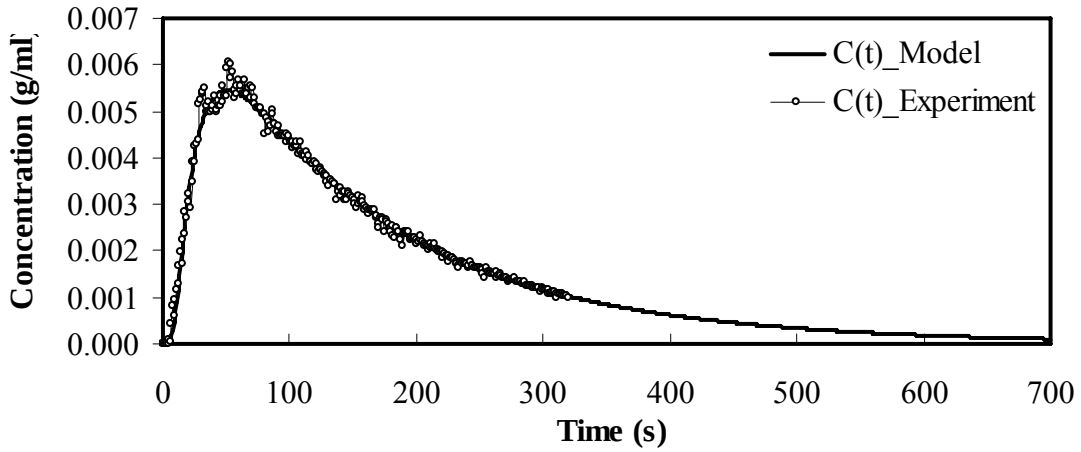

Appendix Figure F34 Relation of $C(t)-curve$ that were obtained from the experiment and dispersion model in the downcomer at the superficial gas velocity in the riser of 4.09 cm/s and in the downcomer of 3.07 cm/s

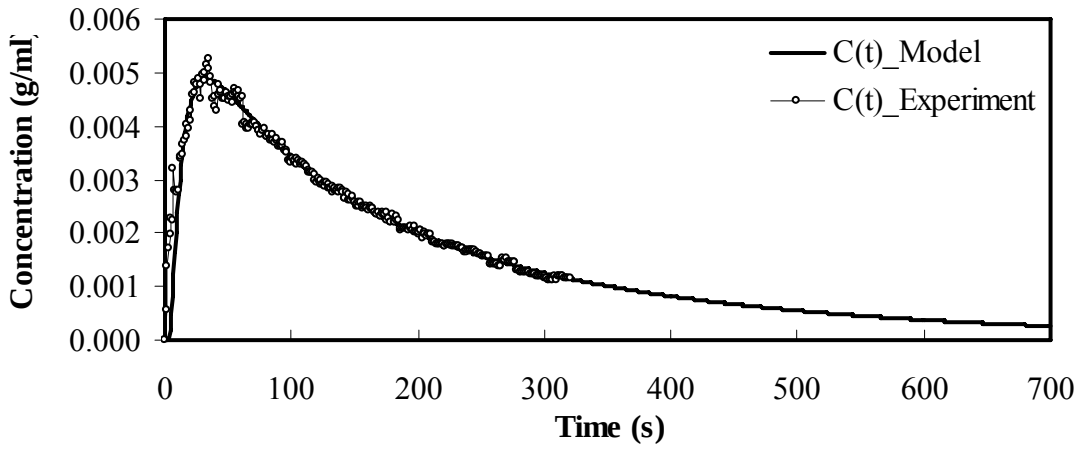

Appendix Figure F35 Relation of $C(t)-curve$ that were obtained from the experiment and dispersion model in the riser at the superficial gas velocity in the riser of 6.14 cm/s and in the downcomer of 3.07 cm/s

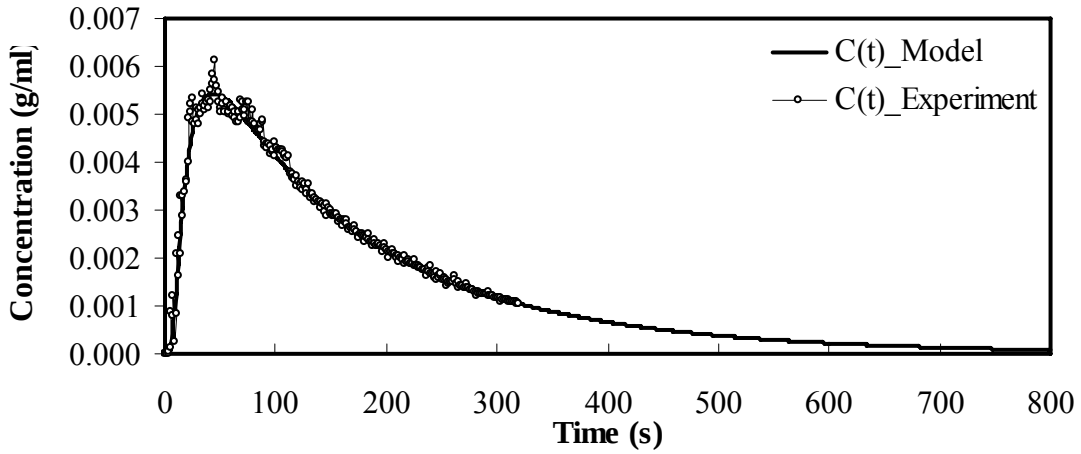

Appendix Figure F36 Relation of $C(t)-curve$ that were obtained from the experiment and dispersion model in the downcomer at the superficial gas velocity in the riser of 6.14 cm/s and in the downcomer of 3.07 cm/s

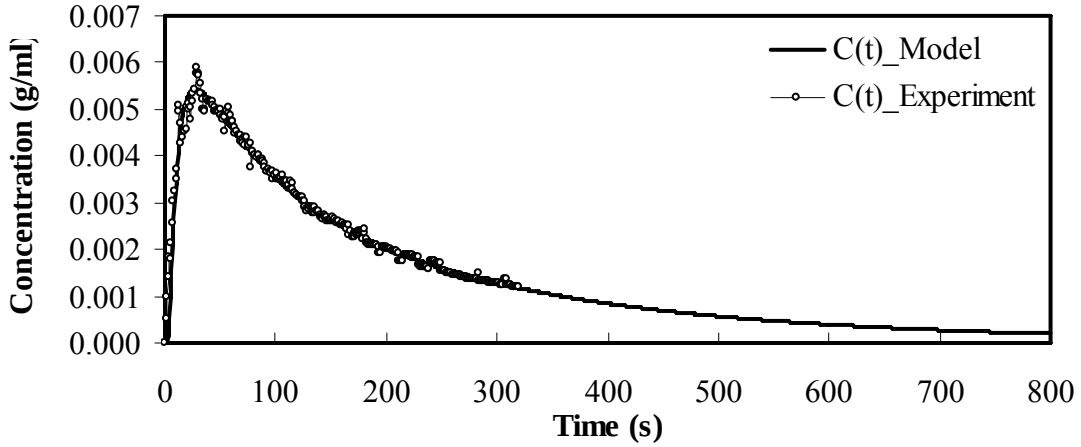

Appendix Figure F37 Relation of $C(t)-curve$ that were obtained from the experiment and dispersion model in the riser at the superficial gas velocity in the riser of 8.19 cm/s and in the downcomer of 3.07 cm/s

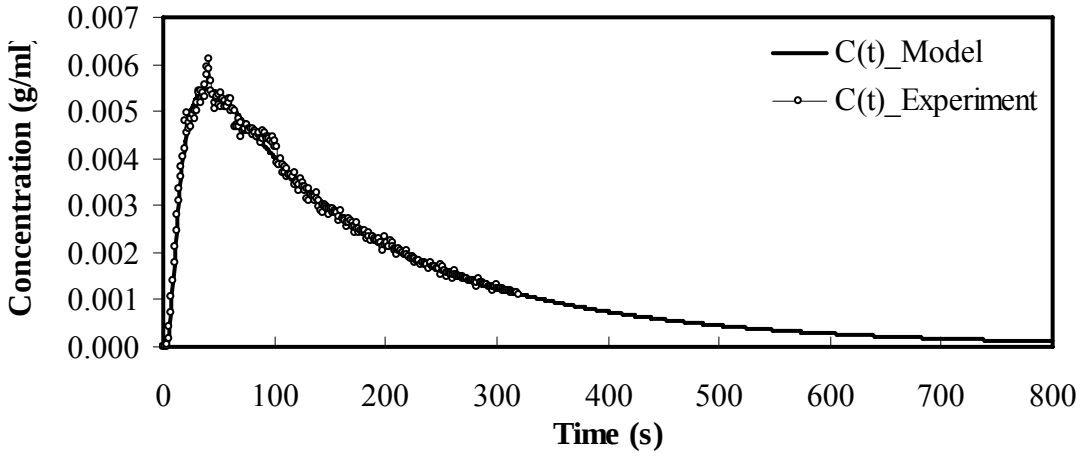

Appendix Figure F38 Relation of $C(t)-curve$ that were obtained from the experiment and dispersion model in the downcomer at the superficial gas velocity in the riser of 8.19 cm/s and in the downcomer of 3.07 cm/s

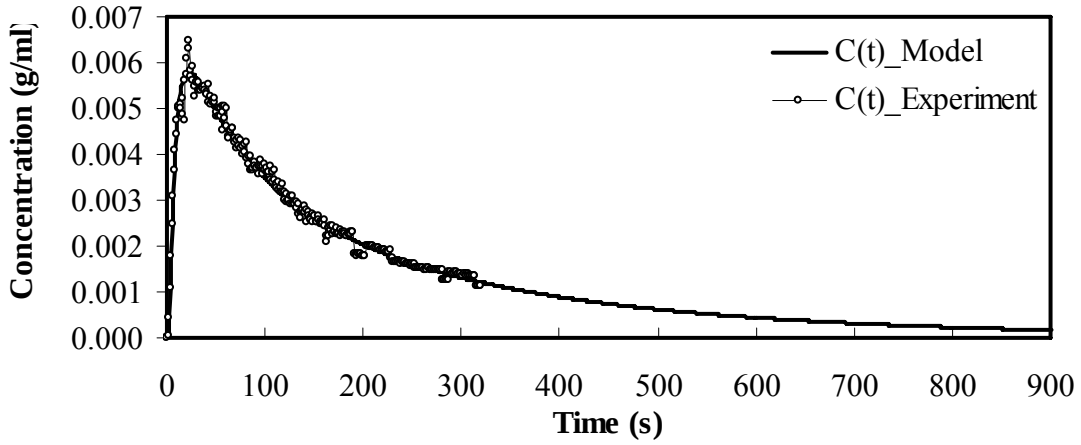

Appendix Figure F39 Relation of $C(t)-curve$ that were obtained from the experiment and dispersion model in the riser at the superficial gas velocity in the riser of 10.23 cm/s and in the downcomer of 3.07 cm/s

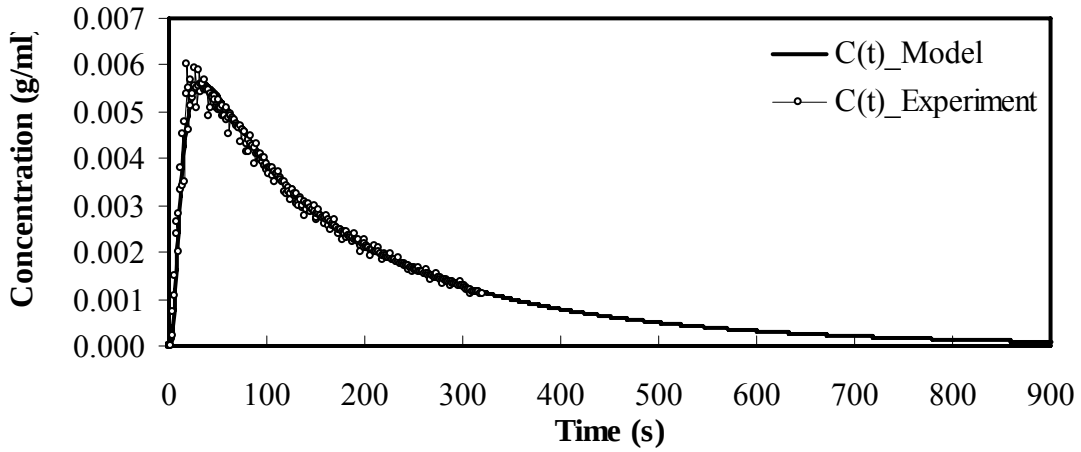

Appendix Figure F40 Relation of $C(t)-curve$ that were obtained from the experiment and dispersion model in the downcomer at the superficial gas velocity in the riser of 10.23 cm/s and in the downcomer of 3.07 cm/s

CIRRICULUM VITAE

NAME : Miss Olrarat Wongsirikajorn

BIRTH DATE : March 5, 1984

BIRTH PLACE : Bangkok, Thailand

EDUCATION :

YEAR	**INSTITUTE**	**DEGREE/DIPLOMA**
2005	Kasetsart Univ.	B.Eng. (Chemical)
2008	Kasetsart Univ.	M.Eng. (Chemical)

POSITION/TITLE : Teacher Assistant

WORK PLACE : Faculty of Engineering, Kasetsart University

SCHOLARSHIP/AWARDS : Thai Asahi Glass Public Co., Ltd. Scholarship 2004
: Asian Development Bank (ADB) Scholarship 2006-2008